

HIGH RESOLUTION SEQUENCE STRATIGRAPHY AND
RESERVOIR CHARACTERIZATION OF MISSISSIPPIAN STRATA
IN CENTRAL AND EASTERN OKLAHOMA

By

C.J. APPLESETH

Bachelor of Arts in Business Administration

University of Central Oklahoma

Edmond, OK

2008

Submitted to the Faculty of the
Graduate College of the
Oklahoma State University
in partial fulfillment of
the requirements for
the Degree of
MASTER OF SCIENCE
May, 2019

HIGH RESOLUTION SEQUENCE STRATIGRAPHY AND
RESERVOIR CHARACTERIZATION OF MISSISSIPPIAN STRATA
IN CENTRAL AND EASTERN OKLAHOMA

Thesis Approved:

Dr. G. Michael Grammer

Thesis Adviser

Dr. James Puckette

Dr. Jack Pashin

ACKNOWLEDGEMENTS

I would like to thank Dr. Michael Grammer for his guidance throughout my research. His questions and insights made me a better geologist. “So what?” was a common question that he used to force me to focus on what is important in what I’m trying to convey. I would also like to thank my committee members, Dr. Jack Pashin and Dr. Jim Puckette for their support as well. Dr. Pashin did not hesitate to join my committee to fill-in for a member who could not serve at the last minute. Dr. Puckette was the first faculty member that I met when I was considering coming back to school. His positive attitude and encouragement cemented my decision to come to Oklahoma State. I cannot thank him enough for his help throughout my studies at the Boone Pickens School of Geology.

I would also like my colleagues in the Carbonate Reservoir Characterization Group. They helped with my research through bouncing ideas off of them and general brainstorming. Other members outside of this group also helped with my research. Ethan Hill had a comparable data set and we talked at length about some of the similar issues with our respective projects. Drew Davis, Connor Cain, Scott Shelley, and Ethan were some of the best friends I could have asked for as a graduate student. They each served as an outlet for general frustrations as a graduate student, and we each knew that the other would always be there to listen and help out.

I would like to thank my family. Their encouragement and support throughout this study was appreciated. My parents, Jim and Joy Appleseth, always believed in me and encouraged me to pursue this when I was still deciding if I wanted to come back to school. I am thankful that I did.

Finally, I want to thank my wife, Rachel. Words fall short of the gratitude and love that I have for you. We met right as I was beginning graduate school and you have been there with me every step of the way. I cannot imagine doing this without you by my side, and I cannot wait to meet our child, Norah Elaine, sometime in the next few weeks. I love both of you more than I can describe.

Name: C.J. APPLESETH

Date of Degree: DECEMBER, 2018

Title of Study: HIGH RESOLUTION SEQUENCE STRATIGRAPHY AND RESERVOIR
CHARACTERIZATION OF MISSISSIPPIAN STRATA IN CENTRAL AND
EASTERN OKLAHOMA

Major Field: GEOLOGY

Abstract: The “Mississippian Limestone” of the Mid-Continent has a geologically complex arrangement of facies. These complexities span throughout the region and have proven problematic in prediction of subsurface facies variations. Until recently, a number of studies on the “Mississippian Lime” were focused on large-scale variations in lithofacies. More recent work has defined a sequence stratigraphic hierarchy detailing facies changes that occur due to high-frequency sea level changes. This study expands on previous work in the region by developing a sequence stratigraphic framework in Okfuskee County, Oklahoma. This will allow for better prediction of subsurface variations in the region, as well as correlation of facies and the sequence stratigraphic architecture to other parts of Oklahoma.

The “Mississippian Limestone” is an aerially extensive mixed carbonate and siliciclastic system containing a variety of carbonate environments and subenvironments. Each of these settings has a variety of associated characteristics, including: rock texture, allochems, sedimentary structures, fossils, and pore types along with probable variations in facies and reservoir distribution. Significant lateral and vertical heterogeneity at multiple scales, from kilometer to meter or smaller, commonly occurs in carbonates and has been documented in the Mississippian system of the Mid-Continent. This study integrates multiple data sets (core, wireline logs, and thin sections) to interpret facies and reservoir variability within a sequence stratigraphic framework. Construction of 2-D regional to sub-regional cross sections tied to the sequence stratigraphy should lead to better predictability of reservoir distribution and architecture.

TABLE OF CONTENTS

Chapter	Page
I. INTRODUCTION	1
Problem Statement.....	1
Fundamental Questions and Hypothesis.....	2
Objectives.....	3
II. GEOLOGIC BACKGROUND.....	4
Tectonics	4
Paleogeography and Climate	7
Sea Level	10
III. DATA & METHODS	13
Core Descriptions.....	13
Thin Section Analysis.....	15
X-Ray Diffractions (XRD).....	16
Sequence Stratigraphy and Framework	16
Wireline Logs.....	17
Subsurface Mapping	19
Limitations.....	19
IV. RESULTS	22
Core Facies Types.....	22
Fissile Clay-Rich Siltstone	22
Glauconitic Sandstone	24
Massive Bedded Peloidal Siltstone	26
Laminated Peloidal Siltstone	28
Mottled Peloidal Siltstone	30
Skeletal Mudstone-Wackestone.....	32
Skeletal Packstone-Grainstone	34
Core Facies Stacking Patterns	36

Chapter	Page
V. DISCUSSION	38
Facies Interpretations	40
Fissile Clay-Rich Siltstone (Facies 1)	40
Glaucconitic Sandstone (Facies 2)	41
Massive Bedded Peloidal Siltstone (Facies 3)	41
Laminated Peloidal Siltstone (Facies 4)	41
Mottled Peloidal Siltstone (Facies 5)	42
Skeletal Mudstone-Wackestone (Facies 6)	43
Skeletal Packstone-Grainstone (Facies 7)	43
Sequence Stratigraphic Framework.....	44
Idealized Facies Stacking Pattern.....	44
Sequence Stratigraphic Hierarchy	45
2 nd Order Supersequence	45
3 rd Order Sequence	46
4 th Order High-Frequency Sequence.....	46
Wireline Log Correlations	47
Gamma Ray	49
Resistivity	49
Caliper	50
Sequence Stratigraphically Defined Architecture.....	51
Stratigraphic Cross Sections.....	53
Dip Oriented Cross Sections.....	53
Strike Oriented Cross Sections.....	56
Thickness Maps.....	59
3 rd Order Sequence Thickness Maps.....	60
4 th Order High Frequency Sequence Thickness Maps	57
Reservoir Considerations	59
Silt Origins and Method of Transport	73
VI. CONCLUSIONS.....	76
REFERENCES	78
APPENDICES	85
Appendix A: Angell 1-23.....	86
Whole Core Photographs.....	87
Core Descriptions.....	129

Chapter	Page
Thin Section Photomicrographs.....	134
X-Ray Diffraction Analysis	173
Appendix B: Wise 1-20.....	174
Whole Core Photographs.....	175
Core Descriptions.....	212
X-Ray Diffraction Analysis	216
Appendix C: Mississippian Stratal Architecture	217
Subsurface Cross Section Reference Map	218
Subsurface Cross Sections	SEE ATTACHED
Depth to Mississippian-Pennsylvanian Contact Structure Map	220
Depth to Basal Mississippian Contact (Top of Woodford Shale) Structure Map	221
“4 th Order” Sequence Thickness Maps	222

LIST OF TABLES

Table		Page
1	Cycle hierarchy.....	12
2	General information on cored wells utilized in this	13
3	Wireline logs used in this study	18
4	Primary depositional facies described in this study	39
5	Core image labels for the Angell 1-23 and Wise 1-20	88
6	Bioturbation index utilized for core descriptions	130
7	XRD analysis for the Angell 1-23	173
8	XRD analysis for the Wise 1-20	216

LIST OF FIGURES

Figure		Page
1	Map of Oklahoma showing prominent structural components throughout the state	4
2	Fault Database and Interpretive Fault Map of Oklahoma	6
3	Theoretical shoreline shift in response to a 100 meter sea level change	9
4	Diagram showing the nature and temporal duration of the different elements of Milankovitch orbital variations.....	12
5	The Dunham (1962) carbonate classification scheme based on depositional texture observed.....	14
6	Pore systems observed in carbonates	15
7	Facies 1 Fissile clay-rich siltstone.....	23
8	Facies 2 Glauconitic Sandstone.....	25
9	Facies 3 Massive bedded peloidal siltstone.....	27
10	Facies 4 Laminated peloidal siltstone	29
11	Facies 5 Mottled peloidal siltstone	31
12	Facies 6 Skeletal mudstone-wackestone	33
13	Facies 7 Skeletal packstone-grainstone	35
14	Lithologic columns	37
15	Idealized facies stacking pattern.....	44
16	The sequence stratigraphic framework.....	48
17	Stratigraphic cross sections constructed throughout the study area	52
18	Stratigraphic cross section A-A'	55
19	Stratigraphic cross section B-B'	58
20	Detail of northern sector of Cross Section A-A'	61

21	3 rd order sequence 1	63
22	3 rd order sequence 2	64
23	3 rd order Sequence 3.....	65
24	3 rd order Sequence 4.....	66
25	Series of high frequency sequence maps	68
26	Porosity and permeability categorized by facies.....	70
27	Porosity and permeability categorized from samples in the different 3 rd order sequences.....	72
28	Porosity and permeability categorized according to transgressive/regressive legs of the sequence stratigraphic framework	72
29	Hjulström-Sundborg diagram	74
30	Proposed location of Batesville Delta showing environments and types of sediment deposits.....	75
31	Key for core description of Angell 1-23	131
32	Thin section image label key.....	135
33	Key for core description of Wise 1-20	213

CHAPTER I

INTRODUCTION

Problem statement: The “Mississippian Lime” of the Mid-Continent has a geologically complex arrangement of facies. These complexities span throughout the region and have proven problematic in predicting subsurface facies variations (Wilhite et al., 2011). Until recently, studies were focused on large-scale variations in lithofacies (Gutschick and Sandberg, 1983). More recent work has defined a sequence stratigraphic hierarchy detailing facies changes that occur due to high frequency sea level changes in parts of the region (Childress and Grammer, 2018; Price and Grammer, 2017; Childress and Grammer, 2015; LeBlanc, 2014). Expanding upon these studies with subsurface data from Okfuskee County, Oklahoma, and applying a detailed stratigraphic framework will allow for better prediction of regional subsurface variations in this area and allow for a correlation to facies and sequence stratigraphic architecture in other parts of the basin.

The “Mississippian Lime” is an aerially extensive, mixed carbonate and siliciclastic system containing a variety of carbonate environments and sub-environments (Mazzullo et al., 2011). Each of these environments have a variety of characteristics associated with them including rock texture, allochems, sedimentary structures, fossils, ichnofacies, pore types, and overall geometries (Wilhite et al., 2011).

Significant lateral and vertical heterogeneity at multiple scales, from kilometer to millimeter or smaller, commonly occurs in carbonates and has been documented in the Mississippian system of the Mid-Continent (Childress and Grammer, 2018; Shelley et al., 2018; Price and Grammer, 2017; Childress and Grammer, 2015; LeBlanc, 2014). Integrating multiple data sets (core, wireline logs, and thin sections) and using modern and ancient analogs of depositional environments is required to better predict regional facies assemblages in the subsurface.

The “Mississippian Lime” is characterized by low porosity and low permeability. As a result, various stimulation techniques (hydraulic fracture treatment, well acidizing) are oftentimes needed to enhance recoveries (Roundtree et al., 2010). In addition, “Mississippian Lime” wells are often plagued by high water/oil ratios, with water cuts exceeding 70% (Watney, 2014; Watney et al., 2001). Consequently, understanding the role of how depositional facies and the sequence stratigraphic framework control porosity and permeability is vital to accurate characterization of the “Mississippian Lime.”

Fundamental questions and project hypothesis: The following are fundamental questions that are addressed in this study:

1. Can a sequence stratigraphic framework be constructed which accounts for high frequency eustatic sea level changes (probable 4th and 5th order, 100,000 – 20,000 years) using core in Okfuskee County?

2. Can incorporating multiple data sets (core, petrographic analysis, and wireline logs) produce sufficient controls to predict and map facies assemblages in the subsurface?
3. How do primary depositional facies and the sequence stratigraphic hierarchy control development and preservation of porosity and permeability?

The main hypotheses of this work is that a hierarchical sequence stratigraphic framework correlated with high frequency eustatic sea level changes will help to explain the development and distribution of porosity and permeability, and that the utilization of multiple data sets will yield sufficient controls to accurately map subsurface Mississippian strata in east-central Oklahoma.

Objectives: The objective of this study is to describe facies utilizing core and thin sections to 1) characterize variations in depositional facies in order to discern trends and expand predictability, 2) construct a sequence stratigraphic framework by examining the vertical stacking patterns of facies, 3) determine how porosity and permeability correlates to the depositional facies and the sequence stratigraphic framework, and 4) utilize wireline logs to establish key stratigraphic surfaces to aid in subsurface mapping around Okfuskee County and construct regional cross sections to describe platform/basin geometry.

CHAPTER II

GEOLOGIC BACKGROUND

Tectonics: The study area is located in Okfuskee County in east central Oklahoma near the boundary between the Cherokee Platform and the Arkoma Basin (Northcutt and Campbell, 1996). The area is bounded by several prominent structural features. Figure 1 shows the locations, estimated size, and alignment of these features.

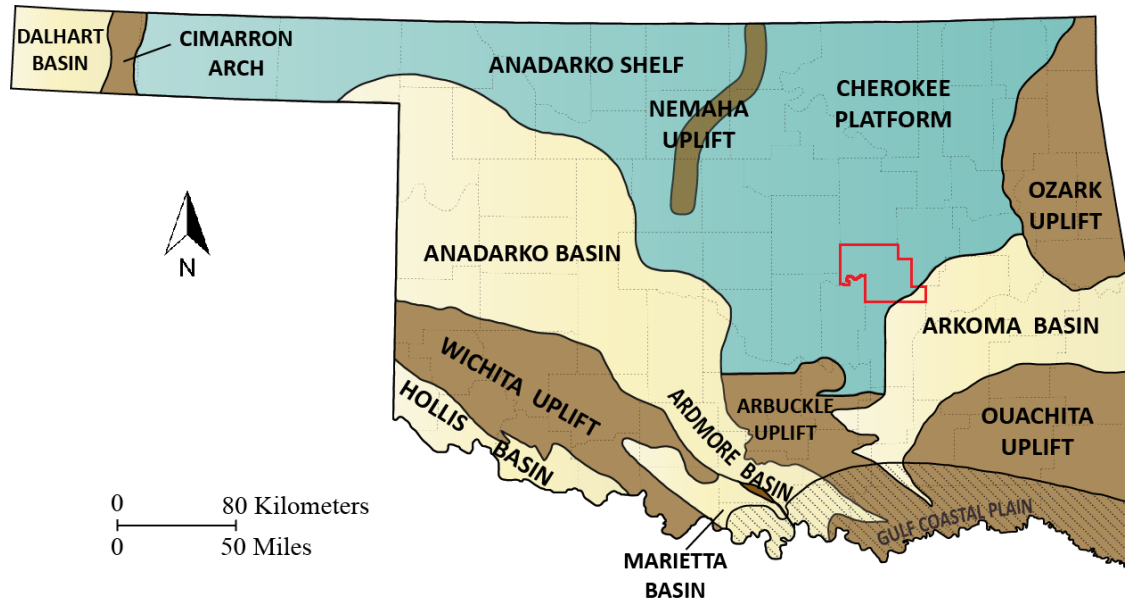


Figure 1: Map of Oklahoma showing prominent structural components throughout the state. Uplifted regions are in brown, structural lows are in tan, and shelf/platform areas are shown as green. The cores used in this study come from Okfuskee County (outlined in red). Adapted from Northcutt and Campbell, 1996.

Mississippian carbonates in northern Oklahoma were deposited in a shallow tropical sea across a broad ramp (Gutschick and Sandberg, 1983). Therefore in general, relatively shallower water, higher energy proximal facies can be found to the north, and relatively deeper water, lower energy facies are located toward the south.

The study area is situated on the edge of the Arkoma Basin. This basin is the product of the collision of the North American and Gondwanan Plates from the Early Mississippian through the Middle Pennsylvanian (Suneson, 2012). It is characterized as a foreland basin because it formed adjacent and parallel to a compressional orogenic belt, the Ouachita fold-and-thrust belt (Suneson, 2012).

Numerous faults are known throughout the study area (Figure 2, blue on map) and are generally oriented from SSW to NNE. These data were collected from published literature and from energy industry submissions to the Oklahoma Geological Survey (OGS). It is important to note that this is not a comprehensive collection of faults. The OGS database is being continually updated through the cooperation of academia and industry (Oklahoma Fault Database, 2017).

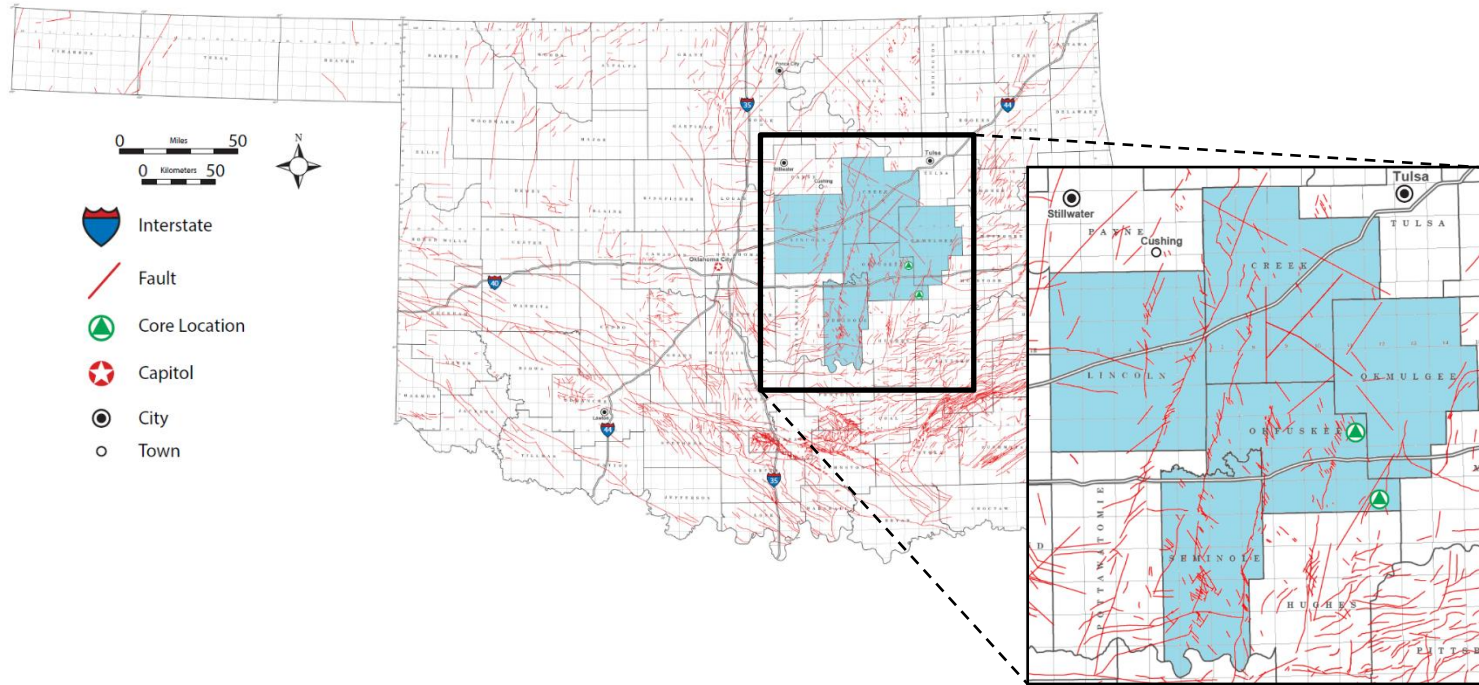


Figure 2: Fault Database and Interpretive Fault Map of Oklahoma: From the Oklahoma Geological Survey with information collected from published literature and energy industry data. Study area indicated by blue fill. Fault orientations primarily occur in a SSW to NNE trend across the study area. Adapted from Marsh and Holland (2016).

Paleogeography and climate: During the Mississippian the southern mid-continent was dominated by a shallow, subtropical sea (Gutschick and Sandberg, 1983). The study area was located approximately 30° south of the equator at this time. Work from Mazzullo and others (2009) suggests paleo-winds were from the (present day) east-northeast.

The “Mississippian Lime” of Oklahoma is interpreted to have been deposited on part of a distally steepened ramp (Childress and Grammer, 2018; Mazzullo et al. 2011; Wilhite et al., 2011). Ramps are divided into two broad categories; homoclinal and distally steepened. Homoclinal ramps are characterized by a gentle (less than 1°) constant slope from shoreline to basin. They can be 10’s to > 100 km wide (Read, 1982). Distally steepened ramps are similar, but with a distinct increase in dip (up to several degrees) located 10’s to over 100 kilometers from shore (Read, 1985).

Platform geometries control energy regimes and therefore what facies types are formed. Proximal locations on distally steepened ramps experience the highest energy regimes, and relative energy decreases moving down dip (offshore). Muddier facies and mass transport deposits (MTDs), such as slumps, breccias, and turbidites may be found in downdip/distal locations (Read, 1982). These geometries give insight as to how facies belts shift in response to sea level changes.

The low declivity of ramps allows for broad migrations of facies belts (from 10’s up to 100’s of kilometers) as global sea level fluctuates. Figure 3 displays lateral

migration of shoreline that is possible with a 100 meter (328.1 feet) sea level change across platforms with varying dip angles. Variations in the dip across the platform, as well as antecedent topography, could greatly influence actual migration distance. The purpose of this figure is to simply illustrate how sensitive low declivity slopes are to sea level rise and fall.

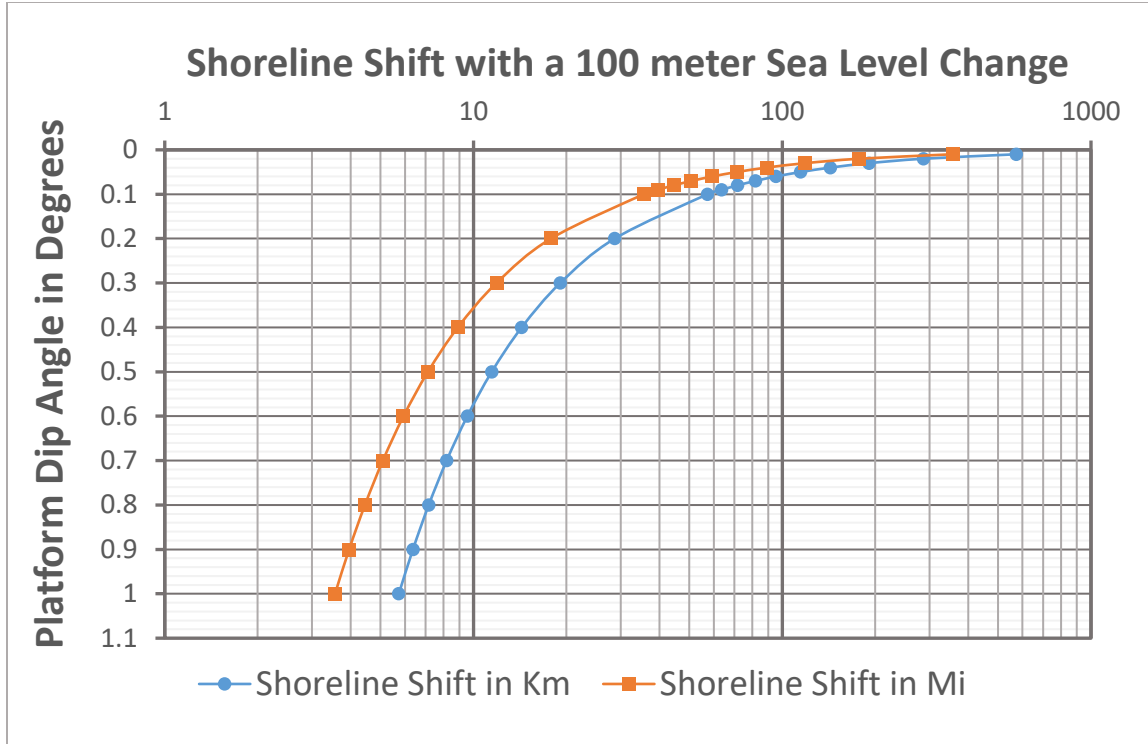
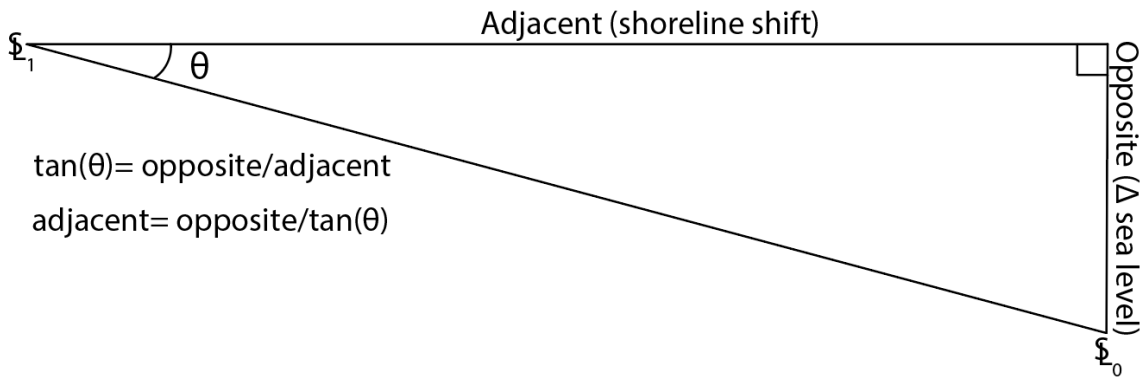


Figure 3: Theoretical shoreline shift in response to a 100 meter sea level change. Calculated by the following equation: $\tan \theta = \frac{\text{Opposite}}{\text{Adjacent}}$

Where θ represents platform dip, opposite refers to sea level change, and adjacent (the variable to be solved) is the shoreline shift. See below. Ramp gradients were observed in this study to be $\approx 0.03^\circ$.



Climate during the Mississippian was transitioning from the greenhouse conditions of the Devonian to icehouse conditions of the Pennsylvanian (Haq and Schutter, 2008; Read, 1995). Greenhouse conditions are marked by little or no continental ice sheets. In response, sea level changes are small, on the order of 10 meters or less (Read, 1995, & Goldhammer et al., 1990). Conversely, amplitudes of sea level change during icehouse conditions, when there is extensive continental glaciation, may approach 100 meters (Read, 1995).

Sea Level: Sea level and deposition of carbonates are inextricably linked (Goldhammer et al., 1990). Most carbonate depositional systems occur in relatively shallow water, so even small changes can have broad impacts on facies expression and overall carbonate deposition. There are several mechanisms that control changes in sea level. Tectonics and sedimentation rates can influence local changes in sea level. The global, or eustatic sea level is partly controlled by orbital variability (Kerans and Tinker, 1997).

Orbital variability directly controls some of the lower orders of eustatic sea level cyclicity. These lower orders of cyclicity are referred to as Milankovitch Cyclicity (Read, 1995). The mechanism controlling eustatic sea level can be observed in the higher latitudes as solar radiation intensity and distribution is controlled by variations in the Earth's orbit (Read, 1995). Continental glaciation increases during periods when solar radiation intensity and distribution are weaker, thus lowering sea level. Three variations have been observed, and each has a different temporal signal. Sometimes these

variations work in-phase with one another, compounding the effect (increased glaciation), and other times, they are out-of-phase and lessen the impact (Read, 1995).

The three Milankovitch signals are:

1. Eccentricity (100-400 ky cycle): a function of the elliptical shape of Earth's orbit as it revolves around the Sun
2. Obliquity (~40 ky cycle): is a function of the variation in Earth's tilt of its axis
3. Precession (~21 ky cycle): is a function of the "wobble" of Earth's rotation

Eccentricity is likely the main driver of 4th order high-frequency sequences (Read, 1995). The 400 ky cycle is the longest and most stable periodic signal attributed to Earth's elliptical orbit (Kent et al., 2018). Recent work shows, "the 400 ky eccentricity cycle can reliably pace Earth's climate back to at least 215 Ma, well back in the Late Triassic Period" (Kent et al., 2018, p. 1). The 5th order high frequency cycles correspond to changes in relative amounts of ice due to climate variability tied to obliquity and precession (Read, 1995). Read (1995) points out that obliquity cycles appear to have more influence during icehouse and transitional times. Refer to Figure 4 for a simplified depiction of these orbital fluctuations, and Table 1 for an overview of frequencies and amplitudes seen in eustatic sea level changes.

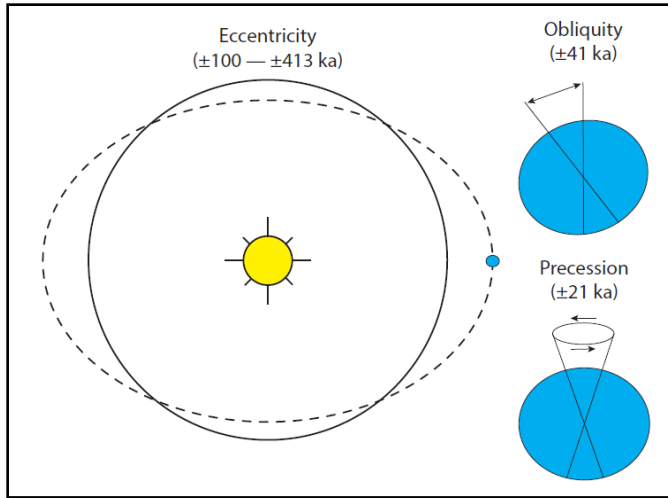


Figure 4: Diagram showing the nature and temporal duration of the different elements of Milankovitch orbital variations. From Read (1995).

Cycle Hierarchy				
Tectono-Eustatic Cycle Order	Sequence Stratigraphic Unit	Duration (n = Ma)	Relative Sea Level Amplitude (m)	Relative Sea Level Rise/Fall Rate (cm/ka)
First	Supersequence	> 100		< 1
Second	Supersequence	10 - 100	50 - 100	1 - 3
Third	Depositional Sequence or Composite Sequence	1 - 10	50 - 100	1 - 10
Fourth	High-Frequency Sequence	0.1 - 0.4	1 - 150	40 - 500
Fifth	High-Frequency Cycle	0.02 - 0.04	1 - 150	60 - 700

Table 1: Cycle hierarchy: Table defining the difference between the multiple orders of eustatic sea level changes. This study utilizes high-resolution sequence stratigraphy which concentrates on the 3rd, 4th, and 5th orders of cyclicity. Modified from Goldammer et al., (1991).

CHAPTER III

DATA & METHODS

The two cores (725.1 total linear feet, 221.0 meters) described in this study are located in eastern Okfuskee County and separated by 13 miles (20.9 kilometers). Refer to Table 2 for general data attributes for the cores in this study. The locations of these cores are significant in that they provide insight into more distal localities of the “Mississippian” system than many previous studies which were focused on more proximal locations (Leblanc, 2014; Flinton, 2016; Jaeckel, 2016; & Shelley et al., 2017). 37 thin sections were cut throughout the “Mississippian” interval of the Angell 1-23. Analysis of bulk mineralogy of 43 samples from the two cores was done through x-ray diffraction (XRD).

Lease Name	Well Number	Location	County	“Mississippian” Interval (SSTVD)	“Mississippian” Thickness
Angell	1-23	Sec. 23-12N-11E	Okfuskee	3010.0 - 3390.9 feet	380.9 feet
Wise	1-20	Sec. 20-10N-12E	Okfuskee	3737.0 - 4081.2 feet	344.2 feet

Table 2: General information on cored wells utilized in this study.

Core Descriptions: Core work is the first step in examining and classifying rock properties. Both cores were analyzed and a lithologic column was constructed for each (Figure 14). First, a detailed facies analysis was conducted. It consisted of observations

of lithology, color, skeletal allochems, sedimentary structures, burrowing, bedding, cross-stratification, and porosity type.

Siliciclastic-rich facies were described based upon dominant grain type, secondary minerals observed, sedimentary structures, and the degree of bioturbation. The degree of bioturbation was determined using a bioturbation index chart from Bann and others (2008). Color was classified according to the Geological Rock-Color Chart (Goddard et al., 1951). Carbonate dominant facies were described using the classification system developed by Dunham (1962). The pore type descriptors are outlined by Choquette and Pray (1970). Refer to Figures 5 and 6 for a description of the Dunham and Choquette & Pray classification methods, respectively. This analysis allowed for the identification of primary depositional facies types. These facies were placed in a depositional environment consistent with the rock properties observed, and then the environments were used to construct an ideal stacking pattern consistent with responses to sea level changes.

DEPOSITIONAL TEXTURE RECOGNIZABLE					DEPOSITIONAL TEXTURE NOT RECOGNIZABLE
Components not bound together during deposition				Components bound together during deposition	CRYSTALLINE CARBONATE
Contains carbonate mud (clay/fine silt) (< 30 μm)		Grain-supported	Lacks mud and is grain-supported		
Mud-supported					
Less than 10% grains	More than 10% grains				
MUDSTONE	WACKESTONE	PACKSTONE	GRAINSTONE	BOUNDSTONE	

Figure 5: The Dunham (1962) carbonate classification scheme based on depositional texture observed. From Scholle and Ulmer-Scholle (2003).

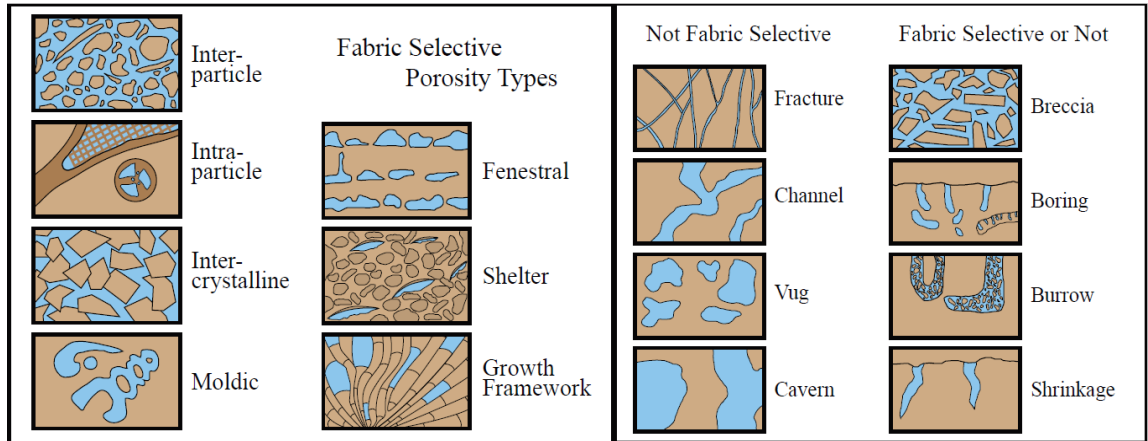


Figure 6: Pore systems observed in carbonates. Developed by Choquette and Pray (1970). From Scholle and Ulmer-Scholle (2003).

Thin Section Analysis: Thin sections facilitated the identification and quantification of rock attributes that are unable to be observed in core hand sample alone due to the fine-grained nature of these deposits. These attributes include grain size, pore types, allochems, and textural classification. The thin sections were all blue epoxy impregnated to visualize open pore space, and stained with alizarin red to distinguish calcite from dolomite. Potassium ferricyanide stain was also used to indicate iron content. The same classification scheme used for core work was also utilized in petrographic analysis (Dunham, 1962; Choquette and Pray, 1970). Relative abundance of allochems was estimated using standard visual estimation charts (Baccelle & Bosellini, 1965, from Flügel, 2010). Integrating thin sections with the overall core analysis improves interpretations and is fundamental to identifying facies, depositional

environments, facies stacking patterns, and constructing a sequence stratigraphic framework.

X-Ray Diffraction (XRD): X-ray diffraction is used to identify crystalline minerals in rocks and can give quantitative estimates of bulk and clay mineralogy (Poppe et al, 2001; USGS XRD, 2000). Devon collected 43 samples total, 37 from the Angell 1-23 and 6 from the Wise 1-20. The samples were evaluated using whole rock bulk mineralogy to identify mineral assemblages and quantify their relative abundance. These assemblages include clay types: illite/smectite, illite/mica, kaolinite, and chlorite; cements: quartz, feldspar, calcite, and dolomite; and other mineral assemblages: pyrite and apatite. The XRD data in this study was used to supplement thin section analysis.

Sequence Stratigraphy and Framework: One of the main goals of this project is to construct a sequence stratigraphic framework based on primary depositional facies and stratal patterns that allow for enhanced prediction of facies mosaics in the subsurface throughout the region. This framework uses a chronostratigraphic approach instead of a lithostratigraphic approach. Lithostratigraphy is a branch of stratigraphy that correlates rock units based on similar lithologic traits. This can lead to interpretations that show greater continuity of facies than what truly exists. When applied to reservoir characterization, it can overestimate communication between two reservoirs that might share similar characteristics, but are not genetically related (Bashore et al., 1994). To avoid these pitfalls, this study uses sequence stratigraphy to correlate packages of rocks

using unconformities and their correlative conformities to group sedimentary successions into spatially and temporally constrained sequences. Sequence stratigraphy surpasses lithostratigraphy in its potential to predict both lateral and vertical distribution of facies within a chronostratigraphically constrained framework of unconformity-bound depositional sequences (Handford and Loucks, 1993). High-resolution sequence stratigraphy is therefore the preferred approach to analyzing depositional and stratal patterns at or below reservoir scale (Kerans and Tinker, 1997).

Wireline Logs: The cored wells for this study have an accompanying suite of wireline logs -- gamma ray, caliper, resistivity with various depths-of-investigation, and density-neutron. Gamma ray logs measure radioactivity in the formation and are used as lithology indicators (Asquith and Krygowski, 2004). The caliper log measures borehole diameter. It is used to identify washout zones (areas of borehole collapse often due to poorly indurated lithologies), indicated by an increase in borehole diameter. The caliper log can also be used to identify permeable zones where drilling fluid enters a porous and permeable formation and particulates in the drilling fluid accumulate on the sidewalls of the borehole causing a decrease in borehole diameter. The caliper log was valuable for identifying the Mississippian-Pennsylvanian contact in these wells. The base of the Pennsylvanian is poorly indurated and prone to washout, and the Mississippian section is better cemented and more competent. Resistivity logs measure the response of a formation as an electric current is passed through it. Resistivity logs are used to identify

hydrocarbon-bearing zones versus water-bearing zones, indicate permeable zones, and can be used to determine porosity (Asquith and Krygowski, 2004). Density and neutron logs indicate porosity, lithology, and the presence of natural gas. The density log measures electron density within the formation, and neutron logs measure hydrogen ion concentration (Asquith and Krygowski, 2004). Refer to Table 3 for a general overview of the logs and how they were used in this study.

Wireline Logs			
Log	Property Measured	Units	Use
Gamma Ray	Natural radioactivity (e.g. K, Th, U)	API units	Correlation, lithology
Resistivity	Resistance to electric current flow	Ohm-meters	Correlation, fluid types
Caliper	Borehole diameter	Inches	Borehole integrity, tool/pad contact
Neutron	Hydrogen concentration in pores (water & hydrocarbons)	Percent porosity	Porous zone identification, gas-bearing zone detection (when used in conjunction with density)
Density	Bulk density (specifically electron density, also includes pore fluids in the output)	grams/cubic centimeter	Formation density, gas-bearing zone detection (when used in conjunction with neutron)

Table 3: Wireline logs used in this study. The properties measured, and how they were used in making geologic interpretations (modified from Cant, 1992).

The wireline logs were analyzed using Petra, a geologic software package developed by IHS Markit that allows for the manipulation of a large database of wells.

Petra has multiple geologic functions including well log analysis, subsurface mapping, and construction of geologic cross sections.

Subsurface Mapping: Once the key stratigraphic surfaces were identified and tied to their respective wireline log signature, it was possible to extrapolate to the non-cored wells in the region. Subsurface mapping displays the lateral continuity of sequences and overall geometry of the depositional system. Both structure maps and thickness maps were constructed in Petra. Structure maps show present day depth to the stratigraphic surface being measured, and are important in identifying faults which can affect the thickness of nearby strata.

Limitations: The data utilized in this study was intentionally restricted to data provided by Devon Energy to test the correlation potential of such a data set (i.e. characterized by limited core data). Both cores analyzed in this study contained the basal Woodford-Mississippian contact and the top Mississippian-Pennsylvanian contact, but the distance between the two cores is 13 miles (20.9 km). Therefore, lateral and vertical heterogeneities likely exist that are not accounted for due to the complex nature of carbonates in general (Harris, 2009; Grammer et al., 2001; Major et al., 1996).

Another limitation is that there are no temporal constraints (e.g. biostratigraphy) associated with these cores (i.e. the exact age of this “Mississippian” core is unknown). When core data is temporally unconstrained, it is not possible to say unequivocally that any unit of rock represents a 4th order high frequency sequence or 5th order high

frequency cycle as defined by Milankovitch cyclicity. Some work has been done in other areas of the “Mississippian Lime” in both outcrop and the subsurface utilizing conodonts to help identify 3rd order sequences, but even the highest resolution conodont biostratigraphy (1 Ma) does not approach the resolution necessary for constraining 4th and 5th order cyclicity (40-20 ky) (Boardman et al., 2013; Hunt, 2017; Miller et al., 2017).

Another limitation of the data set is that the available thin sections came from just one of the cores, the Angell 1-23. No thin sections were made available for the Wise 1-20. Consequently, while both cores appear to be relatively similar from a facies standpoint, subtle changes in the Wise 1-20 may be unaccounted for in the data set. The main distinction is that the Wise 1-20 displayed a higher distribution of clay-rich siltstone facies. The average distance between samples for the Angell 1-23 is 9.55' (2.91 m) (see Appendix A-II for thin section core locations), a relatively large spacing to capture the detailed variability observed in the cores. Therefore, a higher sampling density would allow for stronger insights into rapid facies changes. As such, the thin sections used in this study were best suited for refining facies classifications as a whole instead of making broad interpretations into high-frequency changes to the depositional environment. It is noteworthy that the sampling regimen or criteria utilized for thin sections is unknown. Some key stratigraphic surfaces identified in this study have no accompanying thin section for reference.

Limitations for the XRD data used in this study are similar to that of the thin section data. Low sampling density and sampling regimen/criteria are unknown. The density of samples is too low to make any interpretations regarding high-frequency sea level change or subtle variations in the depositional environment. Also, the samples were evaluated using whole rock bulk mineralogy. To identify specific clay types, randomly oriented mounts for x-ray powder diffraction are required (Poppe et al., 2001).

Wireline logs are limited in that the tool sampling frequency is too low to resolve rapid changes in rock characteristics. Vertical resolution of open-hole wireline tools can vary greatly depending on different vintages of logs, vendor tool, and inherent properties of the attribute being measured (e.g. radioactivity, resistivity, potential, or density). Vertical resolution can range from as high as 6 inches (15.2 cm) to exceeding 6 feet (1.8 m) (Everett et al., 1988). Not all wells had the same suites of tools, with gamma ray and resistivity the minimum wireline logs necessary for inclusion in this study.

CHAPTER IV

RESULTS

Core Facies Types

Fissile clay-rich siltstone

The fissile clay-rich siltstone (Facies 1) is dark grey to black, poorly indurated, and fissile along mm-scale laminations. This facies is composed of clay minerals – illite and mixed layer illite/smectite, very fine sand to silt sized quartz grains, and other minor mineral assemblages. It contains isolated bioclastic debris (<10%) composed of thin-shelled brachiopods and crinoid stem fragments. Some fractures observed had been partially healed by carbonate cement. Pyrite is present, often in the form of mm-scale pyritized burrows and rare (<5%) cm-scale horizontal beds. The Wise 1-20 contained thicker intervals of this facies ranging from very thin beds (1-3 cm.) to very thick beds (100+ cm) (Boggs, 2001). The Angell 1-23 contained only very thin beds of this facies. In both cores, this facies is concentrated towards the middle of the section, and most often grades into the other siltstone facies.

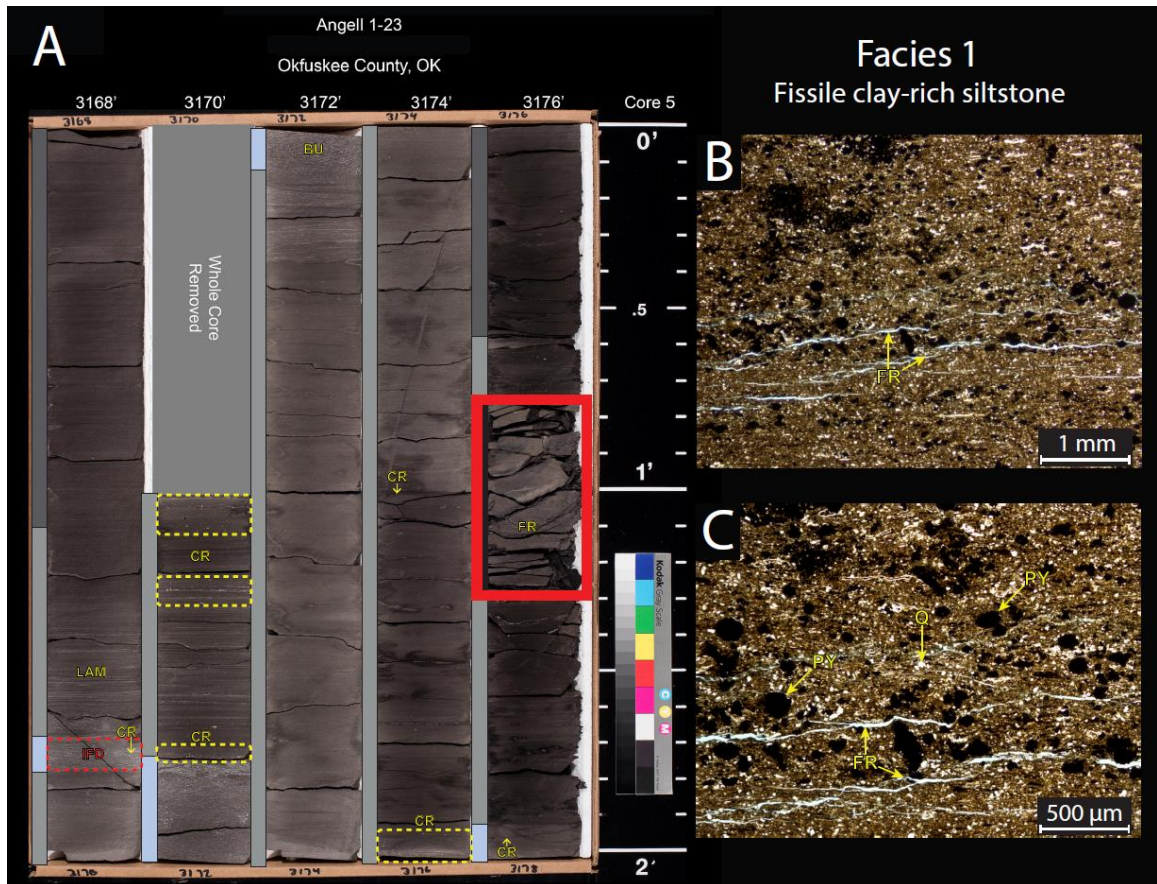


Figure 7: Facies 1 Fissile clay-rich siltstone: **(A)** Core photograph in white light. The scale to the right is in tenths of feet. Core analysis shows that Facies 1 is dark grey to black composed of clay minerals and very fine sand to silt-sized quartz grains. Isolated bioclastic debris composed of thin-shelled brachiopod and crinoid stem fragments. Pyrite is also found in mm-scale pyritized burrows and cm-scale horizontal beds. **(B/C)** Thin section photomicrograph of 3177.20'. Images are in PPL. The sample is blue epoxy impregnated and stained with alizarin red to identify calcite. Clay minerals, quartz silt, and pyrite grains are the main constituents. Clay mineral assemblages appear to be organized horizontally (parallel to bedding planes). Fractures observed are likely induced. All mineral assemblages appear to be fully homogenized.

Glaucconitic Sandstone

The glauconitic sandstone facies (Facies 2) is a dark grey to greenish black, burrowed sandstone. It is composed of primarily (>80%) very fine to medium sand sized grains of glauconite that are sub- to well-rounded, well sorted. This facies also contains isolated (<10%) pyrite and phosphate grains. Centimeter-scale horizontal and vertical burrows are common. This facies is located in the lower portion of the Mississippian section of the core, about 4-5 feet (1.2 – 1.5 meters) above the top of the Woodford Shale. This facies is the least volumetrically significant (<0.2%) facies found in this study. The Angell 1-23 contains 2.4 inches (6.1 centimeters) of glauconitic sandstone and the Wise 1-20 contains 9.6 inches (24.4 centimeters) total, however, this facies is pervasive throughout the region. Previous workers have observed glauconitic sandstone, but only present immediately above the Woodford Shale (LeBlanc, 2014; Flinton, 2016). These studies utilized core data from wells located multiple counties away from the wells used in this study.

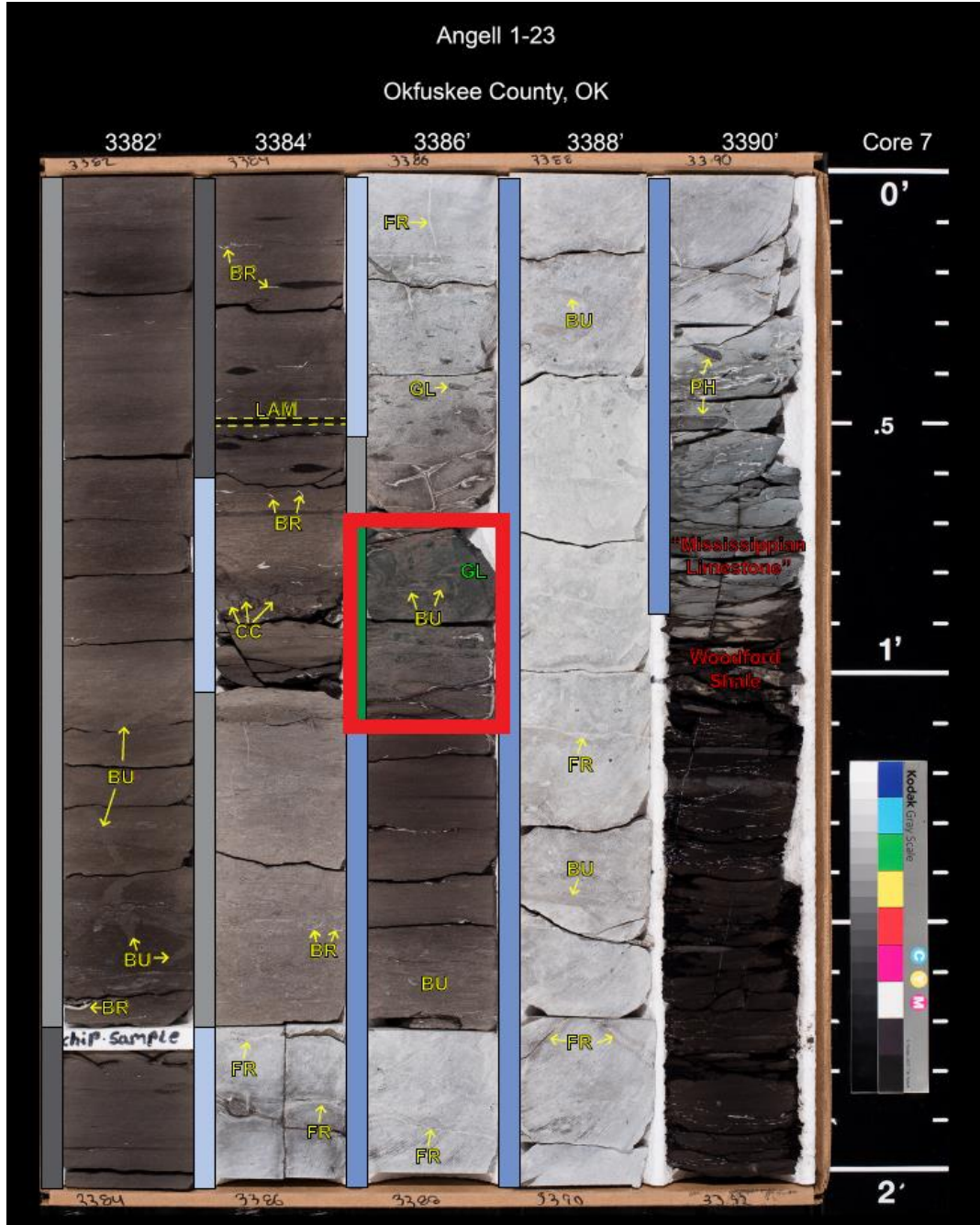


Figure 8: Facies 2 Glauconitic Sandstone: is dark grey to greenish black in color and is commonly burrowed. This facies is composed of very fine to medium sand sized grains of glauconite that are sub- to well-rounded and well-sorted. Core photograph under white light. Scale to the right of the core is in tenths of feet. No thin sections were available in this facies.

Massive bedded peloidal siltstone

The massive bedded peloidal siltstone (Facies 3) is a medium dark grey to black, homogeneous siltstone. It is composed of on average 32% subangular to subrounded quartz silt to very fine sand that is well sorted. There is significant clay and carbonate content associated with this facies, averaging 34% and 22% respectively. The dominant clay types are illite and mixed-layered illite/smectite. The carbonate content is due to the extensive (up to 20%) presence of peloids and rare (<5%) bioclasts (thin shelled brachiopods). In both wells, this facies tends to be interbedded with Facies 4 and 5, the laminated and mottled peloidal siltstone facies. Bed thickness can range from a 2 inches (5.1 centimeters) to over 10 feet (3.04 meters).

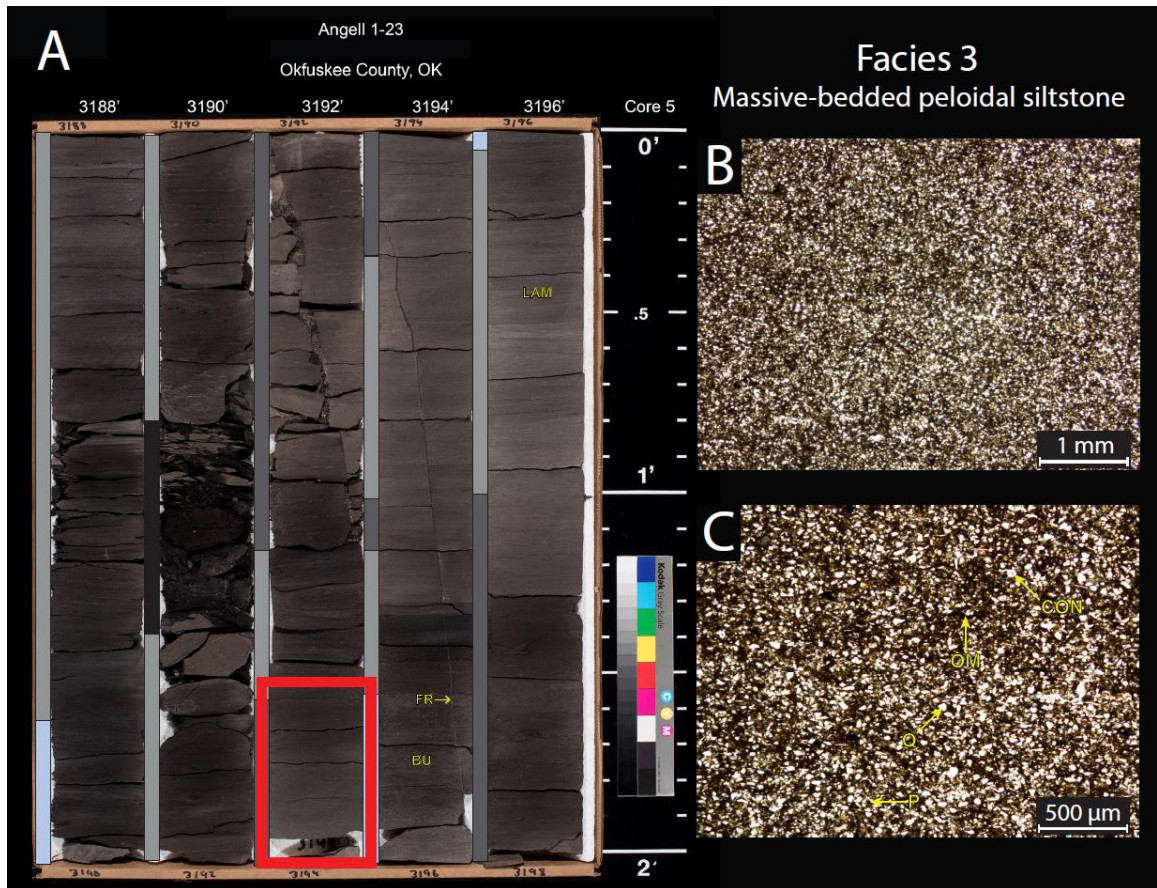


Figure 9: Facies 3 Massive bedded peloidal siltstone: **(A)** Core photograph in white light. The scale to the right is in tenths of feet. Core analysis shows that Facies 3 is medium dark grey to black composed of silt to very fine sand quartz grains that range from subangular to subrounded. Sedimentary structures are limited to absent. **(B/C)** Thin section photomicrograph of 3193.50'. Images are in PPL. The sample is blue epoxy impregnated and stained with alizarin red to identify calcite. Very fine sand to silt quartz grains, carbonate peloids, and clay minerals (illite and mixed-layered illite/smectite) are the main constituents. No apparent bedding or sedimentary structures are observed in this facies. All mineral assemblages appear to be fully homogenized.

Laminated peloidal siltstone

The laminated peloidal siltstone (Facies 4) is medium dark grey to black in color. The primary distinguishing feature of this facies is the presence of visible, intact mm-scale laminae. Compositionally, it is similar to Facies 3 and 5. It averages 29% quartz silt to very fine sand that is subangular to subrounded and moderately sorted. The dominant clay types are illite and mixed-layered illite/smectite. The carbonate content is due to the extensive (up to 20%) presence of peloids and rare (<5%) bioclasts (thin shelled brachiopods and crinoid debris). This facies is commonly interbedded with Facies 3 and 5, the massive bedded and mottled peloidal siltstone facies, respectively. Bed thickness can vary greatly, from 2 inches (5.1 centimeters) to over 20 feet (6.08 meters). Millimeter-scale cross-bedding may also be observed in this facies.

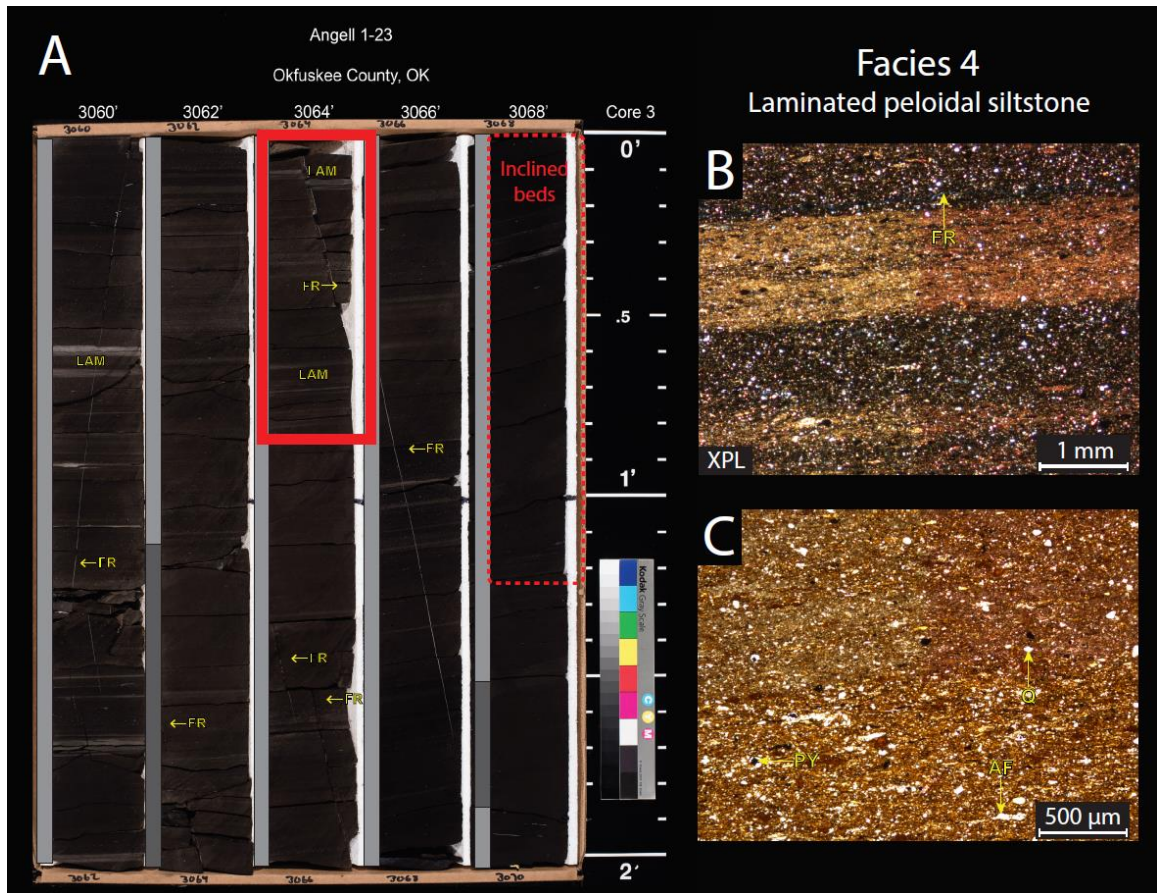


Figure 10: Facies 4 Laminated peloidal siltstone: **(A)** Core photograph in white light. The scale to the right is in tenths of feet. Core analysis shows that Facies 4 is dark grey to black composed of silt to very fine sand quartz grains that range from subangular to subrounded. The composition is similar to the other siltstone facies. Thin (mm to cm-scale) laminations distinguish this facies. Isolated bioclastic debris (thin shelled brachiopod and crinoid fragments) are observed in some footages. **(B/C)** Thin section photomicrograph of 3064.50'. **B** is in XPL and **C** is in PPL. The sample is blue epoxy impregnated and stained with alizarin red to identify calcite. Very fine sand to silt-size quartz grains, carbonate peloids, and clay minerals (illite and mixed-layered illite/smectite) are the main constituents. When viewed through XPL strong preferential deposition of grains is observed with the clay minerals. Some laminations contain abundant clay minerals and other laminations the clays have been winnowed out of the sediment.

Mottled peloidal siltstone

The mottled peloidal siltstone facies (Facies 5) is medium dark grey to black in color. This facies is characterized by increased bioturbation that can vary from moderate to complete homogenization of the sediment as described by Bann and others (2008). The burrowing appears similar to the morphology of the ichnofossil *Phycosiphon incertum*. The burrows are commonly small (from 1 mm to 1 cm), can be near parallel to oblique to observed bedding planes, and filled with clay minerals.

The mineralogical composition is similar to that of Facies 3 and 4 averaging 30% silt to very fine sand sized quartz that is subangular to subrounded and moderately sorted. The dominant clay types are illite and mixed-layered illite/smectite. The carbonate content is due to the extensive (up to 20%) presence of peloids and scattered (<10%) bioclasts (thin shelled brachiopods and crinoid debris). This facies is commonly interbedded with Facies 3 and 4. Bed thickness is often thin, less than 1 foot (0.3 meters). Thicker beds are present towards the base of the Mississippian interval, these beds are over 10 feet (3.0 meters) thick.

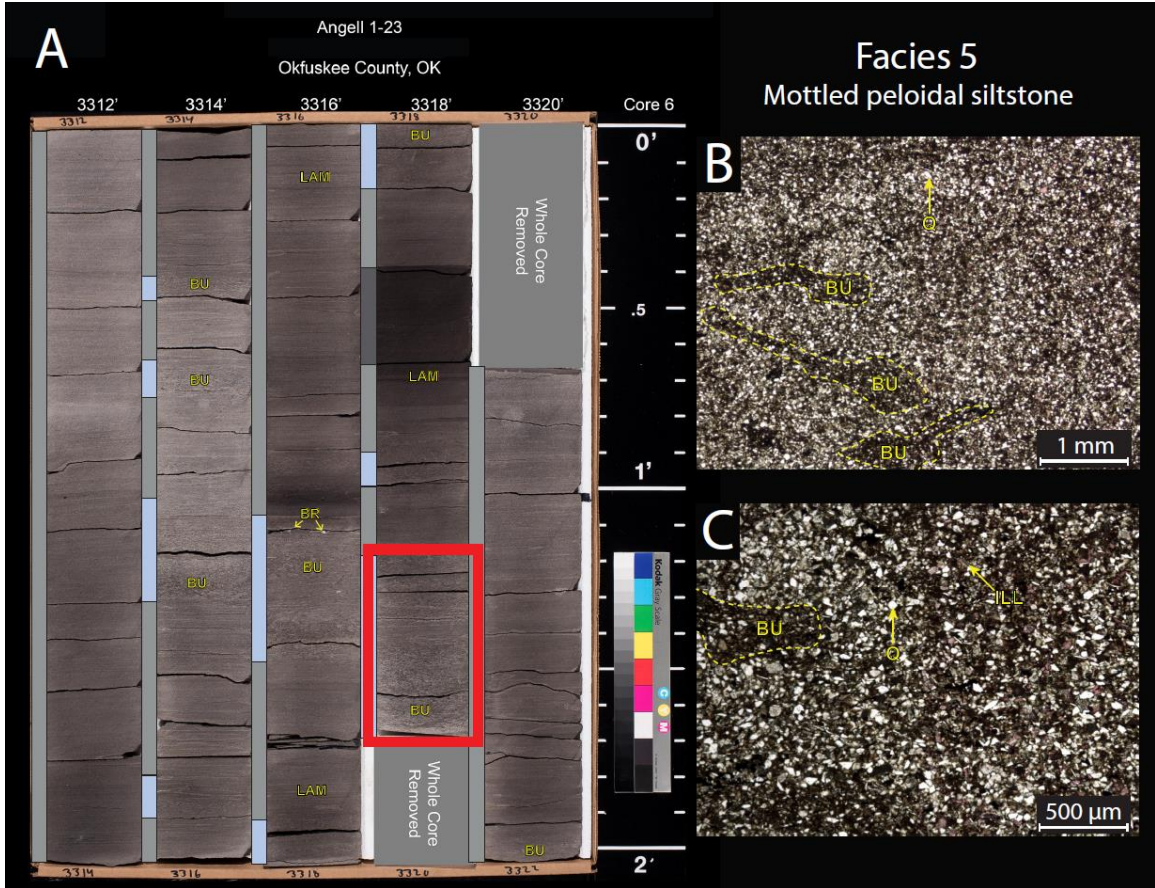


Figure 11: Facies 5 Mottled peloidal siltstone: **(A)** Core photograph in white light. The scale to the right is in tenths of feet. Core analysis shows that Facies 5 is medium dark grey to black composed of silt to very fine sand quartz grains that range from subangular to subrounded. Small (cm to mm-scale) horizontal burrows are abundant throughout. Bioclastic debris (thin shelled brachiopod and crinoid fragments) are common. **(B/C)** Thin section photomicrograph of 3319.00'. Images are in PPL. The sample is blue epoxy impregnated and stained with alizarin red to identify calcite. Very fine sand to silt-size quartz grains, carbonate peloids, and clay minerals (illite and mixed-layered illite/smectite) are the main constituents. Sediment appears to be completely homogenized by biotic activity (burrowing) as no bedding planes are observed via thin section.

Skeletal mudstone-wackestone

The skeletal mudstone-wackestone facies (Facies 6) is medium grey to greyish black in color. This facies has scattered (up to 10%) bioclastic debris (thin shelled brachiopods and crinoid fragments) and cm-scale vertical and horizontal burrows. In contrast to the earlier described facies, calcite is the dominant mineral assemblage. Average calcite content is 86%, clays and quartz average 8% and 5%, respectively. The two main occurrences of this facies are a 4 foot (1.2 meter) interval immediately above the top of the Woodford Shale at the base of the Mississippian section, and an interval near the top of the Mississippian section that is thin bedded and interbedded with facies 3. In this section, this facies shows extensive recrystallization. This made identification of some grains problematic.

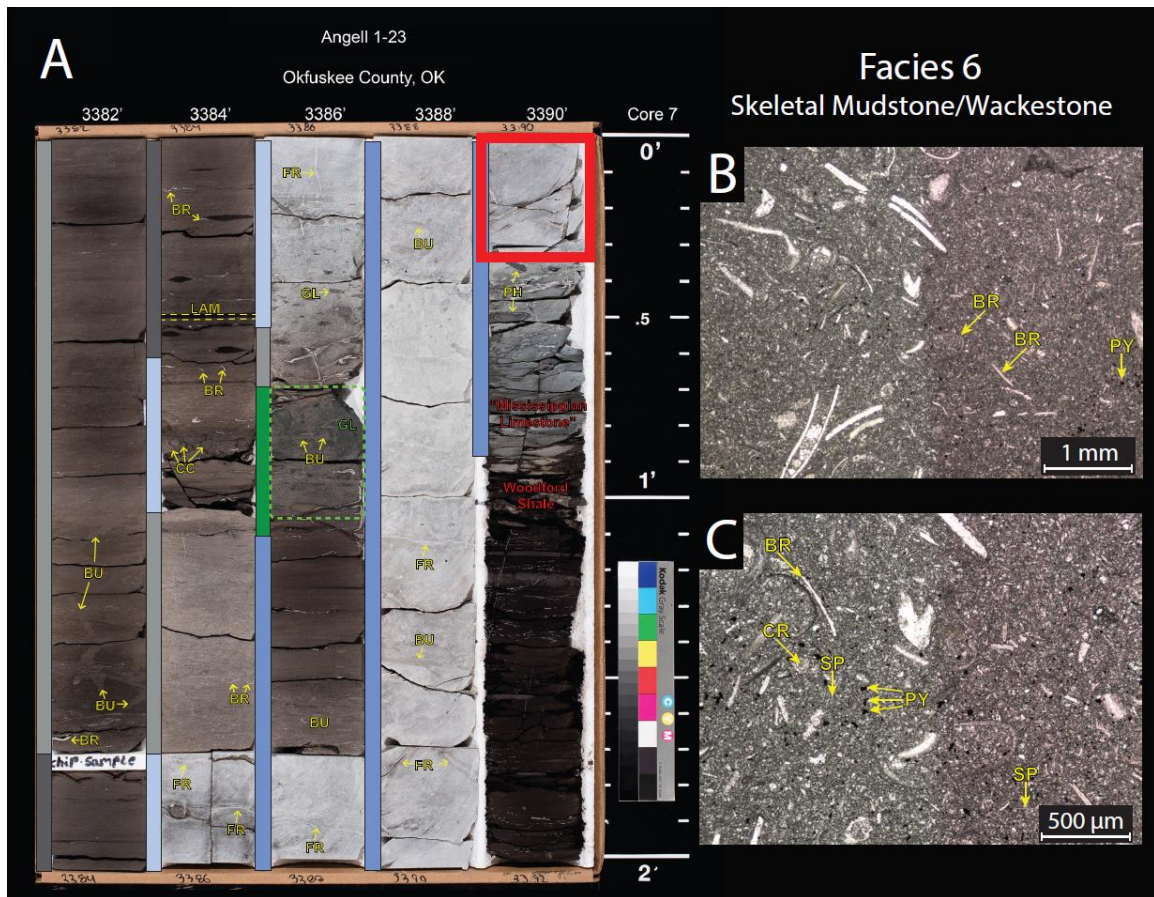


Figure 12: Facies 6 Skeletal mudstone-wackestone: **(A)** Core photograph in white light. The scale to the right is in tenths of feet. Core analysis shows that Facies 6 is medium grey to greyish black composed of primarily calcite from abundant bioclasts (thin shelled brachiopod fragments and crinoids). Burrows are common throughout this facies. **(B/C)** Thin section photomicrograph of 3390.00'. Images are in PPL. The sample is blue epoxy impregnated and stained with alizarin red to identify calcite. Calcite dominates this facies. Fine siliciclastic sediment as well as limited (trace to 2%) pyrite are observed.

Skeletal packstone-grainstone

The skeletal packstone-grainstone facies (Facies 7) is olive black in color. This facies has abundant (> 50%) bioclastic debris (thin shelled brachiopods and crinoid fragments) and cm-scale vertical and horizontal burrows. This facies is only present in the Wise 1-20 at the uppermost portion of the Mississippian interval and towards the middle of the core in a thin (<6 inch) bed. No thin sections or XRD were available for this facies.

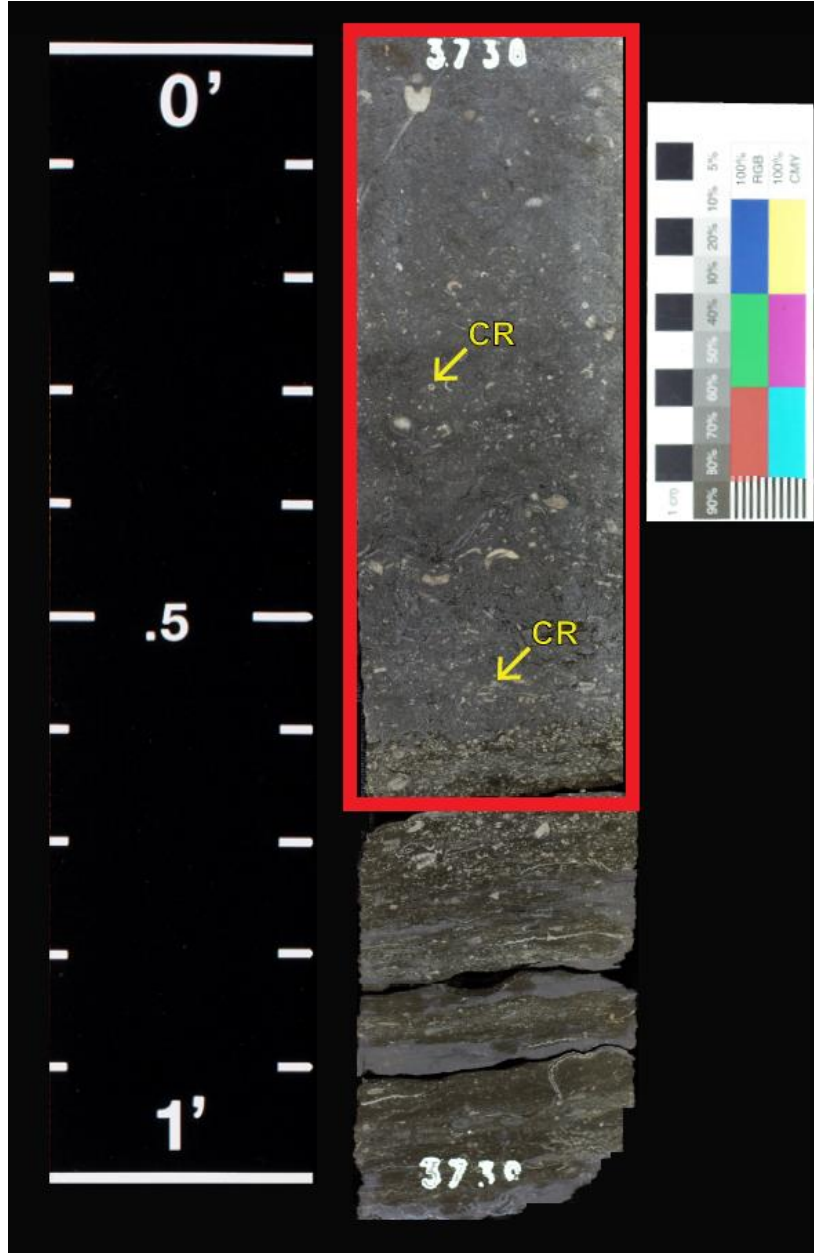
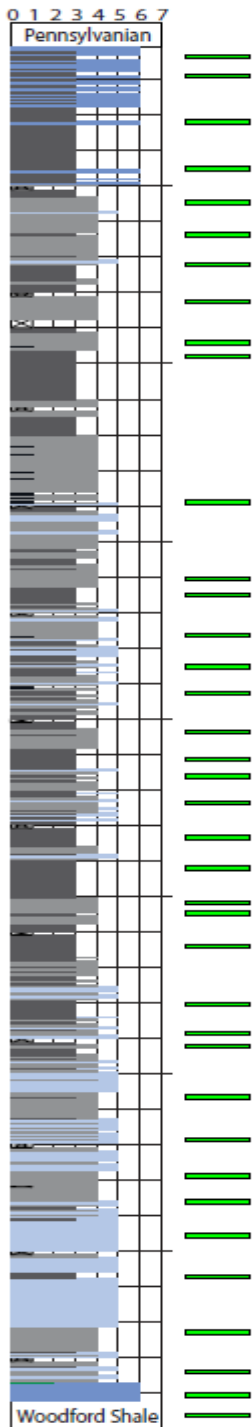


Figure 13: Facies 7 Skeletal packstone-grainstone: is olive black and has abundant bioclastic debris, mostly crinoid fragments and thin shelled brachiopods. This facies is only observed in the Wise 1-20. Core photograph under white light. Scale to the left of the core is in tenths of feet. No thin sections were available in this facies.

Core Facies Stacking Patterns

Once the key core facies were identified and described, the vertical stacking of facies was recorded. Figure 14 displays the facies stacking for each core described in this study and reveals the degree of vertical facies heterogeneity observed in these distally-located cores. The siltstone facies (Facies 3, 4, and 5) are the most prevalent. The carbonate dominant facies (Facies 6 and 7) are found near the top and base of the core. The Angell 1-23 contains multiple 1 foot zones where the whole core was removed and taken for a separate analysis. The Wise 1-20 contains two large (>3 feet) intervals that were not collected during the coring process. Both of these issues result in potential facies changes that are not observable.

ANGELL
1-23



WISE
1-20

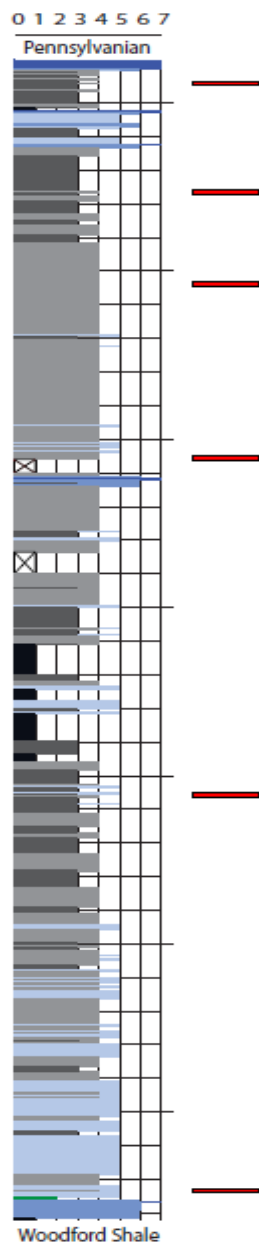


Figure 14: Lithologic columns: Each core in this study was analyzed and the primary depositional facies were identified and plotted. Each rectangle on the background grid represents 10 feet. The green rectangles to the right of the Angell 1-23 core represents locations where thin sections & XRD samples were taken. The red rectangles to the right of the Wise 1-20 core represent locations where only XRD samples were available.

CHAPTER V

Discussion

The facies identified in both cores of this study are presented in a shallowing upward order starting with the facies that is interpreted to be the most distally located. Overall, quartz silt is ubiquitous throughout both cores. Even the more carbonate dominated facies that are interpreted to be located in a more proximal position contain measureable amounts (2-17%). Carbonate content increases with each succeeding facies (2-86%), and clay content displays a negative trend moving from the distal to proximal facies (77-8%). Table 4 gives a brief summary of each of the facies described in this study.


Facies	Color	Mineralogy (Average %)				Sedimentary Features	Dominant Grain Types	Relative Position
		Quartz	Carbonates	Clays	Other			
7 Skeletal packstone-grainstone	Olive black	No samples were taken for XRD analysis				Bioclastic debris, cm-scale vertical and horizontal burrows	Thin-shelled brachiopods, crinoid fragments, skeletal debris	Proximal 
6 Skeletal mudstone-wackestone	Medium grey to greyish black	5	86	8	1	Bioclastic debris, cm-scale vertical and horizontal burrows	Thin-shelled brachiopods, crinoid fragments, skeletal debris	
5 Mottled peloidal siltstone	Medium dark grey to black; brownish black	30	27	29	14	Bioturbated, bioclastic debris, cm-scale vertical and horizontal burrows, zones of pyrite	Subangular to subrounded quartz silt, peloids, shell and crinoid fragments	
4 Laminated peloidal siltstone	Dark grey to black	29	24	36	11	mm to cm-scale planar laminations, mm-scale horizontal burrows	Subangular to subrounded quartz silt, peloids	
3 Massive-bedded peloidal siltstone	Medium dark grey to black; brownish black	32	22	34	12	Massive bedded, relatively featureless siltstone	Subangular to subrounded quartz silt, peloids	
2 Glauconitic sandstone	Dark grey to greenish black	No samples were taken for XRD analysis				cm-scale horizontal and vertical burrows, pyritized grains	Glauconite coated fine to very fine sand sized quartz grains	
1 Fissile clay-rich siltstone	Dark grey to black	16	2	77	5	Poorly indurated fissile cm-scale laminae, pyritized mm-scale burrows	Illite and/or smectite clays, quartz silt grains	

Table 4: Primary depositional facies described in this study. The lowermost facies are interpreted to be the most distally located facies, and the uppermost facies represent the more proximally located facies. The two facies without XRD data had the least amount of core footage available and make up a small percentage of the totality of the facies described. Notable trends include increasing carbonate and decreasing clay content moving up the table. The siltstone facies all contain very similar mineralogies. This suggests that different depositional dynamics played a role in how facies were formed.

Facies Interpretations

Fissile clay-rich siltstone (Facies 1): This facies is interpreted to be deposited on the distal outer ramp to basin region on a distally steepened ramp below both fair weather wave base (FWWB) and storm wave base (SWB). The high clay content and fine siliciclastic sediments suggests deposition occurred in a relatively low-energy environment. That would allow the clay minerals to fall out of suspension and collect on the basin floor. Water conditions in the benthic zone were likely dysoxic, indicated by low abundance and low diversity of fauna preserved, and by the presence of pyrite (Berner, 1981; Canfield and Raiswell, 1991; Canfield et al., 1992; Lobza and Schieber, 1999; Schieber, 2003). It should be noted that the limited bioclastic debris found in this facies is likely washed in from proximal updip locations during energetic storm events, and thus are not found *in situ* (Handford, 1986). The differences in thickness between the two cores may be attributed to the relative position where each core is located. The Wise 1-20 is located in a more distal location than the Angell 1-23, therefore relative water depths should be higher and energy regimes should be lower which would have allowed for more suspension settling and deposition of fine grained sediments. The Wise 1-20 contains 6.1% (20.9 feet of the 344.2 foot long “Mississippian” section) of Facies 1 whereas the Angell 1-23 contains 1.4% (5.3 feet of the 379.9 foot long “Mississippian” section) of Facies 1.

Glauconitic sandstone (Facies 2): This facies is interpreted to be deposited on the distal outer ramp to basin region below SWB. Glauconite formation is commonly associated with low energy conditions, little to no sediment supply, in a submarine environment between 50 and 500 meters (164 – 1640 feet) (Middleton et al.; 2003; Flügel, 2010).

Massive-bedded peloidal siltstone (Facies 3): This facies is interpreted to be deposited on the distal outer ramp region below SWB. Hand sample and thin section analysis show the mineral assemblages are organized homogeneously throughout. The absence of compositional variance within laminae and a lack of bioturbation suggests relatively rapid deposition of this facies in a relatively low energy environment. An energetic environment would likely winnow out the fine grain sediments and transport them further down dip. The mineral assemblages in this facies and Facies 4 and 5 are similar (refer to Table 4). How these facies are expressed could be a function of relative sea level, depositional energy conditions, sedimentation rates, biotic activity, or likely a combination of these factors.

Laminated peloidal siltstone (Facies 4): This facies is interpreted to be deposited on the outer ramp region near or slightly below SWB. The laminae that appear in both hand sample and thin section show preferential deposition and sorting of grain sizes. The preserved laminations and low abundance/diversity of biota, suggest a relatively low-energy environment that occasionally experienced storm events that brought in bioclastic debris from updip and may be responsible for the small scale cross bedding

that is sometimes observed in this facies. The morphology resembles hummocky cross stratification (HCS). However, the cross bedding observed in core is missing key elements to qualify as HCS as defined by Harms and others (1975 and 1982). No erosional bounding surfaces are seen. A scoured bed surface at the base should be present to positively identify as HCS (Harms et al., 1975). However, the following features are consistent with HCS according to Harms and others (1975 and 1982); laminae are nearly parallel to the lower bounding surface, laminae thickness varies both vertically and laterally, and dip angles are low (<10°).

Mottled peloidal siltstone (Facies 5): This facies is interpreted to be deposited on the proximal outer ramp to distal mid-ramp at, or just below, SWB. The proliferation of bioturbation suggests more oxygenated water conditions, which is more hospitable to burrowing biota (Sturdivant et al., 2012). In some areas, the sediment is completely homogenized and all bedding traces are disrupted. Where bioturbation intensity is lower, some bedding planes can be observed. This suggests that water conditions were variable at times, and that colonizing biota required time to proliferate. Bioclastic debris is more common in this facies, but not abundant overall (up to 10%). The average mineralogical content regarding carbonates remains relatively unchanged from Facies 3 and 4. This suggests the sediment source has remained relatively consistent for the 3 middle siltstone facies.

Skeletal mudstone-wackestone (Facies 6): This facies is interpreted to be deposited on the distal mid-ramp below FWWB and above SWB. The abundance of bioclastic debris found within this facies suggests a more proximal environment. Water conditions were likely more oxygenated and conducive to biota proliferation and carbonate formation. A productive carbonate factory in relative close proximity would help explain the dominant carbonate mineral assemblage seen in this facies. Accordingly, the system is interpreted to be prograding during deposition of this facies in order to bring the carbonate factory closer to the locations in this study.

Skeletal packstone-grainstone (Facies 7): This facies is interpreted to be deposited in a more proximal position but still on the distal mid-ramp below FWWB and above SWB. Abundant bioclastic debris suggests a more proximal environment. It is interpreted that this facies was deposited during the maximum sea level regression and that the carbonate factory was at its closest position to the study area. Abundant bioclastic debris was transported and deposited during this time. It is likely that the top of this facies was subject to erosion during Pennsylvanian time as the Mississippian-Pennsylvanian contact is found immediately above this facies in the Wise 1-20. The lack of this facies in the Angell 1-23 can be attributed to erosion as the Pennsylvanian unconformity is more pronounced moving towards the north.

Sequence Stratigraphic Framework

Idealized Facies Stacking Pattern: The facies described in core and thin sections were placed in an idealized facies succession in a shoaling upwards progression to capture one rise (transgression) and fall (regression) in relative sea level see Figure 15. This stacking pattern was used to establish depositional sequences in the cores and identify a hierarchy of nested sequences by utilizing Walther's Law of Facies successions, which connects the idea of lateral continuity based on vertical stacking. It is important to note that a sequence containing the entire progression from the lowermost (distal) facies to the uppermost (proximal) facies was not observed. However, this is an ideal vertical stacking pattern as incomplete successions are to be expected due to a hierarchy of eustatic sea level changes.



Figure 15: Idealized facies stacking pattern: This study identified 7 primary depositional facies utilizing core and thin section analyses. These facies were placed in a shoaling upwards progression. The blue triangle represent the transgressive portion and the red triangle represent the regressive portion of one rise and fall of relative sea level.

Sequence Stratigraphic Hierarchy: The vertical stacking pattern of facies observed in core exhibit different temporal scales of variability. Other studies of the Mississippian system have also identified a hierarchy of cyclicity (LeBlanc, 2014; Jaeckel, 2016; Flinton, 2016; Price and Grammer, 2017; Childress and Grammer, 2018). Two orders of cyclicity were observed in core alone, and another lower order of cyclicity was seen when adding wireline logs to the core data. Table 1 describes the temporal duration and resolution necessary to define these orders of cyclicity. However, temporal relationships for both cores used in this study are not known. The numerical orders used in this study are to note the observations multiple scales of variability and assign them a hierarchy.

Conodont biostratigraphy has been utilized in an attempt to establish a temporal framework for the Mississippian section within the study area (Hunt, 2017). Hunt's (2017) study was successful in providing stage resolution to the study area, with results suggesting that deposition occurred during the Meramecian and Chesterian.

2nd Order Supersequence: Both the Wise 1-20 and Angell 1-23 display one second order supersequence that spans the entirety of the Mississippian interval. The Mississippian/Pennsylvanian unconformity is an erosive contact. It is unknown how much section was eroded from both of the cores analyzed in this study. The erosion is more pronounced to the north, and is most often observed in the subsurface by a wash-out section seen in the caliper curve.

3rd Order Sequence: Four probable 3rd order sequences were identified in both cores. Another partial sequence is observed at the top of the Mississippian interval likely truncated by Pennsylvanian erosion. Sequence thickness ranges from 44 ft. (13.4 meters) to 133 ft. (40.5 meters). Average thickness is 71.5 ft. (21.8 meters). Sequence 3 is the thickest unit in both cores at 133 ft. (40.5 meters) for the Angell 1-23 and 130 ft. (39.6 meters) for the Wise 1-20. Overall, the Angell 1-23 contains the thicker sequences. It is interpreted that the Angell 1-23 was in a more proximal position on the ramp during deposition. This is supported due to the relative abundance of more distal facies (6.1% Facies 1 in the Wise 1-20 compared to 1.4% in the Angell 1-23) observed in the Wise 1-20, denoted in Figure 16.

4th Order High-Frequency Sequence: Multiple high-frequency sequences (HFS) were observed nested within the 3rd order sequences. These were identified by integrating wireline logs to the core data. The logs display a further hierarchy that is difficult to see in core alone. The difficulty lies in the similarity of the facies characterized in core, and the limitations in the data set to properly characterize rock properties below hand sample resolution. Variations in clay mineral content could explain the abrupt increases in gamma ray API units.

The thickness of the HFS ranges from 45 ft. (13.7 meters) to 10 ft. (3.0 meters). The average thickness of the HFS in both cores is 20.8 ft. (6.3 meters). HFS 7 is the thickest for both cores; HFS 1 is the thinnest for both cores. Overall, the Angell 1-23

contains the thicker HFS. This is consistent with the third order sequence observations, and with the interpreted ramp position of both cores. Identification of HFS is vital since these meter-scale units comprise the fundamental reservoir units (Grammer et al., 2004).

Wireline Log Correlations

Wireline logs measure rock properties at and near the borehole. Integrating core analysis to the wireline logs allows for correlation of sequences away from the ground truthed rock data found in the cored wells. The facies and sequences observed in core were tied to their respective wireline log signature and extrapolated to uncored wells in the region. Figure 16 displays the sequence stratigraphic framework and the wireline log tie associated with the third order sequences.

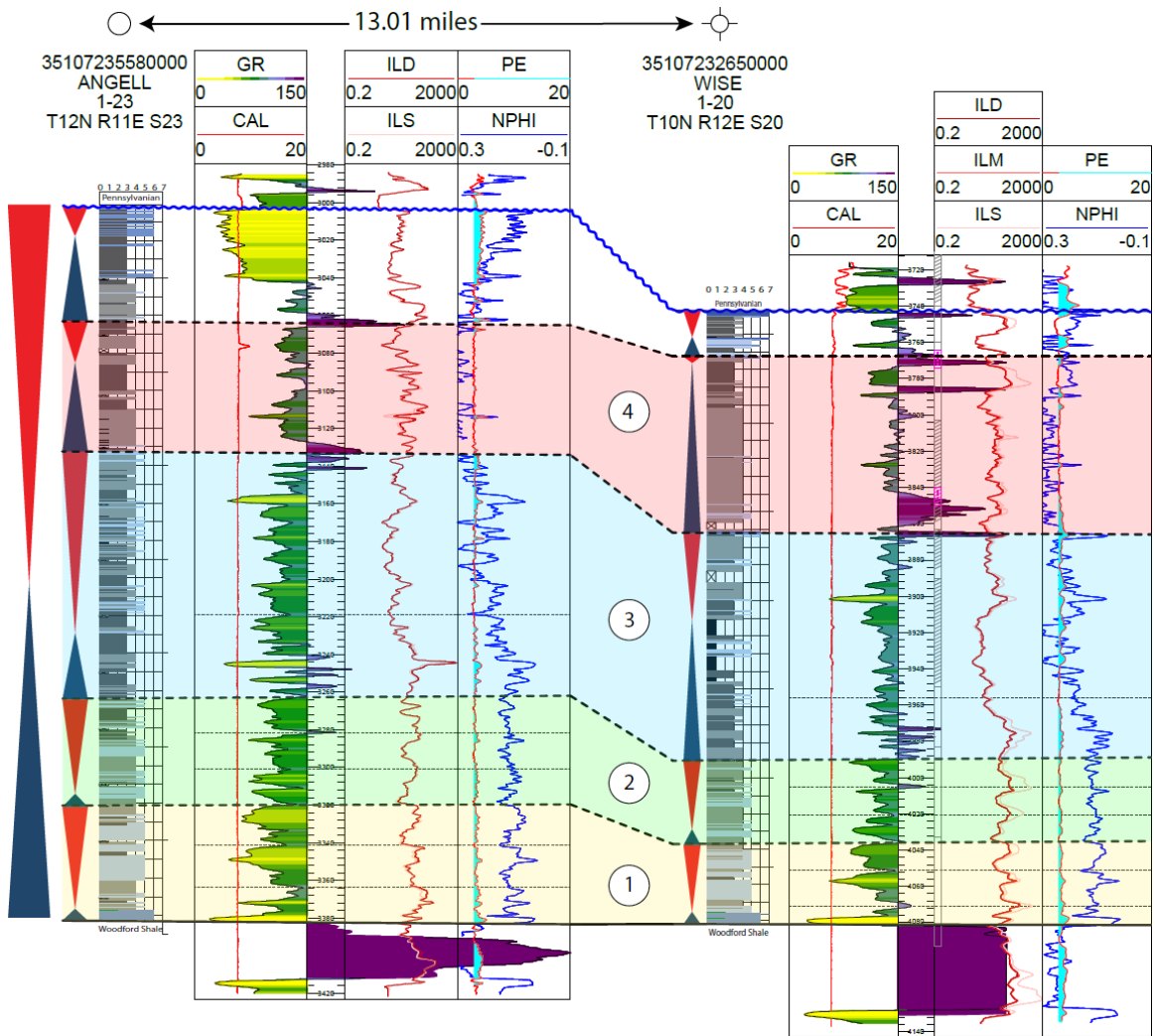


Figure 16: The sequence stratigraphic framework: Constructed by observing facies stacking patterns in core, and linking it to wireline log signatures to enable correlation to non-cored wells. Four complete "3rd" order sequences (bold dashed lines) are observed and a fifth is truncated by the Pennsylvania unconformity (blue sinusoidal line). Multiple "4th" order sequences (dashed lines) are resolvable in wireline logs, however, core correlation has proved problematic due to similarity of facies and limited thin sections to discern small-scale variations. This study utilized the gamma ray curve as the primary log for correlation. It is the curve with the color fill. Some intervals contained API values that went beyond the standard scale and are denoted by the purple fill.

Gamma Ray: The gamma ray curve was found to be the most consistent logging tool for correlation purposes. Each of the third order sequences is bounded by a sharp increase in gamma ray API units. Oftentimes the measurements went beyond the standard scale of 150 API units. In Figure 16 the purple fill that intrudes into the depth column and the resistivity track are examples of this. These “hot” zones in the gamma ray curve are attributed to more distal facies that contain a greater concentration of fine siliciclastic and clay minerals, linked to the transgressive onset of third order sea level change.

Fourth order HFS are also observed in the gamma ray curve. They are also bounded by distinct increases in recorded gamma ray API units. These HFS are able to be correlated throughout the study area and their signature proved to be as predictable as the third order sequences. However, tying the core data to this higher frequency cyclicity observed in the gamma ray curve proved to be difficult. The predicted facies changes associated with sequence boundaries were not always observed. As previously mentioned, this may be attributed to increased fine grained sediment and clays that are not visible in core hand sample. A more robust photomicrograph and XRD data set with a higher sampling density would be needed to help control these variables, and make more unequivocal interpretations.

Resistivity: The resistivity curves for both wells were useful for correlating 3rd order sequences. The resistivity tool can be influenced by formation fluids (brine or oil), therefore this curve is a secondary tool used in conjunction with the gamma ray curve to

enhance the precision and accuracy of correlations. The top of each of the 3rd order sequences is identified by a decrease in resistivity. Overall, the more carbonate-rich facies are more resistive than the fine siliciclastic dominated facies.

Fourth order HFS display correlative signatures when used in tandem with the gamma ray curve. These two logs proved to be the most consistent tools in identifying cyclicity in the subsurface throughout the study area. However, the resistivity curve does not yield a definitive tie to the core data. Figure 16 denotes the HFS boundaries by the thin dashed line on the wireline logs only.

The neutron and density porosity curves were considered for correlation purposes, but proved to be not as useful as the gamma ray and resistivity curves. The gamma ray and resistivity curves are more abundant in this data set. Many of the wells in the study area predate the advent of porosity logs. Having a consistent wireline log criteria throughout the data set allowed for more reliability in correlations.

Caliper: The caliper curve was utilized in this study to help identify the boundary between Mississippian and Pennsylvanian strata. This boundary is an erosional contact that erodes varying amounts of section; generally, more section is lost moving north. The facies immediately above the Mississippian section are poorly indurated, which causes borehole washout and caliper readings to increase in response. This pattern is present throughout the study area and consistently recorded by the caliper. Overall,

the caliper maintains contact with the borehole throughout the entirety of the Mississippian section.

Sequence Stratigraphically Defined Architecture

The sequence stratigraphic architecture of the Mississippian section inside the study area displays low declivity clinoforms prograding and thinning to the south into the present-day Arkoma Basin. The geometries observed in dip-oriented cross sections and sequence thickness maps indicate deposition occurred on a ramp environment (Tucker and Wright, 1990). This interpretation is consistent with previous findings (Bertalott, 2014; LeBlanc, 2014; Flinton, 2016; Childress and Grammer, 2018). Sequence thickness along strike appears relatively consistent, although this should not imply continuity of facies, due to expected lateral heterogeneity inherent to the system. These patterns are consistent for both 3rd order sequences and 4th order HFS. Figure 17 shows the locations of the various cross sections constructed for this study.

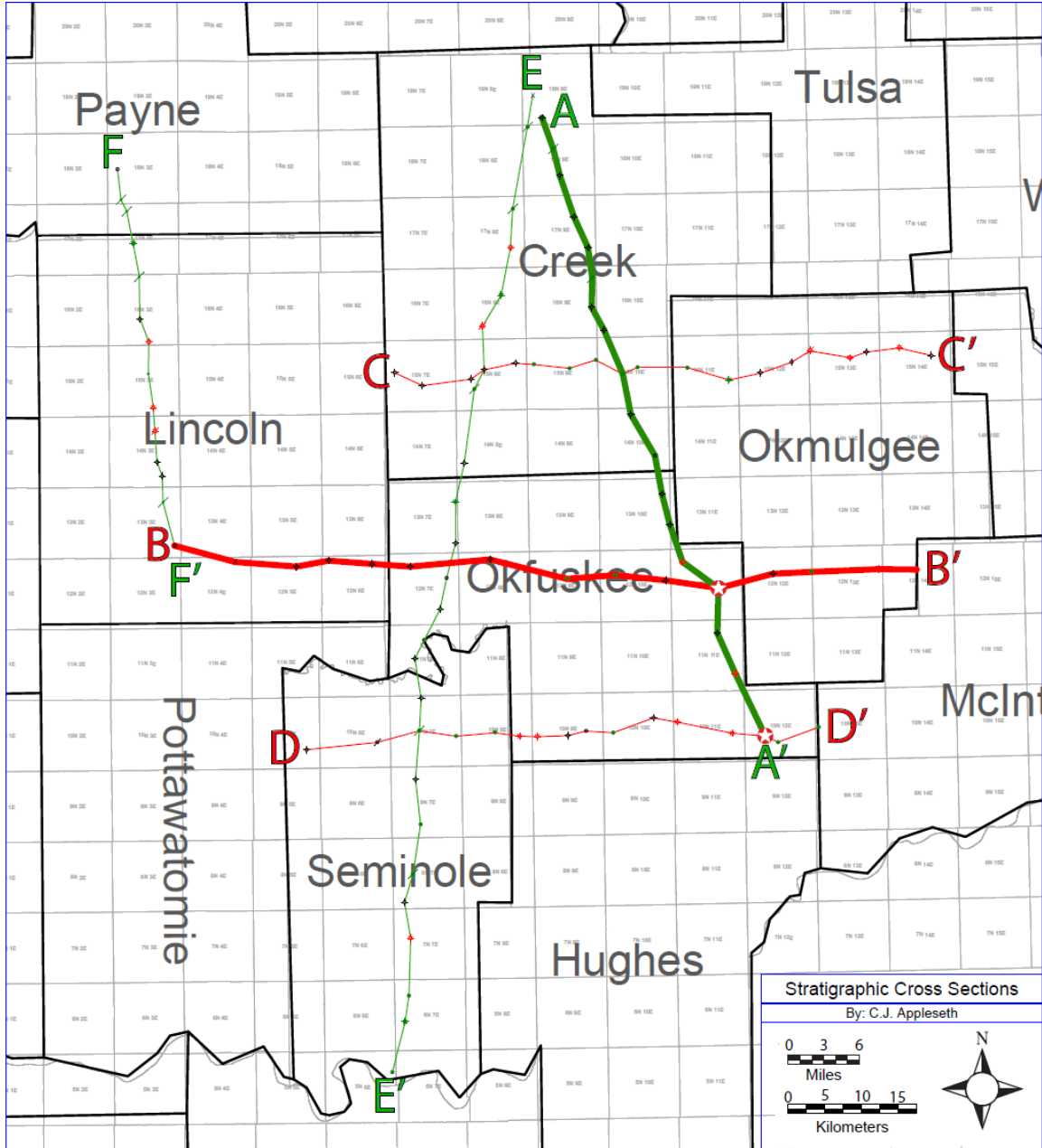


Figure 17: Stratigraphic cross sections constructed throughout the study area. This study highlights A-A' and B-B'. A-A' was constructed along interpreted depositional dip, and B-B' was constructed along depositional strike. Cored wells in this study are denoted by the red stars and located at the intersection of cross sections A and B, and at the south terminus of A-A'. Cross sections C-F may be found in Appendix C-II.

Stratigraphic Cross Sections: Stratigraphic cross sections aid in extrapolating correlations from cored wells and visualize sequence thickness trends across a transect. The primary criteria used to select cross section wells was based on interpreted depositional strike and dip orientation, and the secondary criteria was availability of complete digital wireline logs for the “Mississippian” interval. All stratigraphic cross sections constructed in this study are set to a flat datum on the top of the Woodford Shale, which serves as the base of the “Mississippian” interval.

Dip Oriented Cross Sections: Three cross sections were constructed north to south along interpreted depositional dip. Dip oriented cross sections give the best perspective for determining platform type and evaluating the low declivity geometries associated with this system.

Cross section A-A', Figure 18, is a north-northwest to south-southeast transect spanning 59.01 miles (94.97 km) across 18 wells. It contains two core calibrated wells, the Angell 1-23 and the Wise 1-20. A-A' contains 4 complete “3rd order” sequences. Each of these depositional sequences is denoted by the color fill on the cross sections, and by the bold long-dashed lines. Contained within these sequences are multiple “4th order” high frequency sequences, denoted by the short-dashed lines.

Overall, this dip oriented cross section displays a series of low declivity clinoforms that prograde and thin to the south. The second “3rd order” sequence, shaded in green, is the best example of this geometry. The northern portion is very

gently dipping, the middle portion displays a noticeable increase in dip, and the southern portion returns to a more gentle dip angle. The “4th order” HFS also reflect these geometries at a higher frequency. The wireline log signatures for both “3rd” and “4th order” correlations remain consistent in both proximal and distal directions. This suggests that the stacking patterns observed in core are not the result of localized phenomena (MTDs), but of a larger scale driver, such as high frequency sea level change.

The Mississippian and Pennsylvanian contact differs in proximal to distal locations. The boundary between the two is characterized by an erosional contact in all well locations. Often a poorly indurated bed 2 – 5+ feet thick that washes out during drilling operations is observed in the caliper log by a sharp increase in borehole size. A-A' shows that more section is removed by this unconformity moving towards the north. Depositional sequence 3 and 4 (blue and red filled sequences) are truncated by this unconformity. Numerous faults are known throughout the study area (Marsh and Holland, 2016). The faults are associated with both the Nemaha uplift and formation of the Arkoma Basin. Figure 2 shows known faults throughout the area. The reverse faults related to the Nemaha uplift are likely contributors to increased erosion to the north.

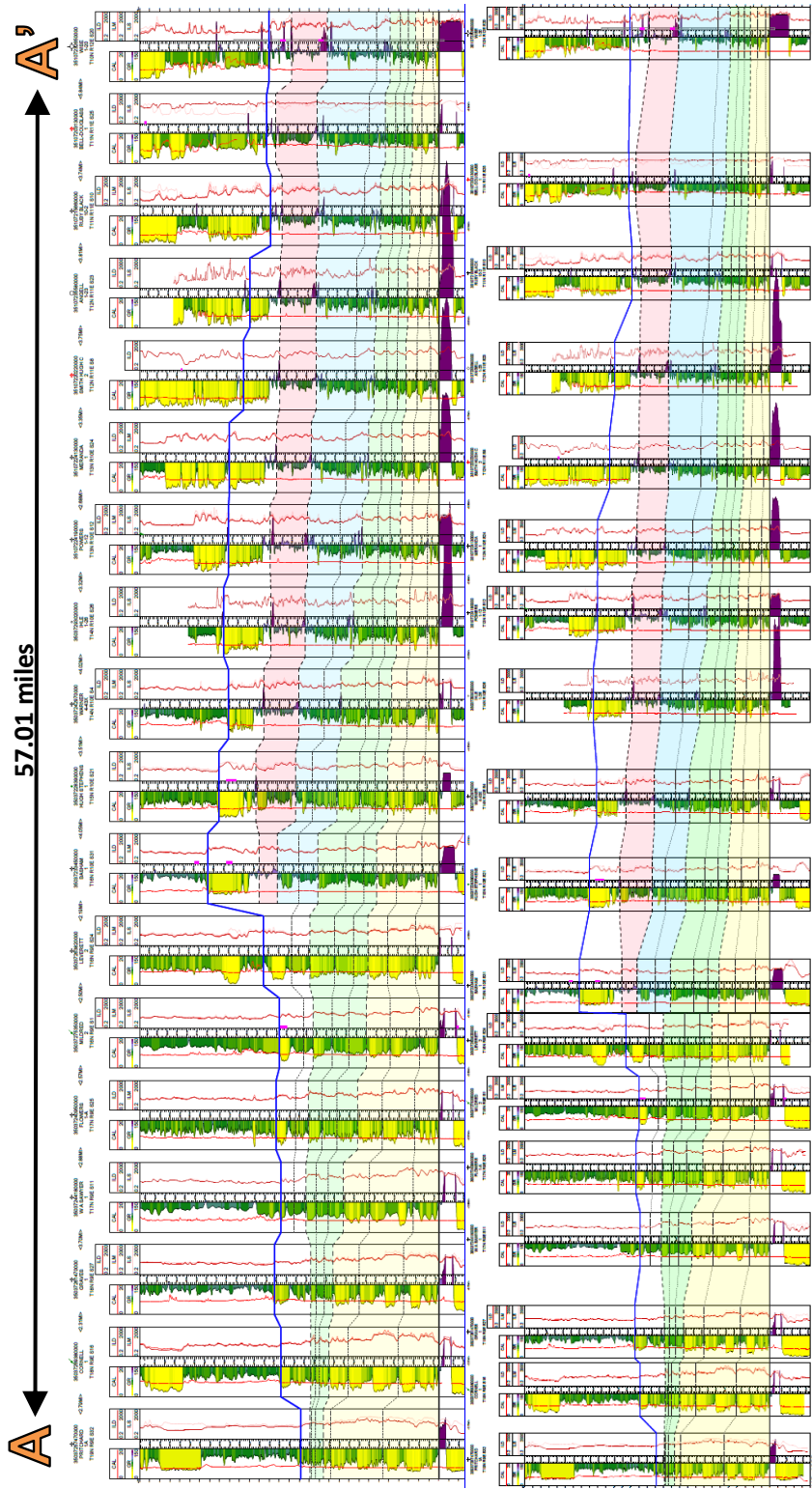


Figure 18: Stratigraphic cross section A-A': Constructed along interpreted depositional dip. The top cross section shows wells with fixed spacing. The bottom cross section displays the same wells, but with relative distance between each well shown. The basal datum is the top of the underlying Woodford Shale; indicated by the solid black bold line. The top of the Mississippian section is indicated by the solid blue bold line. Probable third order sequences are shown in the colored highlighted fill and the bold dashed lines. Nested within are probable fourth order HFS denoted by the light dashed lines. Vertical exaggeration for fixed distance cross section is 106X. Vertical exaggeration for relative distance cross section is 76X.

Strike Oriented Cross Sections: Three cross sections were constructed west to east along interpreted depositional strike. Strike oriented cross sections help constrain the geometry of the system and correlations in a strike direction are generally more consistent in both thickness and wireline log character.

Cross section B-B', Figure 19, is a west to east transect spanning 63.52 miles (102.23 km) across 15 wells. It contains one core calibrated well, the Angell 1-23. B-B' contains 4 complete "3rd order" sequences. Each of these depositional sequences is denoted by the color fill on the cross sections, and by the bold long-dashed lines. Contained within these sequences are multiple "4th order" high frequency sequences; denoted by the short-dashed lines.

Overall, this strike oriented cross section displays relative lateral continuity of sequence thicknesses, both for the "3rd order" depositional sequences and "4th order" HFS. However, continuity of thickness should not imply continuity of facies. Core analysis revealed that several of the facies are similar in composition, and the differences between most of the facies are subtle. Lateral heterogeneity of facies should be expected in this system.

B-B' was selected based on interpreted depositional strike. The sequence thickness trends mostly reflect this interpretation. However, on the western two most wells of B-B' thickening of the sequences is observed. This could be due to the length of this cross section (over 60 miles long) and the strike of the system changes sub-

regionally near these wells. Also, the Mississippian and Pennsylvanian unconformity changes across this transect with “3rd order” sequences 4 and 5 being truncated to the west. This suggests erosion is more prevalent moving west towards the Nemaha uplift. Extensive faulting is known throughout the study area (Marsh and Holland, 2016). See Figure 2 for a detailed map that displays known faults in the region.

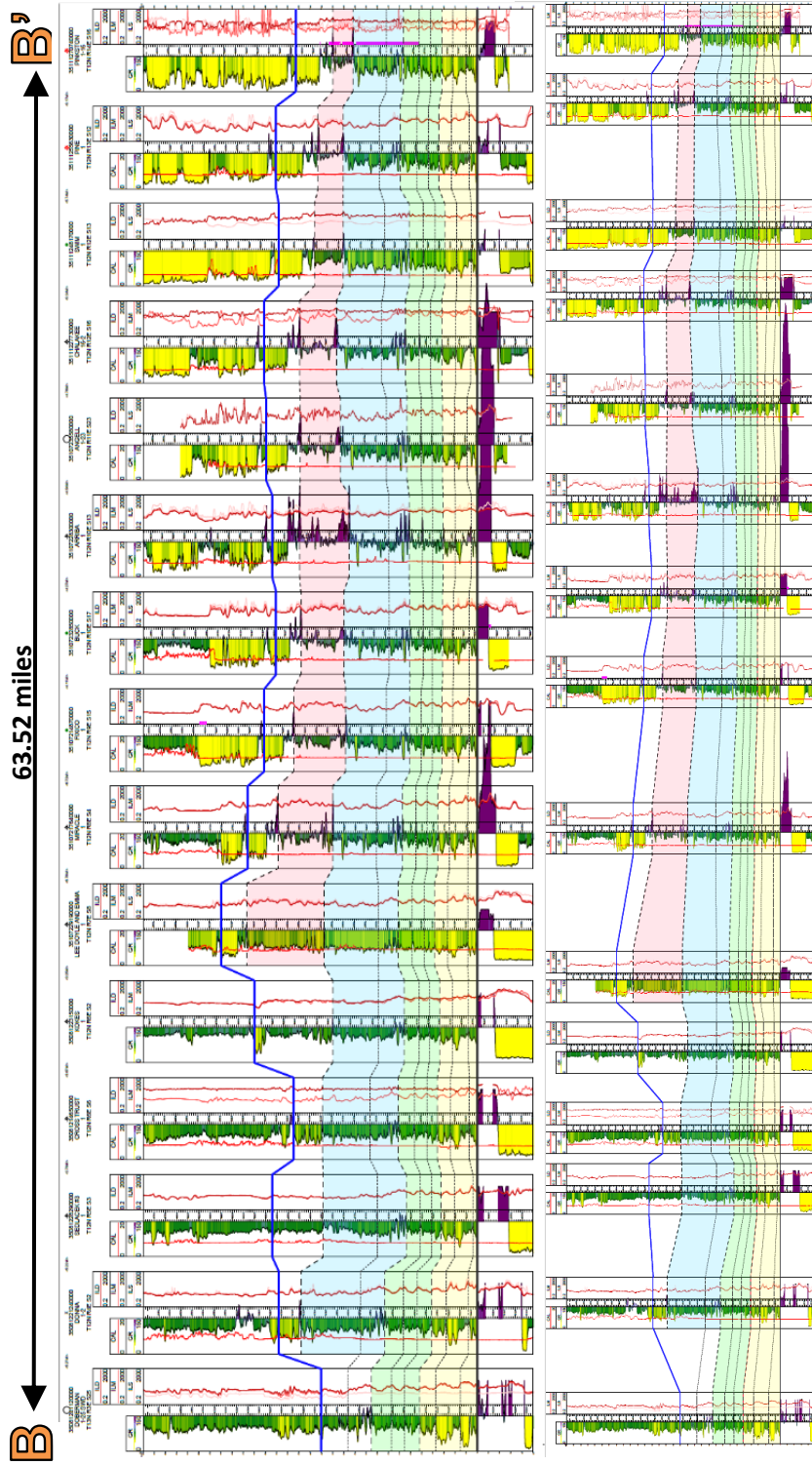


Figure 19: Stratigraphic cross section B-B': Constructed along interpreted depositional strike. The top cross section shows wells with fixed spacing. The bottom cross section displays the same wells, but with relative distance between each well shown. The basal datum is the top of the underlying Woodford Shale, indicated by the solid black bold line. The top of the Mississippian section is indicated by the solid blue bold line. Probable third order sequences are shown in the colored highlighted fill and the bold dashed lines. Nested within are probable fourth order HFS denoted by the light dashed lines. Vertical exaggeration for fixed distance cross section is 135X. Vertical exaggeration for relative distance cross section is 84X.

Thickness Maps: Thickness maps allow for 3-dimensional structures to be viewed on a 2-dimensional surface where X and Y are referenced to a location on a map, and the Z values are referenced to the thickness of the interval being mapped. The contour maps in this study measure the sequence thickness changes across the study area. All maps in this study utilize the same color scheme to indicate variations in thickness. Warmer colors (reds, oranges, and yellows) represent thicker intervals, and cooler colors (white, blues, and greens) represent thinner intervals. Contour intervals for all maps are denoted in the map key and are either 5 or 10 feet (1.5 to 3.0 meters). The wells located on each map represent the control points where tops were picked on the wireline logs. Areas with a high density of control points possess the lowest degree of uncertainty. Areas with a low density of control points (i.e. wells), such as the edges of the maps, have a higher degree of uncertainty. These maps are valuable because they delineate depositional trends, such as strike/dip, platform gradient, and help identify the degree of faulting and erosion.

Overall, sequence thickness trends appear to strike along a west-southwest to east-northeast bearing, and thin in a basinward direction to the south into the present-day Arkoma Basin. Thickness changes are very gradual across wide portions of the platform. This is consistent with previous studies that interpreted that deposition occurred on a distally-steepened ramp (LeBlanc, 2014; Flinton, 2016; Jaeckel, 2016; Price and Grammer, 2017; Childress and Grammer, 2018). Thickness trends show that

intervals in the upper Mississippian section were subject to intense erosion and major changes in depositional patterns are observed.

3rd Order Sequence Thickness Maps: Figure 20 shows the presence of strata that predate the sequences seen in core and throughout the majority of the study area. These older sequences display similar geometry and likely thinned out before reaching the cored wells, or were only deposited as a thin zone that is not recognizable in either core or wireline logs. Sequence 1 (Figure 21) strikes along a west-southwest to east-northeast transect. It dips gently to the south. The northern edge contains the thickest intervals of this sequence.

Sequence 2 (Figure 22) strikes in a west to east orientation. Its top boundary in wireline logs is characterized by a serrated interval on the gamma ray curve that oftentimes will show greater than 150 API units. The resistivity curve is less consistent than the gamma ray for this pick. The resistivity will often begin to read higher resistivity shortly before the gamma ray increases. Sequence 2 progrades and thins to the south. Laterally along strike, thicknesses remain relatively consistent throughout.

Sequence 3 (Figure 23) differs from the previous two in that changes in the depositional trends yield two distinct areas with different strikes. The northern section in Lincoln, Creek, Okfuskee, and Okmulgee County display a general west to east strike which is consistent with the previously deposited sequences. However, Seminole County's strike is more north to south. The definitive cause for this change is not

known. Cross section E-E' (See Appendix C-II) shows the section thickening southward for Sequence 3. This could be in response to increased accommodation space in response to eustatic sea level rise.

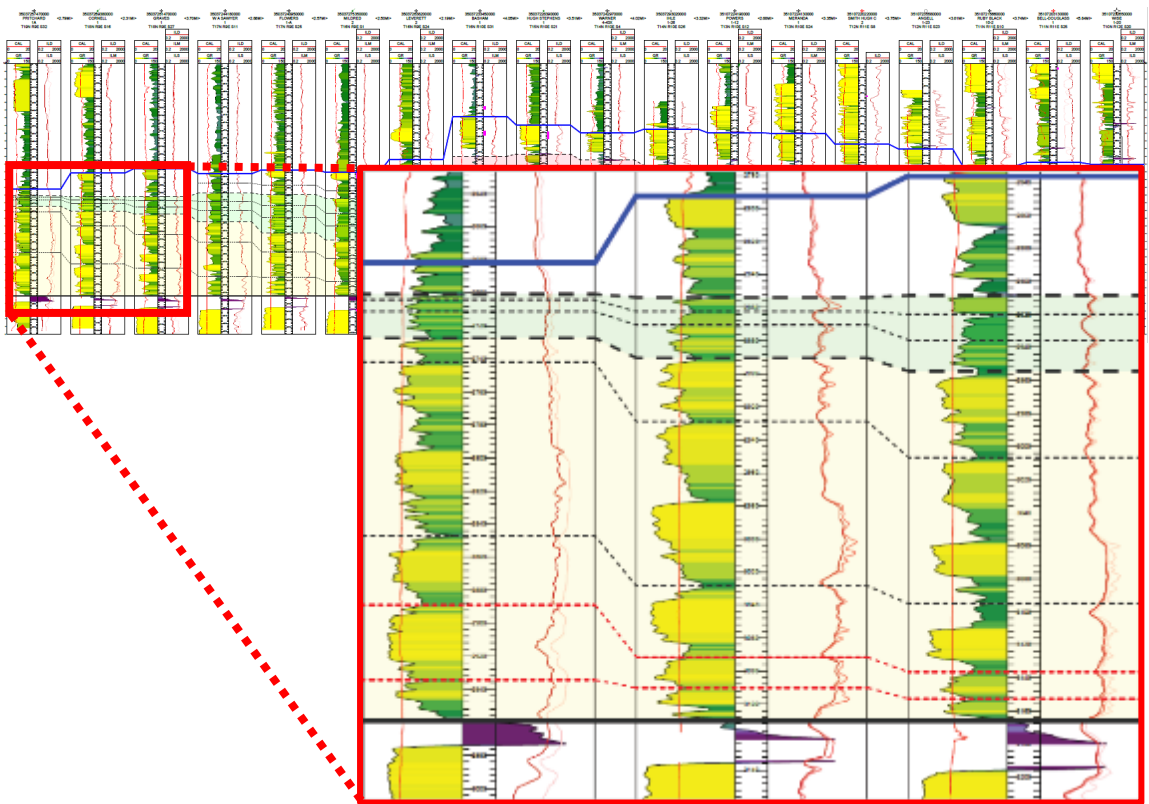


Figure 20: Detail of northern sector of Cross Section A-A': The wells highlighted in the red box show the sequence stratigraphic surfaces that have been extrapolated from the cored wells. These surfaces are denoted by the black dashed lines. The red dashed lines that are between the basal Woodford Shale and high frequency sequence 1 are likely other sequence boundaries that predate the deposition of the sequences defined in core. These sequences either thinned out prior to reaching the cored wells, or only deposited as a thin zone not recognizable in either core or wireline logs.

Sequence 4 (Figure 24) displays similar trends to Sequence 3. Thinning is more pronounced as the pre-Pennsylvanian unconformity removes more Mississippian section to the north and the western townships of Seminole County display thinning. This may be attributed to known faulting in the region, which enhances erosion. Figure 2 shows extensive faulting in the area along strike on Sequence 4.

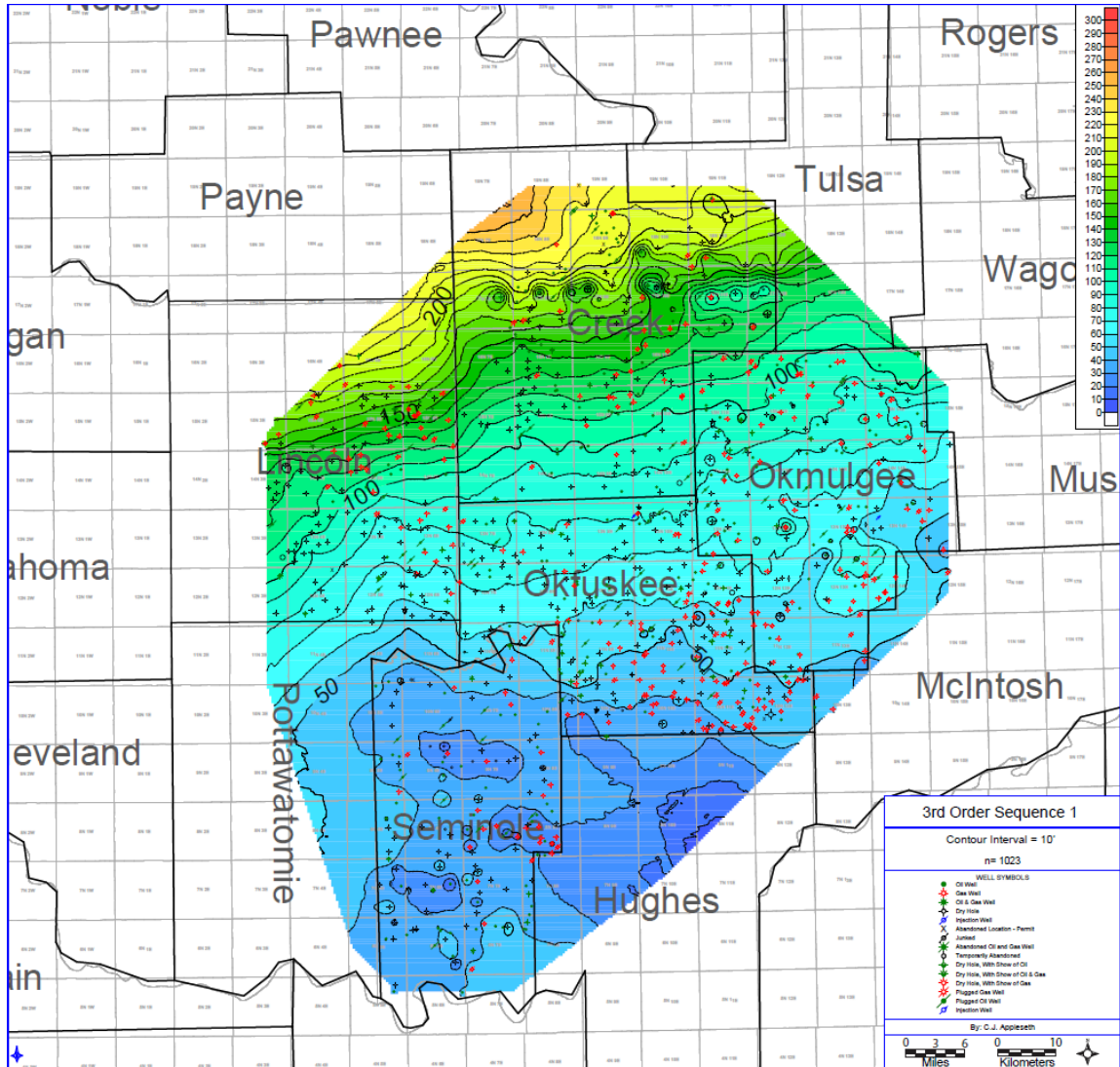


Figure 21: 3rd order sequence 1: Deposited atop the Woodford Shale. Overall strike of this sequence is west-southwest to east-northeast and dips gently to the south. Wells displayed represent control points where tops were picked on the wireline logs. The contour interval is 10 feet. Cooler colors (white, blues, and greens) represent thinner intervals and warmer colors (yellows, oranges, and reds) represent thicker intervals.

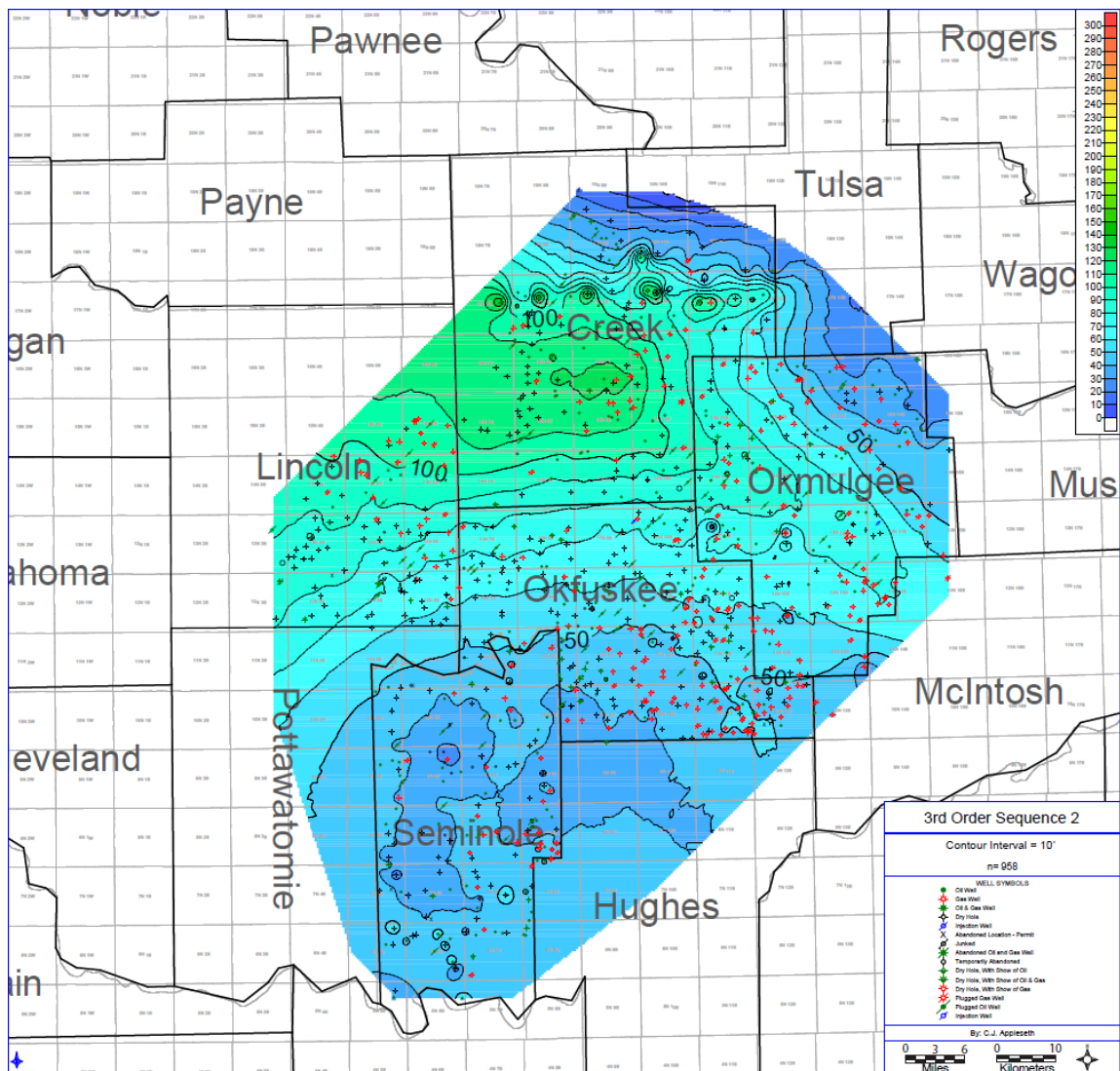


Figure 22: 3rd order sequence 2: Overall strike of this sequence is west to east and dips gently to the south. Thickness along strike remains consistent. Wells displayed represent control points where tops were picked on the wireline logs. The contour interval is 10 feet. Cooler colors (white, blues, and greens) represent thinner intervals and warmer colors (yellows, oranges, and reds) represent thicker intervals.

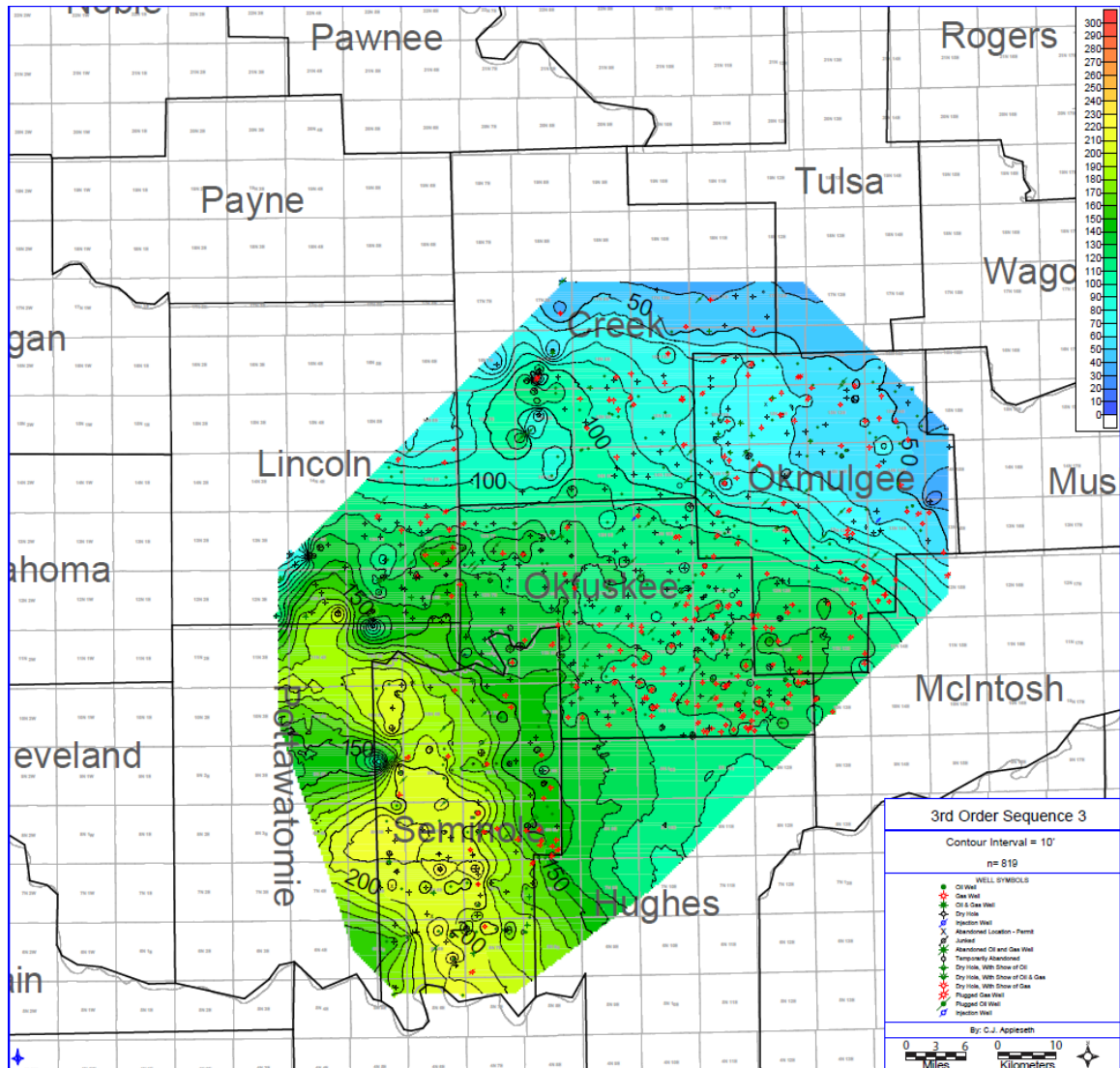


Figure 23: 3rd order Sequence 3: Displays two areas with distinct differences in strike. The northern section in Lincoln, Creek, Okfuskee, and Okmulgee County display a general west to east strike similar to the previous sequences. The strike in Seminole County is more north and south. Wells displayed represent control points where tops were picked on the wireline logs. The contour interval is 10 feet. Cooler colors (white, blues, and greens) represent thinner intervals and warmer colors (yellows, oranges, and reds) represent thicker intervals.

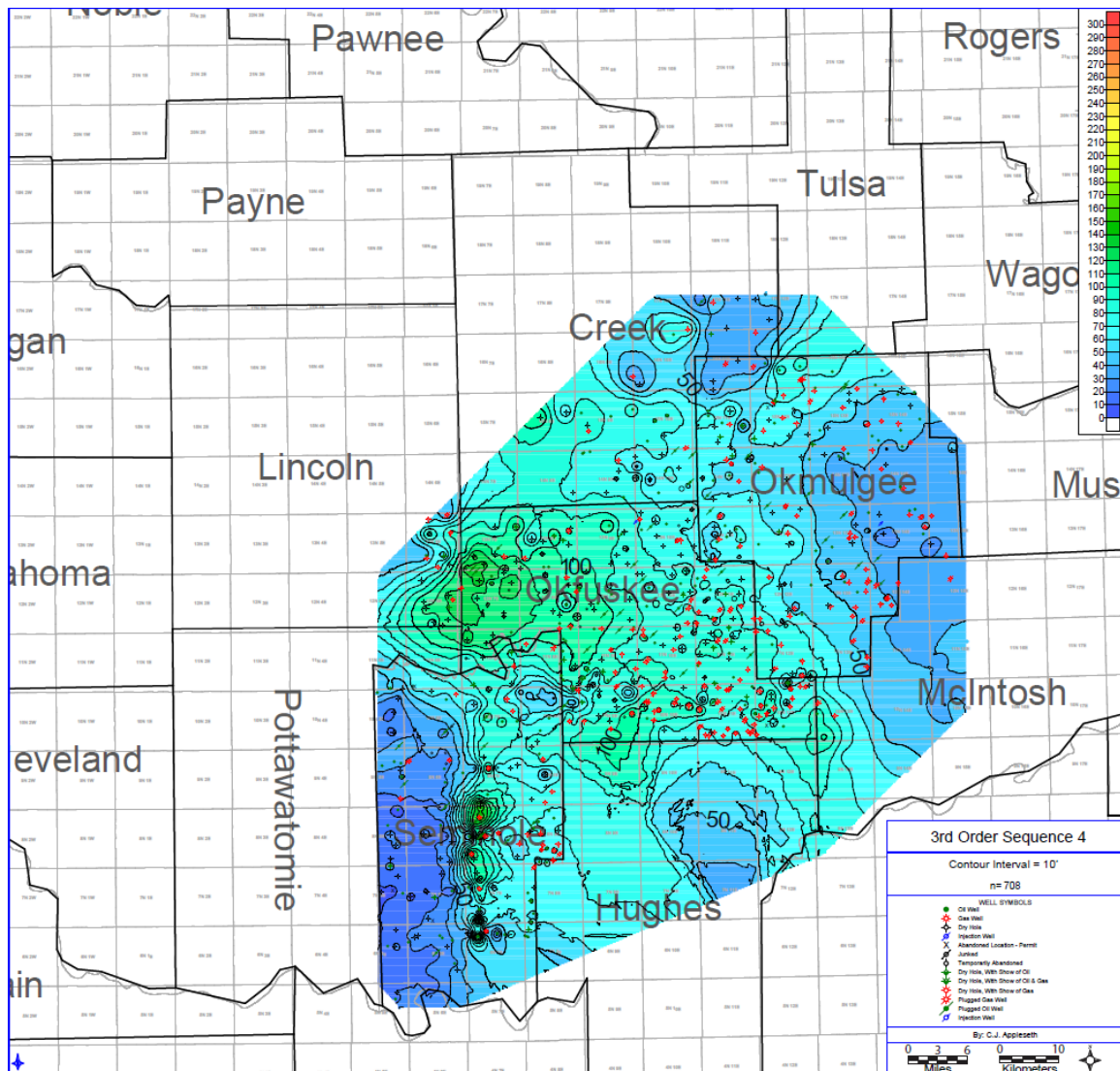


Figure 24: 3rd order Sequence 4: Overall strike of this sequence is similar to Sequence 3. Thinning is more pronounced in the north due to the Pennsylvanian unconformity removing Mississippian section. Wells displayed represent control points where tops were picked on the wireline logs. The contour interval is 10 feet. Cooler colors (white, blues, and greens) represent thinner intervals and warmer colors (yellows, oranges, and reds) represent thicker intervals.

4th Order High Frequency Sequence Thickness Maps

Lower order/higher frequency sequences (HFS) were picked from wireline logs in order to add more granularity to sequence picks to aid in the delineation of thickness trends throughout the study area. The trends observed in the HFS are more readily apparent due to increased density of key stratigraphic surfaces that were selected. Figure 25 shows the sequence thickness trends as they prograde to the south into the present day Arkoma Basin.

Overall, these maps reflect the patterns observed in the 3rd order sequence thickness maps, while also adding additional details. High frequency sequence 1-4 show gradual shifting of the thickness trends towards the south. A hiatus is seen in HFS 5 as the thicker interval appears to remain in the same position observed in HFS 4. Then the southward shift is observed again in HFS 6 and 7. The shift in HFS 6 and 7 appear to be more pronounced than the more gradual shifts seen in the earlier sequences.

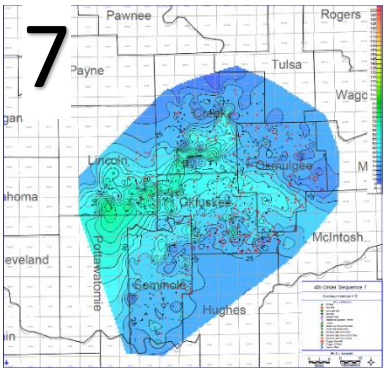
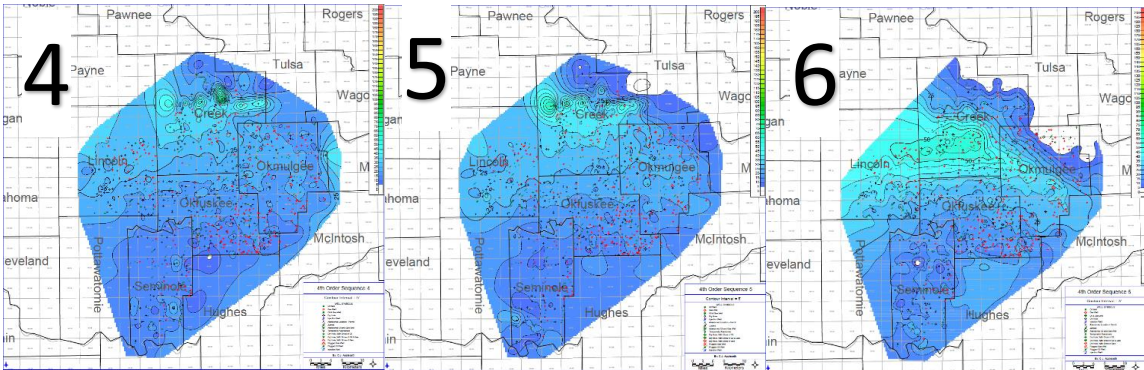
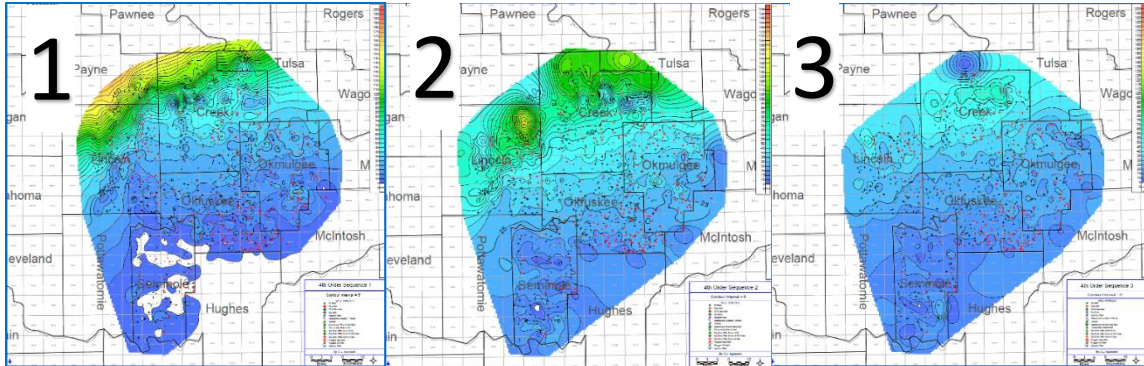


Figure 25: Series of high frequency sequence maps: That display increased detail to the thickness trends observed in the 3rd order sequences. Overall, strike of the system is west to east. Deposition is characterized by a steady progradation to the south. Contour interval is 5 feet for each HFS.

Reservoir Considerations

Porosity and permeability were measured from select samples from the Wise 1-20. These samples were categorized according to facies and position on the sequence stratigraphic framework in order to discern the trends in reservoir development. Defining these factors is vital in understanding reservoir architecture and the extent of reservoir communication. Lateral and vertical heterogeneity can lead to highly compartmentalized reservoirs which can impact well performance.

Facies analysis of the porosity and permeability data show that Facies 3 and 4 display the highest values of porosity and permeability. These are the massive-bedded peloidal siltstones and the laminated peloidal siltstones. The other facies display limited porosity or permeability development. It should be noted that Facies 3 and 4 display a wide range of values for both porosity and permeability. Therefore, facies alone does not, by itself, indicate the presence of a well-developed reservoir.

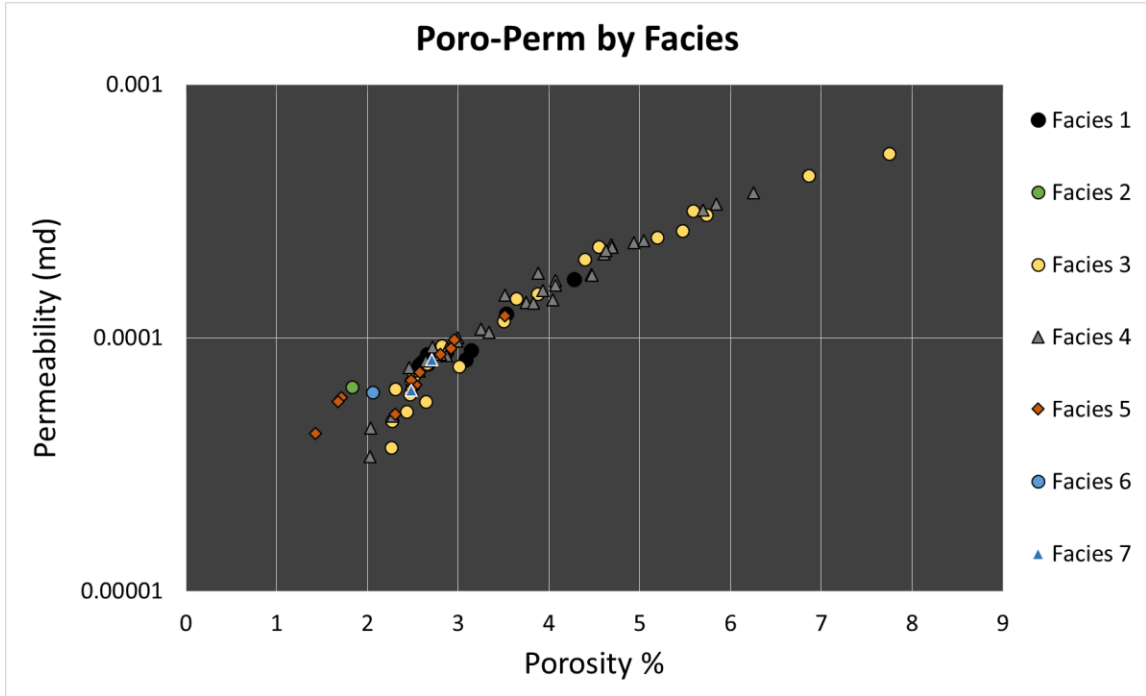


Figure 26: Porosity and permeability categorized by facies. This figure utilizes the facies described in this study to discern if facies partly control reservoir quality. Facies 3 and 4 (massive-bedded peloidal siltstone and laminated peloidal siltstone) display the highest values for porosity and permeability.

The sequence stratigraphic framework was also tied to the porosity and permeability data to determine its role in reservoir development. “3rd order” sequences were established from core analysis and tied to the porosity and permeability data. Also, transgressive versus regressive portions of the “3rd order” sequences were evaluated. Sequence 4 displays the highest potential for reservoir development. The other sequences show either limited porosity-permeability (Sequence 1 and 2) or fluctuate widely (Sequence 3 and 5). The relationship of transgression/regression to porosity and permeability is not clearly delineated and varies widely. Regressive legs

show a lower potential for reservoir development, this may be attributed to the higher likelihood of containing the more carbonate dominated facies, as the increased calcite content (cements) in these facies may occlude porosity. The transgressive legs exhibit similarly low porosity and permeability values as the regressive legs. The lower values may be due to samples with higher percentages of clay minerals (fissile clay-rich siltstone) that can occlude porosity and permeability.

No single factor appears to be the sole driver of reservoir development. It is more likely that each of these variables works in conjunction to produce more porosity and higher permeability. To find optimal reservoir zones, each of these elements should be considered to enhance recoveries and produce more economical wells; with stronger consideration given to facies type and sequence position.

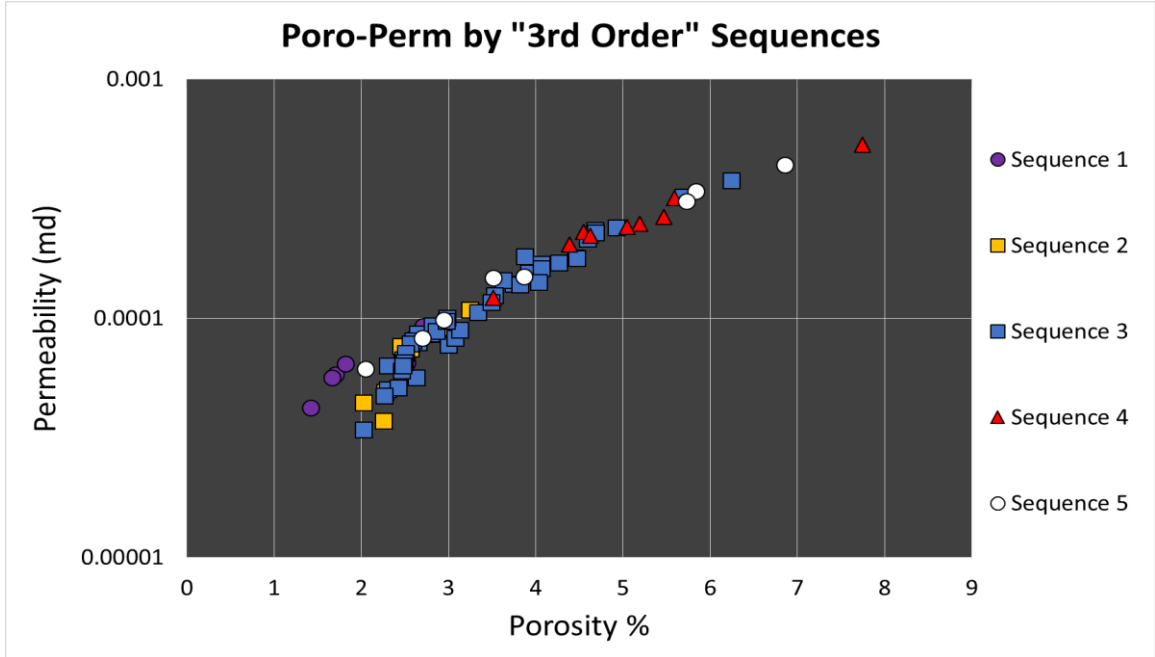


Figure 27: Porosity and permeability categorized from samples in the different 3rd order sequences. Overall, Sequence 4 displays the highest potential for porosity and permeability development.

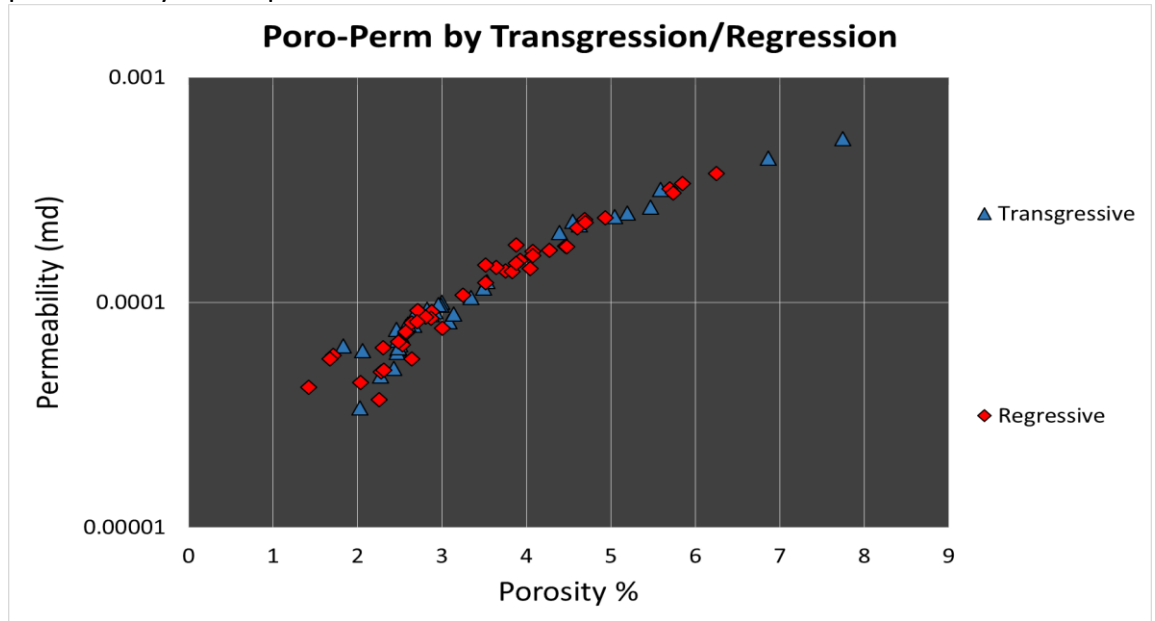


Figure 28: Porosity and permeability categorized according to transgressive/regressive legs of the sequence stratigraphic framework. Overall, the correlation between transgressive/regressive legs and reservoir development is poorly defined.

Silt Origins and Method of Transport

Fine siliciclastic sediment is found throughout the “Mississippian Limestone” in this study and other studies spanning from the Anadarko Basin to the Ozark outcrop belt (Childress, 2015; LeBlanc, 2015; Flinton, 2016; Jaeckel, 2016; Price and Grammer, 2017; Shelley et al., 2017; Childress and Grammer, 2018). Abundant detrital quartz, ranging in size from very fine sand to silt, and illite clay are found in both core locations. The presence of fine siliciclastic sediments is significant due to the sensitivity of carbonate producing organisms in carbonate depositional systems. Siliciclastic sediments suspended in the water column may alter photic zones and inhibit carbonate production (Tucker and Wright, 1990).

The source of the fine siliciclastic sediment is unresolved. Determining the origin of these sediments is problematic due to the minimal energy requirements to keep fine sediment suspended in the water column, and transported away from the source. Figure 29 is a chart that plots the relationship of different sized particles to flow velocity. Once mobilized, fine sediments can be transported under at very low flow velocities. Therefore, these sediments may be transported great distances from their source before settling out of the water column.

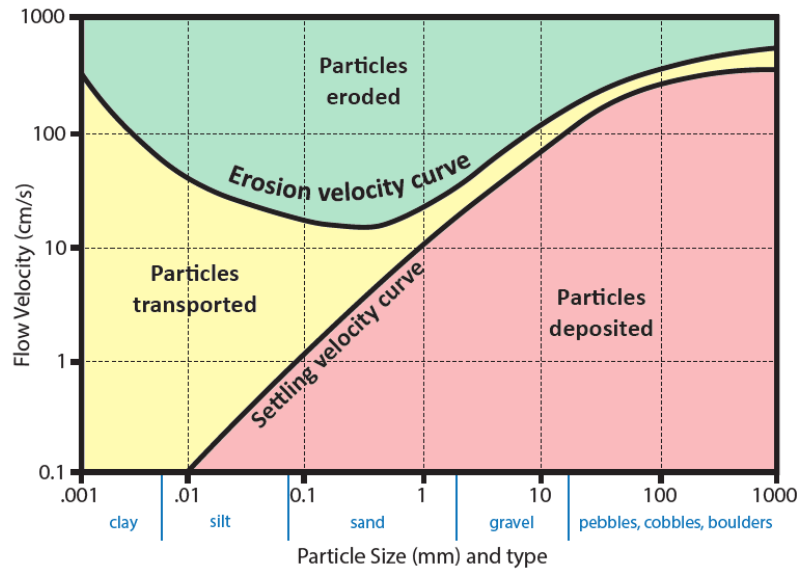


Figure 29: Hjulström-Sundborg diagram: This figure displays the energy regimes required for erosion, transport, and deposition of sediment of various sizes. Fine grains of sediment require minimal flow velocities to remain suspended and transported. Modified from Earle (2014) after Hjulström (1935).

Potential sources for the siliciclastic sediment that have been proposed include the Ozark Uplift, which is believed to have been a paleogeographic high during the Mississippian (Huffman, 1958). The Batesville Delta in northeast Arkansas is proposed as a fluvial-deltaic source that supplied siliciclastic sediments in the Late Mississippian (Chesterian) (Glick, 1979). Recent conodont work has indicated that cores located in the study area are predominantly Chesterian in age (Hunt, 2017). Figure 30 shows the relative position of the Batesville Delta as well as the sediment types and interpreted ocean current flow direction. It is probable that each of these played a role in contributing sediment into the Mississippian system.

A fluvial-deltaic system can provide large amounts of sediment. The Amazon River creates a plume of sediment spanning thousands of square kilometers that inhibits both the photic and oxic zones, which partially restricts carbonate production (Moura et al., 2016). This plume is transported by longshore currents and deposited into the Atlantic Ocean. This modern analog may provide insight in explaining how fine siliciclastic sediments came to dominate the composition of both cores in this study.

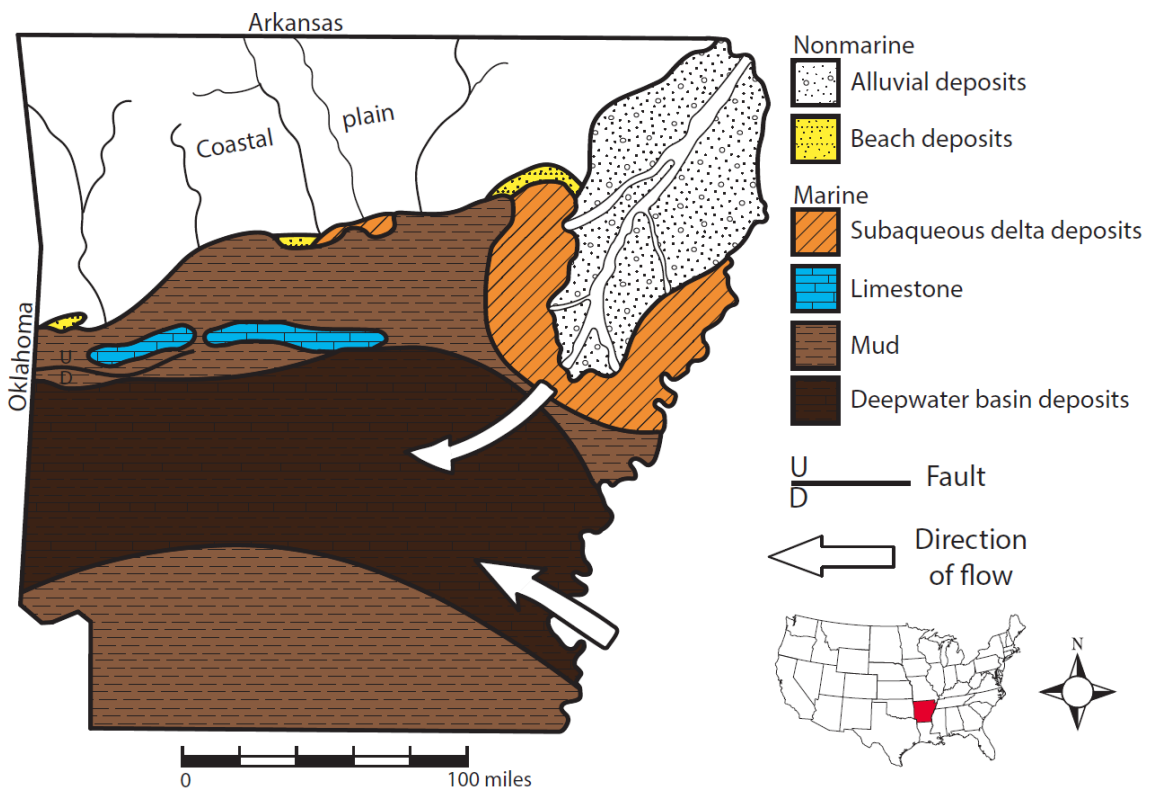


Figure 30: Proposed location of Batesville Delta showing environments and types of sediment deposits. Current flows from East to West into present day Oklahoma. Modified from Glick (1979).

CHAPTER VI

Conclusions

This study utilizes an integrated approach to enhance the predictability of facies assemblages away from cored intervals within Okfuskee County. The sequence stratigraphic framework established in this study used detailed core descriptions and thin section data to identify key sequence stratigraphic surfaces that were then tied to wireline log signatures. Surfaces were found to be regionally correlative. Construction of cross sections and thickness maps offer an improved understanding of the Mississippian system in East-Central Oklahoma. The key conclusions from this study are:

1. Seven primary depositional facies were identified utilizing core and thin section analysis. The facies observed are consistent with deposition on a distally-steepened ramp from beneath FWWB to below SWB. Core and thin sections revealed that fine siliciclastics (very fine sand, silt, and clay) dominate the system with episodic deposition of thin beds of skeletal carbonate grains, likely washed in from up-dip locations.
2. These seven facies were used to define an idealized vertical stacking pattern. Fine siliciclastic sediments dominate the transgressive phases and more carbonate-rich sediments cap the regressive phases.

3. Analysis of the idealized vertical stacking patterns of facies and vertical heterogeneity established a hierarchy of amplitudes of eustatic sea level cyclicity. The hierarchy consists of a probable 2nd order supersequence that contains five 3rd order sequences, and multiple 4th order high frequency sequences.
4. The 3rd order sequence boundaries established in the cores are tied to resolvable wireline log signatures. The gamma-ray tool provided the most consistent signature for subsurface mapping. Resistivity curves were used as a secondary tool in identifying key stratigraphic boundaries in the subsurface. The wireline log signatures associated with the 3rd order sequence boundaries proved to be consistent across multiple townships, and allowed for a regional correlation.
5. Strike elongate cross sections (West to East) display relative lateral continuity of sequence thickness but this should not imply lateral continuity of facies. Dip oriented cross sections display a series of low declivity ($\approx 0.03^\circ$) clinoforms prograding and thinning to the south into the present-day Arkoma Basin. The geometry and distribution of the probable 3rd and 4th order sequences identified in this study are consistent with previous workers' interpretations that Mississippian deposition occurred on a distally-steepened ramp.

REFERENCES

- Asquith, G., and Krygowski D., 2004, Basic Well Log Analysis, Tulsa, American Association of Petroleum Geologists, 244 p.
- Baccelle, L., and Bosellini, A., 1965, Diagrammi per la stima visive della composizione percentuale nelle rocche sedimentary. –Annali dell'Università di Ferrara (Nuova Serie), Sezione 9, Scienze geologiche e paleontologiche, Vol. 1, No. 3, 59-62, 15 Pls.
- Bann, K.L., Tye, S.C., MacEachern, J.A., Fielding, C.R., and Jones, B.G., 2008, Ichnological Signatures and Sedimentology of Mixed Wave- and Storm-dominated Deltaic Deposits: Examples from the Early Permian, Southern Sydney Basin of Southeastern Australia, in Hampson, G., Steel, R., Burgess, P., and Dalrymple, R. (eds.), Recent Advances in Models of Siliciclastic Shallow-Marine Stratigraphy, SEPM Special Publication 90, p. 293-332.
- Bashore, W.M., Araktingi, U.G., Levy, M., Schweller, W.J., 1994, Importance of a Geological Framework and Seismic Data Integration for Reservoir Modeling and Subsequent Fluid-Flow Predictions, in Yarus, J.M., Chambers, R.L. (eds.), Stochastic Modeling and Geostatistics: Principles, Methods, and Case Studies, AAPG Special Volumes Computer Applications 3, p. 159 – 179.
- Berner, R.A., 1981, A New Geochemical Classification of Sedimentary Environments. *Journal of Sedimentary Petrology*, v.51, p. 359 -- 366.
- Bertalott, J., 2014, Core and log based stratigraphic framework of the Mississippian limestone in portions of north-central Oklahoma: unpublished M.S. thesis, Oklahoma State University, 132 p.
- Boardman, D.R., Thompson, T.L., Godwin, C., Mazzullo, S.J., Wilhite, B.W., Morris, B.T., 2013, High-Resolution Conodont Zonation for Kinderhookian (Middle Tournaisian) and Osagean (Upper Tournaisian Lower Visean) Strata of the Western Edge of the Ozark Plateau, North America, *Shale Shaker*, September/October, p. 98 – 151.
- Boggs, S. Jr., 2001, Principles of sedimentology and stratigraphy 3rd. ed. Prentice-Hall, Upper Saddle River, New Jersey: 726 p.

- Canfield, D.E., and Raiswell, R., 1991, Pyrite Formation and Fossil Preservation, in Allison, P.A., and Briggs, D.E.G., eds., *Taphonomy: Releasing the Data Locked in the Fossil Record*: Plenum Press, New York, p. 337 -- 387.
- Canfield, D.E., Raiswell, R., and Bottrell, S., 1992, The Reactivity of Sedimentary Iron Minerals Toward Sulfide. *American Journal of Science*, v. 292, p. 659 – 683.
- Cant, D. 1992. Subsurface facies analysis. In *Facies Models: Response to Sea Level Change*, Geological Association of Canada, *GeoText* 1. p. 27–45.
- Childress, M. and G.M. Grammer, 2015, High-resolution sequence stratigraphic architecture of a Mid-Continent Mississippian outcrop in Southwestern Missouri, *Shale Shaker*. p. 206-234.
- Childress, M. and G.M. Grammer, 2018, Characteristics of Debris Flows and Outrunner Blocks - Evidence for Mississippian-age Deposition on a Distally Steepened Ramp, in Grammer, G.M., J. Gregg, J. Puckette, P. Jaiswal, M. Pranter, S. Mazzullo, and R. Goldstein, editors, *Mississippian Reservoirs of the Mid-Continent, U.S.A.*, American Association of Petroleum Geologists Memoir 116, doi: 10.1306/13632145M1163786
- Choquette, P.W., and Pray, L.C., 1970, Geologic Nomenclature and Classification of Porosity in Sedimentary Carbonates, *AAPG Bulletin*, v. 54, no. 2, p. 207-250.
- Dunham, R.J., 1962, Classification of Carbonate Rocks According to Depositional Texture, *AAPG Special Volumes, Memoir 1: Classification of Carbonate Rocks*, v. 1, p. 108-121.
- Earle, S., 2014, *Physical Geology*, BC Open Textbook Project, p. 338.
- Everett, R.V., McDonald, J.E., and Herron, M.M., 1988, Wireline Geochemical Log Analysis of Thin Bed Reservoirs Gulf of Mexico, *AAPG, Offshore Louisiana Oil and Gas Fields*, Vol. 2, pg. 37-79.
- Flinton, K., 2016, The effects of high-frequency cyclicity on reservoir characteristics of the “Mississippian Limestone”, Anadarko basin, Kingfisher County, Oklahoma, M.S. Thesis, Oklahoma State University, Stillwater, Oklahoma, 175 p.
- Flügel, E., 2010, *Microfacies of Carbonate Rocks: Analysis, Interpretation, and Application*, 2nd Ed., Springer-Verlag, Berlin, Heidelberg, New York, 1007 p.

- Glick, E.E., 1979, Arkansas: in Paleotectonic Investigations of the Mississippian System in the U.S.: Part I, Introduction and Regional Analysis of the Mississippian System: Geological Survey Prof. Paper 1010, pp. 125-145.
- Goddard, E.N., Trask, P.D., De Ford, R.K., Rove, O.N., Singewald, J.T., and Overbeck, R.M., 1951, Rock Color Chart, Geological Society of America, Boulder, Colorado.
- Goldhammer, R.K., Dunn, P.A., and Hardie, L.A., 1990, Depositional cycles, composite sea-level changes, cycle stacking patterns, and the hierarchy of stratigraphic forcing: Examples from Alpine Triassic platform carbonates, Geological Society of America Bulletin, v. 102, p. 535-562.
- Goldhammer, R.K., Oswald, E.J., & Dunn, P. A., 1991, Hierarchy of stratigraphic forcing: Example from Middle Pennsylvanian shelf carbonates of the Paradox Basin, Kansas Geological Survey, Bulletin 233, p. 361-413.
- Grammer, G.M., Harris, P.M., Eberli, G.P., 2001, Carbonate Platforms: Exploration- and production-scale Insight from Modern Analogs in the Bahamas, The Leading Edge, Society of Economic Geophysicists, v. 20, p. 252-261.
- Grammer, G.M., Harris, P.M., Eberli, G.P., 2004, Integration of Outcrop and Modern Analogs in Reservoir Modeling: Overview with Examples from the Bahamas, in G.M. Grammer, P. M. Harris, and G. P. Eberli, eds., Integration of Outcrop and Modern Analogs in Reservoir Modeling: American Association of Petroleum Geologists Memoir 80, p. 1-22.
- Gutschick, R., and Sandberg, C.A., 1983, Mississippian Continental Margins of the Conterminous United States, SEPM Special Publication, no. 33, p. 79-96.
- Handford, C.R., 1986, Facies and Bedding Sequences in Shelf-Storm-Deposited Carbonates – Fayetteville Shale and Pitkin Limestone (Mississippian), Arkansas, Journal of Sedimentary Petrology, v. 56, no. 1, p. 123-137.
- Handford, C.R., and Loucks, R.G., 1993, Carbonate Depositional Sequences and Systems Tracts-Responses of Carbonate Platforms to Relative Sea-Level Changes, In: Loucks, Robert G., and Sarg, Frederick (eds.), Carbonate Sequence Stratigraphy: Recent Developments and Applications, AAPG Memoir 57, p. 3-42.
- Haq, B.U., and Schutter, S.R., 2008, A Chronology of Paleozoic Sea-Level Changes, Science, v. 322, p. 64-68.

- Harms, J.C., Southard, J.B., Spearing, D.R., and Walker, R.G., 1975, Depositional environments as interpreted from primary sedimentary structures and stratification sequences: SEPM, Short Course 2, 161 p.
- Harms, J.C., Southard, J.B., and Walker, R.G., 1982, Structure and Sequence in Clastic Rocks, SEPM Short Course Notes, V. 9, 51 p.
- Harris, P.M., 2009, Heterogeneity within Carbonate Reservoirs – Guidelines from Modern Analogs, AAPG Search and Discovery Article #60039, 97 p.
- Hjulström, F. (1935). Studies of the morphological activity of rivers as illustrated by the River Fyris, Bulletin, Geological Institute Upsalsa, 25, p. 221-527.
- Huffman, G. G., 1958, Geology of the Ozark Uplift, Northeastern Oklahoma, Oklahoma City Geological Society, The Shale Shaker Digest I, v. I-V, p. 36-42.
- Hunt, J.E., 2017, Conodont biostratigraphy in middle Osagean to upper Chesterian strata, north-central Oklahoma, USA, M.S. Thesis, Oklahoma State University, Stillwater, 167 p.
- Jaeckel, J., 2016, High Resolution Sequence Stratigraphy and Reservoir Characterization of Mid-Continent Mississippian Carbonates in North-Central Oklahoma and South Central Kansas, M.S. Thesis, Oklahoma State University, Stillwater, Oklahoma, 357 p.
- Kent, D.V., Olsen, P.E., Rasmussen, C., Lepre, C., Mundil, R., Imis, R.B., Gehrels, G.E., Giesler, D., Geissman, J.W., and Parker, W.G., 2018, Empirical Evidence for Stability of the 405-Kiloyear Jupiter –Venus Eccentricity Cycle Over Hundreds of Millions of Years, Proceedings of the National Academy of Sciences of the United States of America, www.pnas.org/cgi/doi/10.1073/pnas.1800891115 accessed May 2018.
- Kerans, C., and Tinker, S.W., 1997, Sequence stratigraphy and characterization of carbonate reservoirs: SEPM, Short Course Notes no. 40, p. 1-130.
- LeBlanc, S.E., 2014, High Resolution Sequence Stratigraphy and Reservoir Characterization of the “Mississippian Limestone” in North-Central Oklahoma, M.S. Thesis, Oklahoma State University, Stillwater, Oklahoma, 443 p.
- Lobza, V., and Schieber, J., 1999, Biogenic Sedimentary Structures Produced by Worms in Soupy, Soft Muds: Observations from the Chattanooga Shale (Upper

Devonian) and Experiments. *Journal of Sedimentary Research*, v. 69, p. 1041-1049

- Major, R.P., Bebout, D.G., and Harris, P.M., 1996, Facies Heterogeneity in a Modern Ooid Sand Shoal – an Analog for Hydrocarbon reservoirs: Bureau of Economic Geology, Geological Circular 96-1, University of Texas at Austin, 30 p.
- Marsh, S., and Holland, A., 2016, Comprehensive Fault Database and Interpretive Fault Map of Oklahoma, Oklahoma Geological Survey Open-File Report, OF2-2016.
- Mazzullo, S.J., Wilhite, B.W., and Woolsey, I.W., 2009, Rhythmic Carbonate Versus Spiculite Deposition in Mississippian Hydrocarbon Reservoirs in the Midcontinent USA: Causative factors and resulting reservoir petrophysical attributes, AAPG Search and Discovery Article #10209, 6 p.
- Mazzullo, S.J., Wilhite, B.W., and Morris, B.T., 2011, Mississippian Oil Reservoirs in the Southern Midcontinent: New exploration concepts for a mature reservoir objective, AAPG Search and Discovery Article #10373, 34 p.
- Middleton, G.V., Church, M.J., Coniglio, M., Hardie, L.A., and Longstaffe, F.J., 2003, *Encyclopedia of Sediments and Sedimentary Rocks*, Kluwer Academic Publishers, The Netherlands, 821 p.
- Miller, J.D., Puckette, J.O., Godwin, C.J., 2017, Conodont biostratigraphy-constrained diachronous lithofacies, Boone Group (upper Osagean to lower Meramecian), western Ozarks: breakdown of lithostratigraphic correlations at the regional Scale, in Grammer, G. M., Gregg, J. M., Puckette, J. O., Jaiswal, P., Mazzullo, S. J., Pranter, M. J., and Goldstein, R. H., editors, *Mississippian Reservoirs of the Mid-Continent, U.S.A.*, American Association of Petroleum Geologists Memoir 116, doi:10.1306/13632143M1163785
- Moura, R.L., Amado-Filho, G.M., Moraes, F.C., Brasileiro, P.S., Salomon, P.S., Mahiques, M.M., 2016, An extensive reef system at the Amazon River mouth. *Science Advances* 2:e1501252
- Northcutt, R.A., and Campbell, J.A., 1996. Geologic provinces of Oklahoma, transactions of the 1995 AAPG mid-continent section meeting, 1996, p. 128-134.
- Oklahoma Fault Database, 2017. Oklahoma Geological Survey. Retrieved from <http://www.ou.edu/ogs/data/fault> accessed October 2018.

- Poppe, L.J., Paskevich, V.F., Hathaway, J.C., and Blackwood, D.S., 2001, A Laboratory Manual for X-Ray Powder Diffraction; U.S. Geological Survey Open-File Report 01-041.
- Price, B. and G.M. Grammer, 2017, High Resolution Sequence Stratigraphy and Reservoir Characterization of the Mississippian Burlington/Keokuk Formation, Northwestern Arkansas, in Grammer, G.M., J. Gregg, J. Puckette, P. Jaiswal, M. Pranter, S. Mazzullo, and R. Goldstein, editors, Mississippian Reservoirs of the Mid-Continent, U.S.A., American Association of Petroleum Geologists Memoir 116, doi: 10.1306/13632147m1163787
- Read, J.F., 1982, Carbonate platforms of passive (extensional) continental margin-types, characteristics and evolution, *Tectonophysics*, 81, p. 195-212.
- Read, J.F., 1985, Carbonate Platform Facies Models, *The American Association of Petroleum Geologists Bulletin*, v. 69, no. 1, p. 1-21.
- Read, J.F., 1995, Overview of Carbonate Platform Sequences, Cycle Stratigraphy and Reservoirs in Greenhouse and Icehouse Worlds, In: Read, J. F., Kerans, C., Weber, L. J., Sarg, J. F., and Wright, F. M. (eds.), *Milankovitch Sea Level Changes, Cycles, and Reservoirs on Carbonate Platforms in Greenhouse and Ice-House Worlds: SEPM Short Course 35*, p. 1-102.
- Roundtree, R., Wright, J., and Miskimins, J., 2010, Unconventional Resource Recovery Improvement Using Conventional Reservoir Engineering Strategies, *AAPG Search and Discovery Article #80088*, 15 p.
- Schieber, J., 2003, Simple Gifts and Buried Treasures –Implications of Finding Bioturbation and Erosion Surfaces in Black Shales, *The Sedimentary Record*, v. 1, no. 2, p. 4 – 8.
- Scholle, P.A., and Ulmer-Scholle, D.S., 2003, A Color Guide to the Petrography of Carbonate Rocks: Grains, Textures, Porosity, Diagenesis, *AAPG Memoir 77*, Tulsa, The American Association of Petroleum Geologists, 474 p.
- Shelley, S., Grammer, G.M., and Pranter, M.J., 2017, Reservoir Characterization and Modeling of a Subsurface Meramec Analog from a Quarry in Northeastern Oklahoma, *Shale Shaker*, vol. 68, no. 5, p. 224-243.
- Shelley, S., Grammer, G.M., and Pranter, M.J., 2018, Outcrop-based reservoir characterization and modeling of an Upper Mississippian mixed carbonate-siliciclastic ramp, Northeastern Oklahoma, *in* Grammer, G.M., J. Gregg, J.

- Puckette, P. Jaiswal, M. Pranter, S. Mazzullo, and R. Goldstein, editors, Mississippian Reservoirs of the Mid-Continent, U.S.A., American Association of Petroleum Geologists Memoir 116, doi:10.1306/136321482158M1163788
- Sturdivant, S.K., Diaz, R.J., Cutter, G.R., 2012, Bioturbation in a Declining Oxygen Environment, *in situ* Observations from Wormcam, PLoS ONE 7(4): e34539. doi: 10.1371/journal.pone.0034539
- Suneson, N.H., 2012, Arkoma Basin petroleum – past, present, and future, Shale shaker, July – August 2012, p. 38-70.
- Tucker, M.E., and V.P. Wright, 1990, Carbonate Sedimentology: Blackwell Scientific Publications, 482 p.
- USGS XRD, 2000, United States Geological Survey. Retrieved from <https://pubs.usgs.gov/info/diffraction/html/> accessed October, 2018.
- Watney, L., Guy, W.J., and Byrnes, A.P., 2001. Characterization of the Mississippian chat in south-central Kansas. AAPG Bulletin v. 85 no. 1 p. 85-113
- Watney, L., 2014, Fluid migration and accumulation within the Mississippian: Why 2% oil cut here, 15% oil cut one mile away, AAPG Search and Discovery Article # 50953.
- Wilhite, B.W., Mazzullo, S.J., Morris, B.T., and Boardman, D.R. II, 2011, Syndepositional Tectonism and its Effects on Mississippian (Kinderhookian to Osagean) Lithostratigraphic Architecture: Part 1 – Based on Exposures in the Midcontinent USA, AAPG Search and Discovery Article #30207, 4 p.

APPENDICES

Appendix A: Angell 1-23

- I. Whole Core Photographs
- II. Core Descriptions
- III. Thin Section Photomicrographs
- IV. X-Ray Diffraction Analysis

Appendix B: Wise 1-20

- I. Whole Core Photographs
- II. Core Descriptions
- III. X-Ray Diffraction Analysis

Appendix C: Mississippian Stratal Architecture

- I. Subsurface Cross Section Reference Map
- II. Subsurface Cross Sections
- III. Depth to Mississippian-Pennsylvanian Contact Structure Map
- IV. Depth to Basal Mississippian Contact (Top of Woodford Shale) Structure Map
- V. "4th Order" Sequence Thickness Maps

Appendix A:

Angell 1-23

I. Angell 1-23 Whole Core Photographs

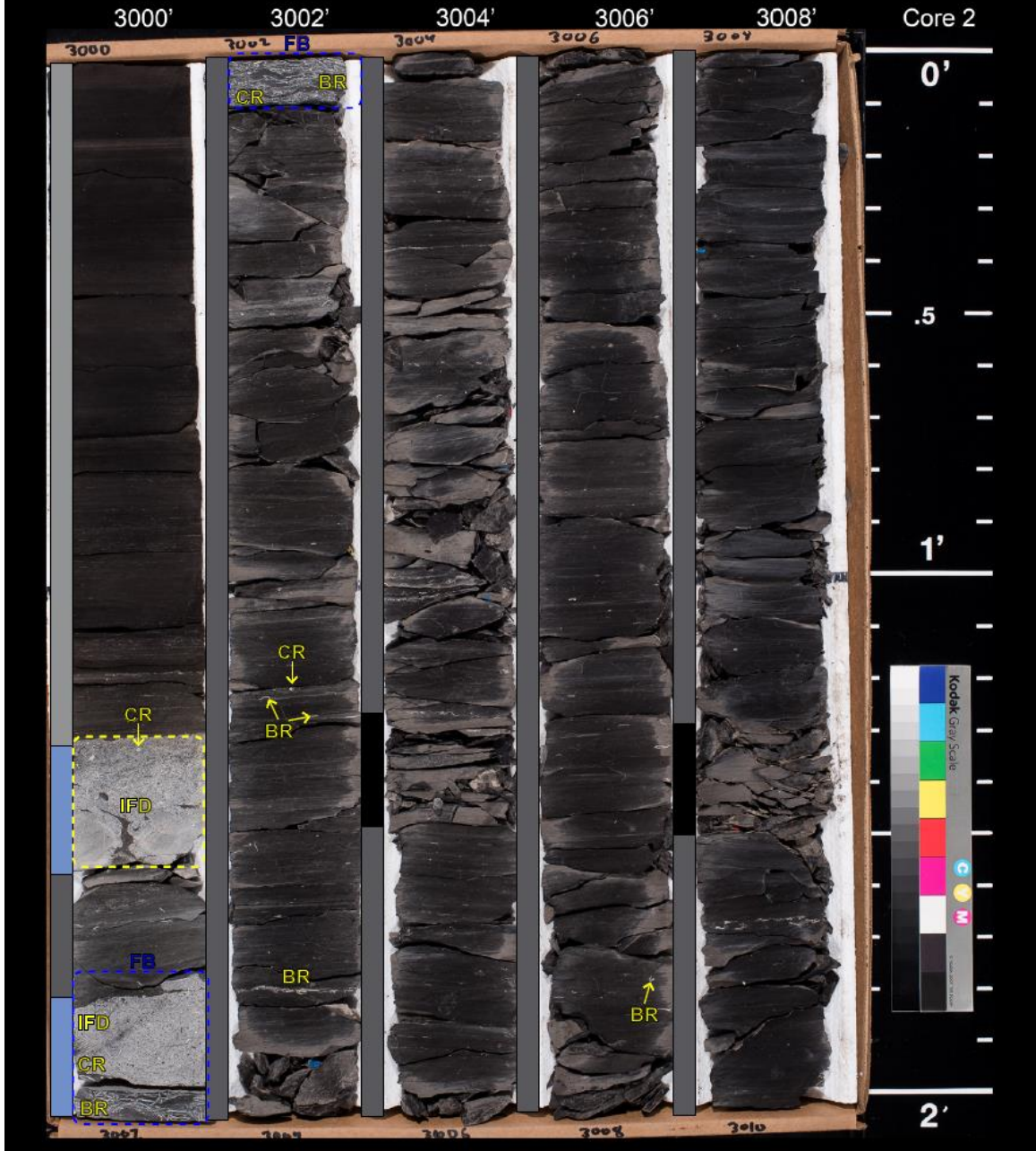
Core Photographs are shown under white light and are labeled with the abbreviations in the table shown below (Table 5). The core is in boxes containing 10 feet of core (when full) and within each box, cores are split into 2 foot intervals. The shallowest depths are located in the top left corner of the boxes, while the deepest depths are in the bottom right corner. The scales next to the core boxes are in tenths of feet. The contacts between the “Mississippian Limestone” and differing strata are marked where present. Next to the cores are colored rectangles that correspond to the facies stacking pattern colors (see Figure 15).

Core Image Labels			
AM	Ammonite	LAM	Lamination
BR	Brachiopod	MTD	Mass transport deposit
BU	Burrow	Oo	Ooid
CC	Clay clast	PH	Phosphate
CR	Crinoid	PSD	Possible Storm Deposit
FB	Fossil Bed	PY	Pyrite
FR	Fracture	PY-BU	Pyritized Burrow
G	Glauconite	RMC	Rip-up mud clast
IFD	Indistinguishable fossil debris	XB	Cross bedding

Table 5: Core image labels for the Angell 1-23 and Wise 1-20

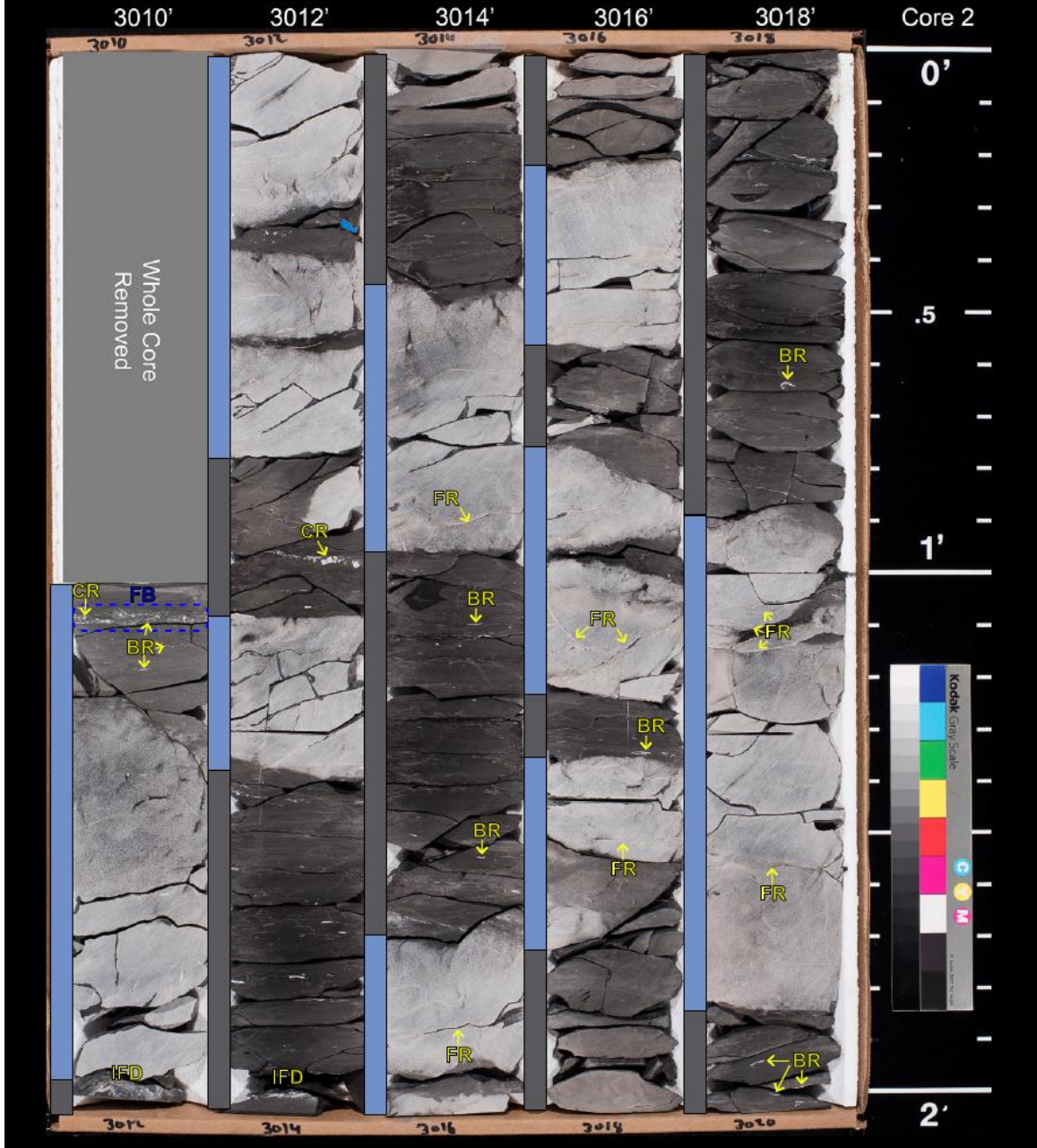
Angell 1-23

Okfuskee County, OK



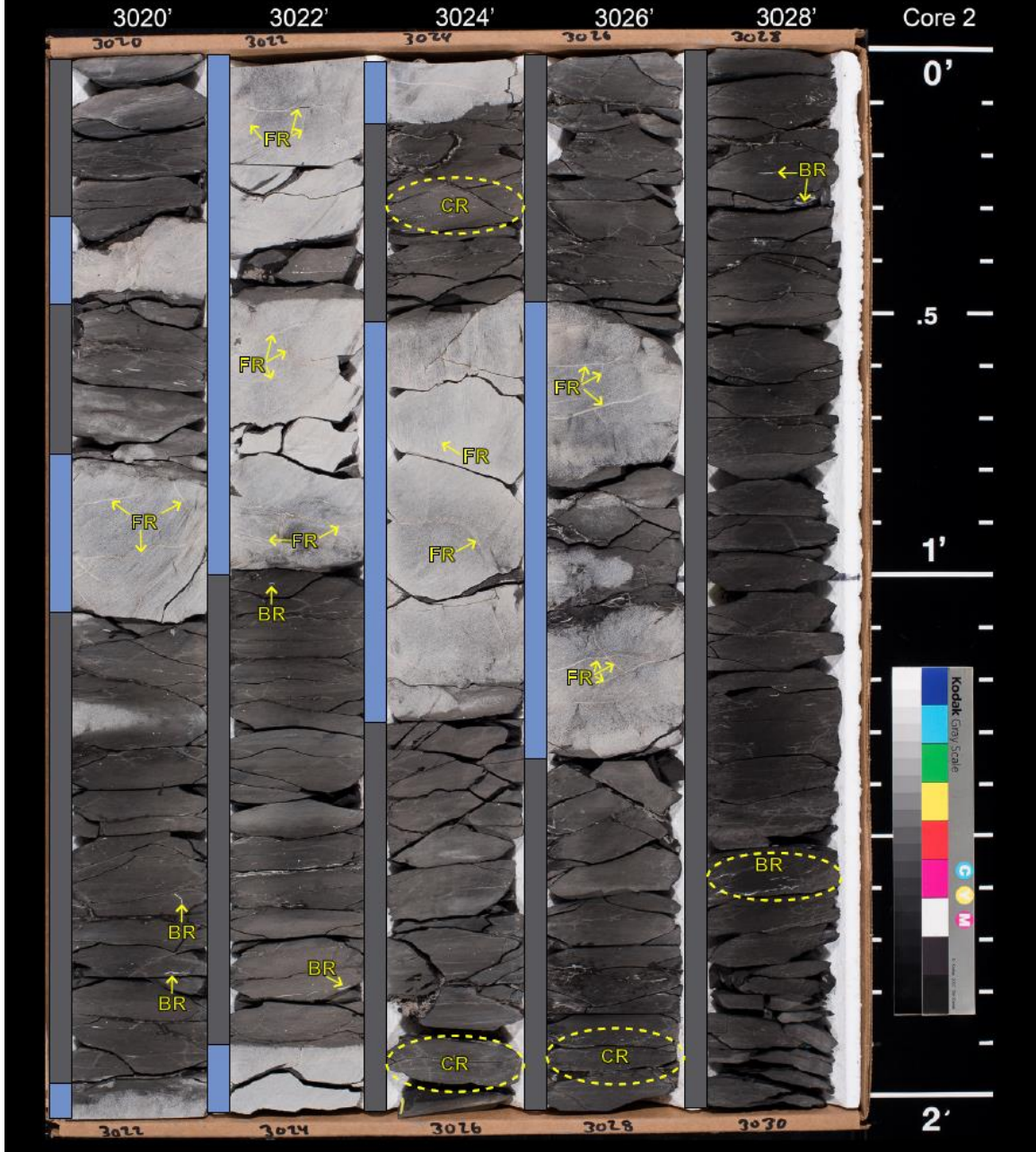
Angell 1-23

Okfuskee County, OK



Angell 1-23

Okfuskee County, OK



Angell 1-23

Okfuskee County, OK

3030'

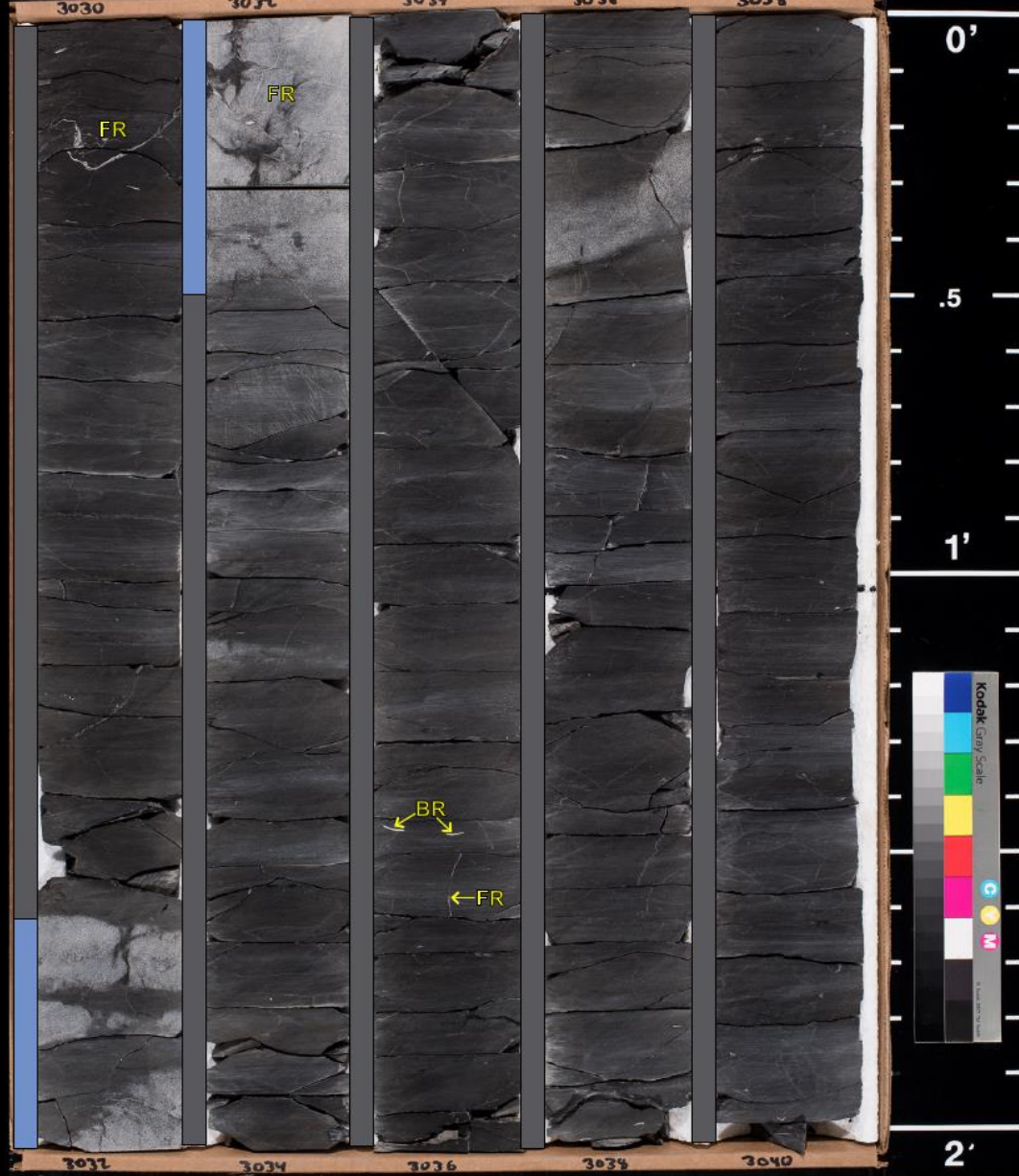
3032'

3034'

3036'

3038'

Core 3



3030

3032

3034

3036

3038

3032

3034

3036

3038

3040

0'

.5

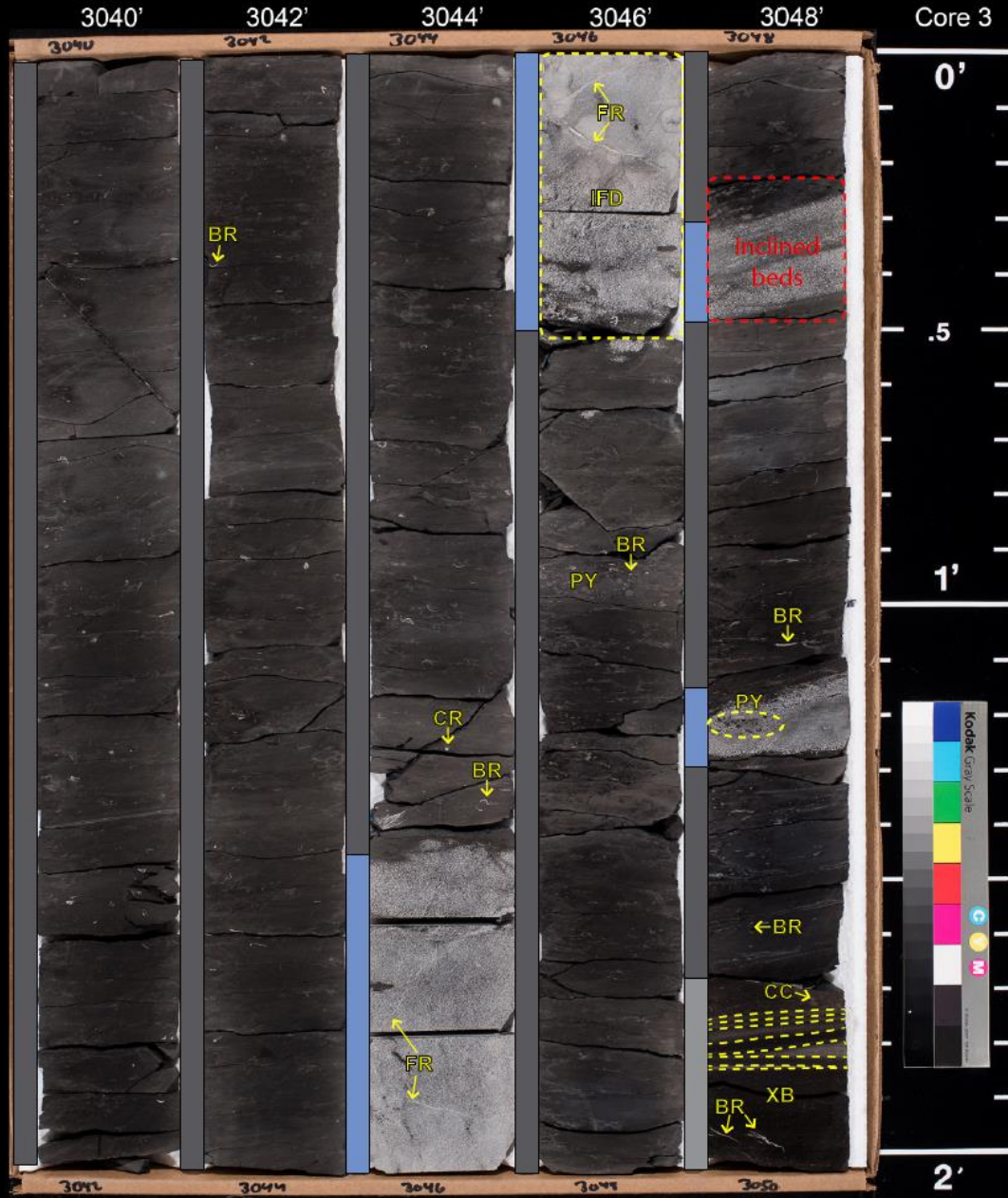
1'

2'



Angell 1-23

Okfuskee County, OK



Angell 1-23

Okfuskee County, OK

3050'

3052'

3054'

3056'

3058'

Core 3

3050

3052

3054

3056

3058

Whole Core
Removed

←FR→

MTD

IFD

Oo

CC

IFD

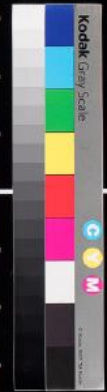
←CR→

0'

.5

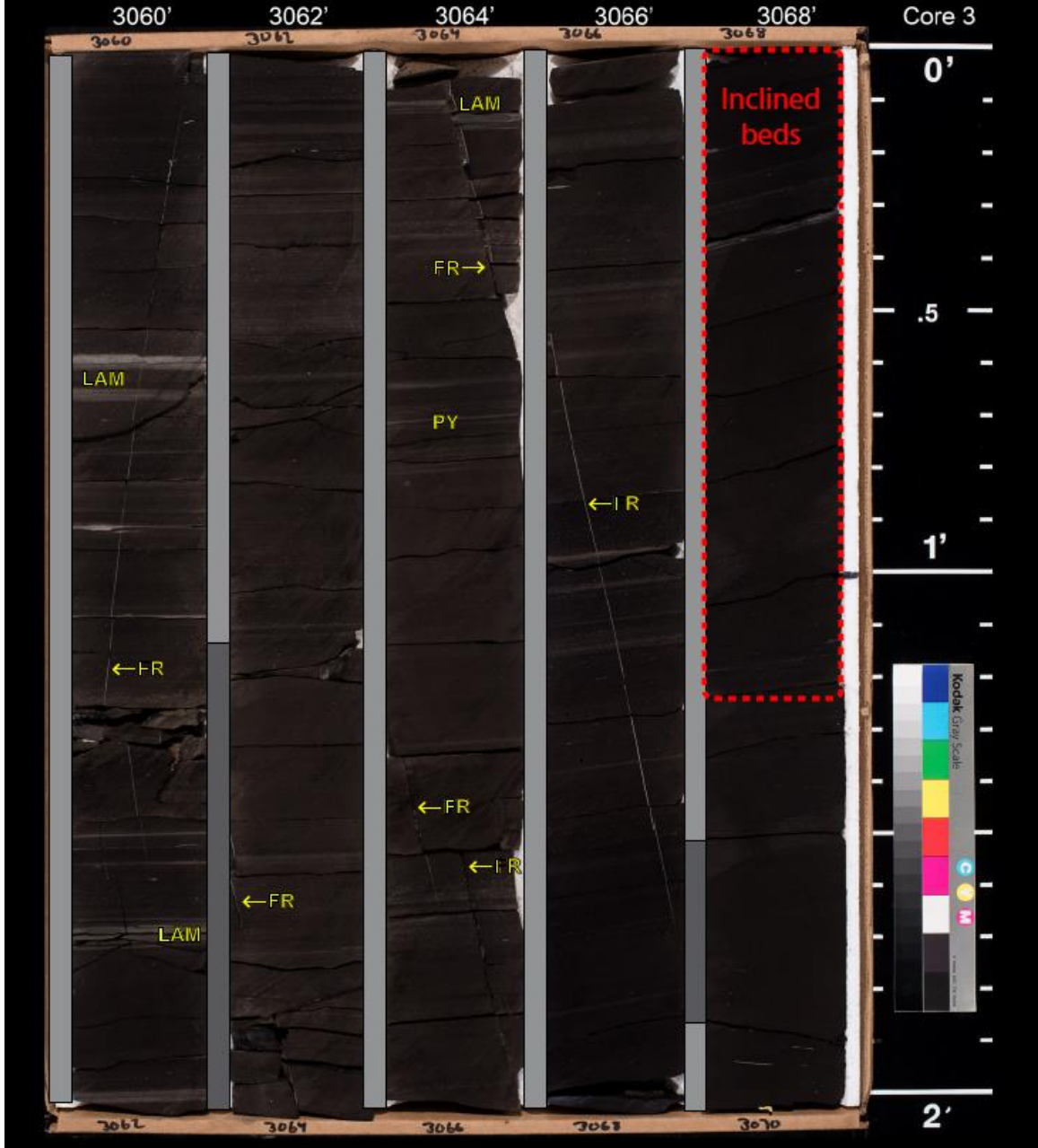
1'

2'



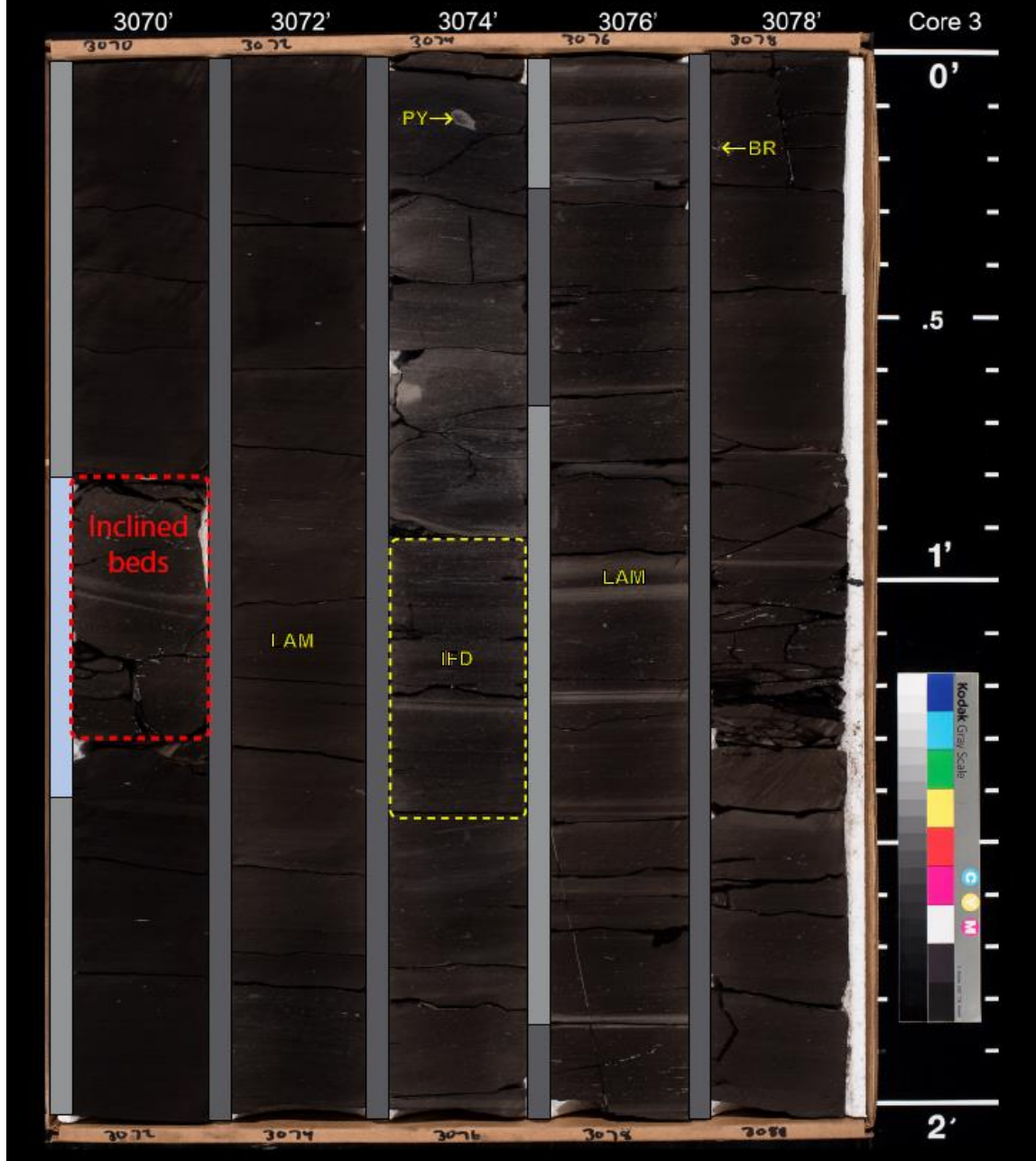
Angell 1-23

Okfuskee County, OK



Angell 1-23

Okfuskee County, OK



Angell 1-23

Okfuskee County, OK

3080'

3082'

3084'

3086'

Core 3



Whole Core
Removed

FR

LAM

End of
Core 3

LAM

0'

.5

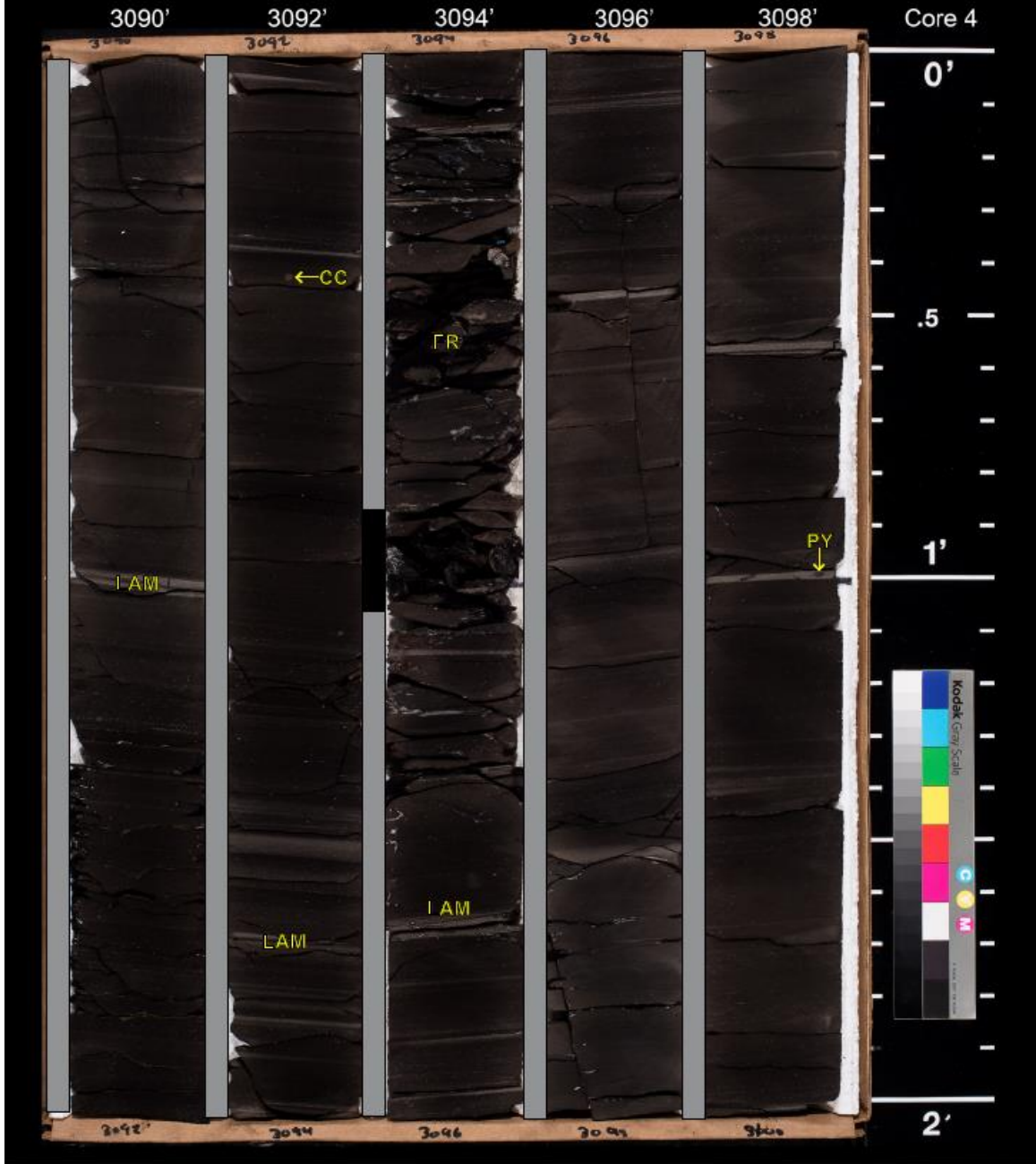
1'

2'



Angell 1-23

Okfuskee County, OK



Angell 1-23

Okfuskee County, OK



Angell 1-23

Okfuskee County, OK



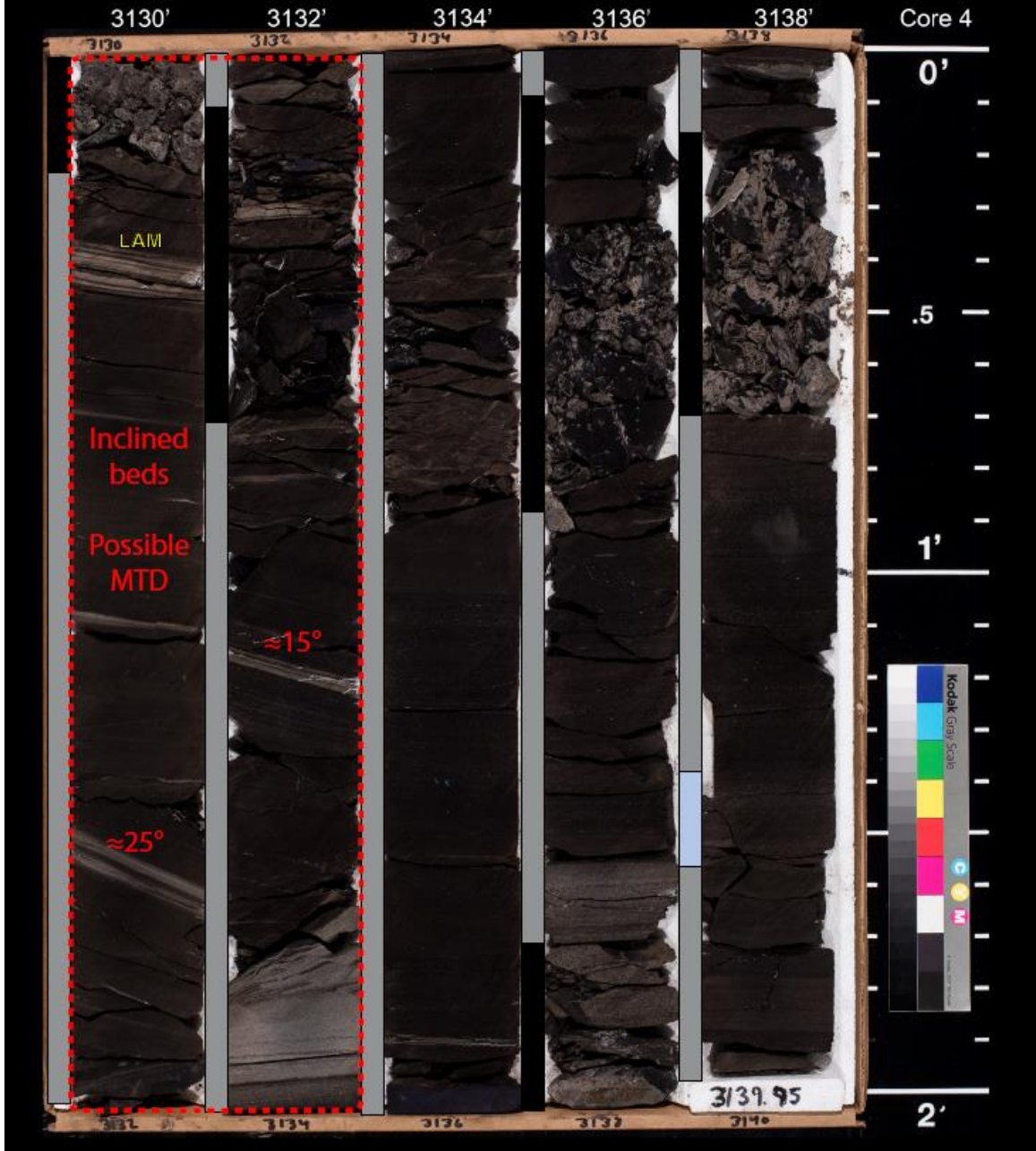
Angell 1-23

Okfuskee County, OK



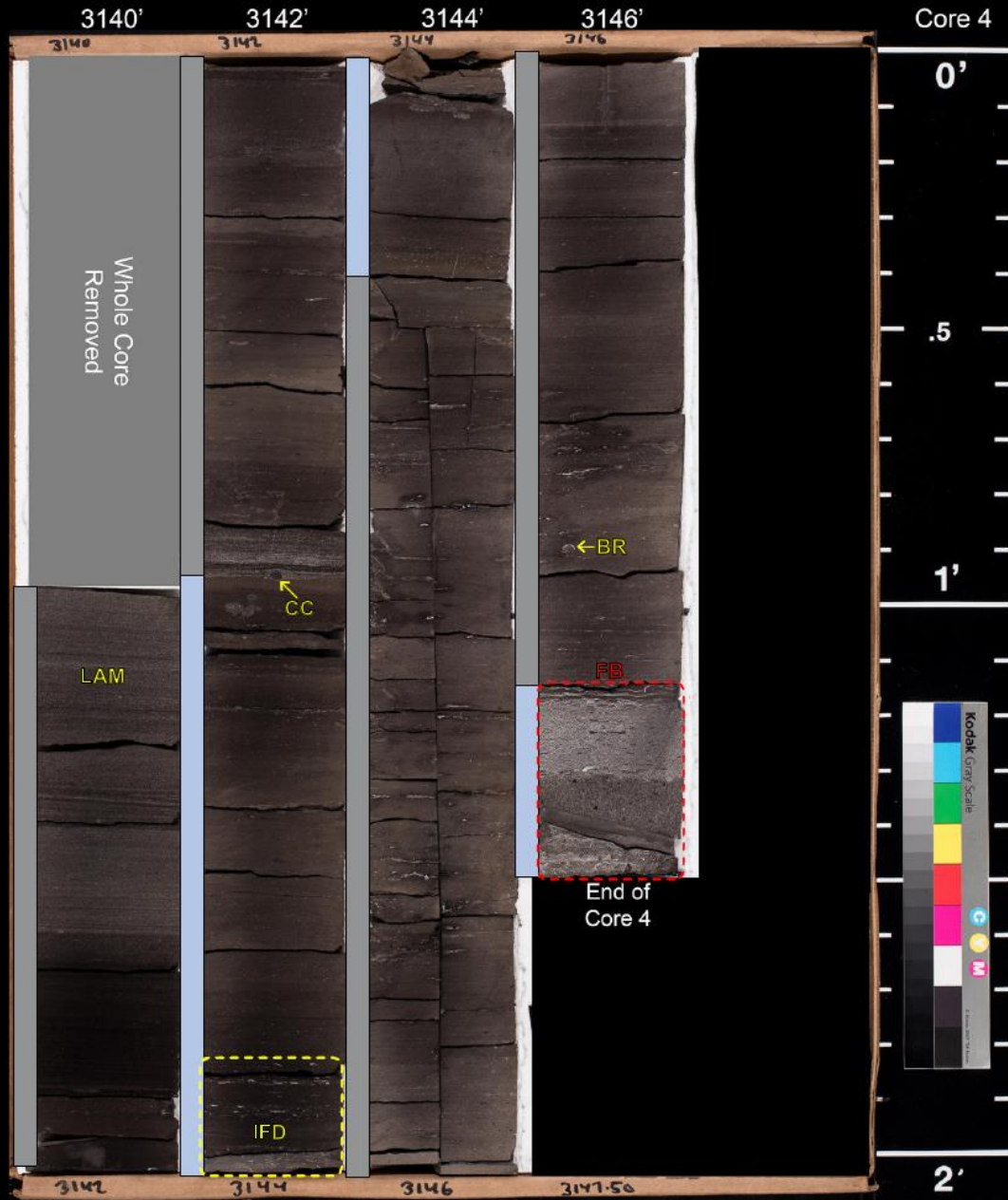
Angell 1-23

Okfuskee County, OK



Angell 1-23

Okfuskee County, OK



3140'

3142'

3144'

3146'

Core 4

0'

.5

1'

2'

3140

3142

3144

3146

3142

3144

3146

3147.50

Whole Core
Removed

LAM

CC

IFD

←BR

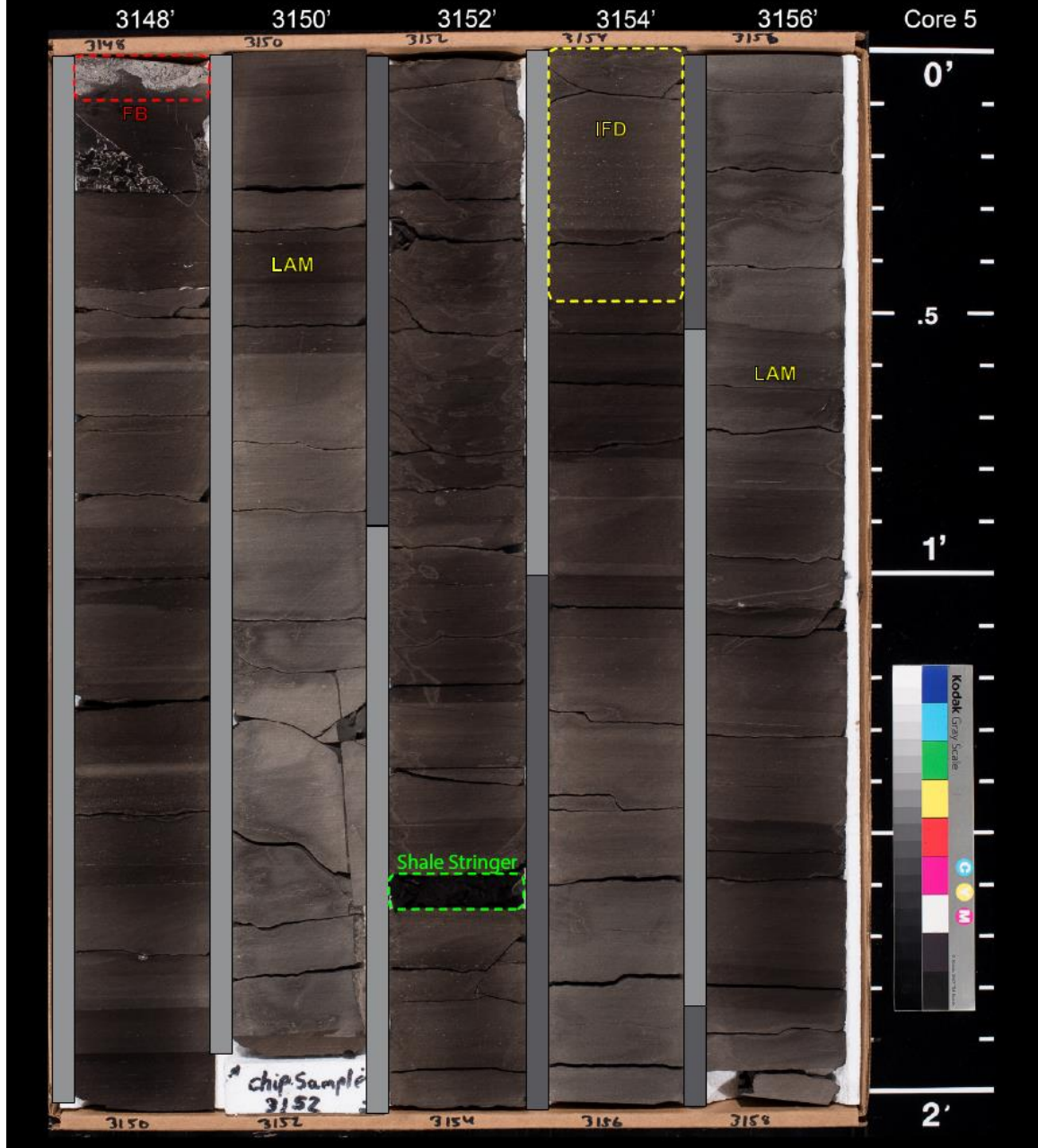
FB

End of
Core 4



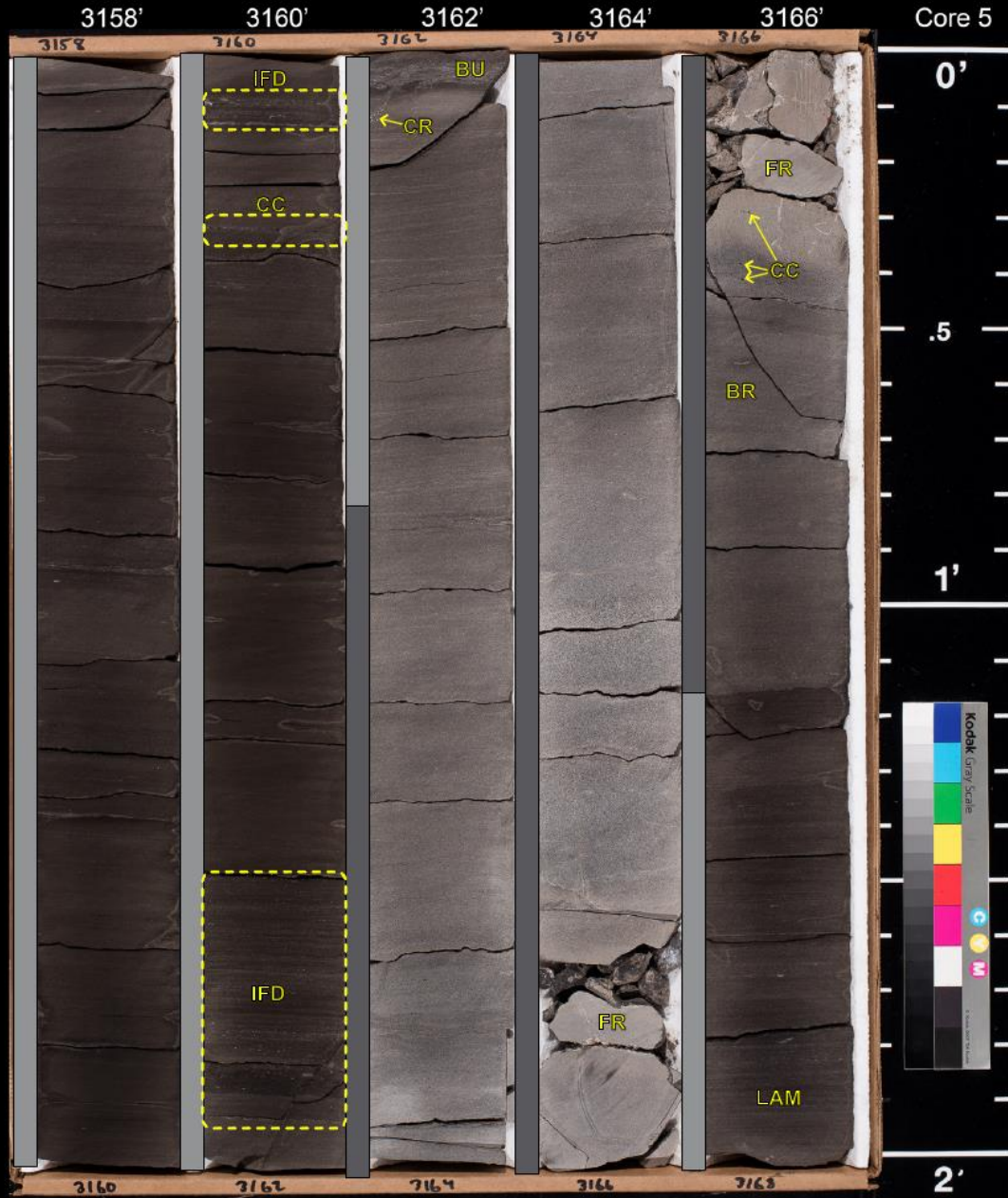
Angell 1-23

Okfuskee County, OK



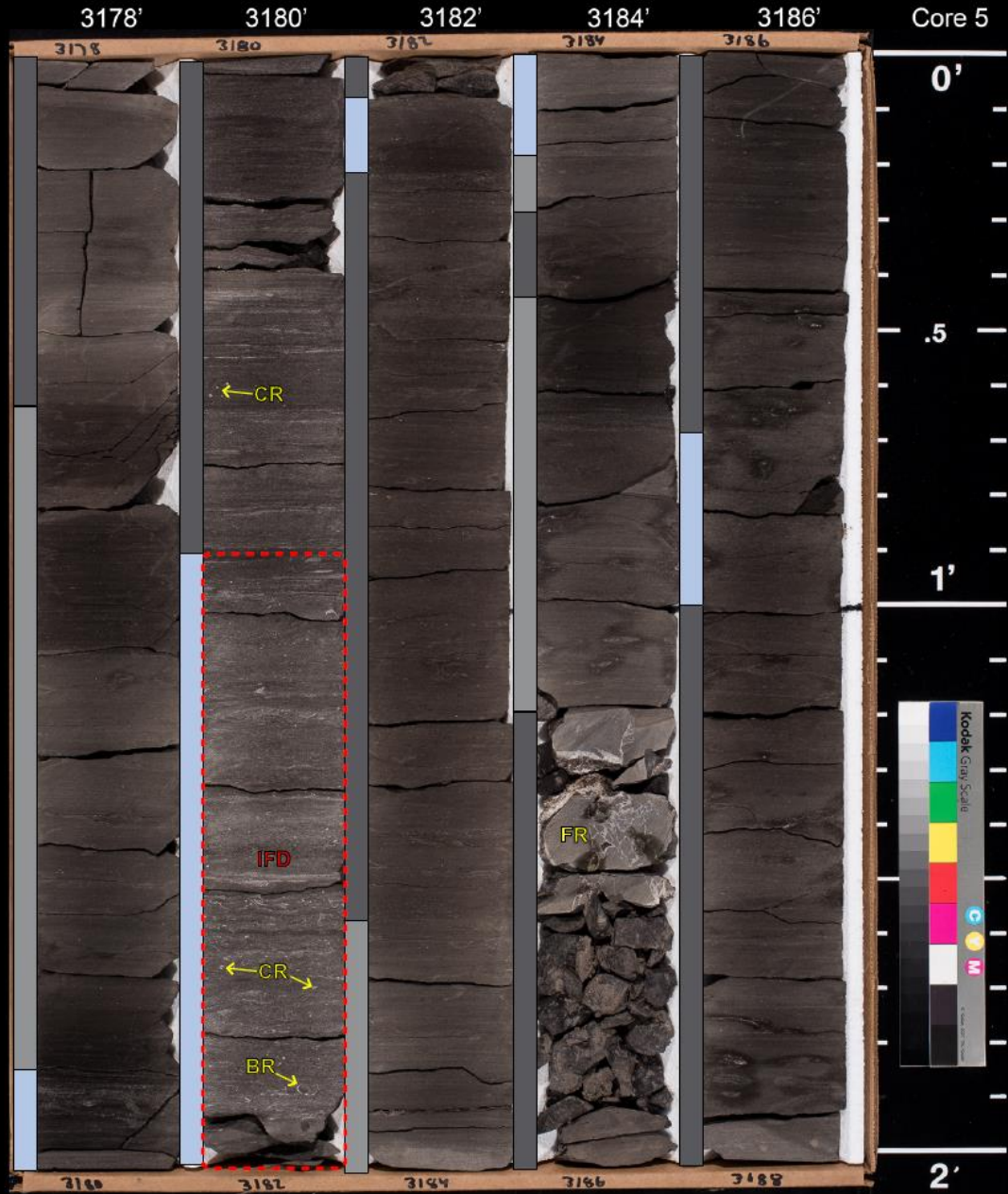
Angell 1-23

Okfuskee County, OK



Angell 1-23

Okfuskee County, OK



Angell 1-23

Okfuskee County, OK

3188'

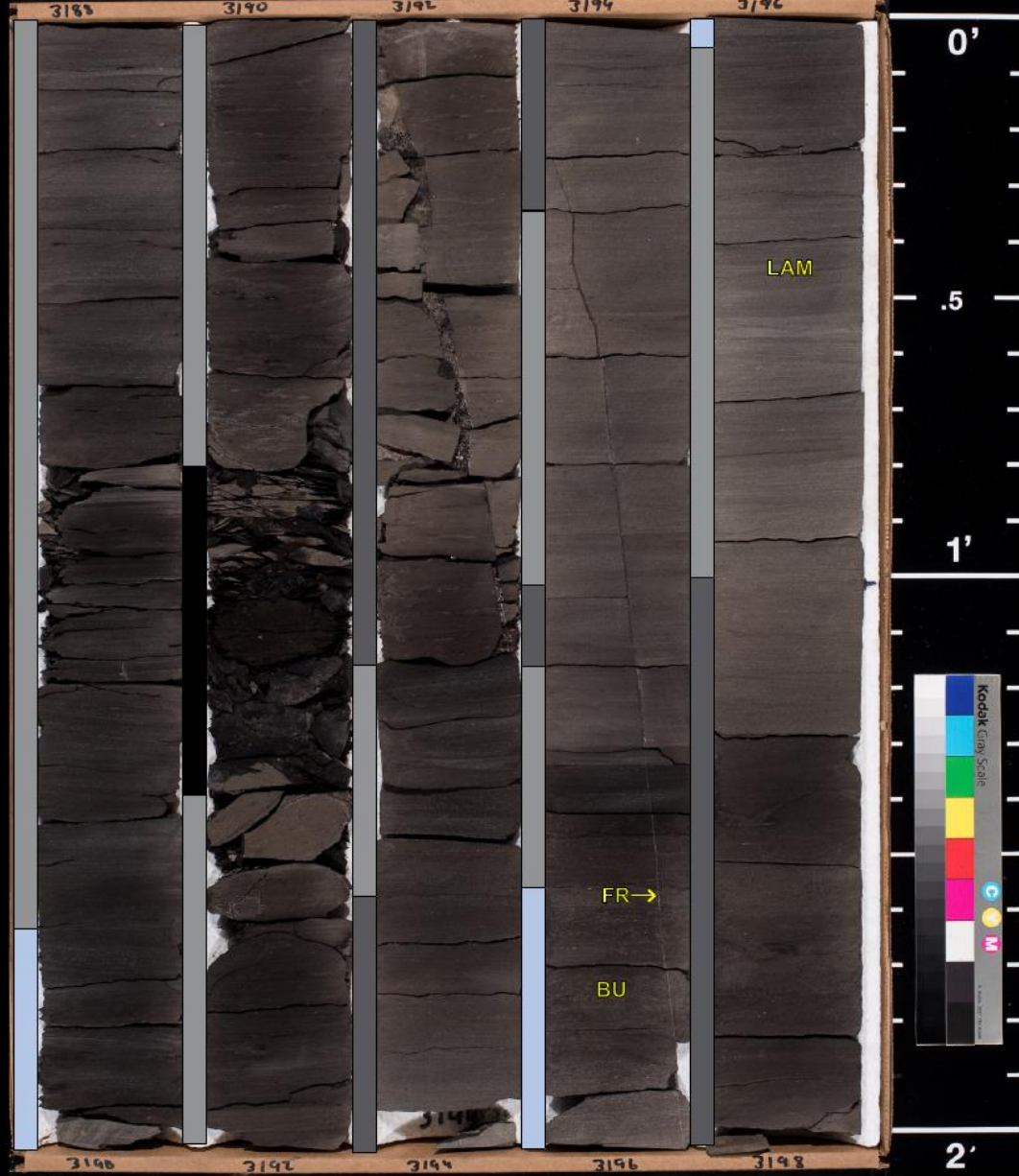
3190'

3192'

3194'

3196'

Core 5



0'

.5

1'

2'

LAM

FR →

BU



3188

3190

3192

3194

3196

3196

3192

3194

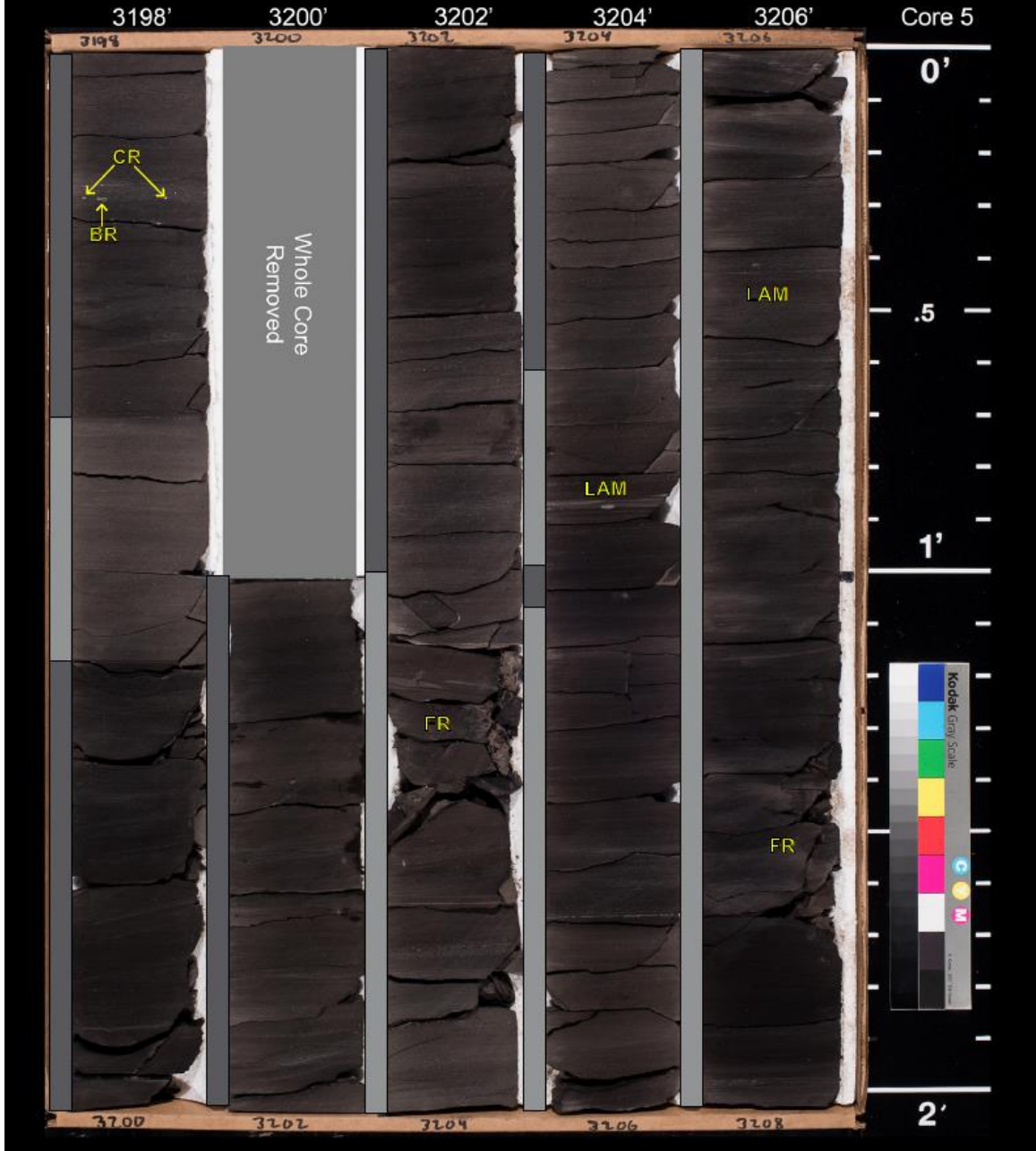
3196

3198

3194

Angell 1-23

Okfuskee County, OK



Angell 1-23

Okfuskee County, OK

3208'

3210'

3212'

3214'

3216'

Core 5

0'

.5

1'

XB

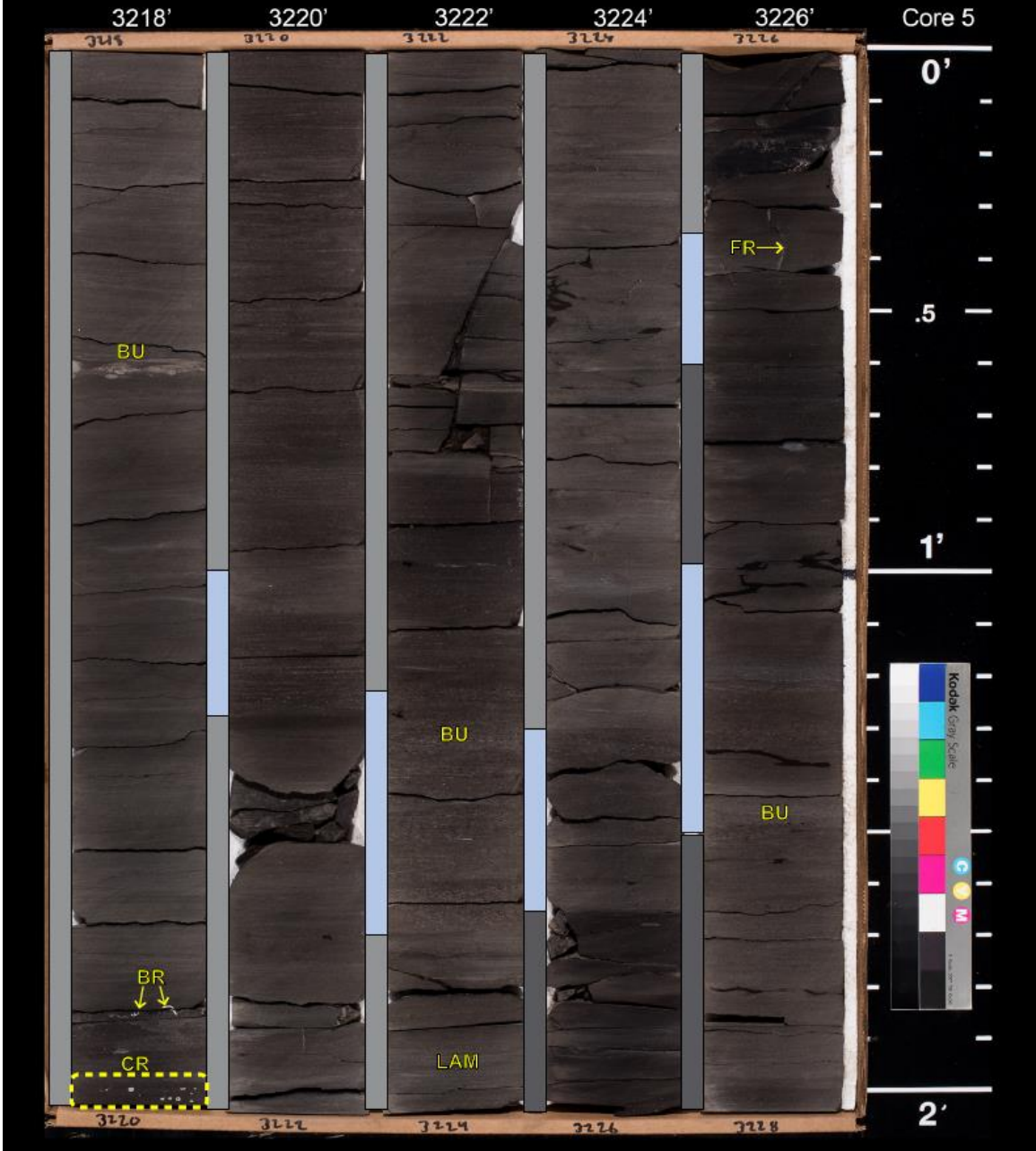
CR

2'



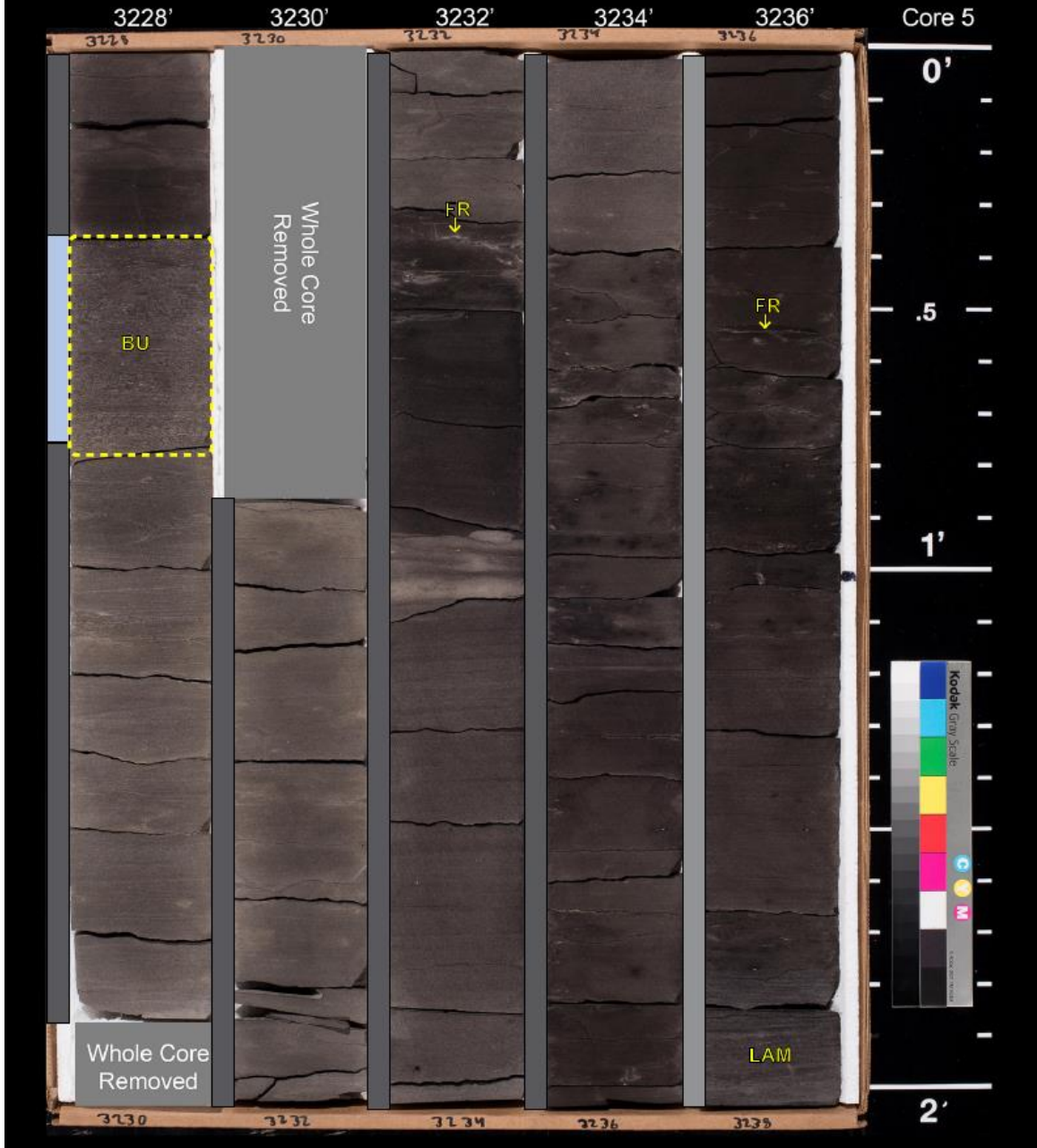
Angell 1-23

Okfuskee County, OK



Angell 1-23

Okfuskee County, OK

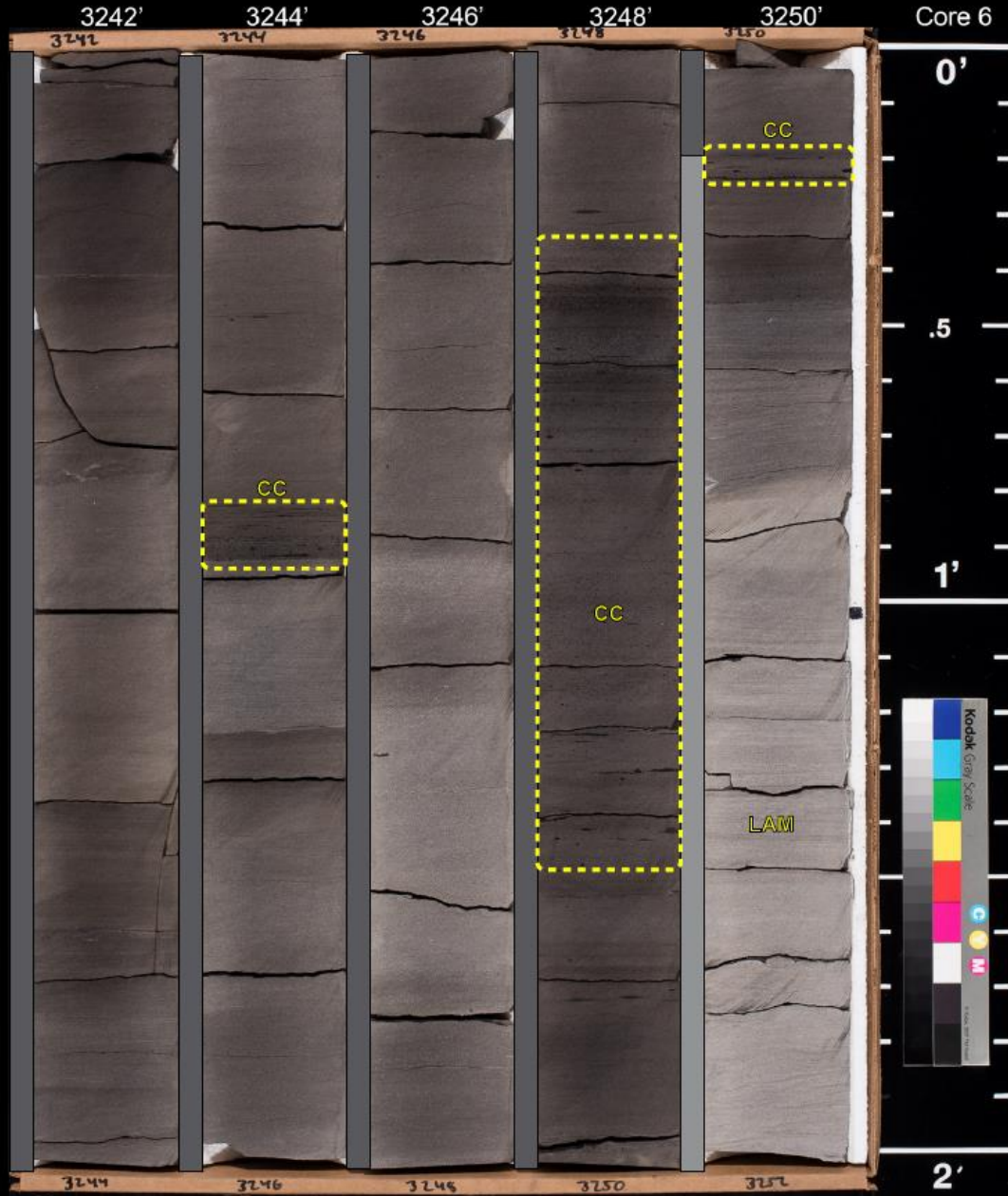


Angell 1-23
Okfuskee County, OK



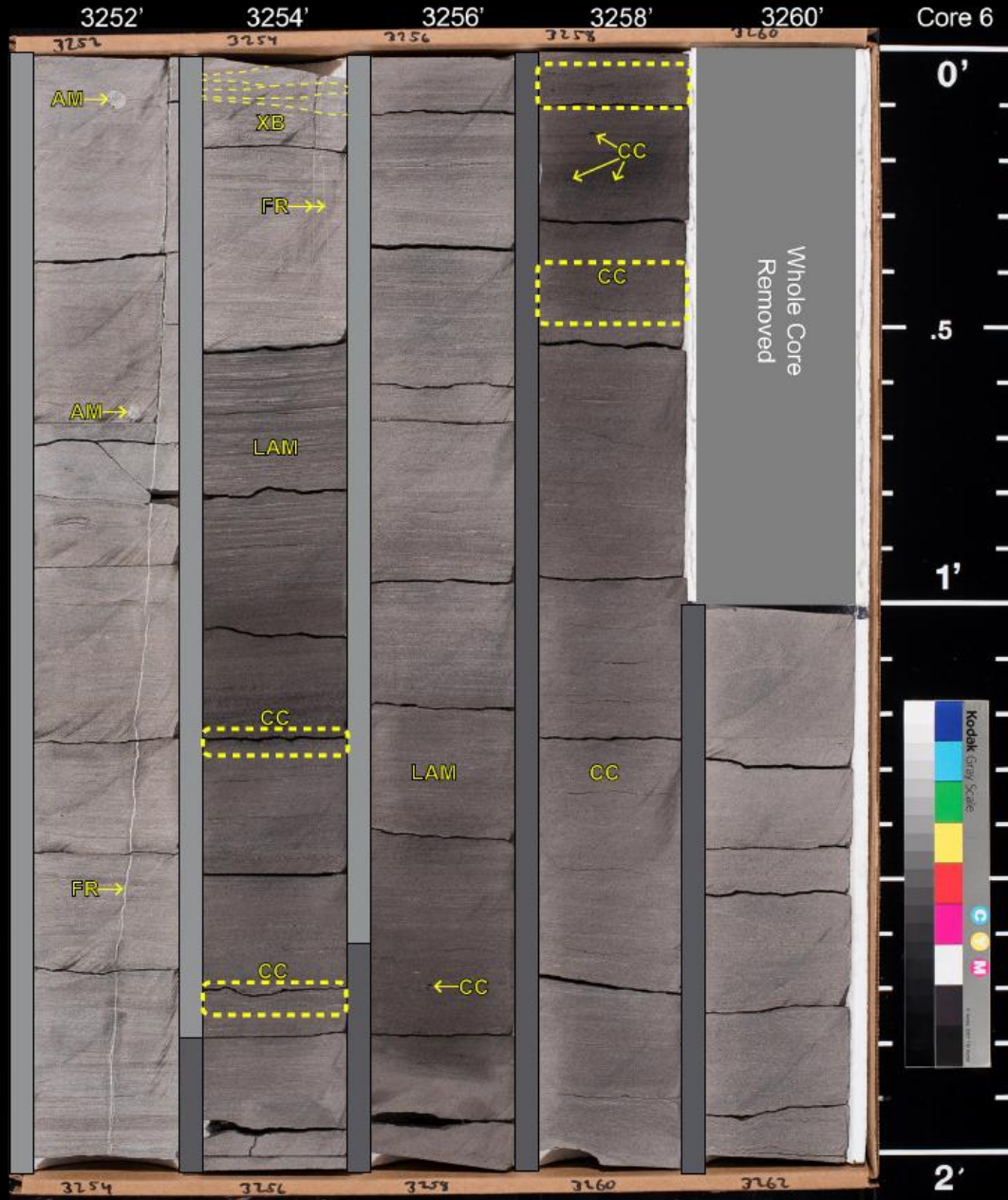
Angell 1-23

Okfuskee County, OK



Angell 1-23

Okfuskee County, OK



Angell 1-23

Okfuskee County, OK

3262'

3264'

3266'

3268'

3270'

Core 6



0'

.5

1'

2'



CC

LAM

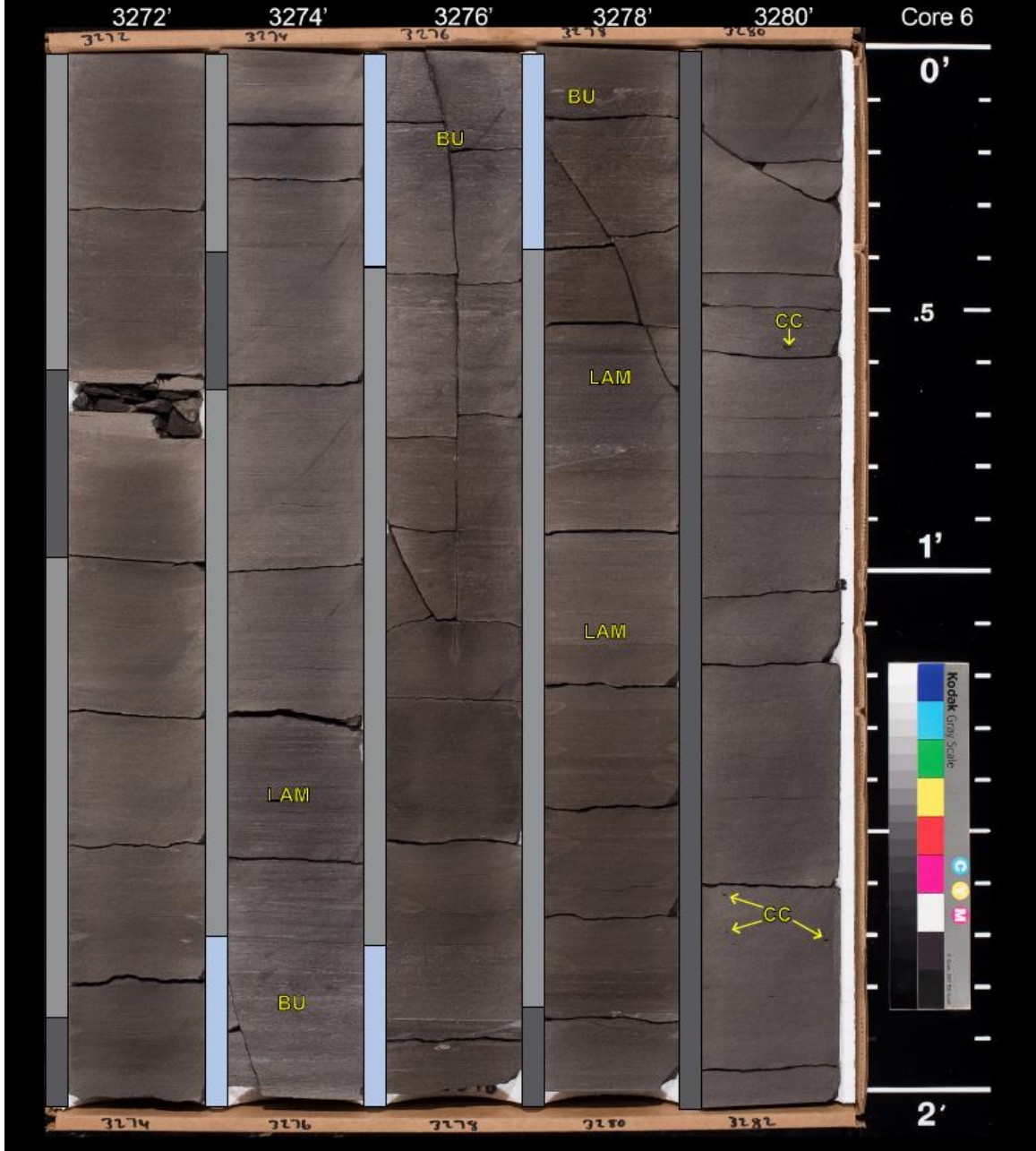
LAM

LAM

CC

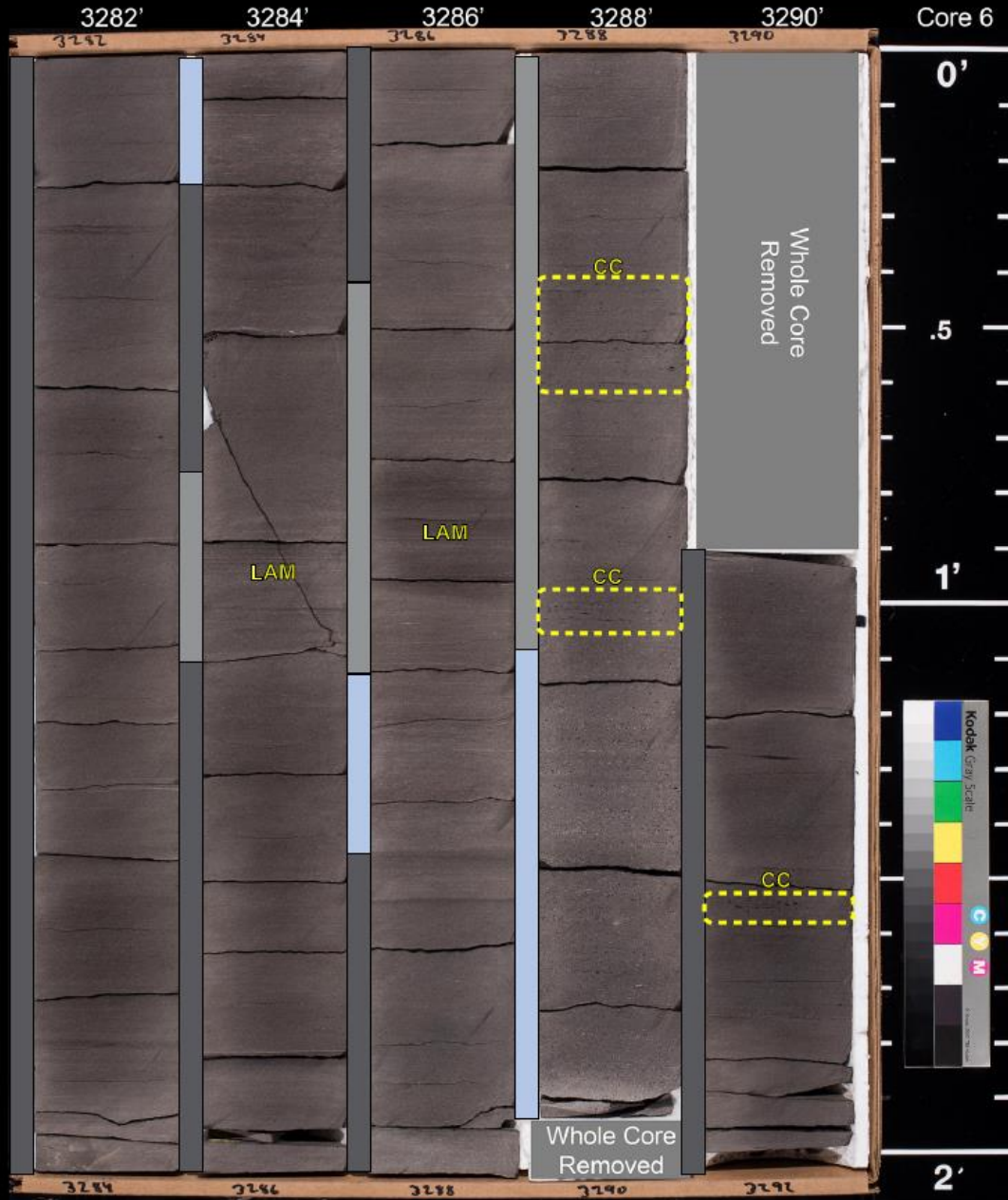
Angell 1-23

Okfuskee County, OK



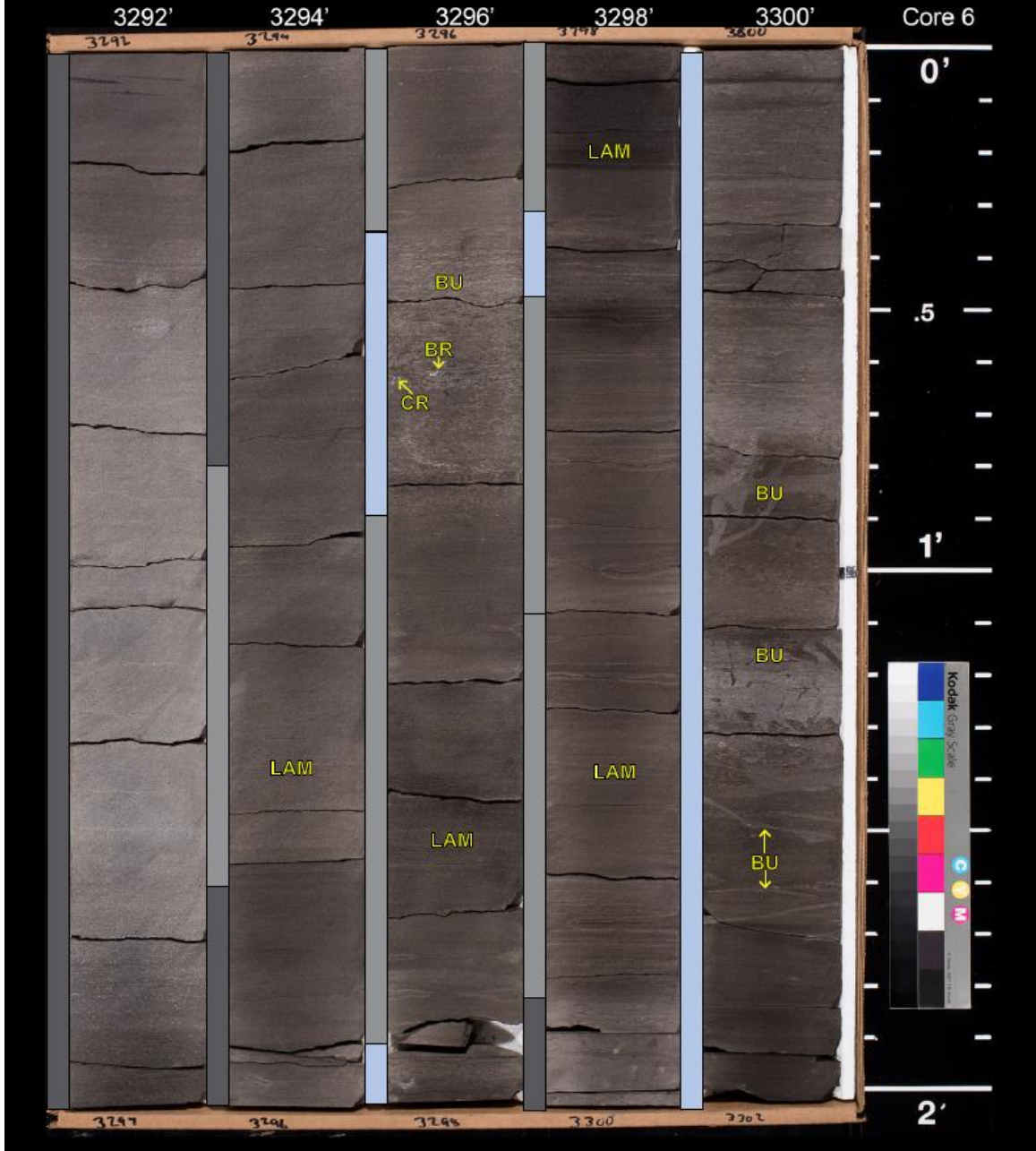
Angell 1-23

Okfuskee County, OK



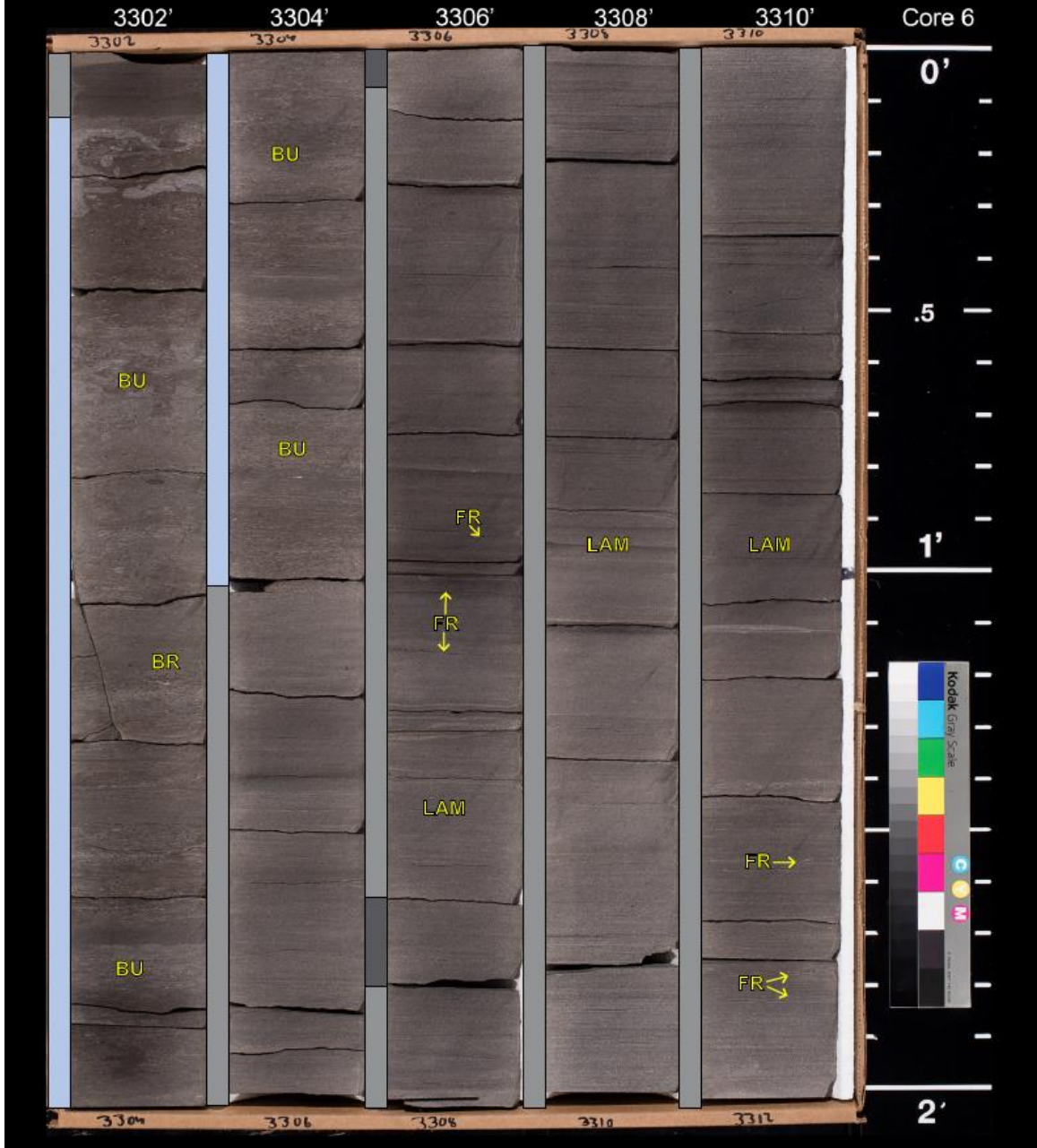
Angell 1-23

Okfuskee County, OK



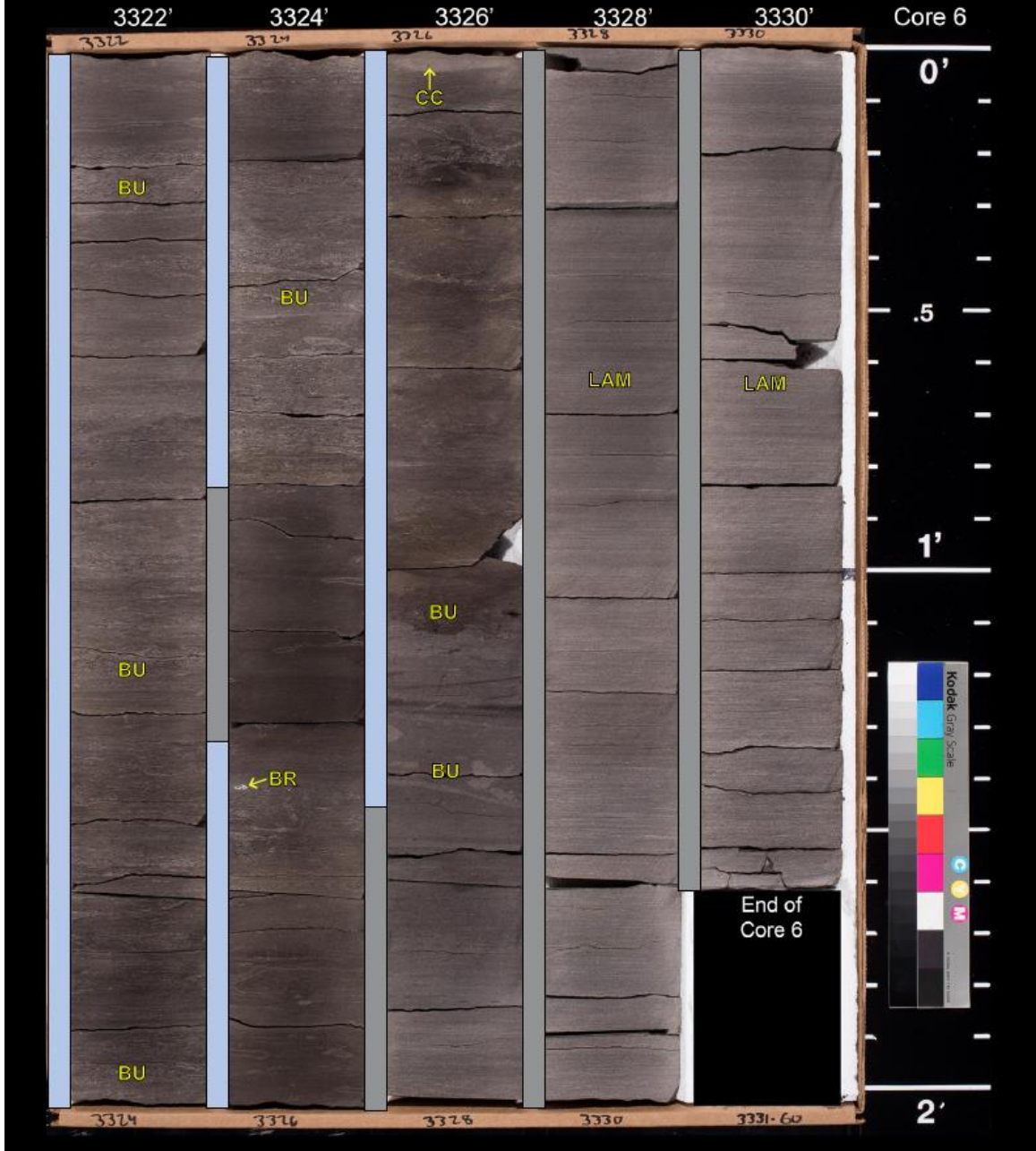
Angell 1-23

Okfuskee County, OK



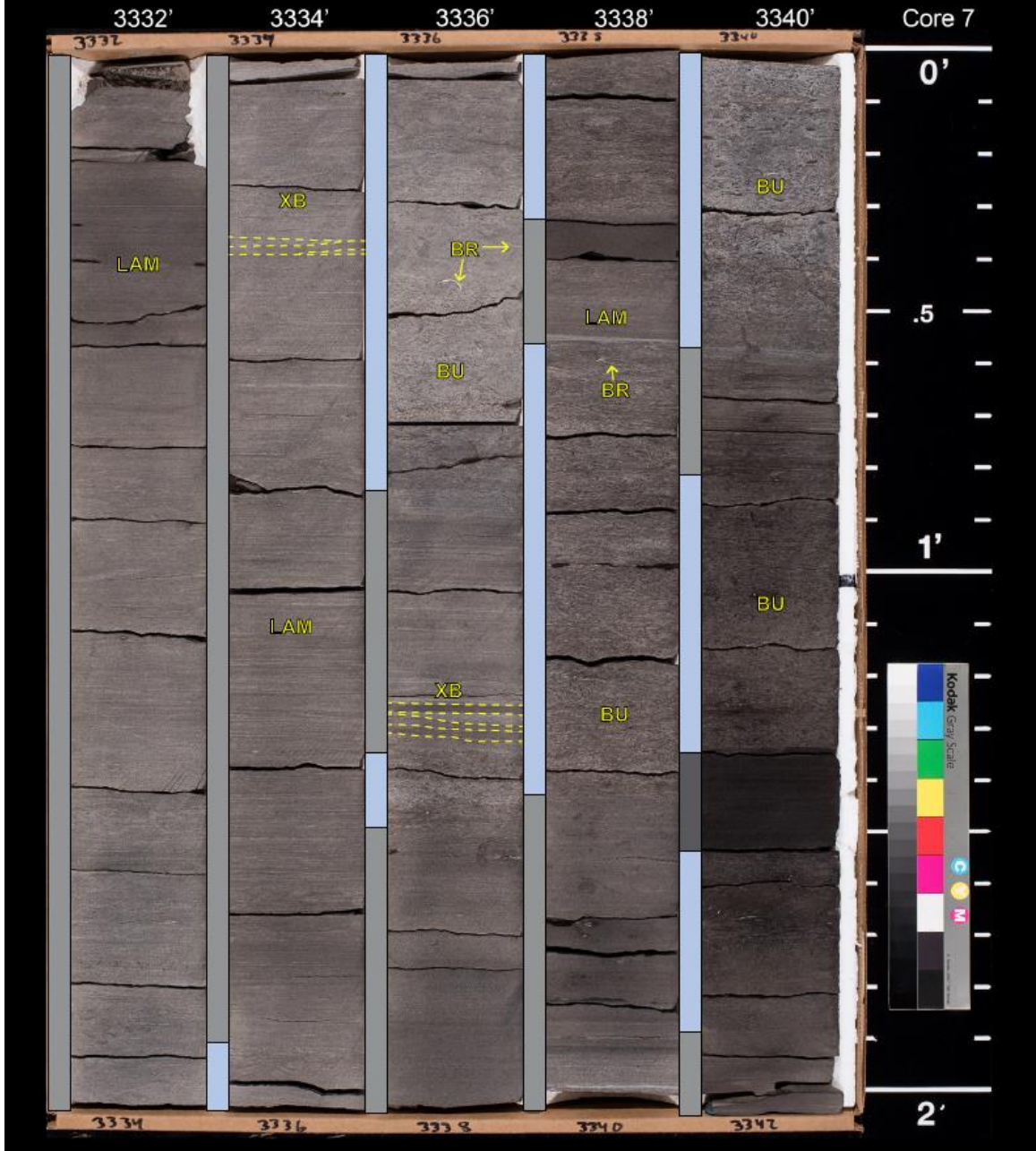
Angell 1-23

Okfuskee County, OK



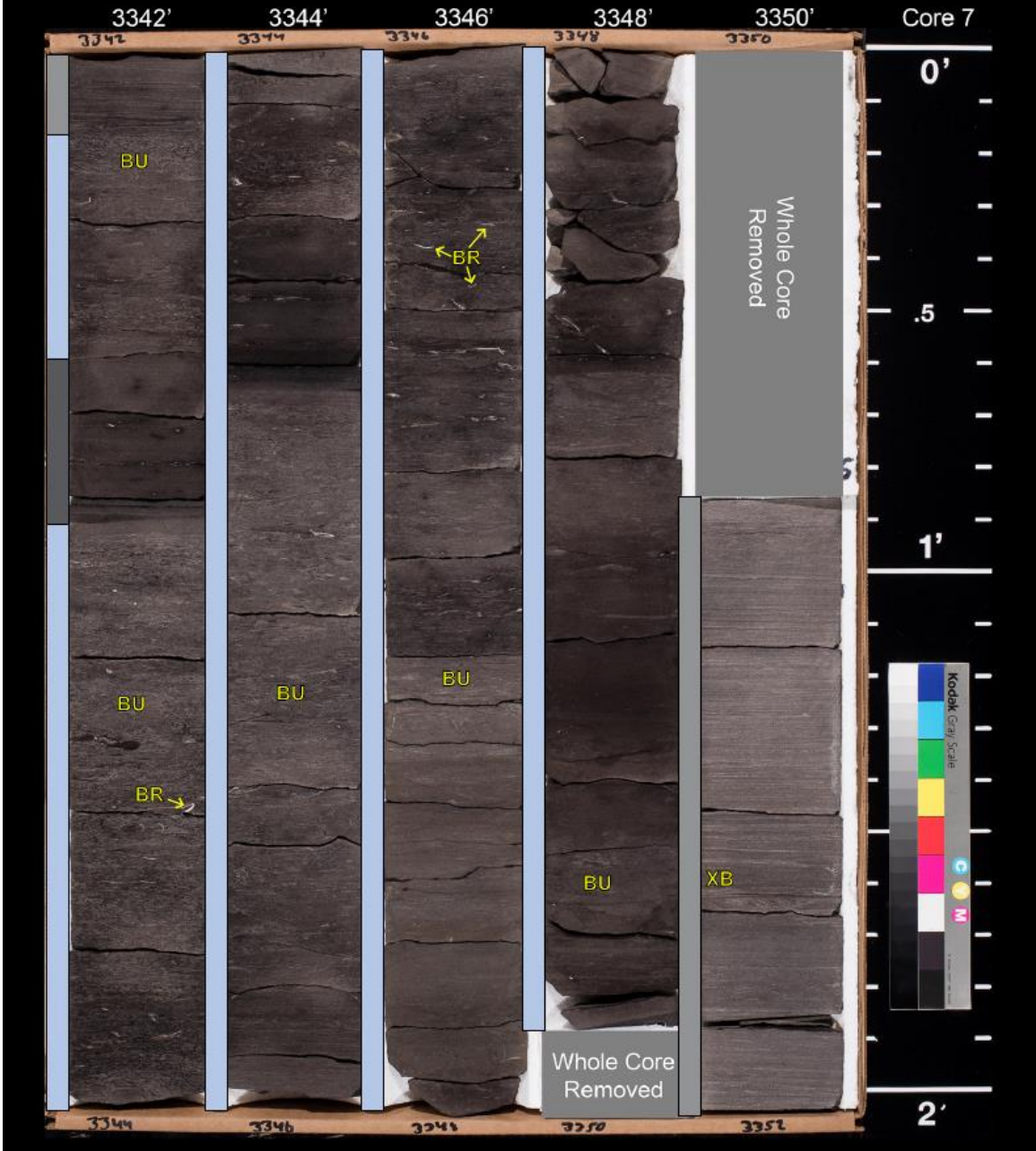
Angell 1-23

Okfuskee County, OK



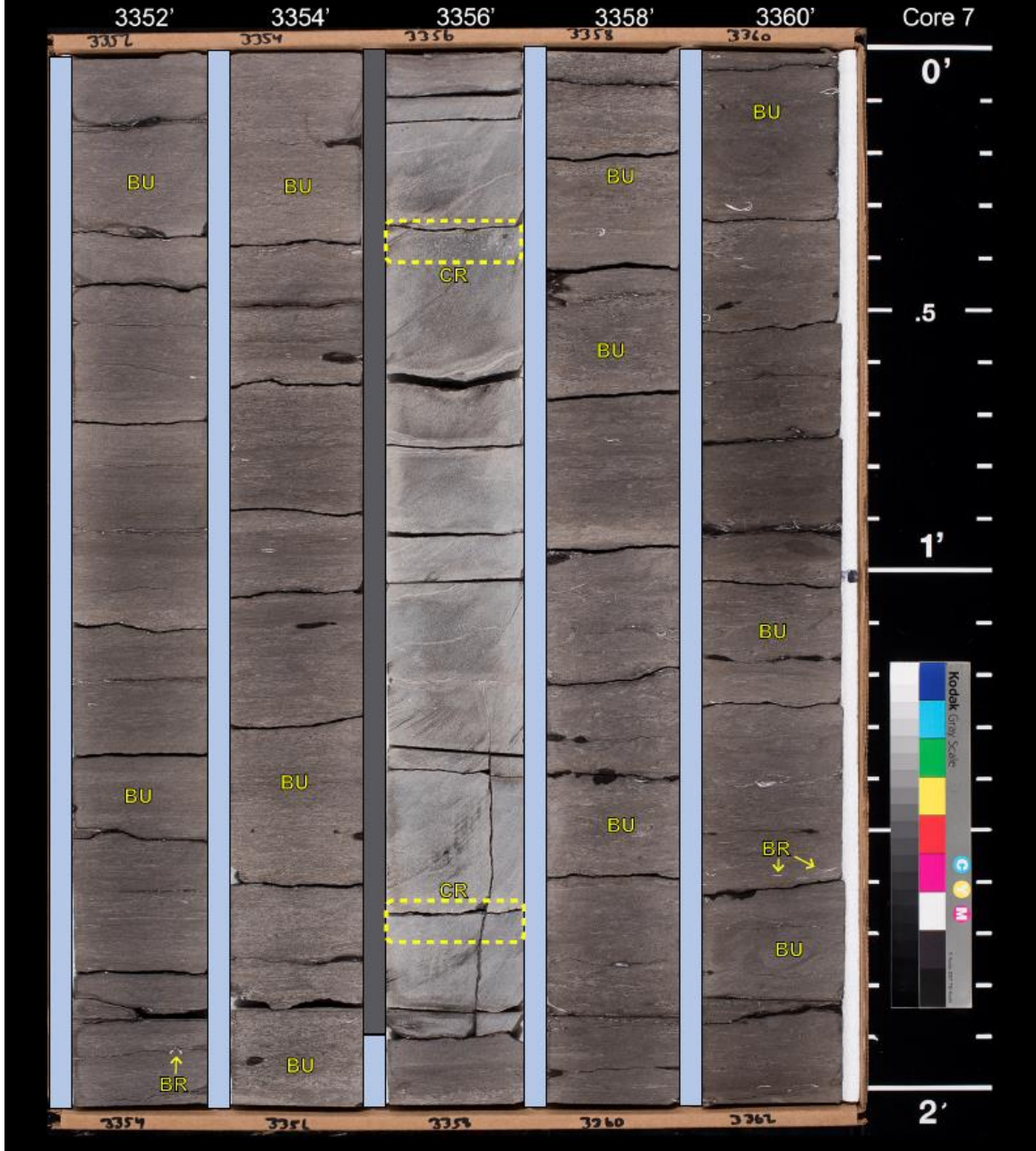
Angell 1-23

Okfuskee County, OK



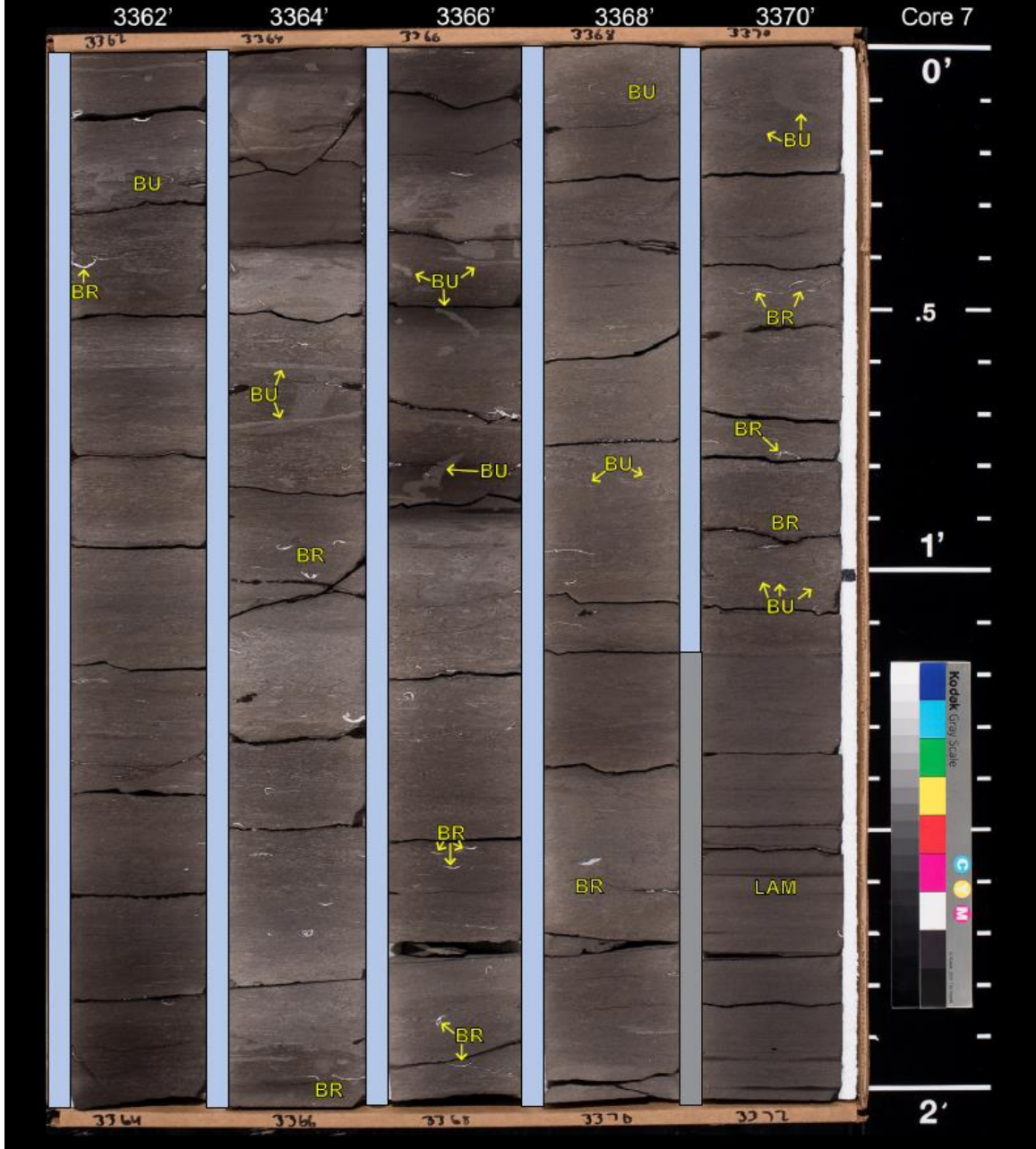
Angell 1-23

Okfuskee County, OK



Angell 1-23

Okfuskee County, OK



Angell 1-23

Okfuskee County, OK

3372'

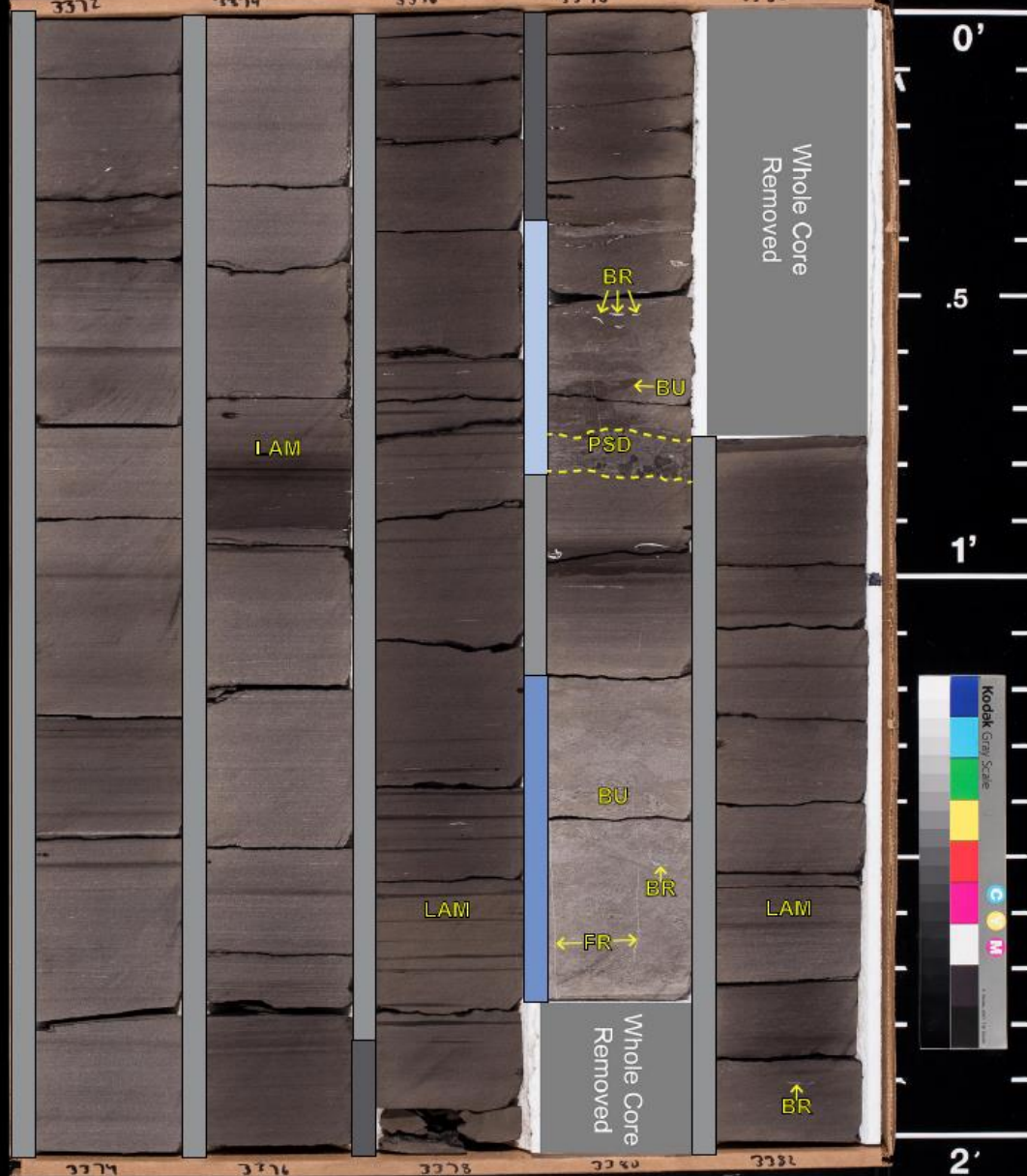
3374'

3376'

3378'

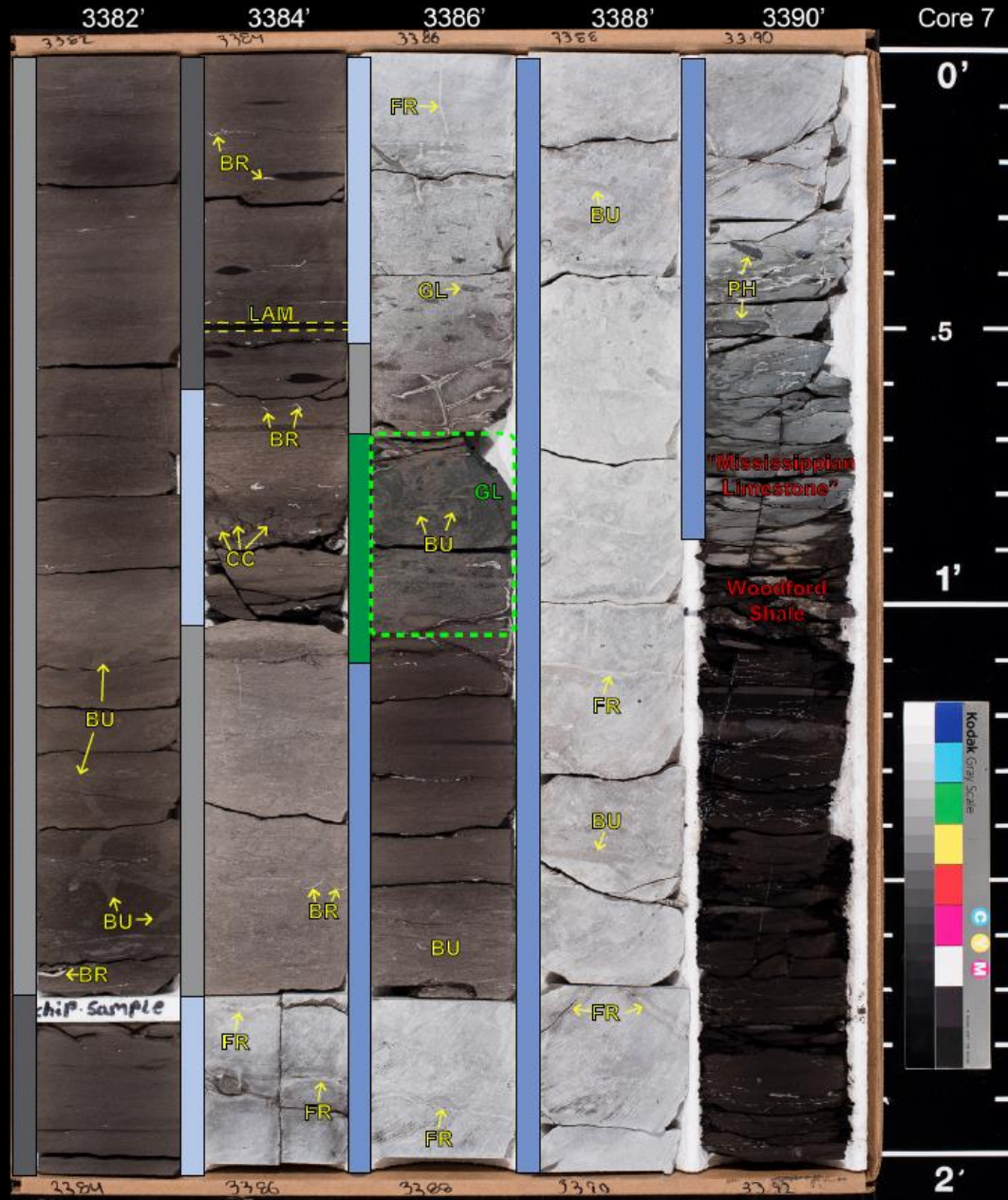
3380'

Core 7



Angell 1-23

Okfuskee County, OK



I. Angell 1-23 Core Description

The Angell 1-23 core was described using the Dunham (1962) classification scheme where applicable (i.e. – carbonate dominant intervals). Siliciclastic dominant intervals were classified based on grain type and composition. The descriptions of bioturbation uses a bioturbation index implemented from Bann et al., 2008 (Table 6).

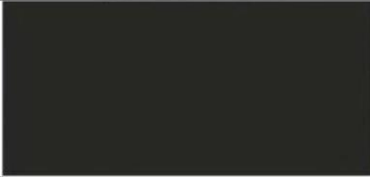
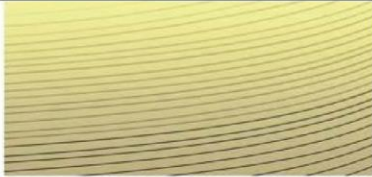

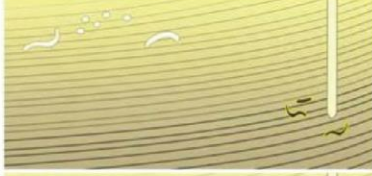


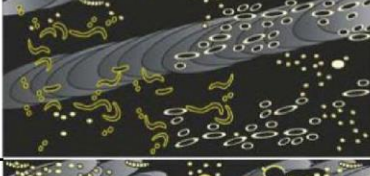







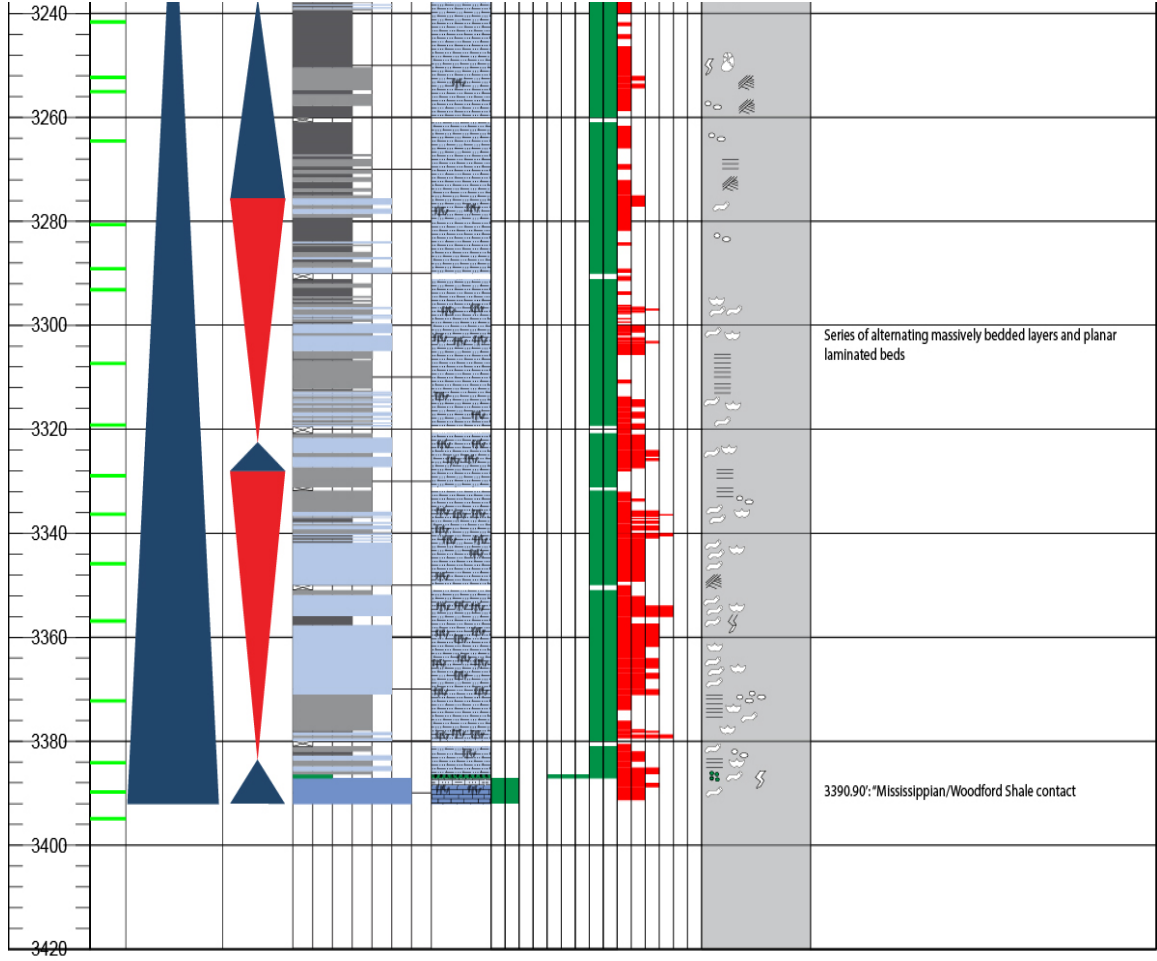
Bioturbation Index			
#	Characteristics	Mud-Dominated Facies	Grain-Dominated Facies
0	Bioturbation absent		
1	Sparse bioturbation, bedding distinct, few discrete traces		
2	Uncommon bioturbation, bedding distinct, low trace density		
3	Moderate bioturbation, bedding boundaries sharp, traces discrete, overlap rare		
4	Common bioturbation, bedding boundaries indistinct, high trace density with overlap common		
5	Abundant bioturbation, bedding completely disturbed (just visible)		
6	Complete bioturbation, total biogenic homogenization of sediment		

Table 6: Bioturbation index utilized for core descriptions. Modified from Bann et al. (2008).

Angell 1-23 Core Description Key

Lithology	Sedimentary Structures
<div style="display: flex; align-items: center; margin-bottom: 5px;"> <div style="width: 30px; height: 30px; border: 1px solid black; margin-right: 10px;"></div> <div>No core recovered</div> </div> <div style="display: flex; align-items: center; margin-bottom: 5px;"> <div style="width: 30px; height: 30px; background-color: #cccccc; border: 1px solid black; margin-right: 10px;"></div> <div>Siltstone</div> </div> <div style="display: flex; align-items: center; margin-bottom: 5px;"> <div style="width: 30px; height: 30px; background-color: #cccccc; border: 1px solid black; margin-right: 10px;"></div> <div>Calcareous Siltstone</div> </div> <div style="display: flex; align-items: center; margin-bottom: 5px;"> <div style="width: 30px; height: 30px; background-color: #cccccc; border: 1px solid black; margin-right: 10px;"></div> <div>Interbedded Limestone & Siltstone</div> </div> <div style="display: flex; align-items: center; margin-bottom: 5px;"> <div style="width: 30px; height: 30px; background-color: #008000; border: 1px solid black; margin-right: 10px;"></div> <div>Glaucconitic Sandstone</div> </div> <div style="display: flex; align-items: center; margin-bottom: 5px;"> <div style="width: 30px; height: 30px; background-color: #cccccc; border: 1px solid black; margin-right: 10px;"></div> <div>Limestone</div> </div>	<div style="display: flex; justify-content: space-between; margin-bottom: 10px;"> <div style="width: 45%;"> <p>Ammonoids </p> <p>Bioturbated </p> <p>Brachiopods </p> <p>Burrows </p> <p>Crinoids </p> <p>Cross-bedded </p> <p>Fracture (filled) </p> </div> <div style="width: 45%;"> <p>Fracture (partially filled) </p> <p>Fracture swarm </p> <p>Glaucconite </p> <p>Horizontal laminae </p> <p>Intraclast </p> <p>Nodule </p> <p>Pyrite </p> </div> </div>

Figure 31: Key for core description of Angell 1-23.



II. Angell 1-23 Thin section photomicrographs

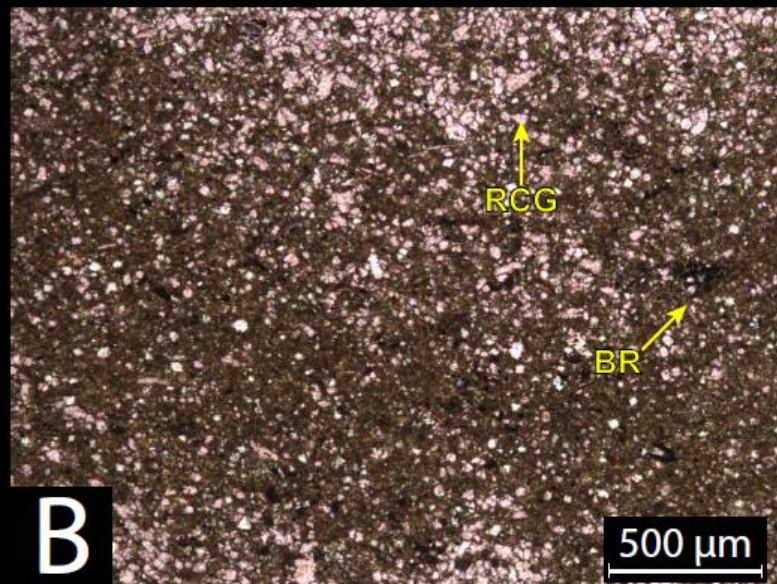
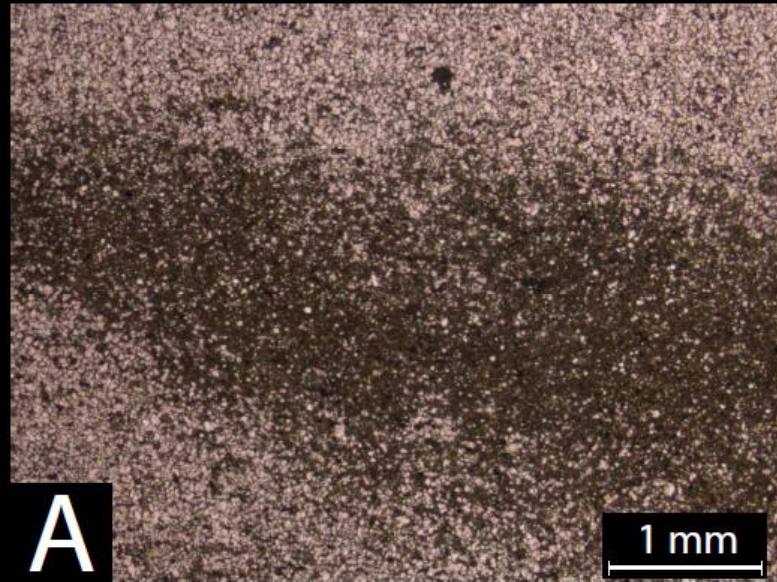
Thin section photomicrographs show enlarged views of samples that have been cut from the core. The samples and images shown are oriented as if looking at core, from shallower at the top of the image and deeper towards the base of the image. The images are formatted in descending order of depth. All thin sections are blue epoxy impregnated, stained with alizarin red and potassium ferricyanide on half of the slide. All photomicrographs are in plane polarized light (unless otherwise stated) and are labeled using the chart below.

Thin Section Image Labels			
AF	Agglutinated Foraminifera	LAM	Lamination
AM	Ammonite	OM	Organic Matter
BI	Bivalve	P	Peloid
BR	Brachiopod	PH	Phosphate
BU	Burrow	PSD	Possible Storm Deposit
CC	Clay Clast	PY	Pyrite
CEM	Cement	PY-BR	Pyritized Brachiopod
CG	Calcite Grain (indistinguishable)	PY-BU	Pyritized Burrow
CON	Conodont	Q	Quartz
CR	Crinoid	RCG	Recrystallized Carbonate Grain
FOR	Foraminifera	RMC	Rip-up Mud Clast
FR	Fracture	SK	Skeletal debris
GL	Glauconite	SP	Spicule
IFD	Indistinguishable Fossil Debris	TAS	Tasmanites
ILL	Illite/mica	XB	Cross Bedding

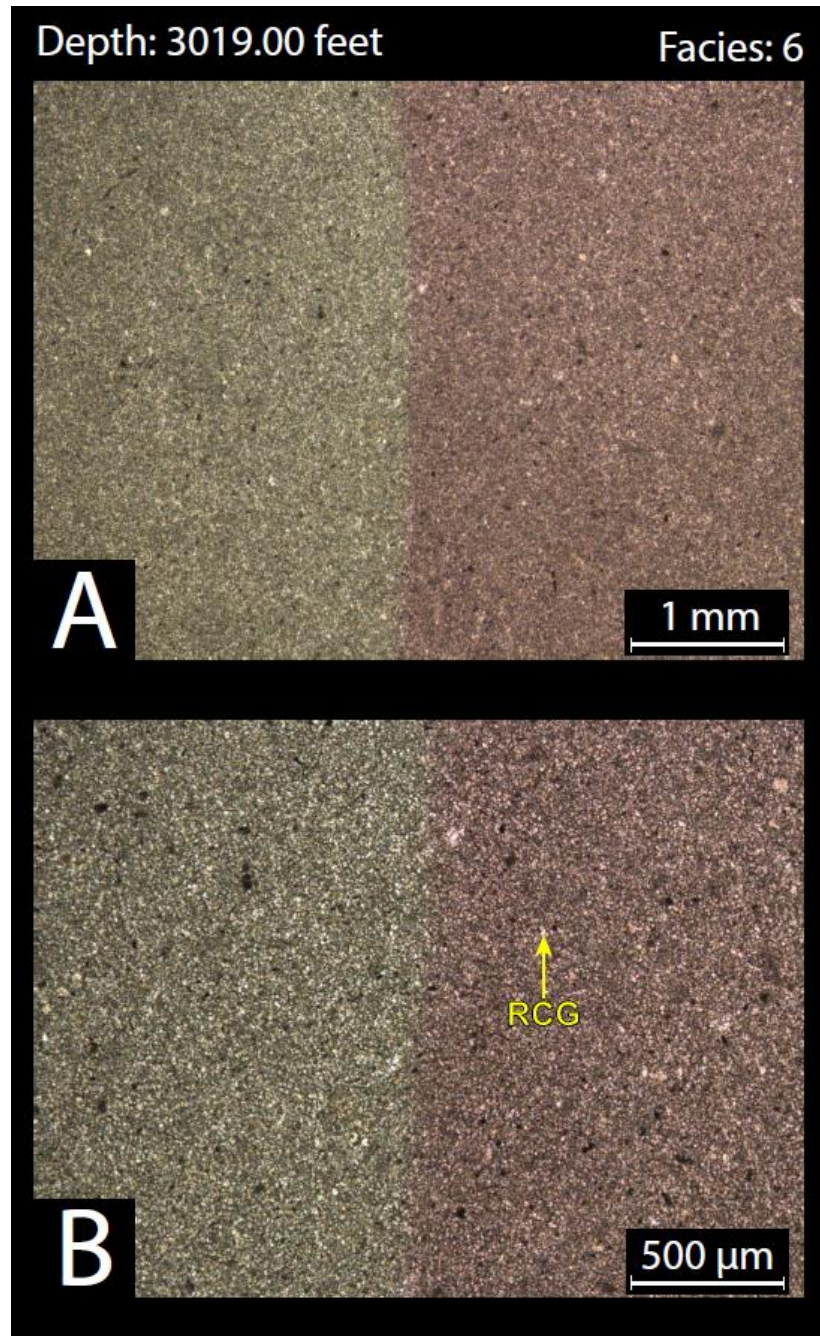
Figure 32: Thin section image label key

Depth: 3013.00 feet

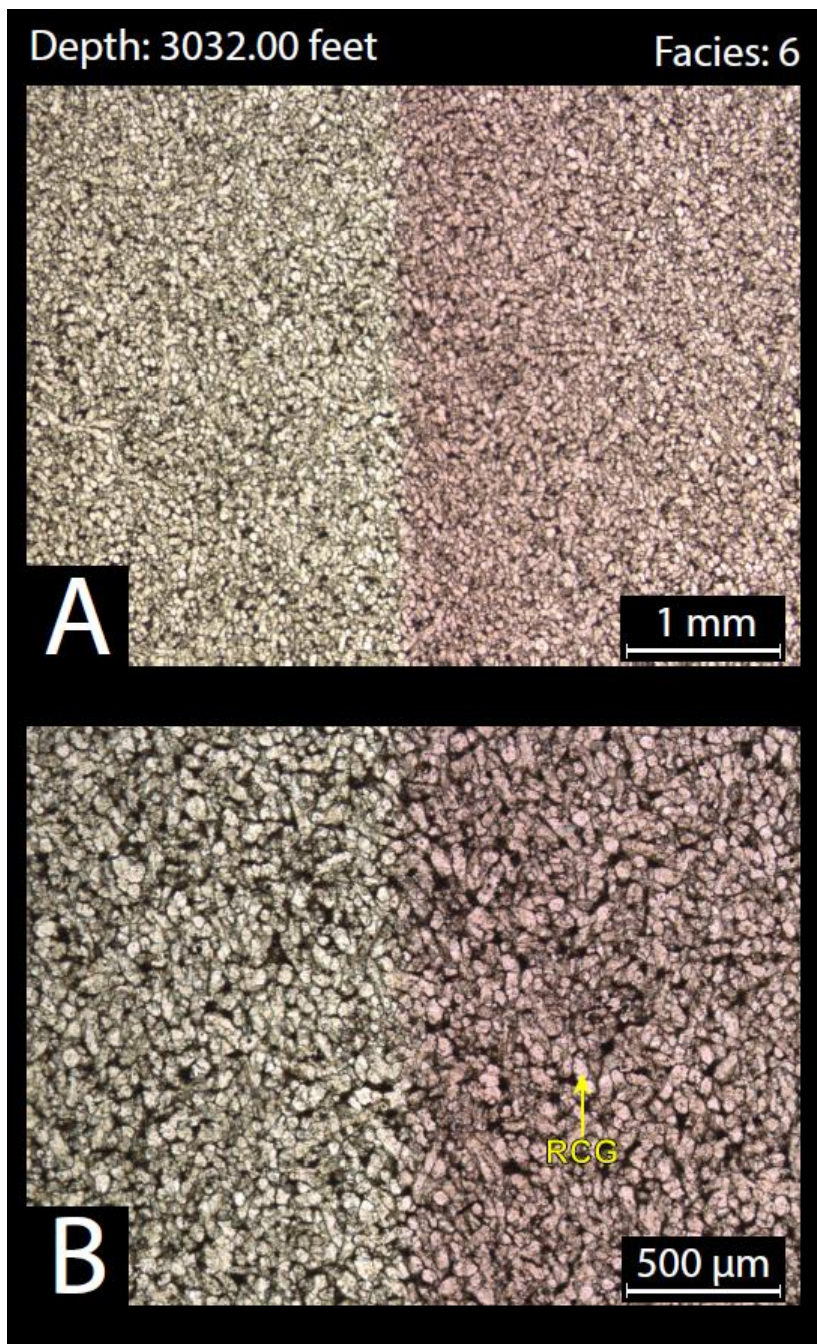
Facies: 6



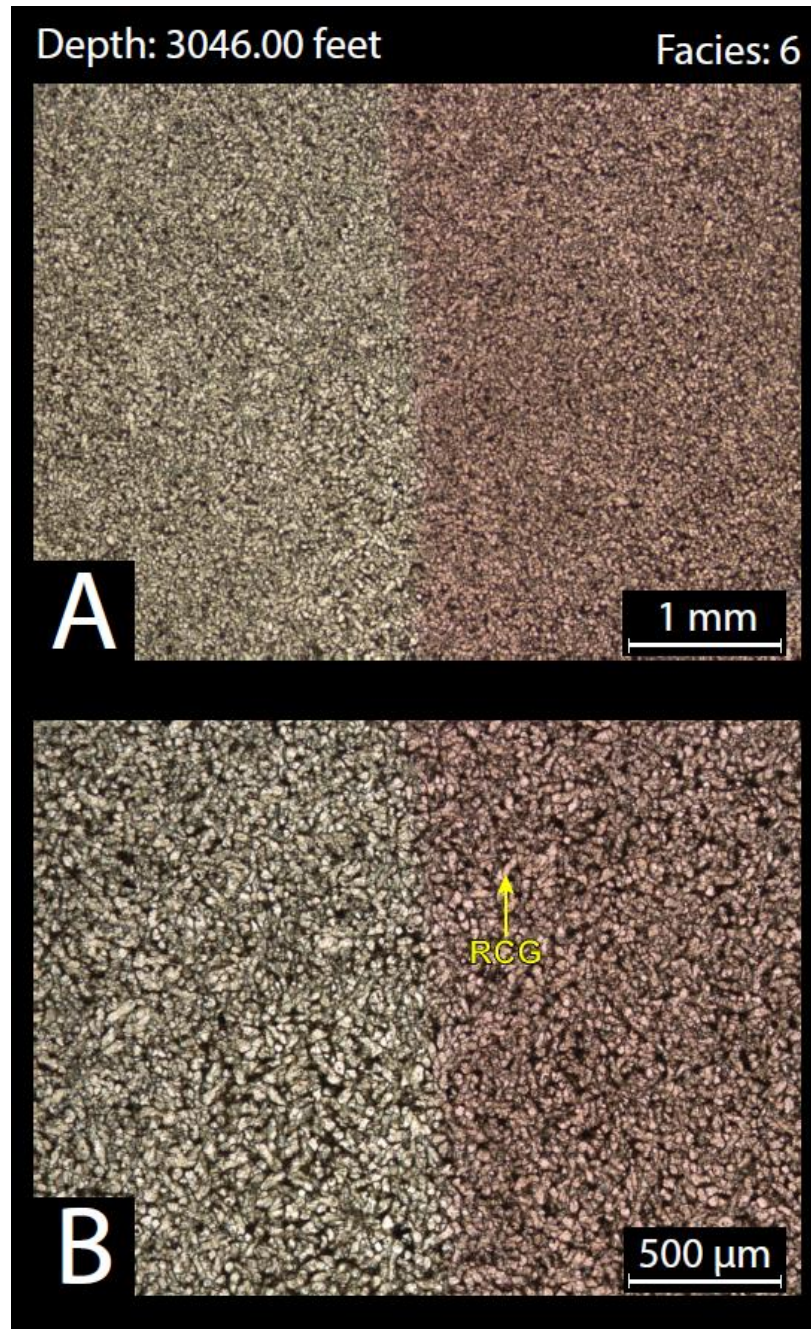
3013.00' – Skeletal Mudstone/Wackestone: Carbonate cement and peloids are the main constituents. Primary depositional facies was likely a carbonate mudstone that has been recrystallized. No apparent bedding or sedimentary structures are observed in this sample. All mineral assemblages appear to be fully homogenized. XRD analysis 89% carbonates (89% calcite and 2% dolomite), 8% clays, 2% quartz, 1% other minerals (trace potassium feldspar, 1% plagioclase feldspar, and trace pyrite).



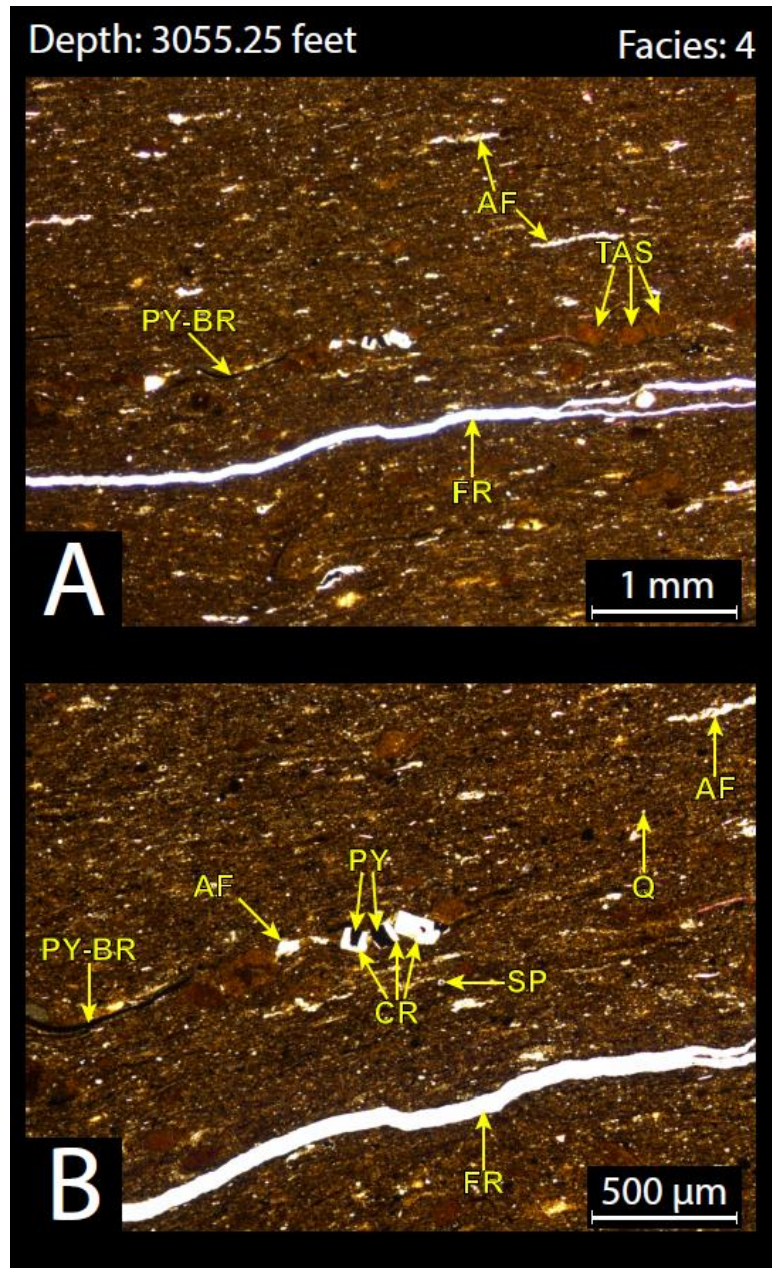
3019.00' – Skeletal Mudstone/Wackestone: Carbonate cement is the dominant constituent. Primary depositional facies was likely a carbonate mudstone that has been recrystallized. No apparent bedding or sedimentary structures are observed in this sample. All mineral assemblages appear to be fully homogenized. XRD analysis 88% carbonates (85% calcite and 3% dolomite), 7% clays, 2% quartz, 1% other minerals (trace potassium feldspar, 1% plagioclase feldspar, and trace pyrite).



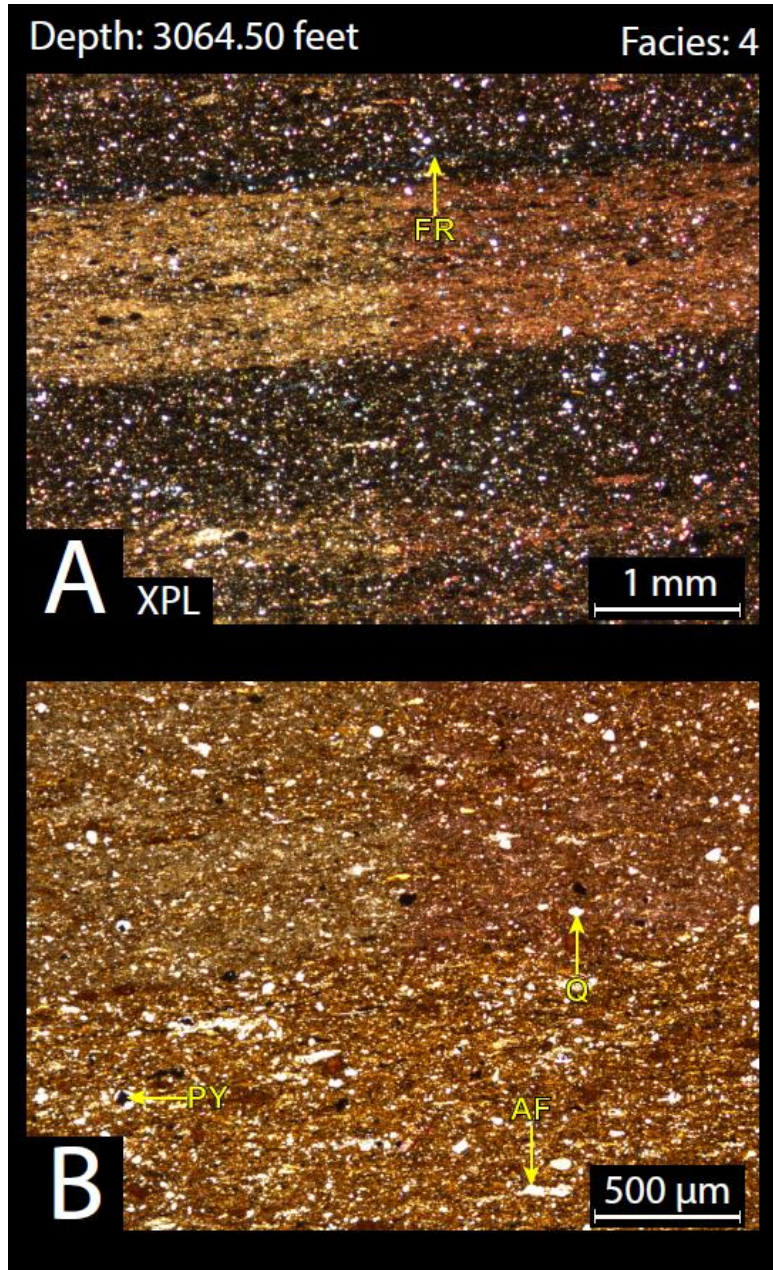
3032.00' – Skeletal Mudstone/Wackestone: Carbonate cement is the dominant constituent. Primary depositional facies was likely a carbonate mudstone that has been recrystallized. No apparent bedding or sedimentary structures are observed in this sample. All mineral assemblages appear to be fully homogenized. XRD analysis 91% carbonates (87% calcite and 4% dolomite), 7% clays, 2% quartz, trace other minerals (trace potassium feldspar, trace plagioclase feldspar, and trace pyrite).



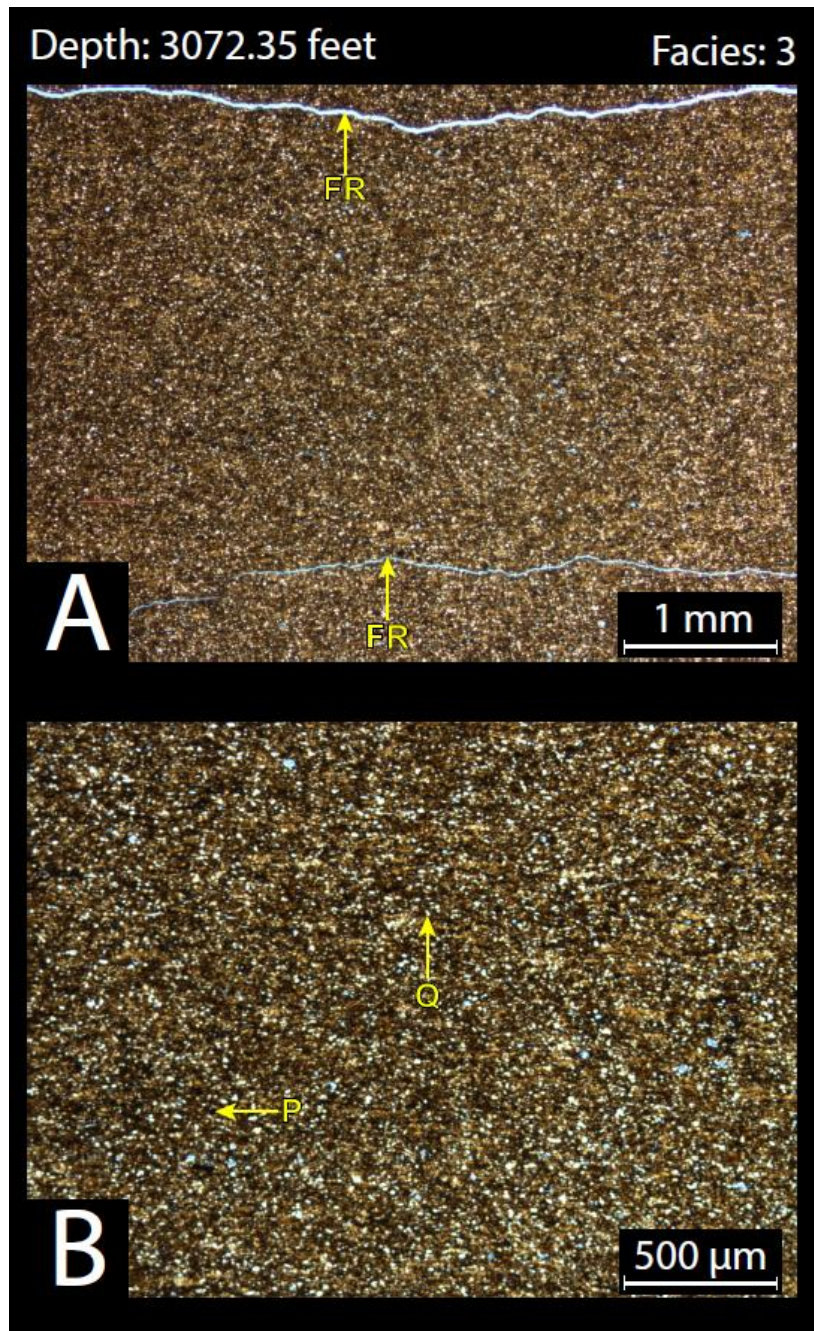
3046.00' – Skeletal Mudstone/Wackestone: Carbonate cement is the dominant constituent. Primary depositional facies was likely a carbonate mudstone that has been recrystallized. No apparent bedding or sedimentary structures are observed in this sample. All mineral assemblages appear to be fully homogenized. XRD analysis 91% carbonates (89% calcite and 2% dolomite), 6% clays, 2% quartz, 1% other minerals (trace potassium feldspar, 1% plagioclase feldspar, and trace pyrite).



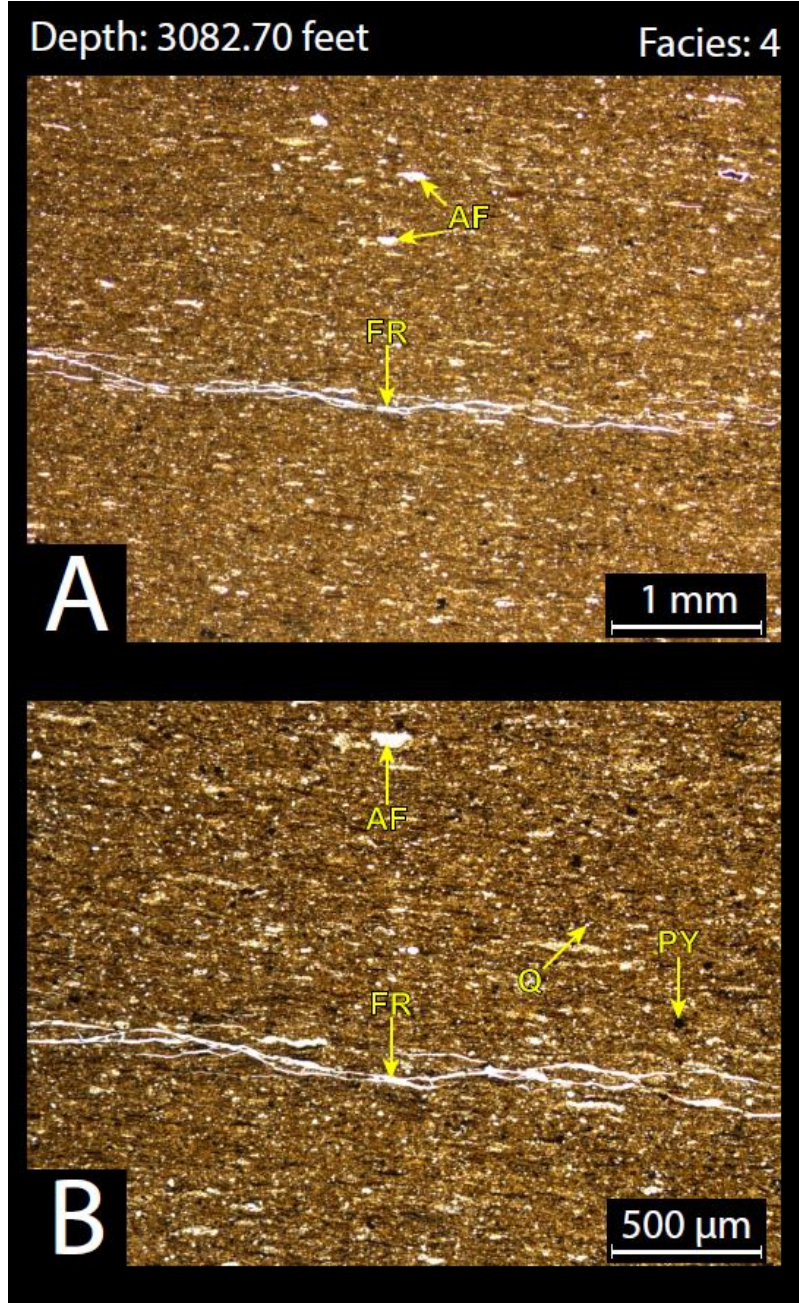
3055.25' – Laminated Peloidal Siltstone: Clay minerals and quartz silt are the main constituents. Pyrite partially replaces calcite in the crinoid stem fragments and scattered microfossils of uncompacted Tasmanites and agglutinated foraminifera are also observed. Clay mineral assemblages appear to be organized horizontally (parallel to bedding planes). Fractures observed are likely induced. All mineral assemblages appear to be fully homogenized. XRD analysis 7% carbonates (7% calcite and trace dolomite), 61% clays, 23% quartz, 9% other minerals (1% potassium feldspar, 3% plagioclase feldspar, 3% pyrite, and 2% apatite).



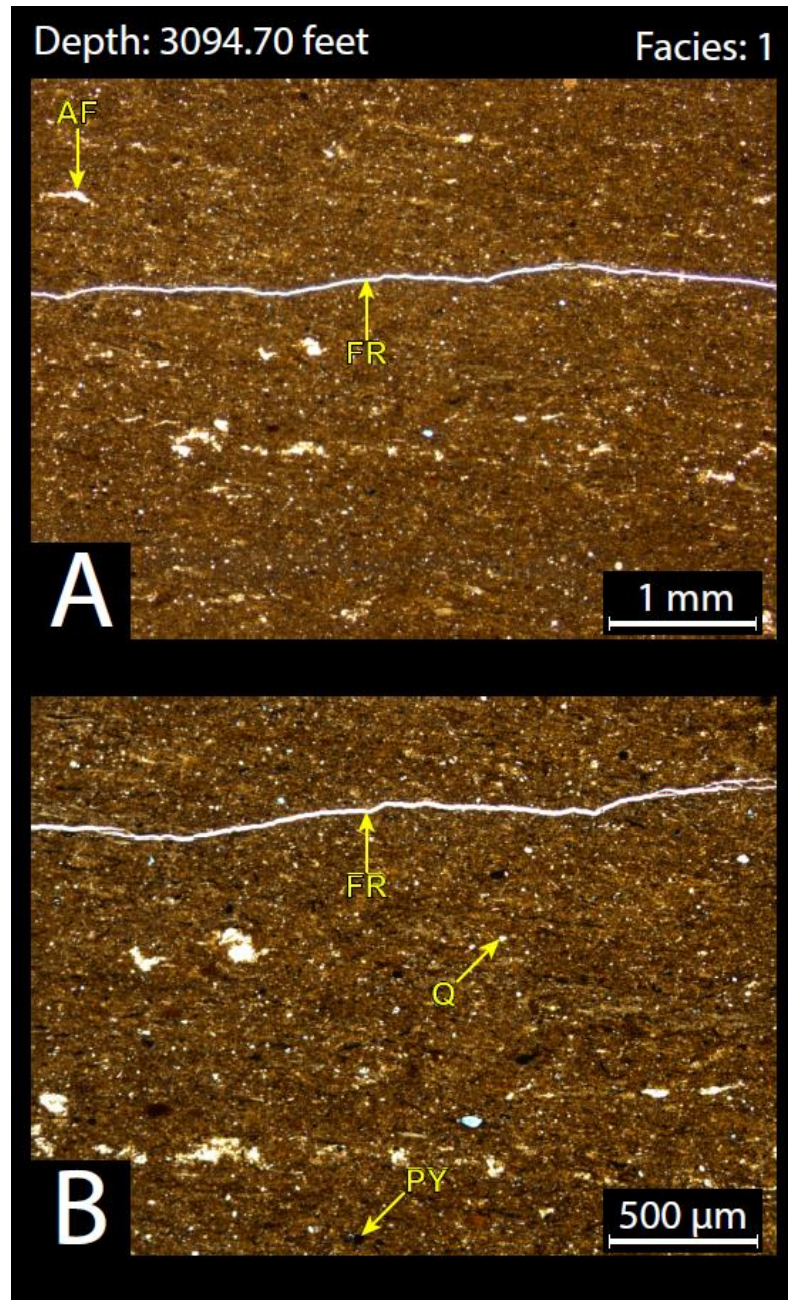
3064.50' – Laminated Peloidal Siltstone: Very fine sand to quartz silt and clay minerals are the main constituents. Pyrite rhombs and scattered microfossils of agglutinated foraminifera are also observed. Clay mineral assemblages appear to be organized horizontally (parallel to bedding planes), and when viewed in XPL display preferential deposition likely due to winnowing from bottom water currents. Fractures observed are likely induced. XRD analysis 9% carbonates (7% calcite and 2% dolomite), 24% clays, 55% quartz, 12% other minerals (1% potassium feldspar, 4% plagioclase feldspar, 2% pyrite, and 5% apatite).



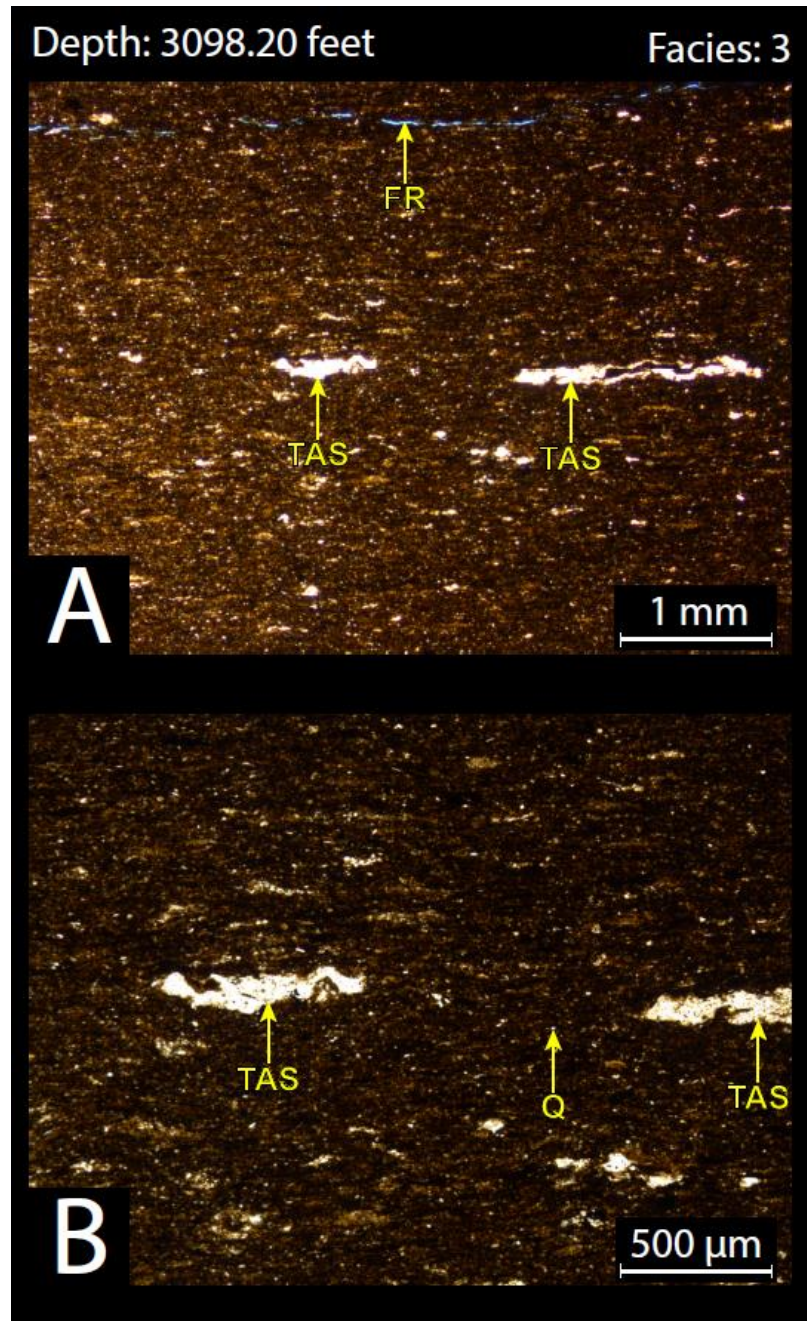
3072.35' – Massive-bedded Peloidal Siltstone: Very fine sand to silt quartz grains, carbonate peloids, and clay minerals are the main constituents. No apparent bedding or sedimentary structures (other than induced fractures) are observed in this sample. All mineral assemblages appear to be fully homogenized. XRD analysis 4% carbonates (3% calcite and 1% dolomite), 54% clays, 31% quartz, 11% other minerals (1% potassium feldspar, 6% plagioclase feldspar, 3% pyrite, and 1% marcasite).



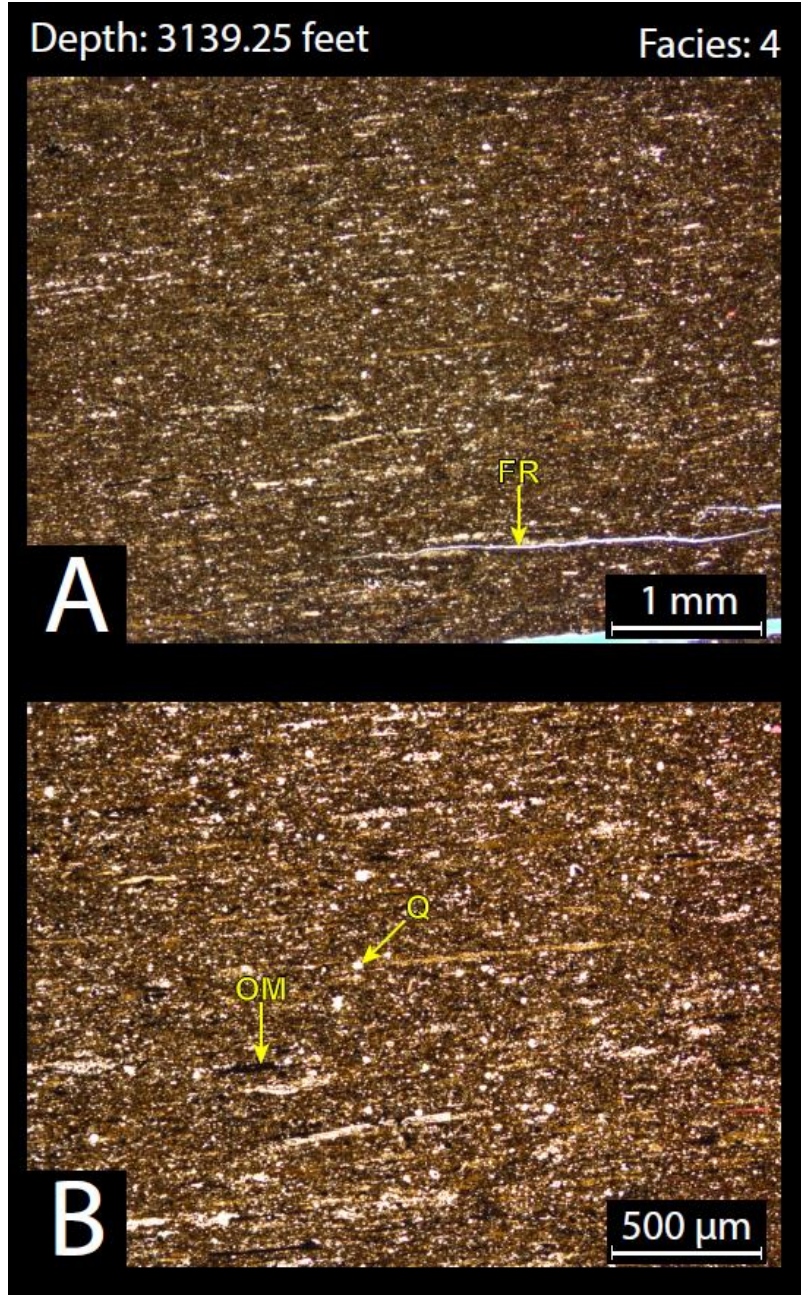
3082.70' – Laminated Peloidal Siltstone: Clay minerals and quartz silt are the main constituents. Pyrite rhombs and scattered microfossils of agglutinated foraminifera are also observed. Clay mineral assemblages appear to be organized horizontally (parallel to bedding planes). Fractures observed are likely induced. All mineral assemblages appear to be fully homogenized. XRD analysis 3% carbonates (2% calcite and 1% dolomite), 67% clays, 19% quartz, 11% other minerals (1% potassium feldspar, 3% plagioclase feldspar, 4% pyrite, 1% marcasite, and 2% apatite).



3094.70' – Fissile Clay-rich Siltstone: Clay minerals and quartz silt are the main constituents. Pyrite rhombs and scattered microfossils of agglutinated foraminifera are also observed. Clay mineral assemblages appear to be organized horizontally (parallel to bedding planes). Fractures observed are likely induced. All mineral assemblages appear to be fully homogenized. XRD analysis 2% carbonates (2% calcite and trace dolomite), 77% clays, 16% quartz, 5% other minerals (trace potassium feldspar, 3% plagioclase feldspar, and 2% pyrite).



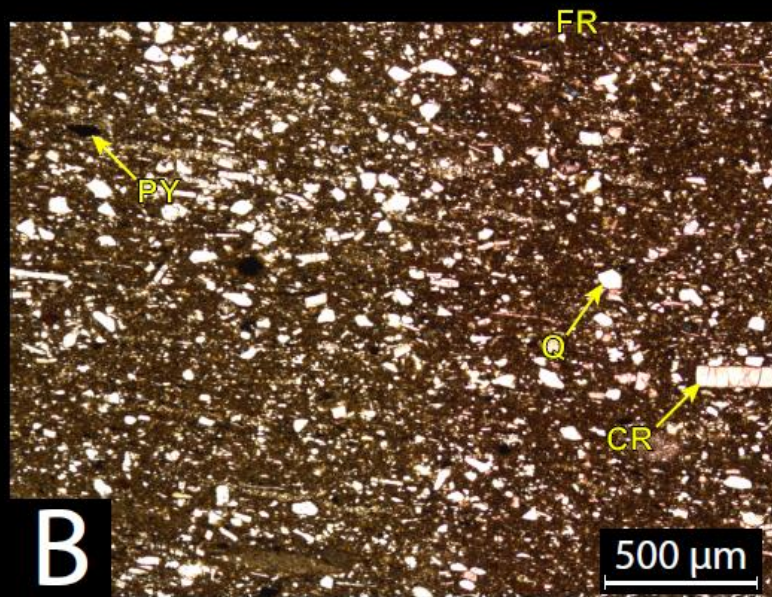
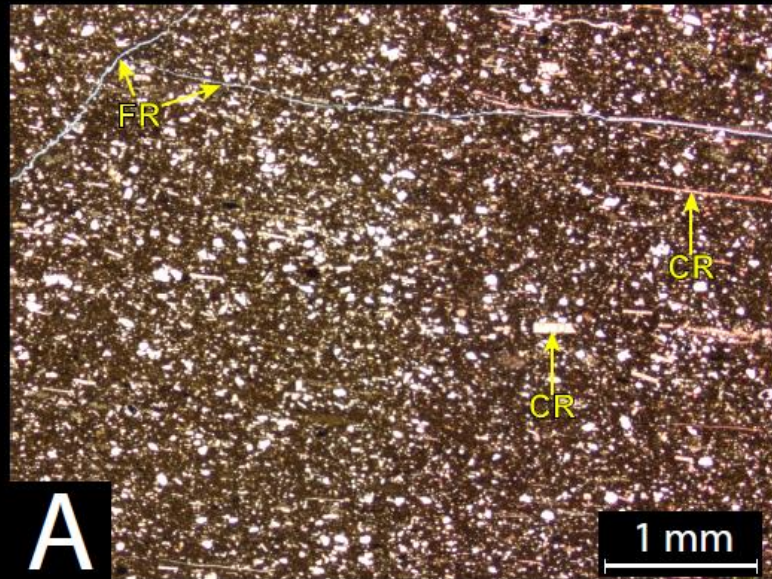
3098.20' – Massive-bedded Peloidal Siltstone: Silt quartz grains and clay minerals are the main constituents. No apparent bedding and few sedimentary structures (flattened Tasmanites, and induced fractures) are observed in this sample. All mineral assemblages appear to be fully homogenized. XRD analysis 2% carbonates (1% calcite and 1% dolomite), 52% clays, 31% quartz, 15% other minerals (2% potassium feldspar, 6% plagioclase feldspar, 4% pyrite, 1% marcasite, and 2% apatite).



3139.25' – Laminated Peloidal Siltstone: Clay minerals and quartz silt are the main constituents. Pyrite rhombs and scattered microfossils of agglutinated foraminifera are also observed. Clay mineral assemblages appear to be organized horizontally (parallel to bedding planes). Fractures observed are likely induced. All mineral assemblages appear to be fully homogenized. XRD analysis 8% carbonates (7% calcite and 1% dolomite), 59% clays, 18% quartz, 15% other minerals (2% potassium feldspar, 4% plagioclase feldspar, and 9% pyrite).

Depth: 3160.25 feet

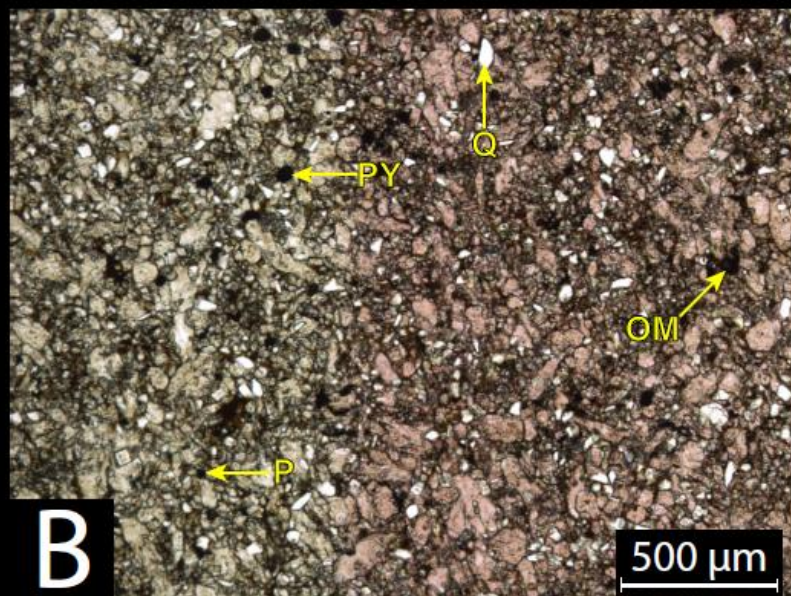
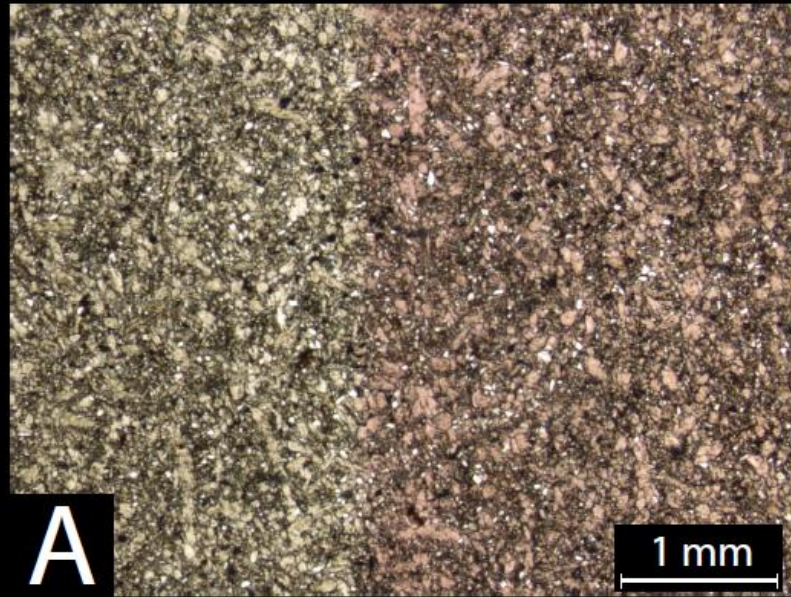
Facies: 4



3160.25' – Laminated Peloidal Siltstone: Clay minerals, very fine sand to quartz silt, crinoid stem fragments, and peloids are the main constituents. Clay mineral assemblages appear to be organized horizontally (parallel to bedding planes). Fractures observed are likely induced. All mineral assemblages appear to be fully homogenized. XRD analysis 21% carbonates (21% calcite and trace dolomite), 47% clays, 24% quartz, 8% other minerals (1% potassium feldspar, 4% plagioclase feldspar, and 3% pyrite).

Depth: 3165.45 feet

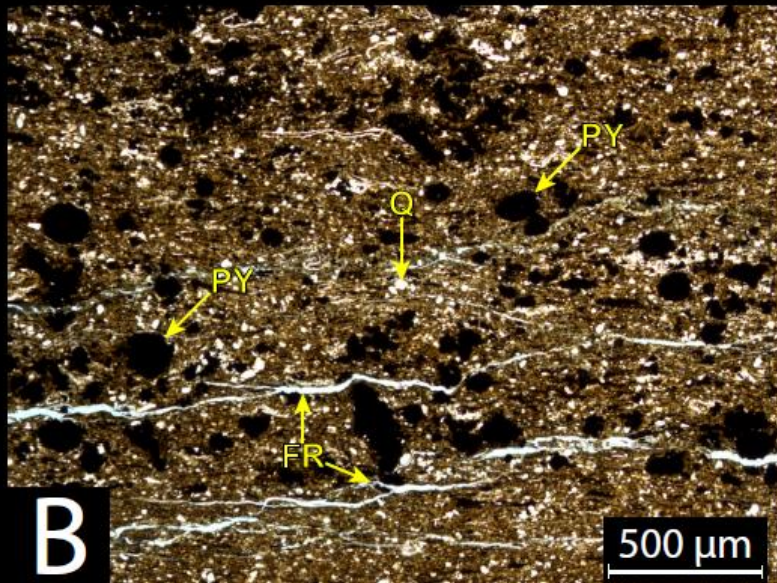
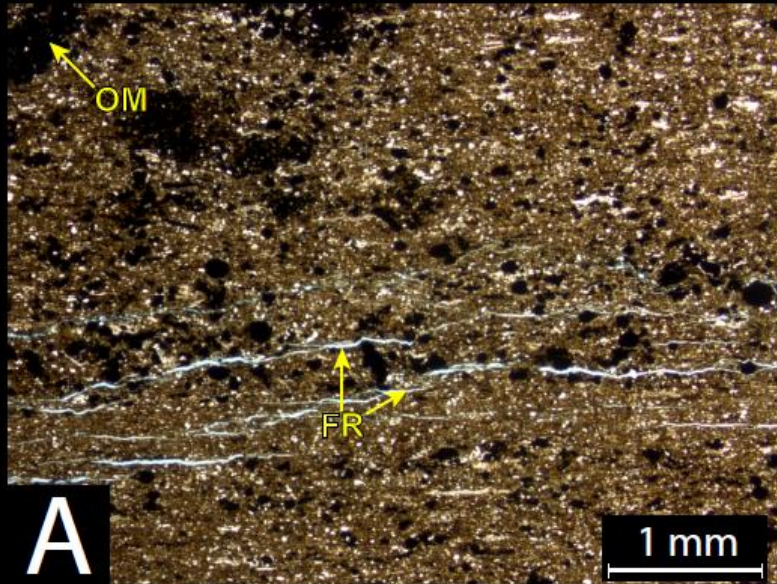
Facies: 3



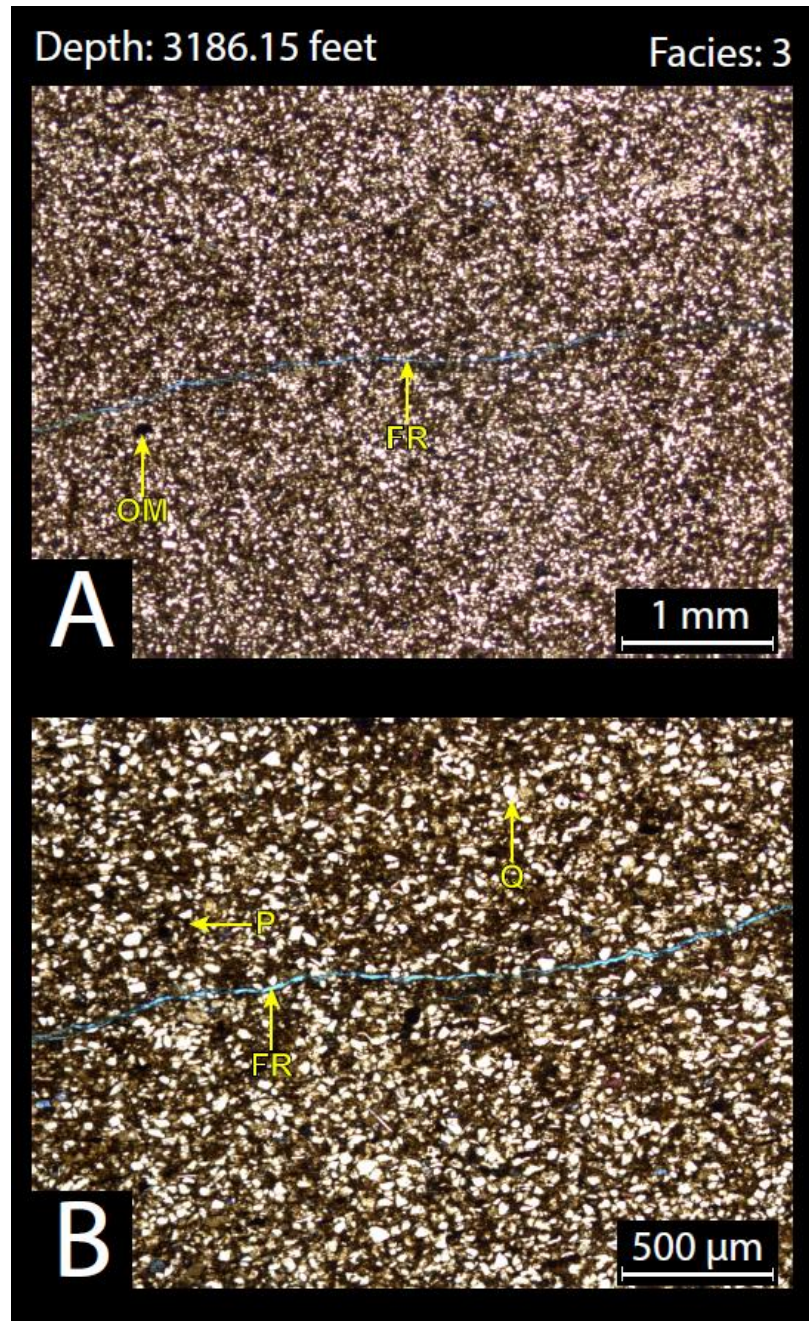
3165.45' – Massive-bedded Peloidal Siltstone: Carbonate cement and peloids are the main constituents. No apparent bedding or sedimentary structures are observed in this sample. All mineral assemblages appear to be fully homogenized. XRD analysis 71% carbonates (60% calcite and 11% dolomite), 13% clays, 12% quartz, 4% other minerals (trace potassium feldspar, 3% plagioclase feldspar, 1% pyrite).

Depth: 3177.20 feet

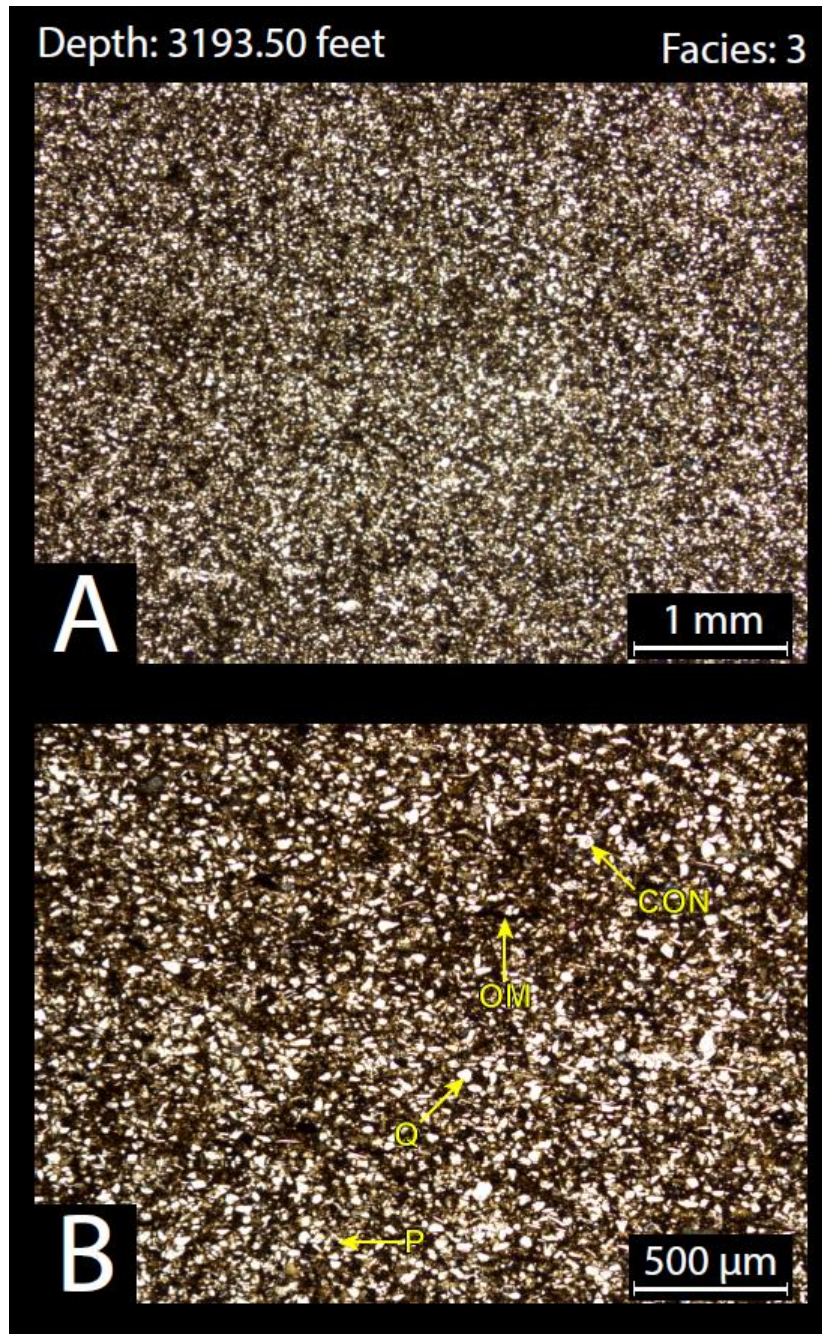
Facies: 1



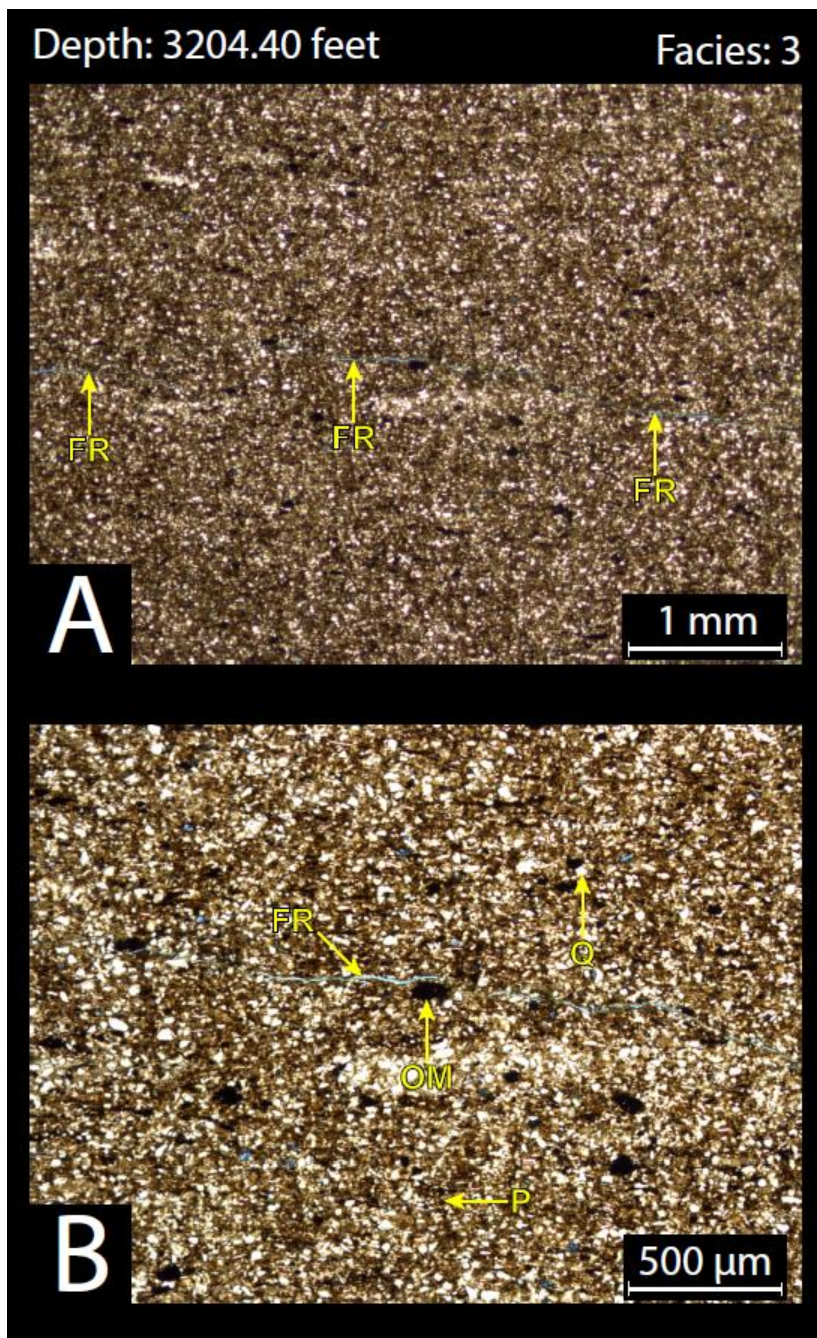
3177.20' – Fissile Clay-rich Siltstone: Clay minerals, quartz silt, and pyrite grains are the main constituents. Clay mineral assemblages appear to be organized horizontally (parallel to bedding planes). Fractures observed are likely induced. All mineral assemblages appear to be fully homogenized. XRD analysis 1% carbonates (1% calcite and trace dolomite), 62% clays, 18% quartz, 19% other minerals (1% potassium feldspar, 2% plagioclase feldspar, 14% pyrite, and 2% marcasite).



3186.15' – Massive-bedded Peloidal Siltstone: Very fine sand to silt quartz grains, carbonate peloids, and clay minerals are the main constituents. No apparent bedding or sedimentary structures (other than induced fractures) are observed in this sample. All mineral assemblages appear to be fully homogenized. XRD analysis 4% carbonates (3% calcite and 1% dolomite), 55% clays, 31% quartz, 10% other minerals (3% potassium feldspar, 5% plagioclase feldspar, and 2% pyrite).



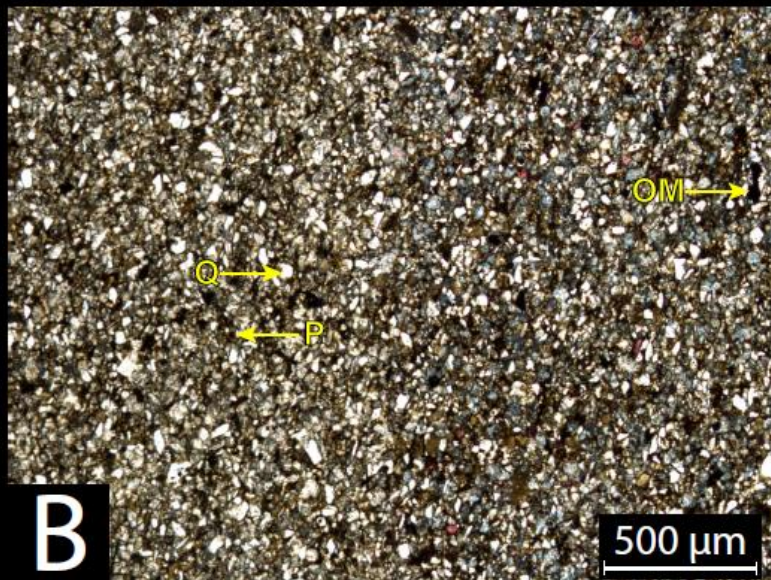
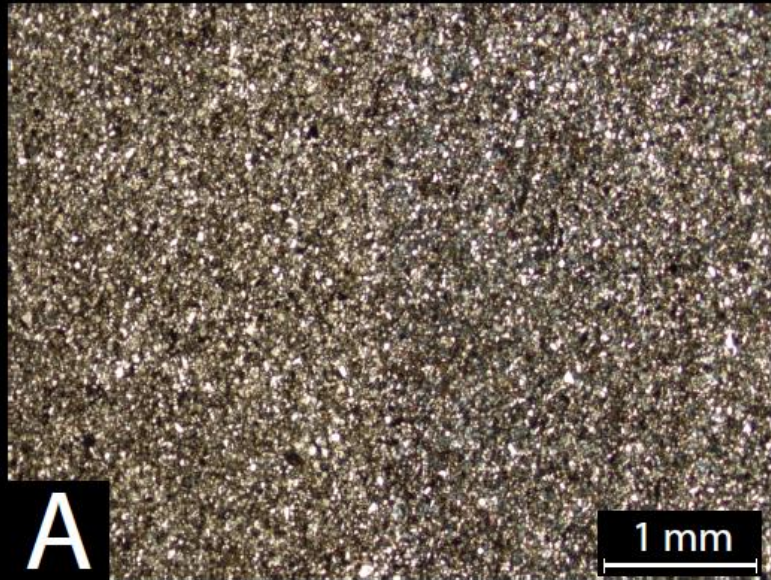
3193.50' – Massive-bedded Peloidal Siltstone: Very fine sand to silt quartz grains, carbonate peloids, and clay minerals are the main constituents. No apparent bedding or sedimentary structures (other than induced fractures) are observed in this sample. All mineral assemblages appear to be fully homogenized. XRD analysis 5% carbonates (3% calcite and 2% dolomite), 43% clays, 38% quartz, 14% other minerals (2% potassium feldspar, 9% plagioclase feldspar, 3% pyrite, and trace marcasite).



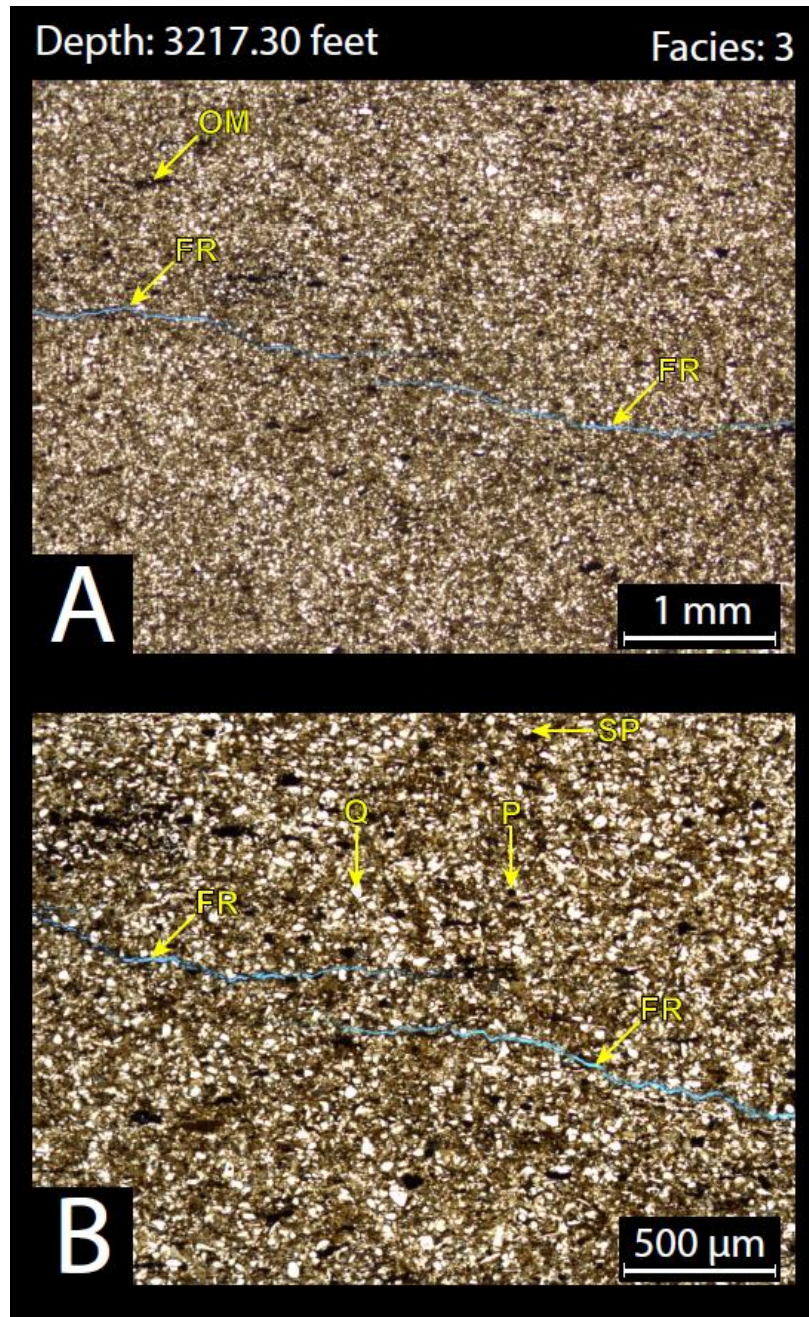
3204.40' – Massive-bedded Peloidal Siltstone: Very fine sand to silt quartz grains and clay minerals are the main constituents. No apparent bedding or sedimentary structures (other than induced fractures) are observed in this sample. All mineral assemblages appear to be fully homogenized. XRD analysis trace carbonates (0% calcite and trace dolomite), 48% clays, 36% quartz, 16% other minerals (5% potassium feldspar, 9% plagioclase feldspar, and 2% pyrite).

Depth: 3211.35 feet

Facies: 3



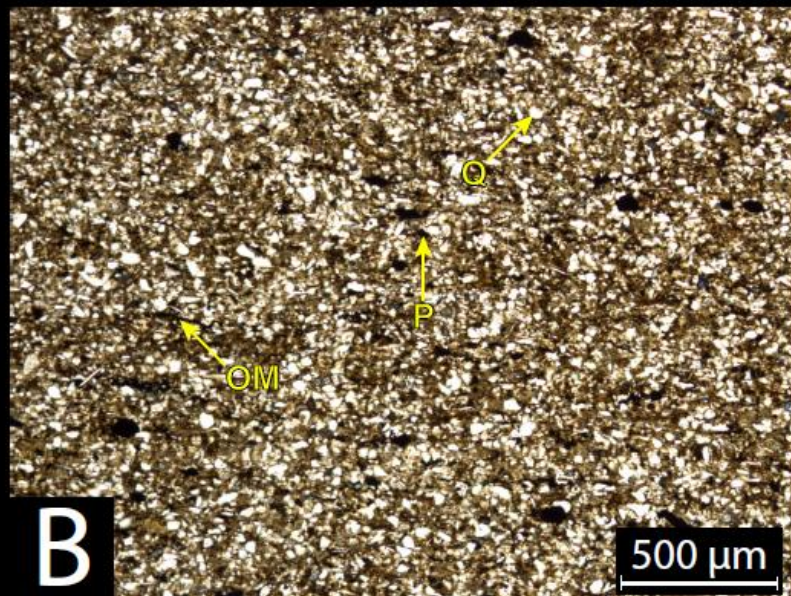
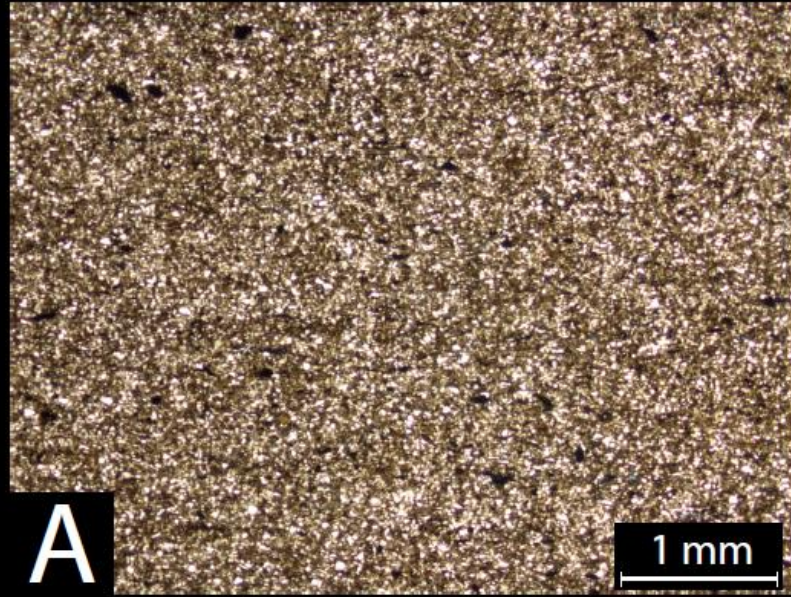
3211.35' – Massive-bedded Peloidal Siltstone: Very fine sand to silt quartz grains, carbonate peloids, and clay minerals are the main constituents. No apparent bedding or sedimentary structures are observed in this sample. All mineral assemblages appear to be fully homogenized. XRD analysis 27% carbonates (4% calcite and 23% dolomite), 29% clays, 34% quartz, 10% other minerals (1% potassium feldspar, 6% plagioclase feldspar, 2% pyrite, and 1% marcasite).



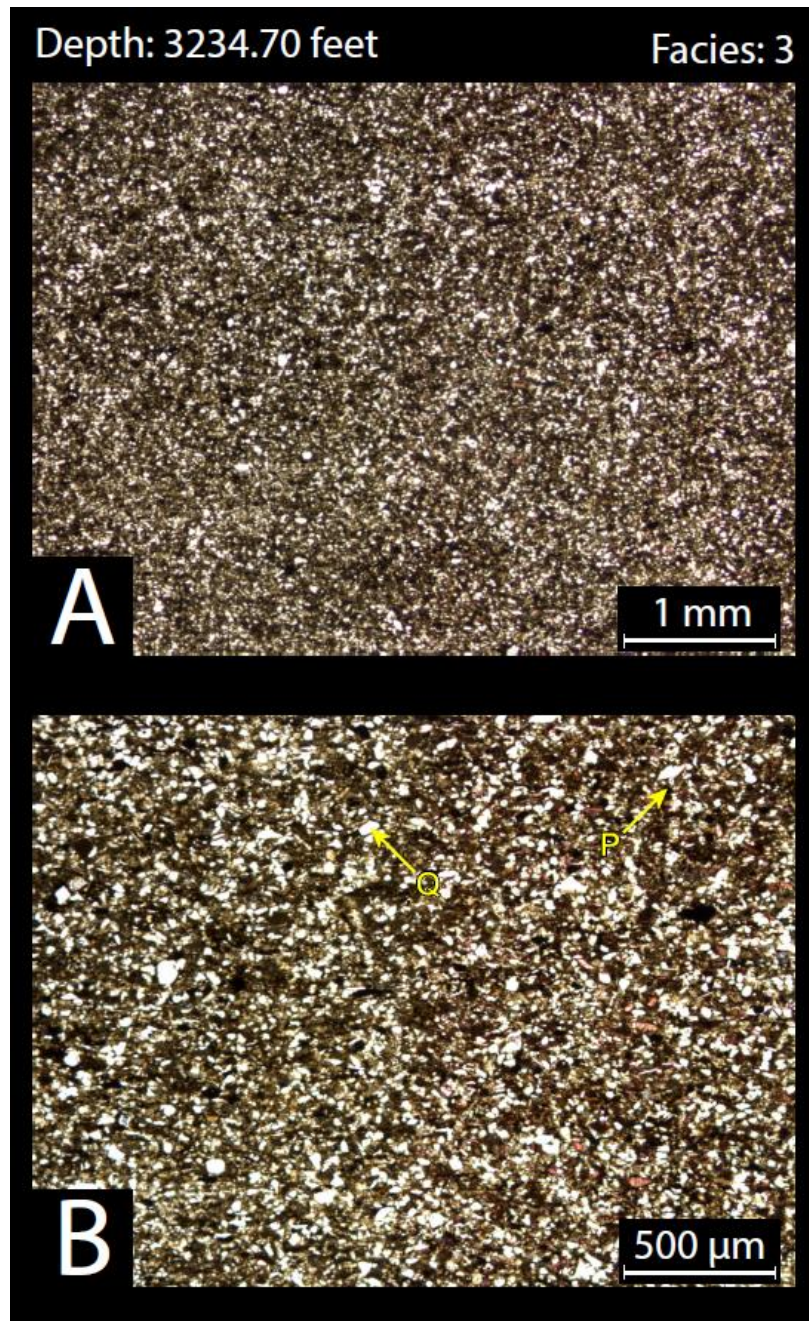
3217.30' – Massive-bedded Peloidal Siltstone: Very fine sand to silt quartz grains, carbonate peloids, and clay minerals are the main constituents. No apparent bedding or sedimentary structures (other than induced fractures) are observed in this sample. All mineral assemblages appear to be fully homogenized. XRD analysis 6% carbonates (5% calcite and 1% dolomite), 42% clays, 38% quartz, 14% other minerals (3% potassium feldspar, 7% plagioclase feldspar, 3% pyrite, and 1% apatite).

Depth: 3224.40 feet

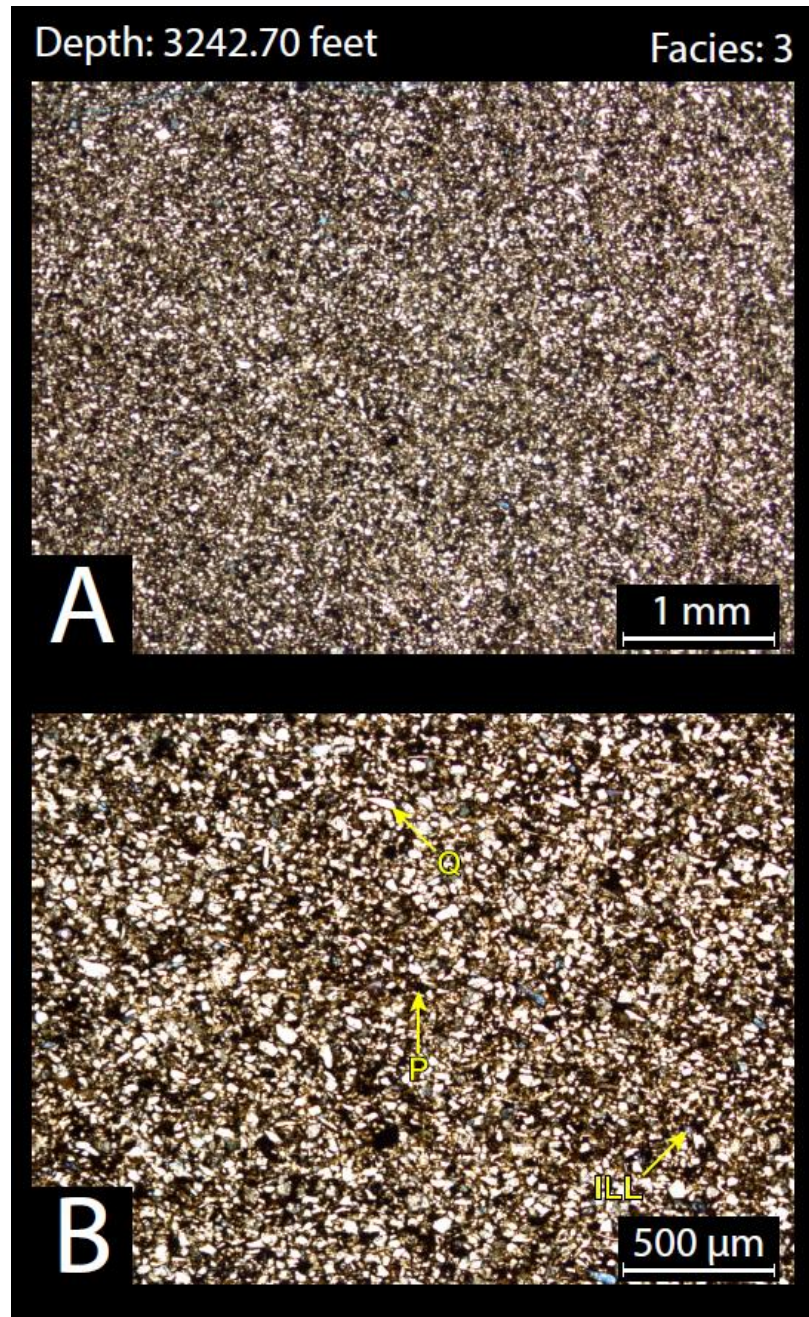
Facies: 4



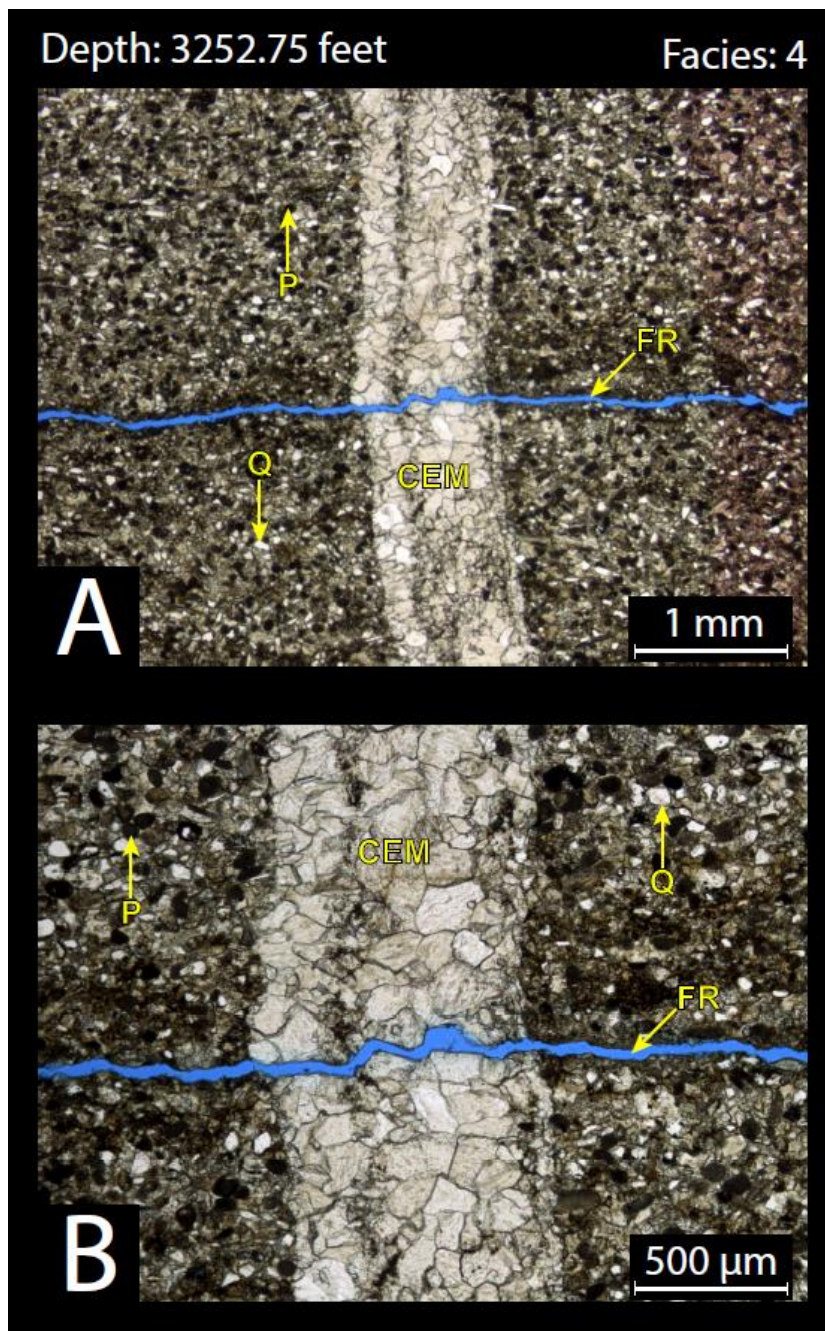
3224.40' – Laminated Peloidal Siltstone: Clay minerals and very fine sand to quartz silt are the main constituents. All mineral assemblages appear to be fully homogenized. XRD analysis 2% carbonates (1% calcite and 1% dolomite), 51% clays, 36% quartz, 11% other minerals (2% potassium feldspar, 6% plagioclase feldspar, and 3% pyrite).



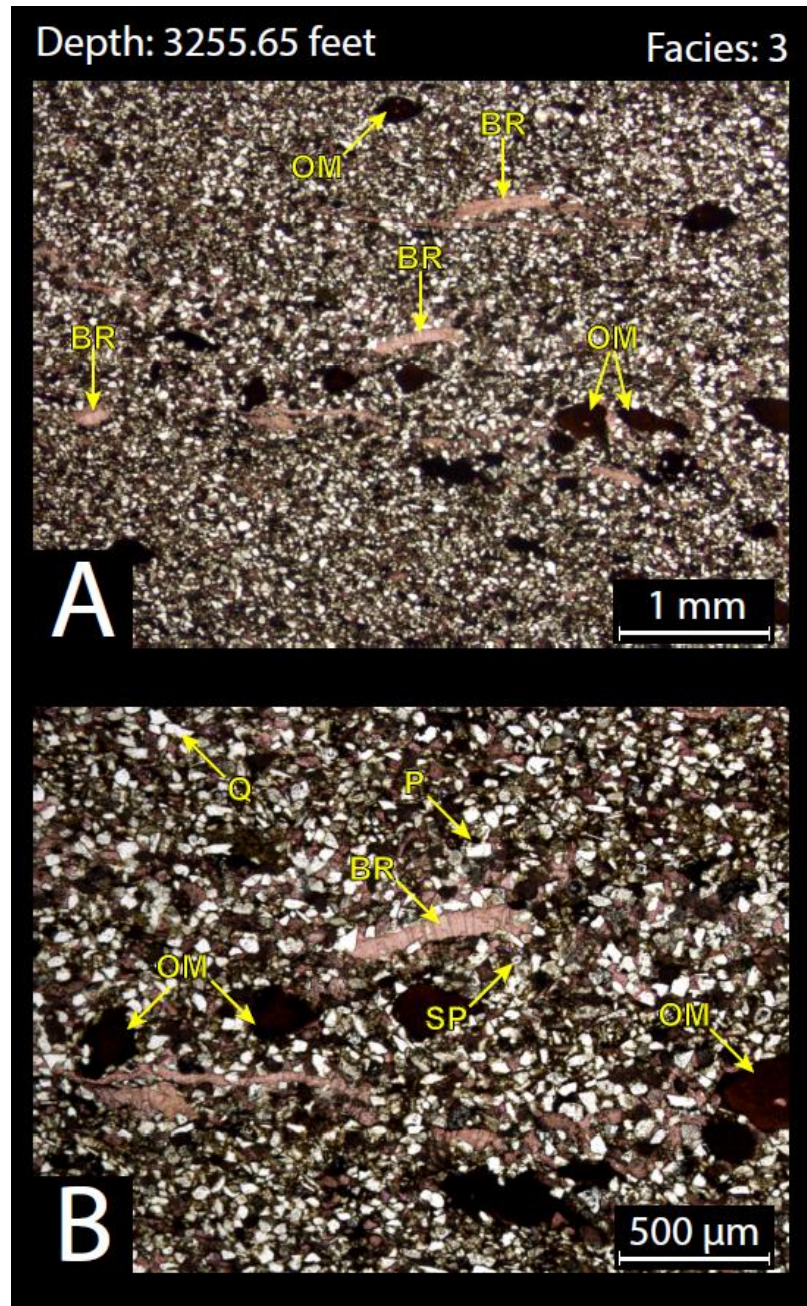
3234.70' – Massive-bedded Peloidal Siltstone: Very fine sand to silt quartz grains, carbonate peloids, and clay minerals are the main constituents. No apparent bedding or sedimentary structures are observed in this sample. All mineral assemblages appear to be fully homogenized. XRD analysis 12% carbonates (12% calcite and trace dolomite), 42% clays, 35% quartz, 11% other minerals (2% potassium feldspar, 6% plagioclase feldspar, and 3% pyrite).



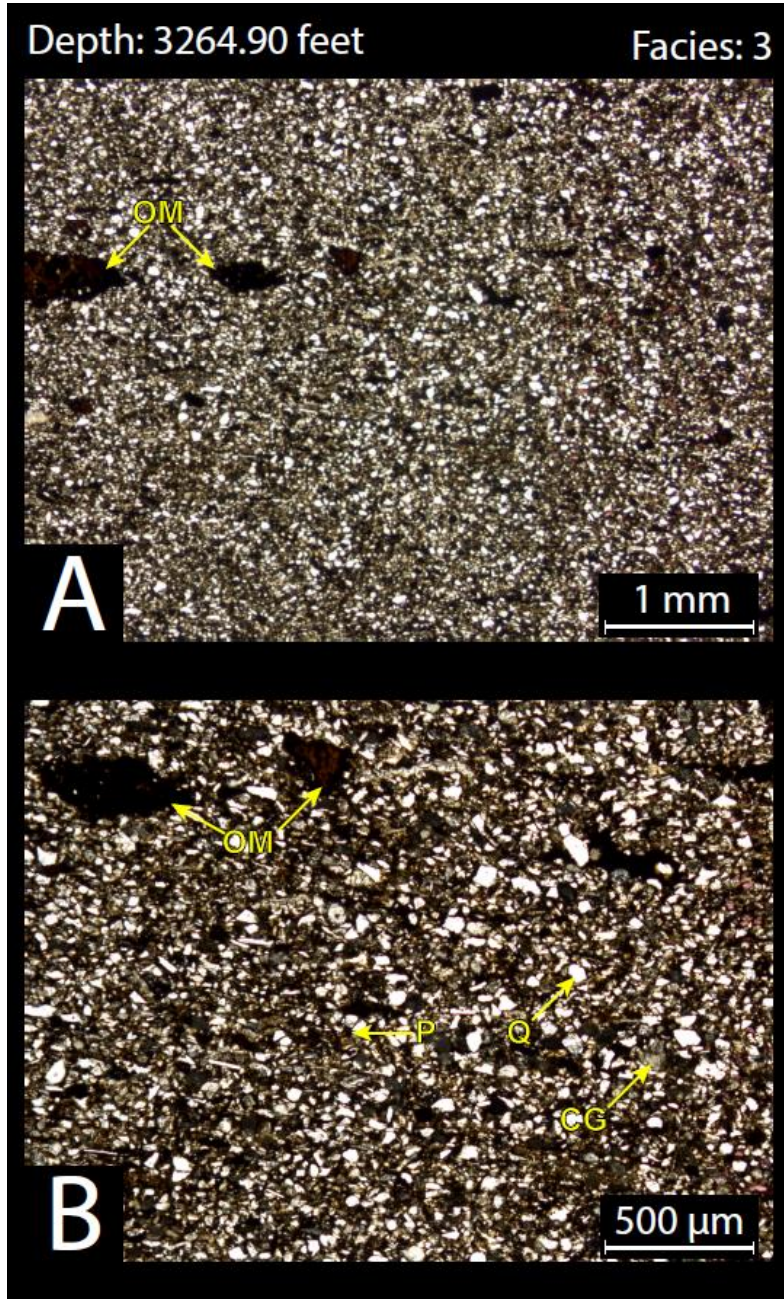
3242.70' – Massive-bedded Peloidal Siltstone: Very fine sand to silt quartz grains, carbonate peloids, and clay minerals are the main constituents. No apparent bedding or sedimentary structures are observed in this sample. All mineral assemblages appear to be fully homogenized. XRD analysis 11% carbonates (4% calcite and 7% dolomite), 28% clays, 44% quartz, 17% other minerals (2% potassium feldspar, 10% plagioclase feldspar, 3% pyrite, and 2% apatite).



3252.75' – Laminated Peloidal Siltstone: Carbonate peloids and very fine sand to quartz silt are the main constituents. The fracture in the center is filled with calcite cement. Open fractures observed are likely induced. All mineral assemblages appear to be fully homogenized. XRD analysis 67% carbonates (66% calcite and 1% dolomite), 5% clays, 20% quartz, 8% other minerals (trace potassium feldspar, 7% plagioclase feldspar, 1% pyrite, and trace apatite).



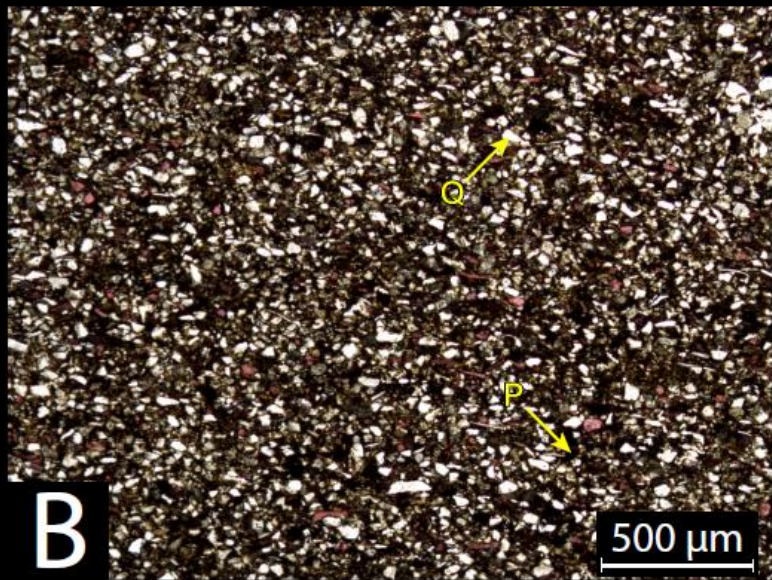
3255.65' – Massive-bedded Peloidal Siltstone: Very fine sand to silt quartz grains, brachiopod shell fragments, and carbonate peloids are the main constituents. Small masses of organic matter scattered throughout the thin section, but not abundant (<5%) overall. No apparent bedding or sedimentary structures are observed in this sample. All mineral assemblages appear to be fully homogenized. XRD analysis 24% carbonates (19% calcite and 5% dolomite), 18% clays, 43% quartz, 15% other minerals (2% potassium feldspar, 8% plagioclase feldspar, 3% pyrite, and 2% apatite).



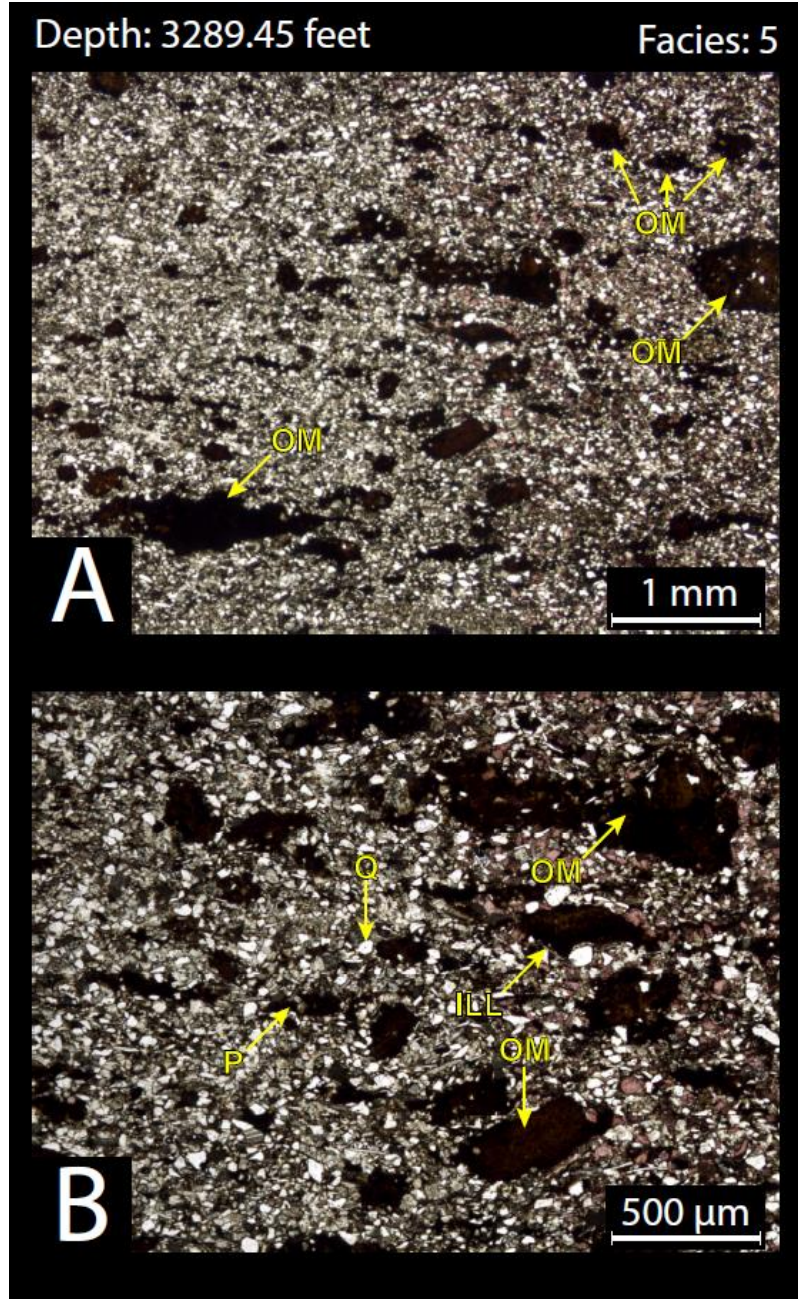
3264.90' – Massive-bedded Peloidal Siltstone: Very fine sand to silt quartz grains, carbonate peloids, and clay minerals are the main constituents. Small masses of organic matter scattered throughout the thin section, but not abundant (<5%) overall. No apparent bedding or sedimentary structures are observed in this sample. All mineral assemblages appear to be fully homogenized. XRD analysis 18% carbonates (15% calcite and 3% dolomite), 25% clays, 40% quartz, 17% other minerals (3% potassium feldspar, 9% plagioclase feldspar, 3% pyrite, and 2% apatite).

Depth: 3280.80 feet

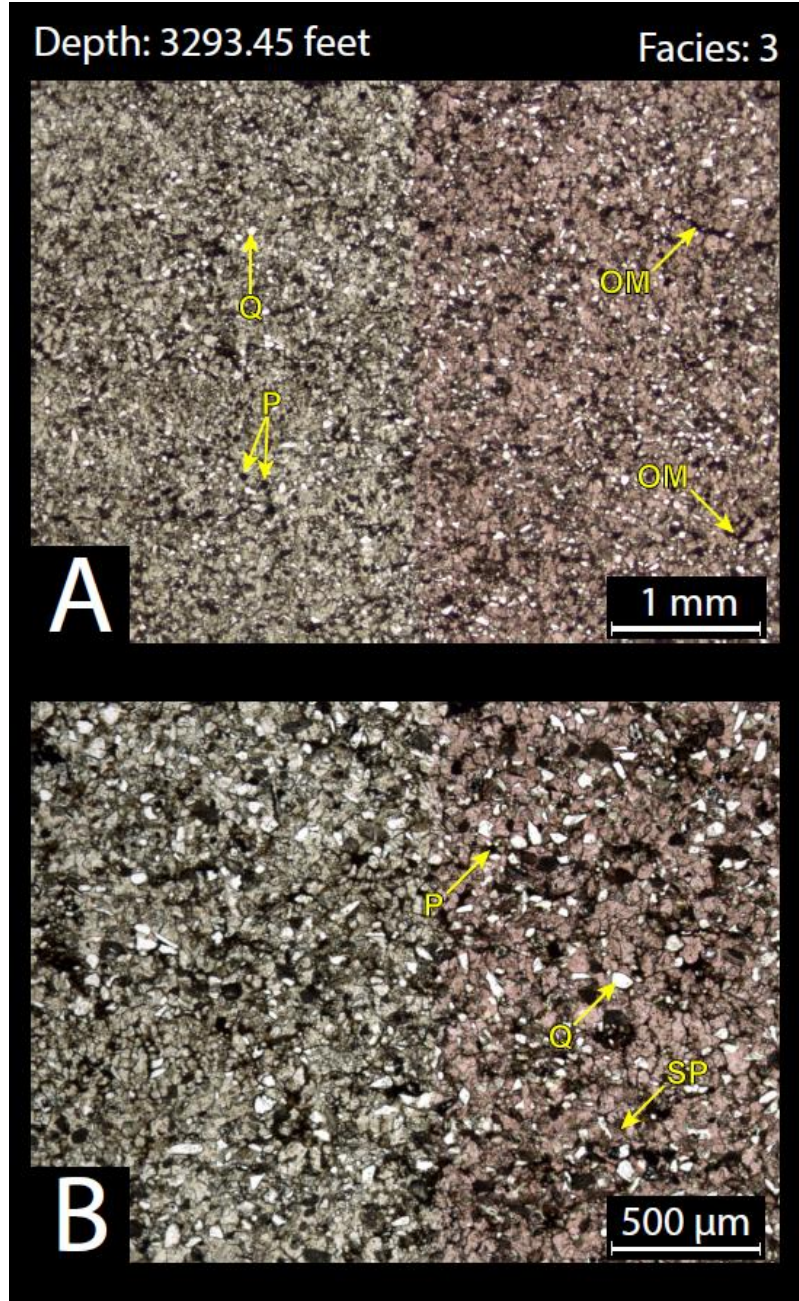
Facies: 3



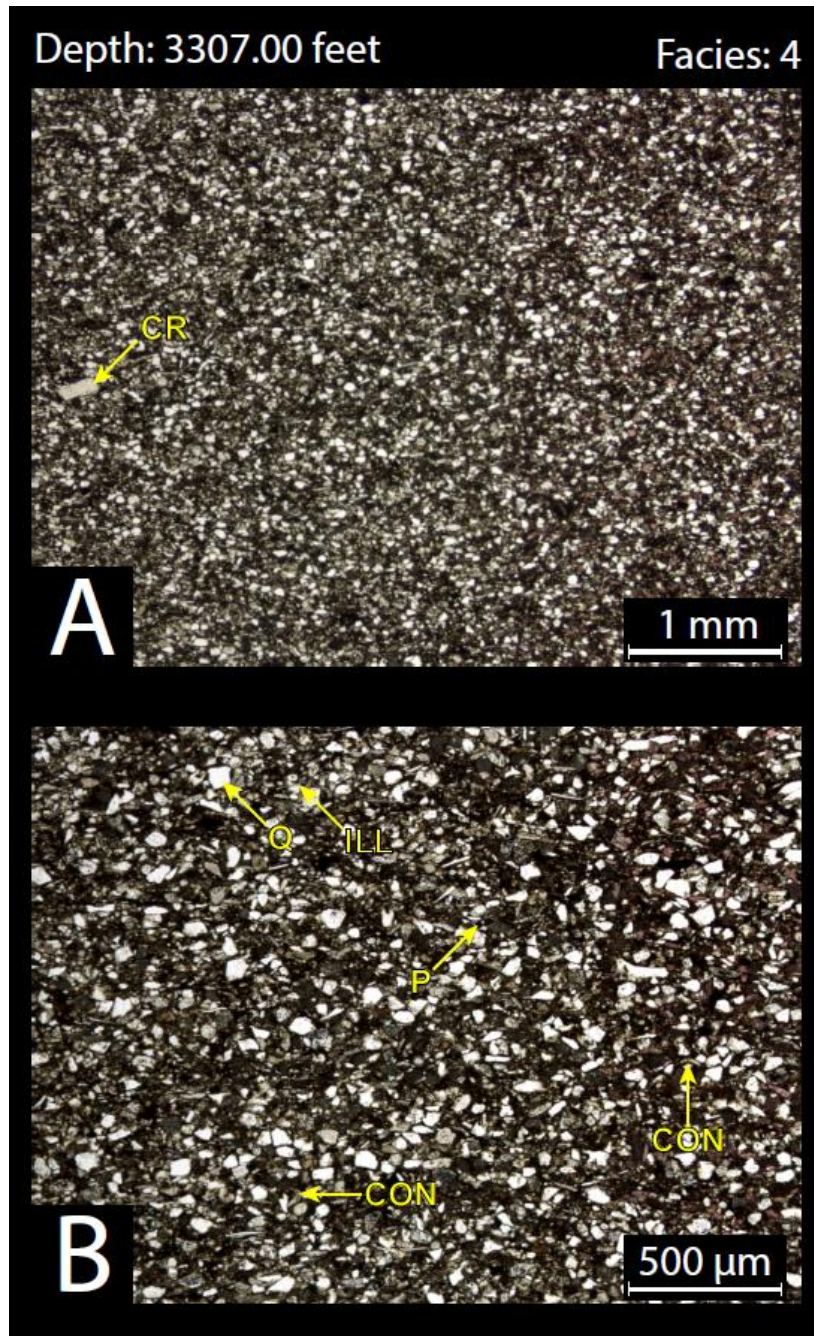
3280.80' – Massive-bedded Peloidal Siltstone: Very fine sand to silt quartz grains, carbonate peloids, and clay minerals are the main constituents. No apparent bedding or sedimentary structures are observed in this sample. All mineral assemblages appear to be fully homogenized. XRD analysis 21% carbonates (15% calcite and 6% dolomite), 22% clays, 43% quartz, 14% other minerals (1% potassium feldspar, 8% plagioclase feldspar, 4% pyrite, and 1% apatite).



3289.45' – Mottled Peloidal Siltstone: Very fine sand to silt quartz grains, carbonate peloids, and clay minerals are the main constituents. Small masses of organic matter scattered throughout the thin section, (relative abundance <15%). No apparent bedding are observed in this sample, likely due to biotic activity. All mineral assemblages appear to be fully homogenized. XRD analysis 26% carbonates (21% calcite and 5% dolomite), 20% clays, 34% quartz, 20% other minerals (2% potassium feldspar, 8% plagioclase feldspar, 2% pyrite, and 8% apatite).



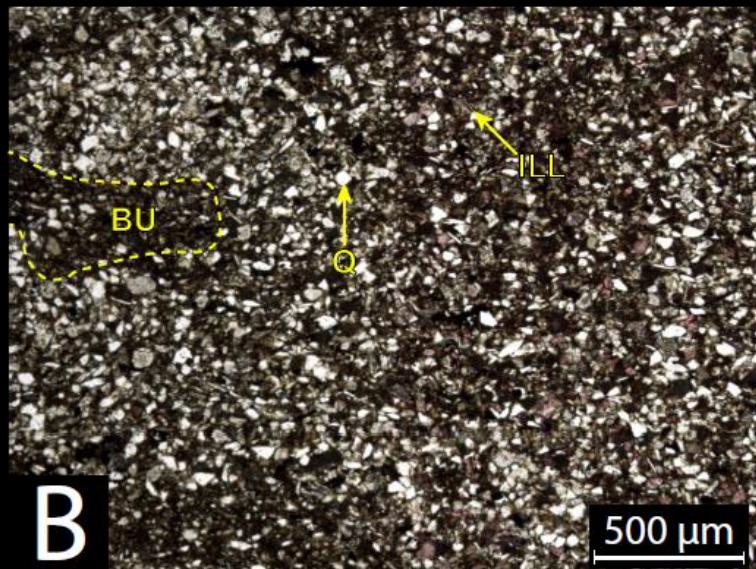
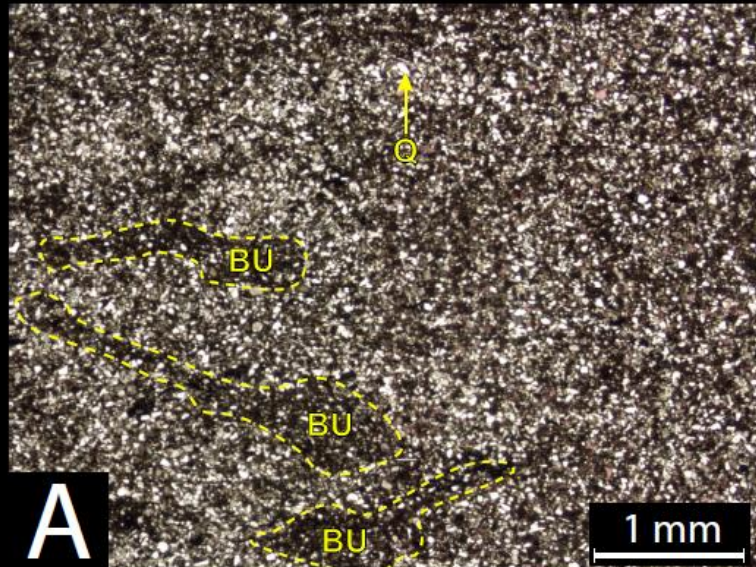
3293.45' – Massive-bedded Peloidal Siltstone: Carbonate cement, peloids, and very fine sand to silt quartz grains are the main constituents. Small masses of organic matter scattered throughout the thin section, but not abundant (<1%) overall. No apparent bedding or sedimentary structures are observed in this sample. All mineral assemblages appear to be fully homogenized. XRD analysis 62% carbonates (61% calcite and 1% dolomite), 10% clays, 19% quartz, 9% other minerals (1% potassium feldspar, 7% plagioclase feldspar, and 1% pyrite).



3307.00' – Laminated Peloidal Siltstone: Very fine sand to quartz silt, clay minerals, crinoid stem fragments, and peloids are the main constituents. Scattered conodonts are also observable, but not abundant overall. Fractures observed are likely induced. All mineral assemblages appear to be fully homogenized. XRD analysis 35% carbonates (31% calcite and 4% dolomite), 21% clays, 34% quartz, 10% other minerals (1% potassium feldspar, 7% plagioclase feldspar, and 2% pyrite).

Depth: 3319.00 feet

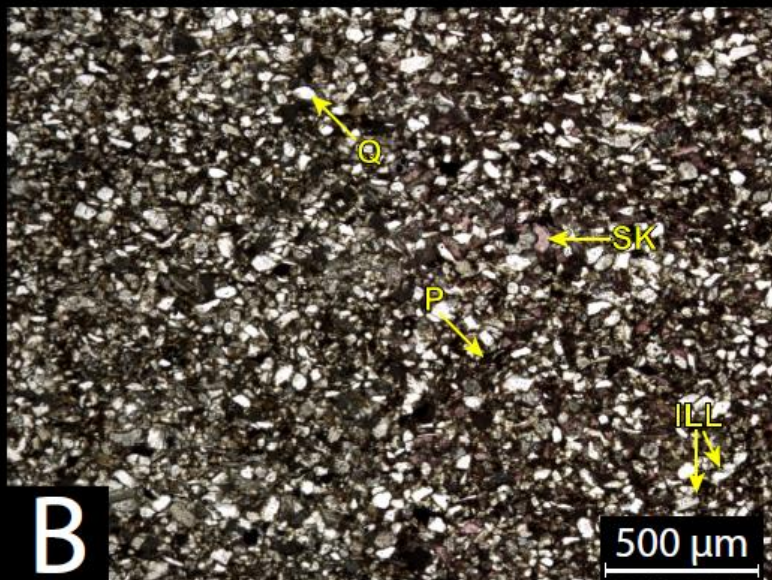
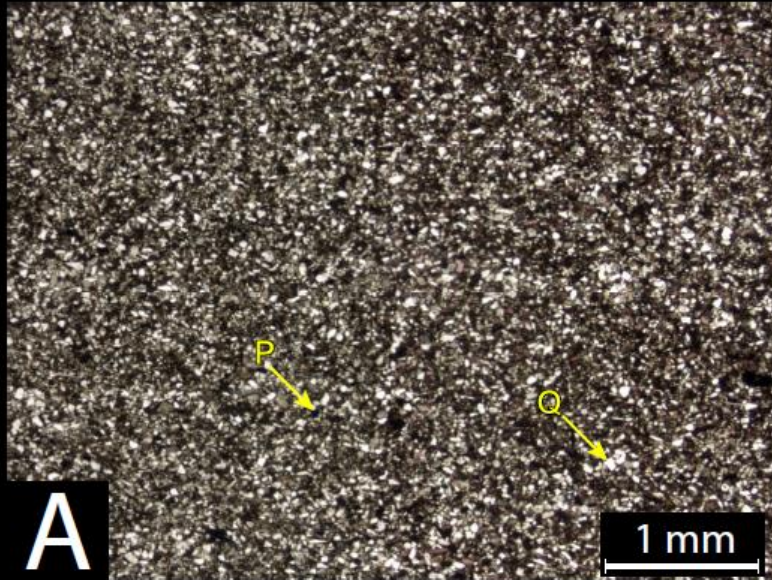
Facies: 5



3289.45' – Mottled Peloidal Siltstone: Very fine sand to silt quartz grains, carbonate peloids, and clay minerals are the main constituents. Burrows in this sample are preferentially filled with clay minerals. No apparent bedding are observed in this sample, likely due to biotic activity. All mineral assemblages outside of the burrows appear to be fully homogenized. XRD analysis 26% carbonates (21% calcite and 5% dolomite), 24% clays, 37% quartz, 13% other minerals (2% potassium feldspar, 8% plagioclase feldspar, and 3% pyrite).

Depth: 3329.60 feet

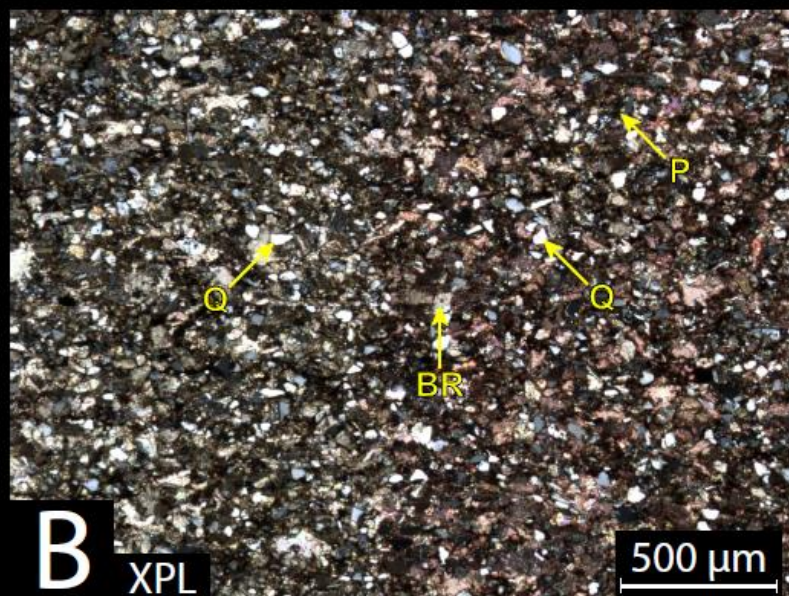
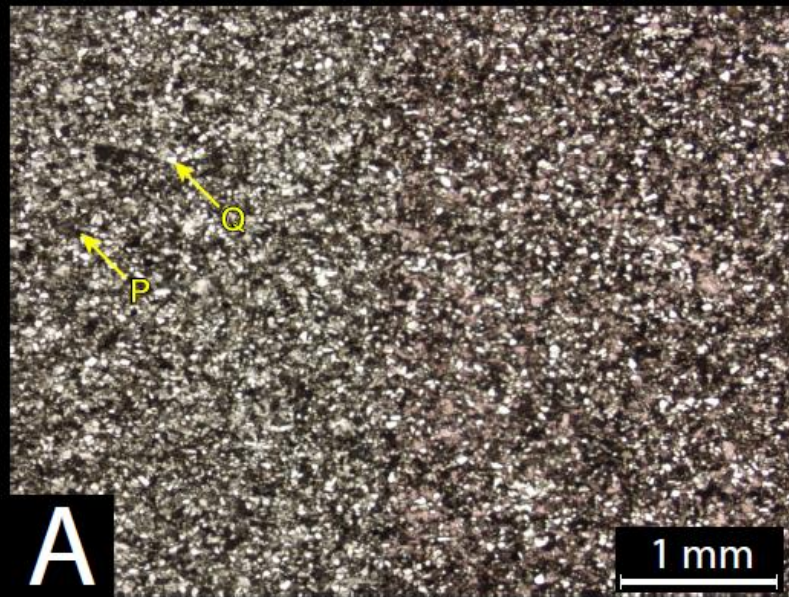
Facies: 4



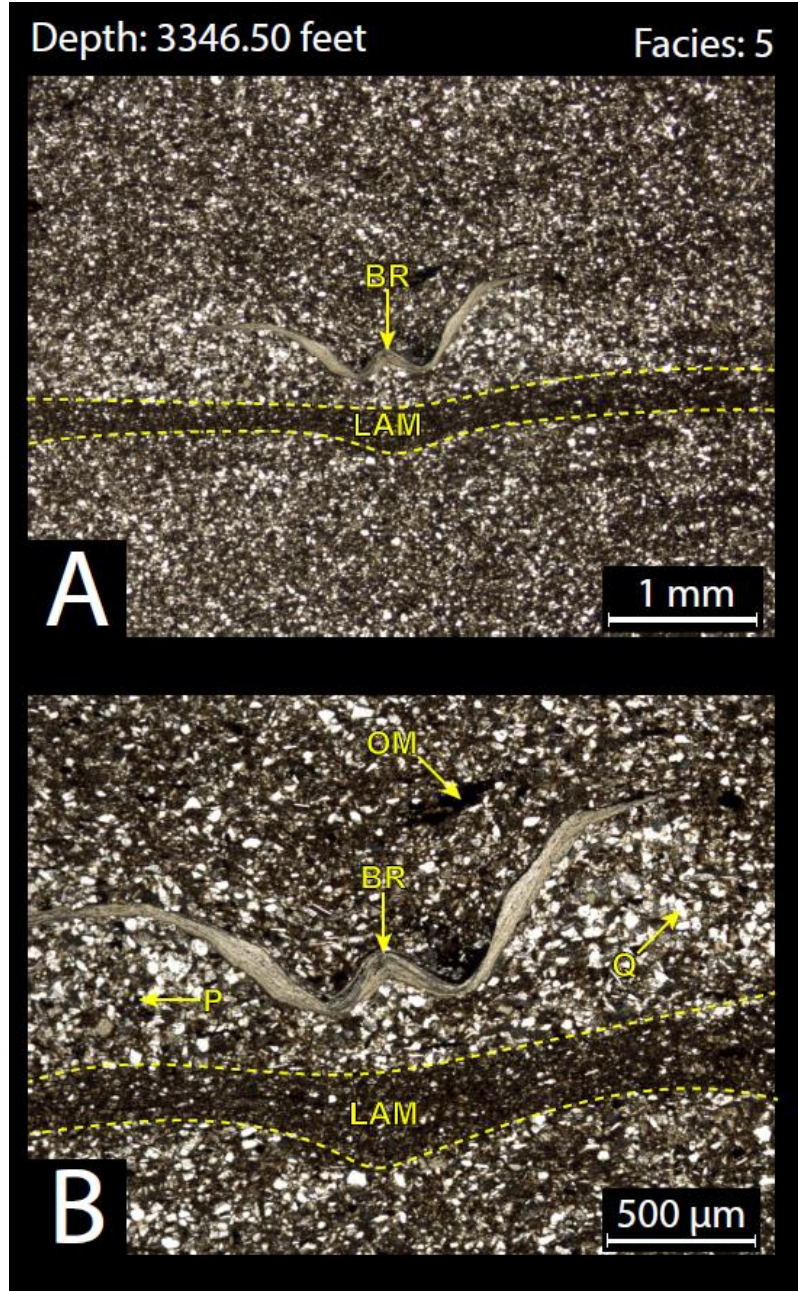
3329.60' – Laminated Peloidal Siltstone: Very fine sand to quartz silt, clay minerals, crinoid stem fragments, and peloids are the main constituents. Fractures observed are likely induced. All mineral assemblages appear to be fully homogenized. XRD analysis 30% carbonates (24% calcite and 6% dolomite), 16% clays, 43% quartz, 11% other minerals (2% potassium feldspar, 7% plagioclase feldspar, 2% pyrite, and trace apatite).

Depth: 3336.70 feet

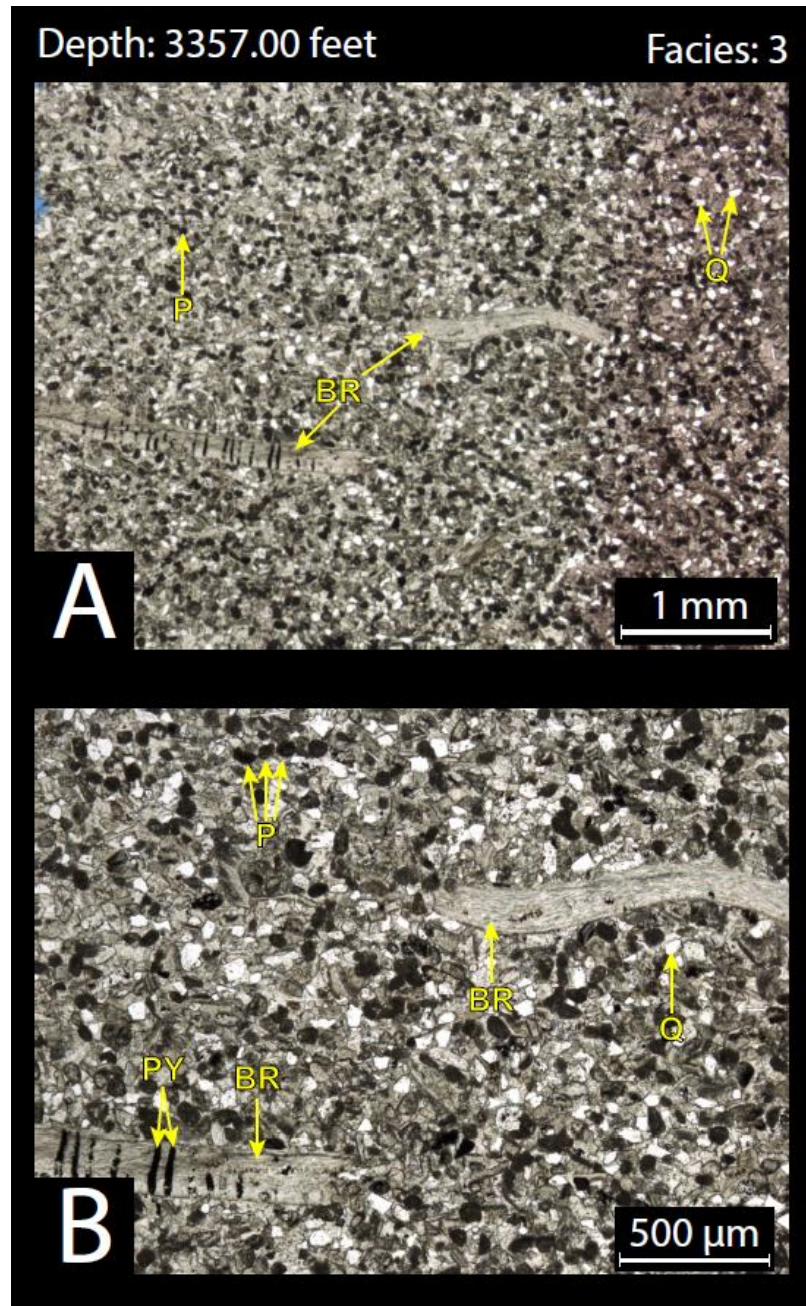
Facies: 4



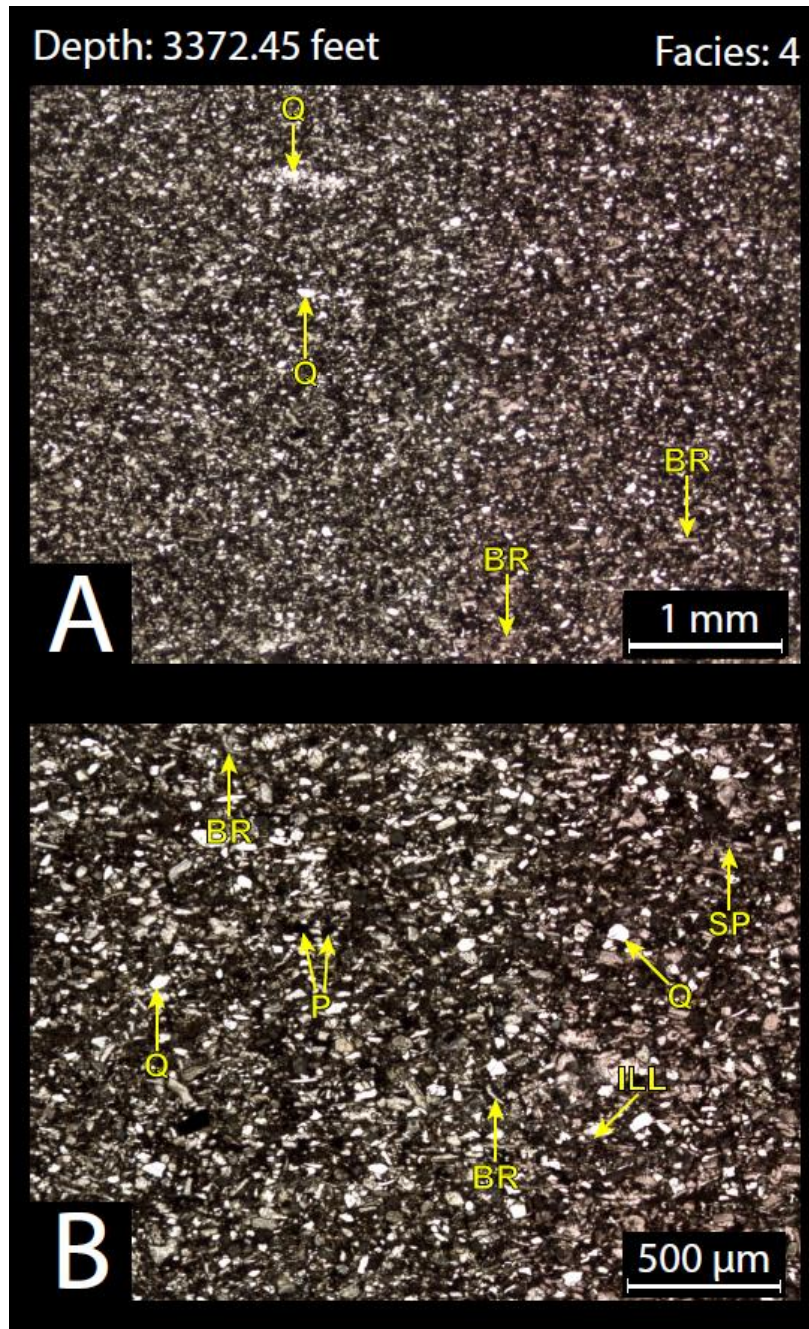
3336.70' – Laminated Peloidal Siltstone: Carbonate peloids, very fine sand to quartz silt, and clay minerals, are the main constituents. Fractures observed are likely induced. All mineral assemblages appear to be fully homogenized. XRD analysis 48% carbonates (43% calcite and 5% dolomite), 13% clays, 28% quartz, 11% other minerals (2% potassium feldspar, 7% plagioclase feldspar, and 2% pyrite).



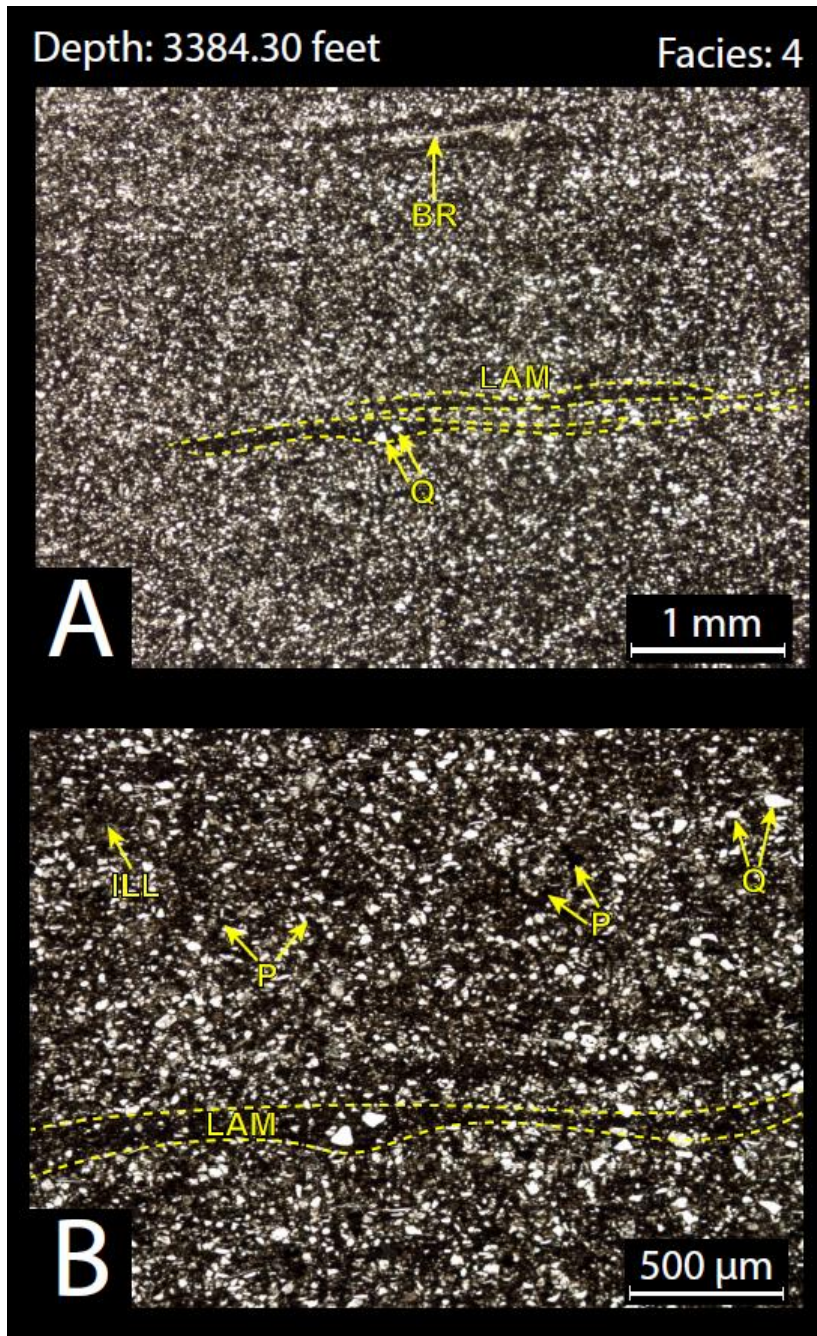
3289.45' – Mottled Peloidal Siltstone: Very fine sand to silt quartz grains, carbonate peloids, brachiopod shell fragments, and clay minerals are the main constituents. Millimeter-scale horizontal burrows are also present in this sample. Some laminations are intact, suggesting lower biotic activity. All mineral assemblages outside of the clay laminations appear to be fully homogenized. XRD analysis 26% carbonates (23% calcite and 3% dolomite), 28% clays, 36% quartz, 10% other minerals (1% potassium feldspar, 6% plagioclase feldspar, 2% pyrite, and 1% marcasite).



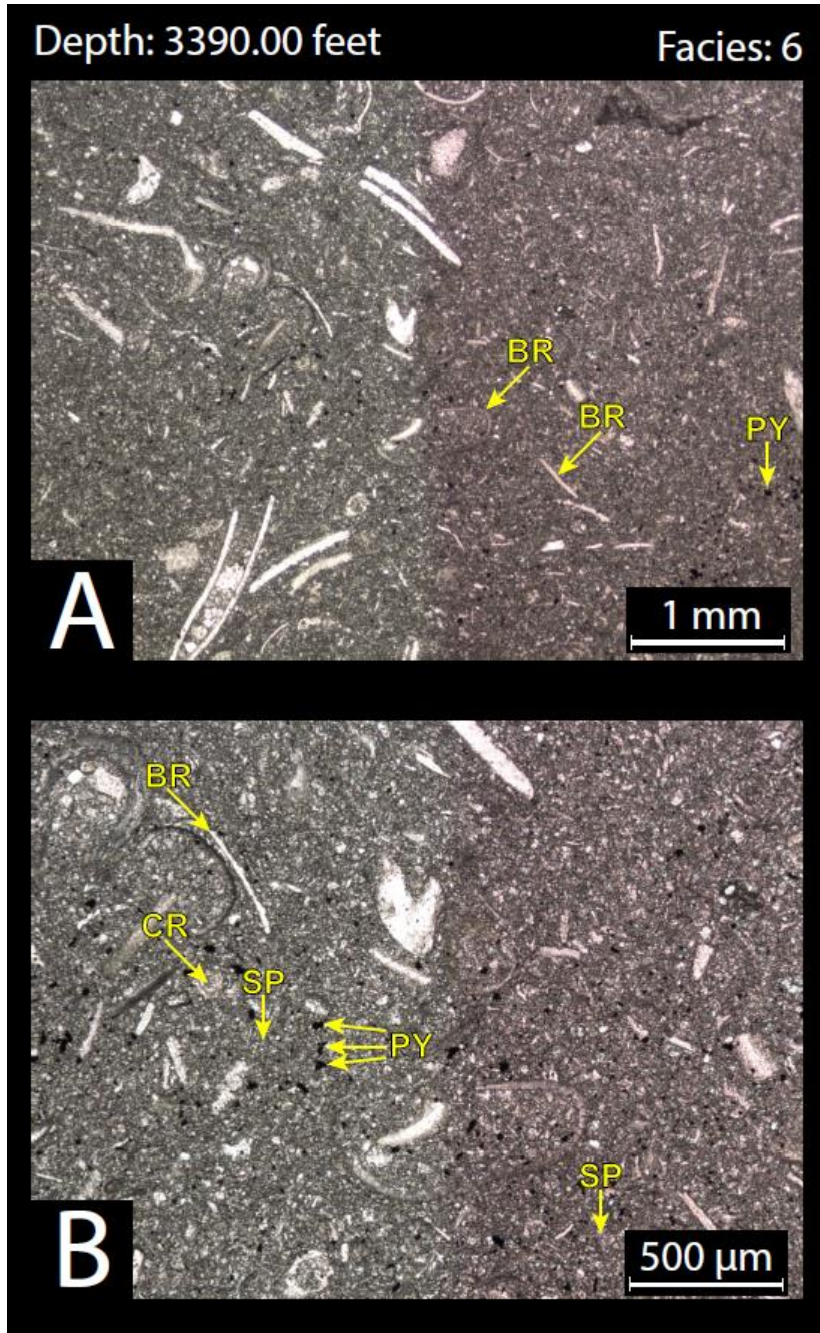
3357.00' – Massive-bedded Peloidal Siltstone: Brachiopod shell fragments, peloids, and very fine sand to silt quartz grains are the main constituents. Trace amounts of pyrite are observed partially replacing segments in brachiopod shell fragments. No apparent bedding or sedimentary structures are observed in this sample. All mineral assemblages appear to be fully homogenized. XRD analysis 78% carbonates (77% calcite and 1% dolomite), 4% clays, 14% quartz, 4% other minerals (trace potassium feldspar, 4% plagioclase feldspar, and trace pyrite).



3372.45' – Laminated Peloidal Siltstone: Carbonate peloids, brachiopod fragments, and very fine sand to quartz silt are the main constituents. Fractures observed are likely induced. All mineral assemblages appear to be fully homogenized. XRD analysis 61% carbonates (60% calcite and 1% dolomite), 9% clays, 20% quartz, 10% other minerals (1% potassium feldspar, 4% plagioclase feldspar, 2% pyrite, and 3% marcasite).



3384.30' – Laminated Peloidal Siltstone: Very fine sand to quartz silt and clay minerals are the main constituents. Brachiopod shell fragments are also observed. Clay mineral assemblages appear to be organized horizontally (parallel to bedding planes). Fractures observed are likely induced. XRD analysis 28% carbonates (25% calcite and 3% dolomite), 28% clays, 32% quartz, 12% other minerals (2% potassium feldspar, 7% plagioclase feldspar, and 3% pyrite).



3390.00' – Skeletal Mudstone/Wackestone: Carbonate cement and bioclastic debris (brachiopod shell fragments and crinoid stem fragments) are the main constituents. Millimeter-scale horizontal burrows are also present in this facies, but not observed in this sample. All mineral assemblages appear to be fully homogenized. XRD analysis 72% carbonates (70% calcite and 2% dolomite), 8% clays, 17% quartz, 3% other minerals (trace potassium feldspar, 1% plagioclase feldspar, and 2% pyrite).

IV. Angell 1-23 X-Ray Diffraction Analysis

X-ray diffraction (XRD) is a diagnostic tool for identifying crystalline materials and provides quantitative estimates of bulk and clay mineralogy. Devon Energy sampled the butt section of the core. These samples were evaluated utilizing whole-rock bulk mineralogy to identify and quantify the abundances of common framework grains and cements.

Facies	Sample Depth (ft)		Carbonates		OTHER MINERALS					TOTALS			
	Top	Bottom	Calcite	Dolomite (Fe/Ca+)	K-spar	Plag.	Pyrite	Marcasite	Apatite	Quartz	Clays	Carb.	Others
6	3013.00'	3013.30'	87	2	Tr	1	Tr	0	0	2	8	89	1
6	3019.00'	3019.30'	85	3	Tr	1	Tr	0	0	2	9	88	1
6	3032.00'	3032.30'	87	4	Tr	Tr	Tr	0	0	2	7	91	0
6	3046.00'	3046.30'	89	2	Tr	1	Tr	0	0	2	6	91	1
4	3055.25'	3055.50'	7	Tr	1	3	3	0	2	23	61	7	9
4	3064.50'	3064.80'	7	2	1	4	2	0	5	55	24	9	12
3	3072.35'	3072.65'	3	1	1	6	3	1	0	31	54	4	11
4	3082.70'	3083.00'	2	1	1	3	4	1	2	19	67	3	11
1	3094.70'	3095.00'	2	Tr	Tr	3	2	0	0	16	77	2	5
3	3098.20'	3098.50'	1	1	2	6	4	1	2	31	52	2	15
5	3139.25'	3139.50'	7	1	2	4	9	0	0	18	59	8	15
4	3160.25'	3160.55'	21	Tr	1	4	3	0	0	24	47	21	8
3	3165.45'	3165.45'	60	11	Tr	3	1	0	0	12	13	71	4
4	3177.20'	3177.50'	1	Tr	1	2	14	2	0	18	62	1	19
3	3186.15'	3186.45'	3	1	3	5	2	0	0	31	55	4	10
3	3193.50'	3193.80'	3	2	2	9	3	Tr	0	38	43	5	14
3	3204.40'	3204.70'	0	Tr	5	9	2	0	0	36	48	0	16
3	3211.35'	3211.35'	4	23	1	6	2	1	0	34	29	27	10
3	3217.30'	3217.60'	5	1	3	7	3	0	1	38	42	6	14
4	3224.40'	3224.70'	1	1	2	6	3	0	0	36	51	2	11
3	3234.70'	3235.00'	12	Tr	2	6	3	0	0	35	42	12	11
3	3242.70'	3243.00'	4	7	2	10	3	0	2	44	28	11	17
4	3252.75'	3252.85'	66	1	Tr	7	1	0	Tr	20	5	67	8
3	3255.65'	3255.65'	19	5	2	8	3	0	2	43	18	24	15
3	3264.90'	3264.90'	15	3	3	9	3	0	2	40	25	18	17
3	3280.80'	3280.80'	15	6	1	8	4	0	1	43	22	21	14
5	3289.45'	3289.45'	21	5	2	8	2	0	8	34	20	26	20
3	3293.45'	3293.45'	61	1	1	7	1	0	0	19	10	62	9
4	3307.00'	3307.30'	31	4	1	7	2	0	0	34	21	35	10
5	3319.00'	3319.30'	21	5	2	8	3	0	0	37	24	26	13
4	3329.60'	3329.90'	24	6	2	7	2	0	Tr	43	16	30	11
5	3336.70'	3337.00'	43	5	2	7	2	0	0	28	13	48	11
5	3346.50'	3346.80'	23	3	1	6	2	1	0	36	28	26	10
3	3357.00'	3357.30'	77	1	Tr	4	Tr	0	0	14	4	78	4
4	3372.45'	3372.75'	60	1	1	4	2	3	0	20	9	61	10
4	3384.30'	3384.60'	25	3	2	7	3	0	0	32	28	28	12
6	3390.00'	3390.30'	70	2	Tr	1	2	0	0	17	8	72	3

Table 7 XRD analysis for the Angell 1-23

Appendix B:

Wise 1-20

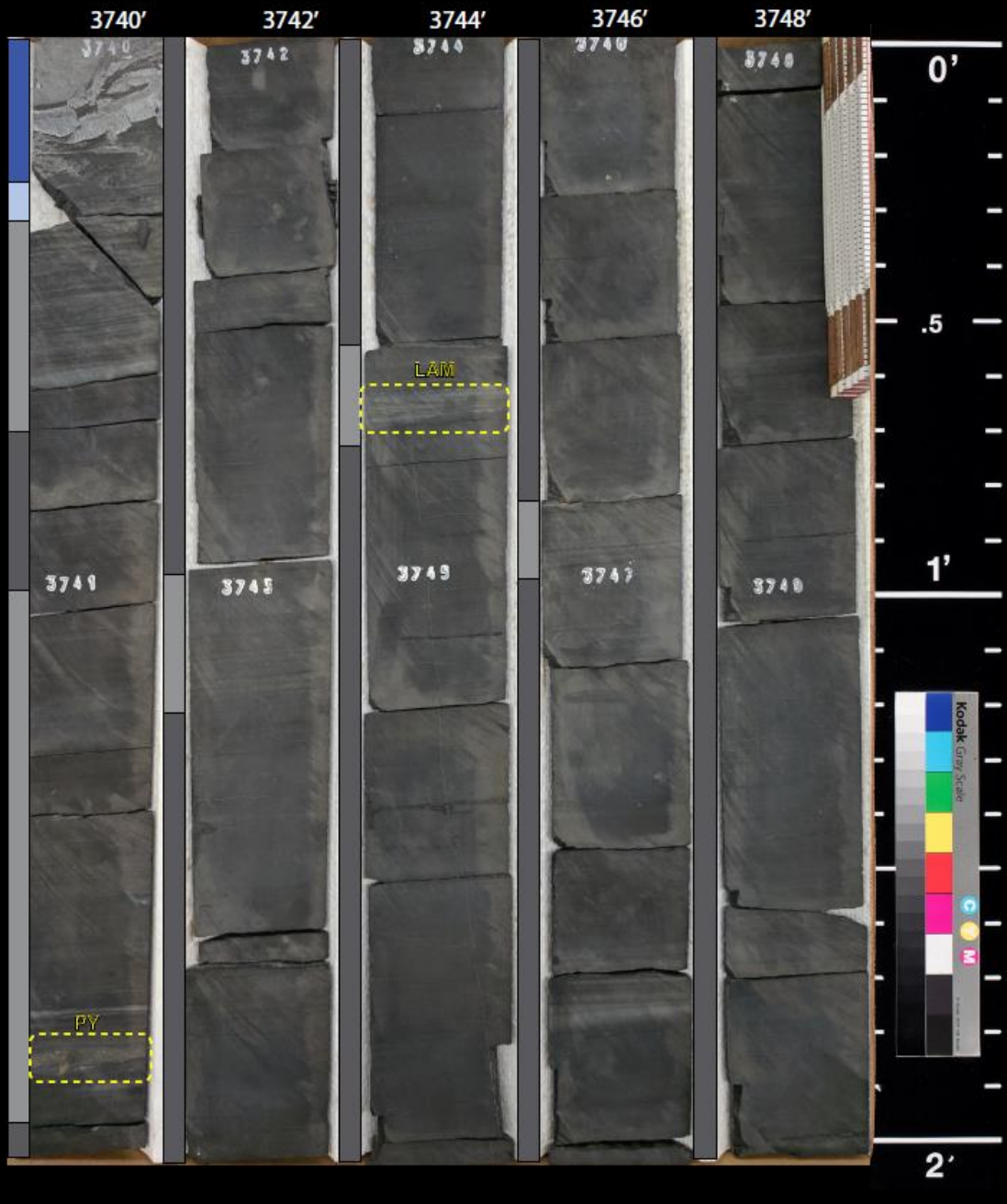
I. Wise 1-20 Whole Core Photographs

Core Photographs are shown under white light and are labeled with the abbreviations in Table 5. The core is in boxes containing 10 feet of core (when full) and within each box, cores are split into 2 foot intervals. The shallowest depths are located in the top left corner of the boxes, while the deepest depths are in the bottom right corner. The scales next to the core boxes are in tenths of feet. The contacts between the “Mississippian Limestone” and differing strata are marked where present. Next to the cores are colored rectangles that correspond to the facies stacking pattern colors (see Figure 15).

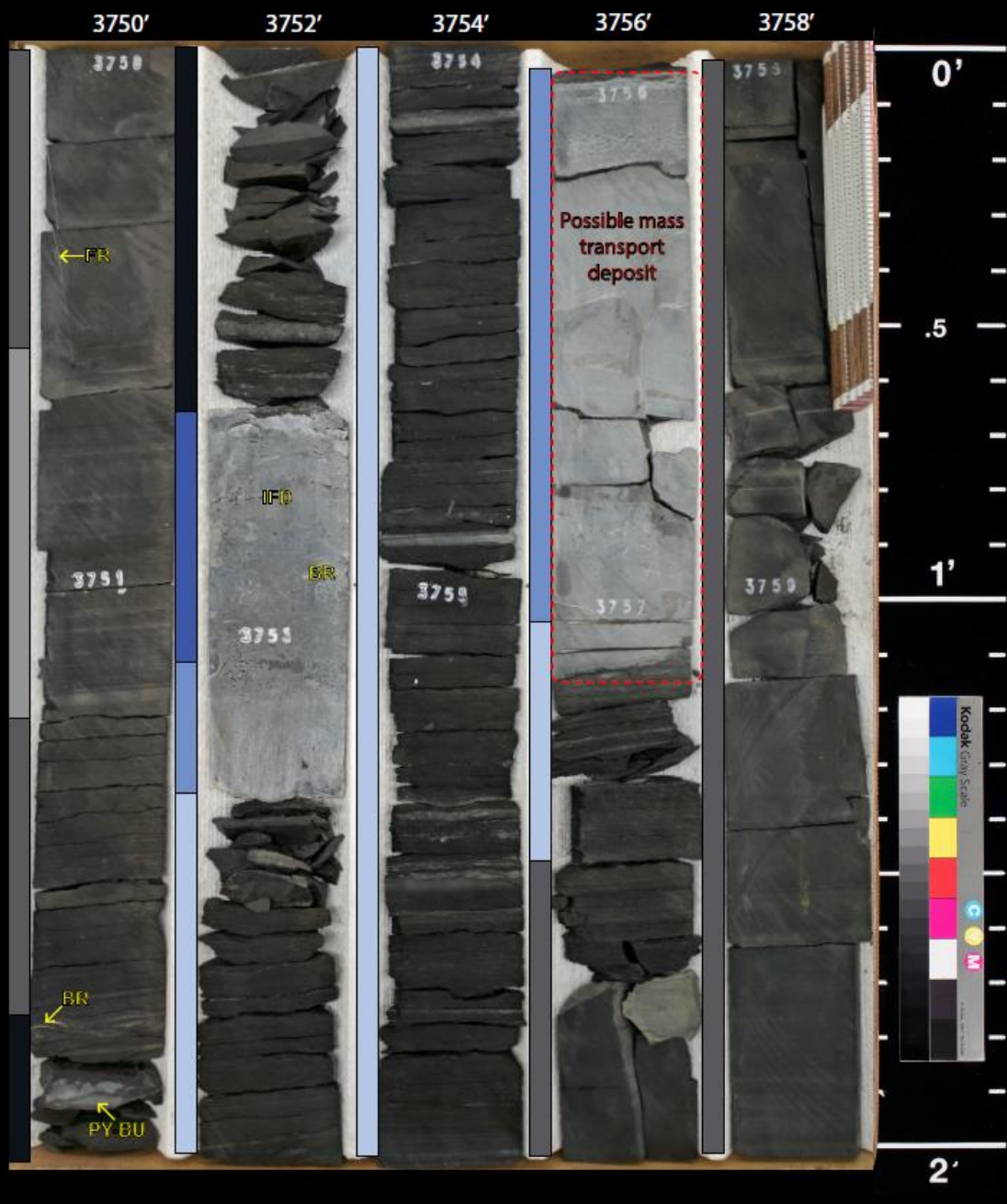
Wise 1-20
Okfuskee County, OK



Wise 1-20
Okfuskee County, OK



Wise 1-20
Okfuskee County, OK



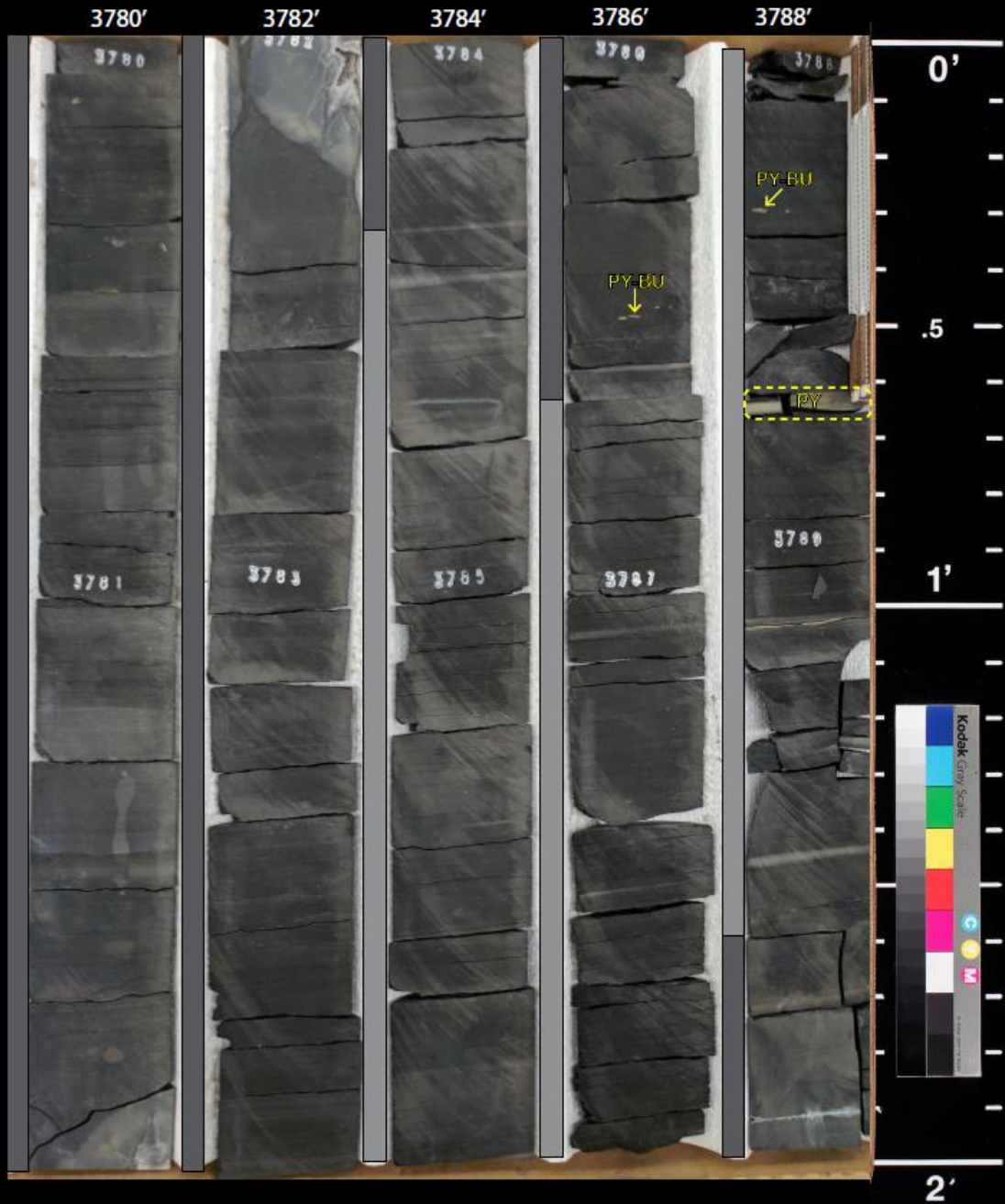
Wise 1-20
Okfuskee County, OK



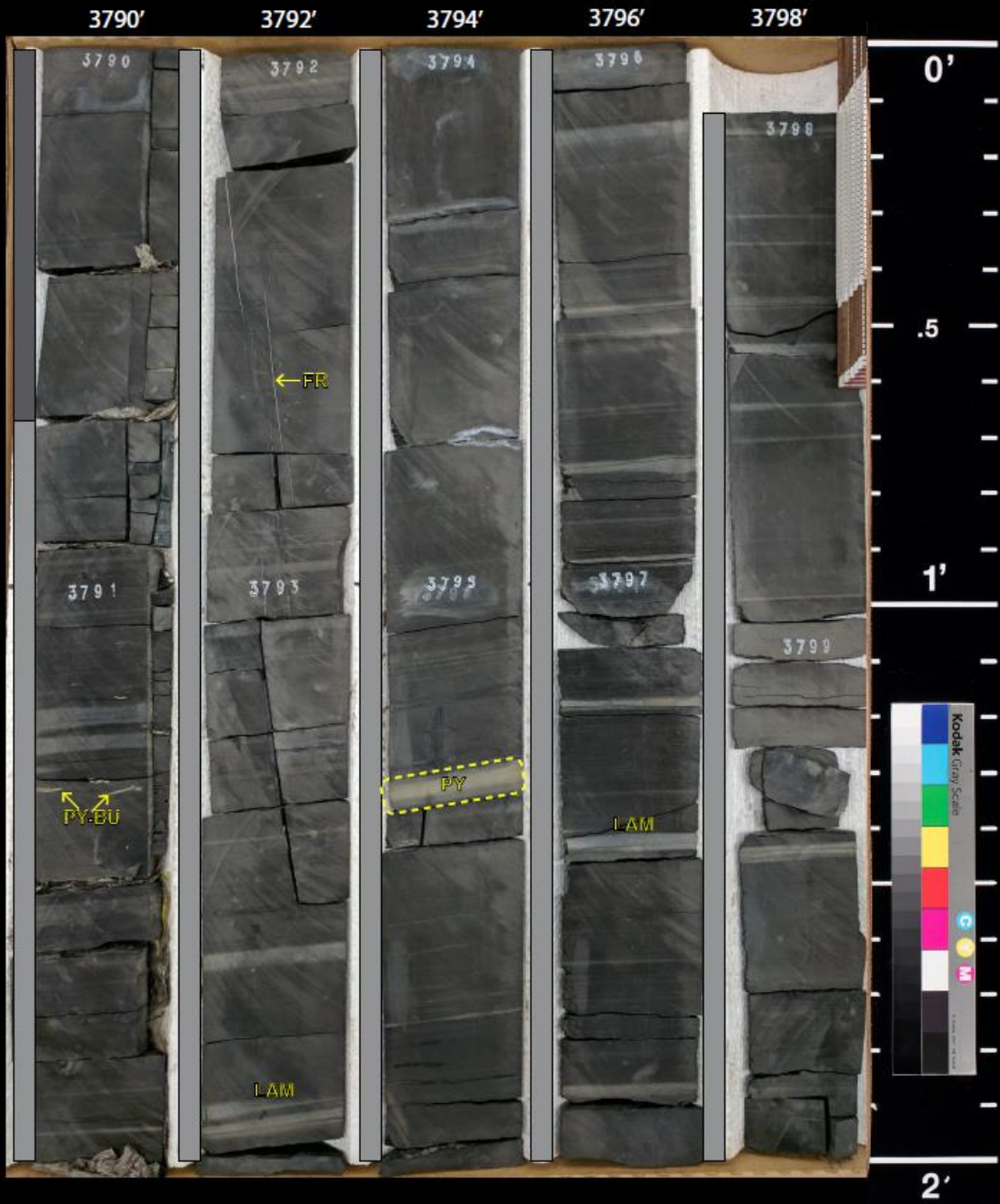
Wise 1-20
Okfuskee County, OK



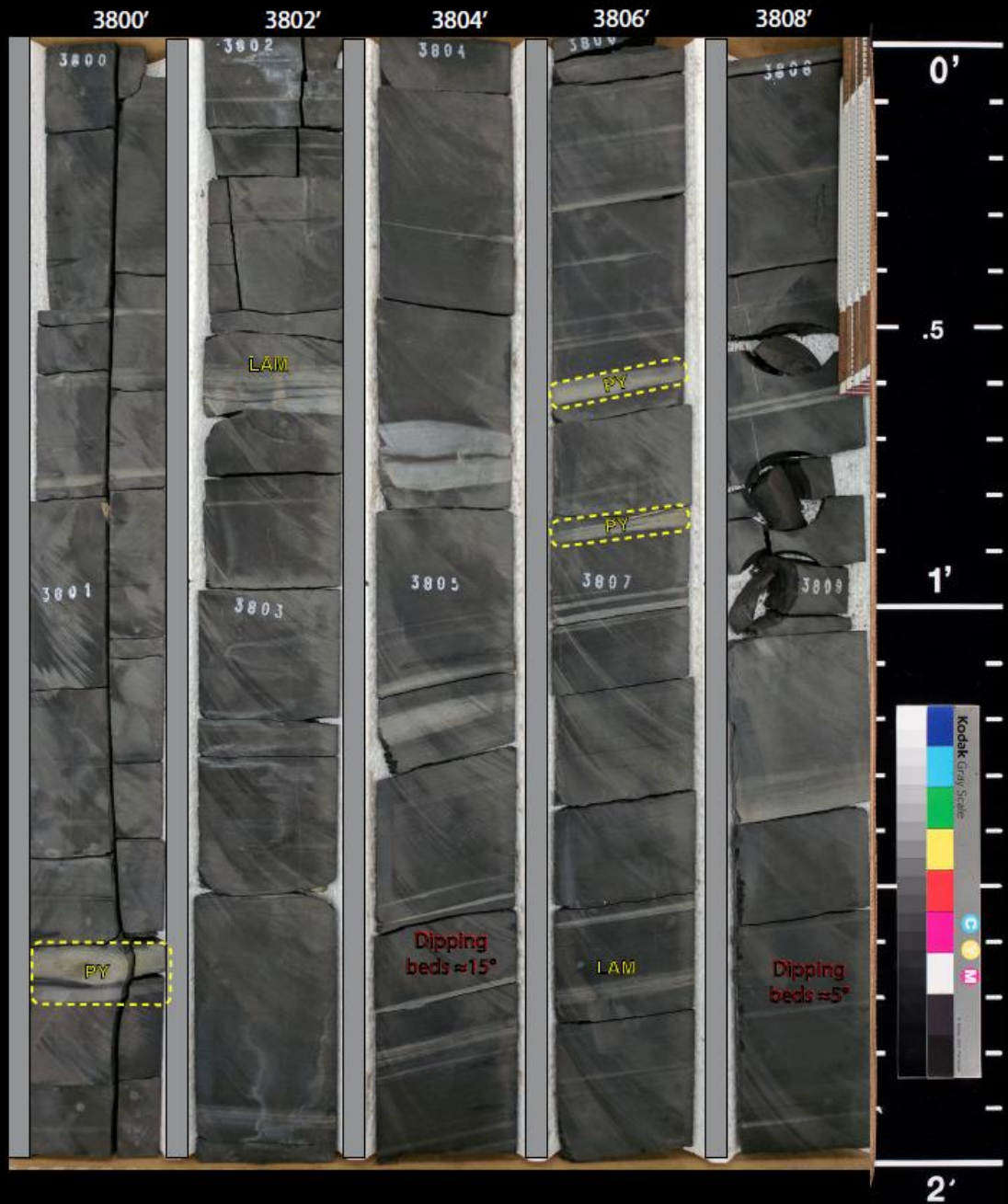
Wise 1-20
Okfuskee County, OK



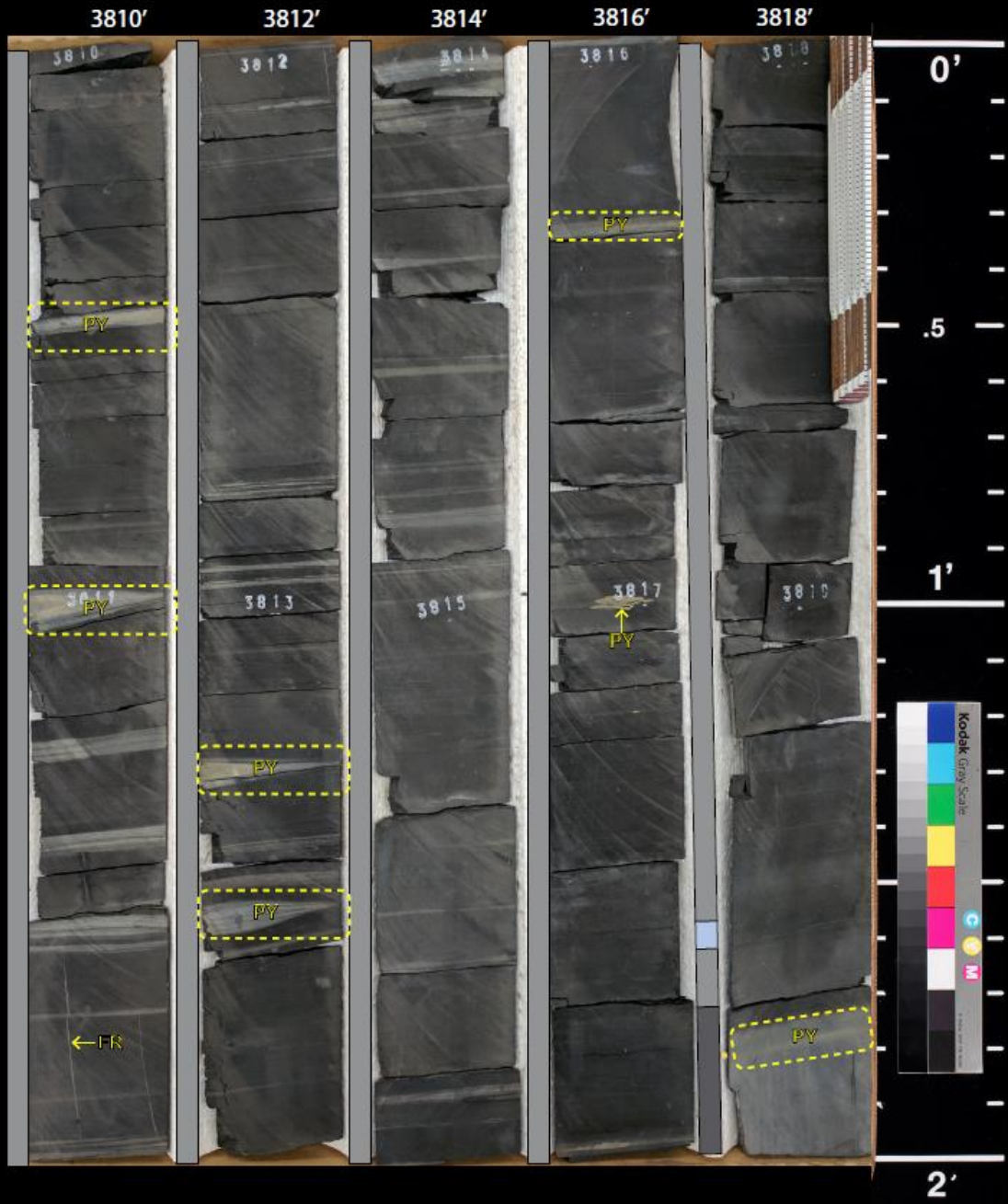
Wise 1-20
Okfuskee County, OK



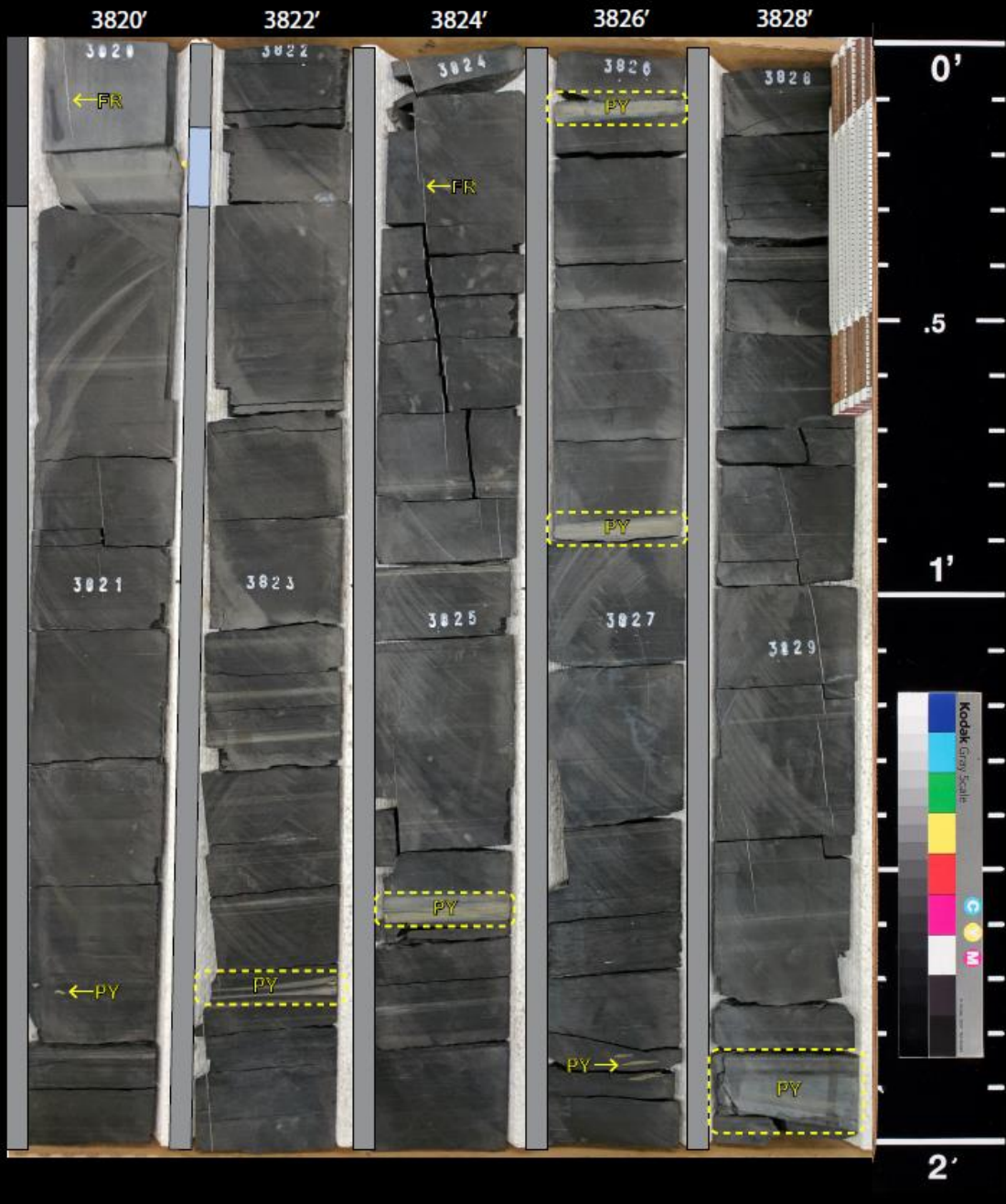
Wise 1-20
Okfuskee County, OK



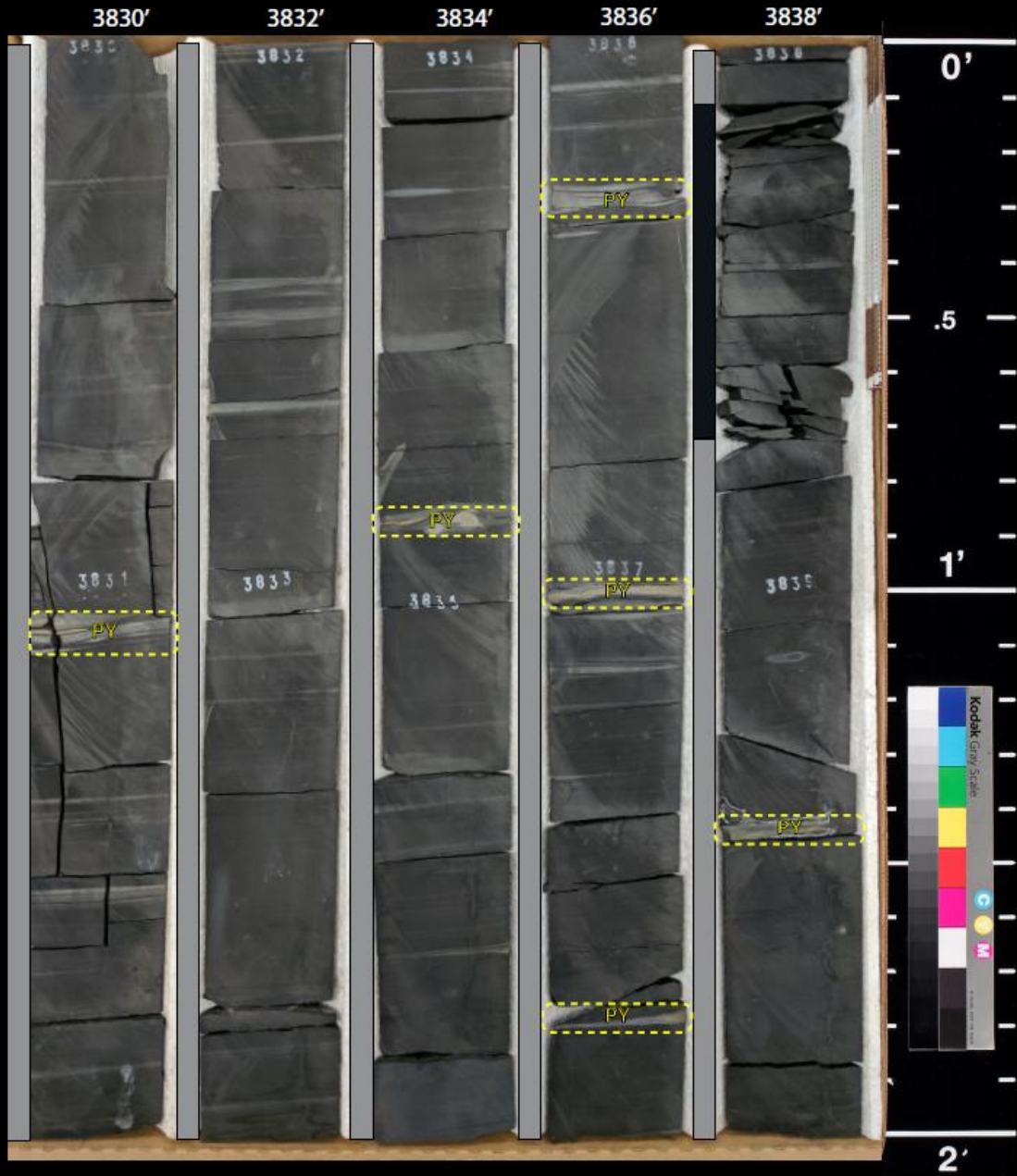
Wise 1-20
Okfuskee County, OK



Wise 1-20
Okfuskee County, OK



Wise 1-20
Okfuskee County, OK



Wise 1-20
Okfuskee County, OK

3840'

3842'

3844'

3846'

3848'

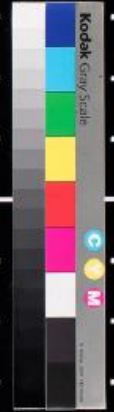


0'

.5

1'

2'



Wise 1-20
Okfuskee County, OK

3850' 3852' 3854' 3856' 3858'



0'

.5

1'

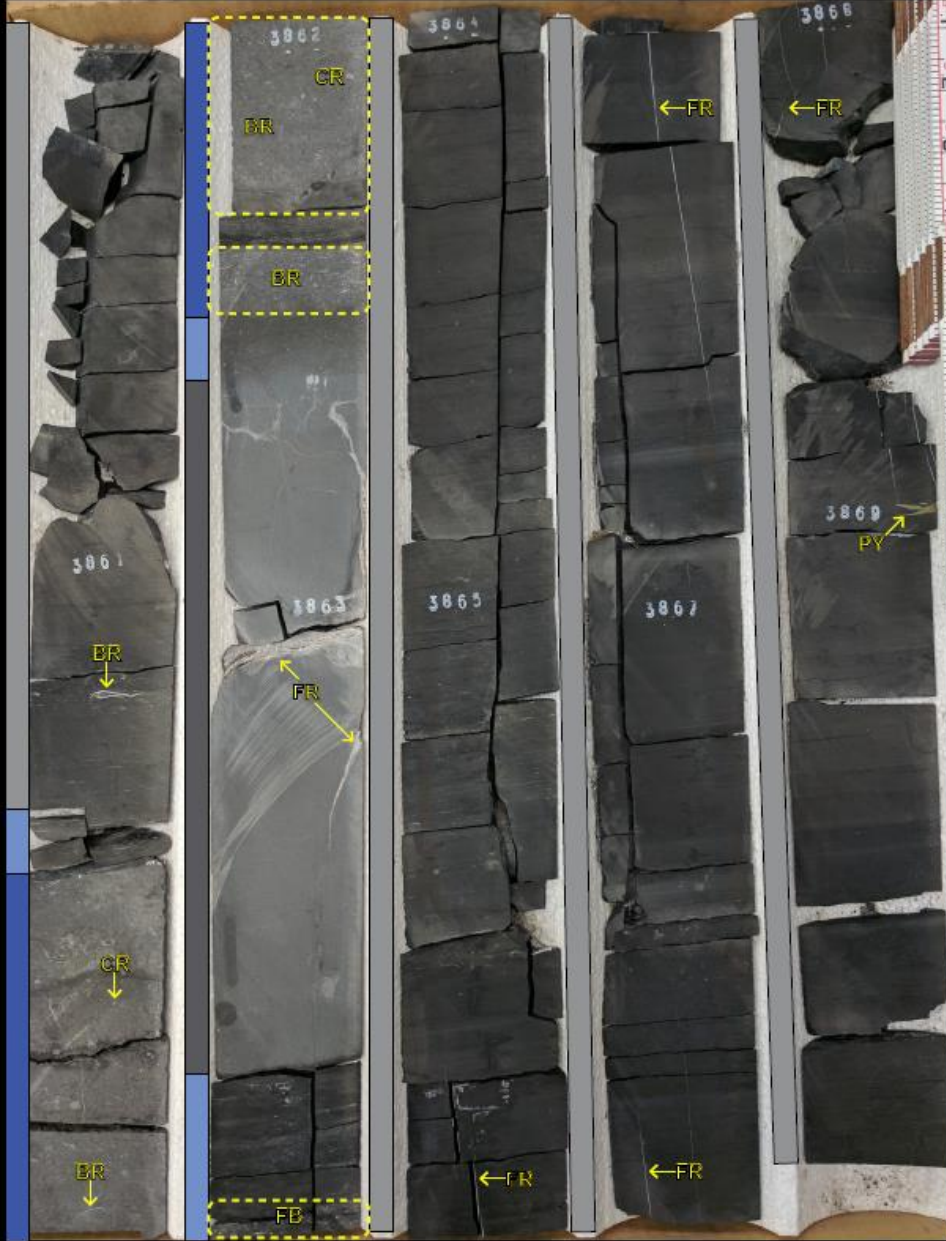
2'

No recovery from
3855.7 feet to
3860.0 feet



Wise 1-20
Okfuskee County, OK

3860' 3862' 3864' 3866' 3868'



0'

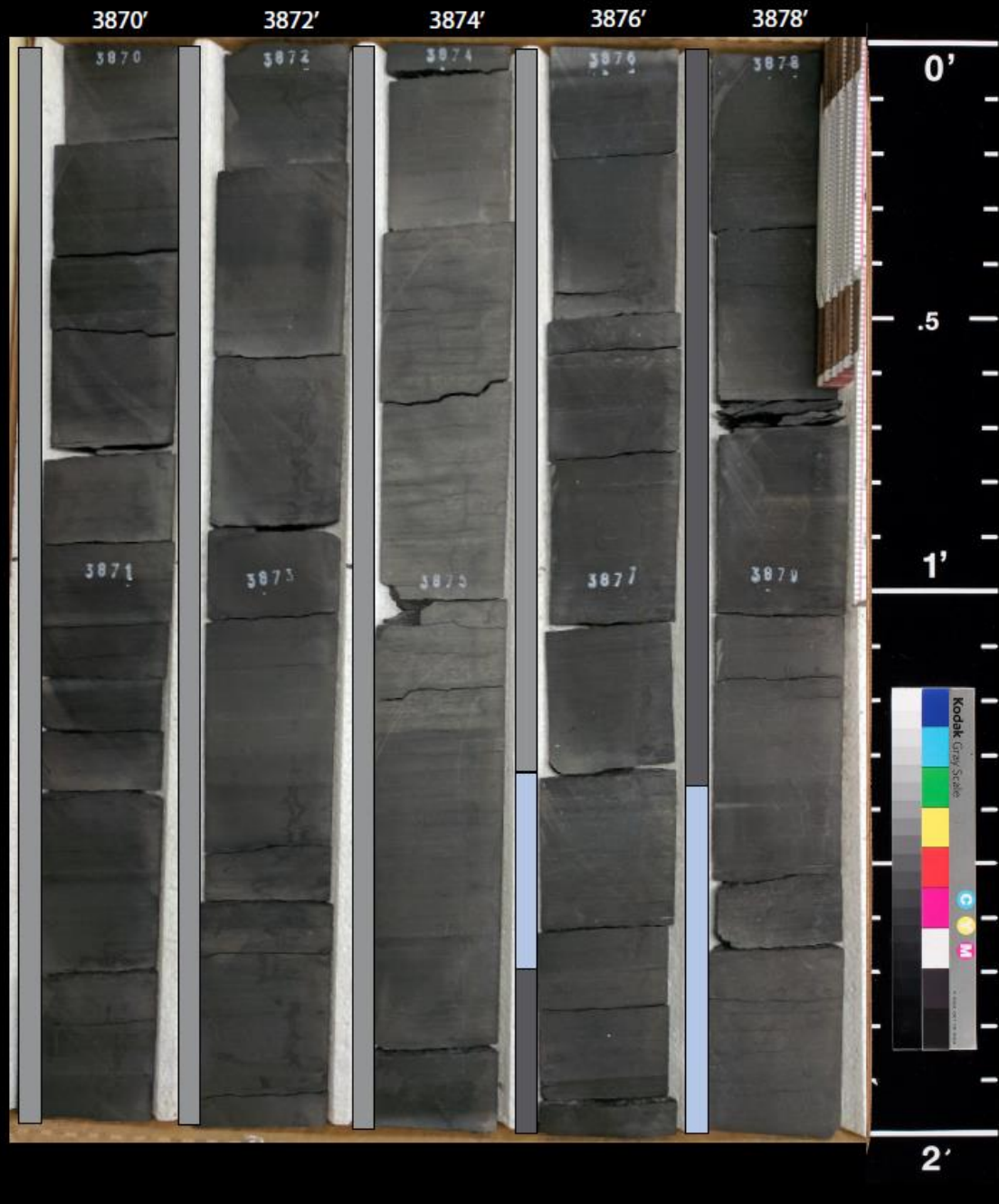
.5

1'

2'



Wise 1-20
Okfuskee County, OK



Wise 1-20
Okfuskee County, OK

3880' 3882' 3884' 3886' 3888'



PY

PY

3881

3883

No recovery from
3883.6 feet to
3890.0 feet

0'

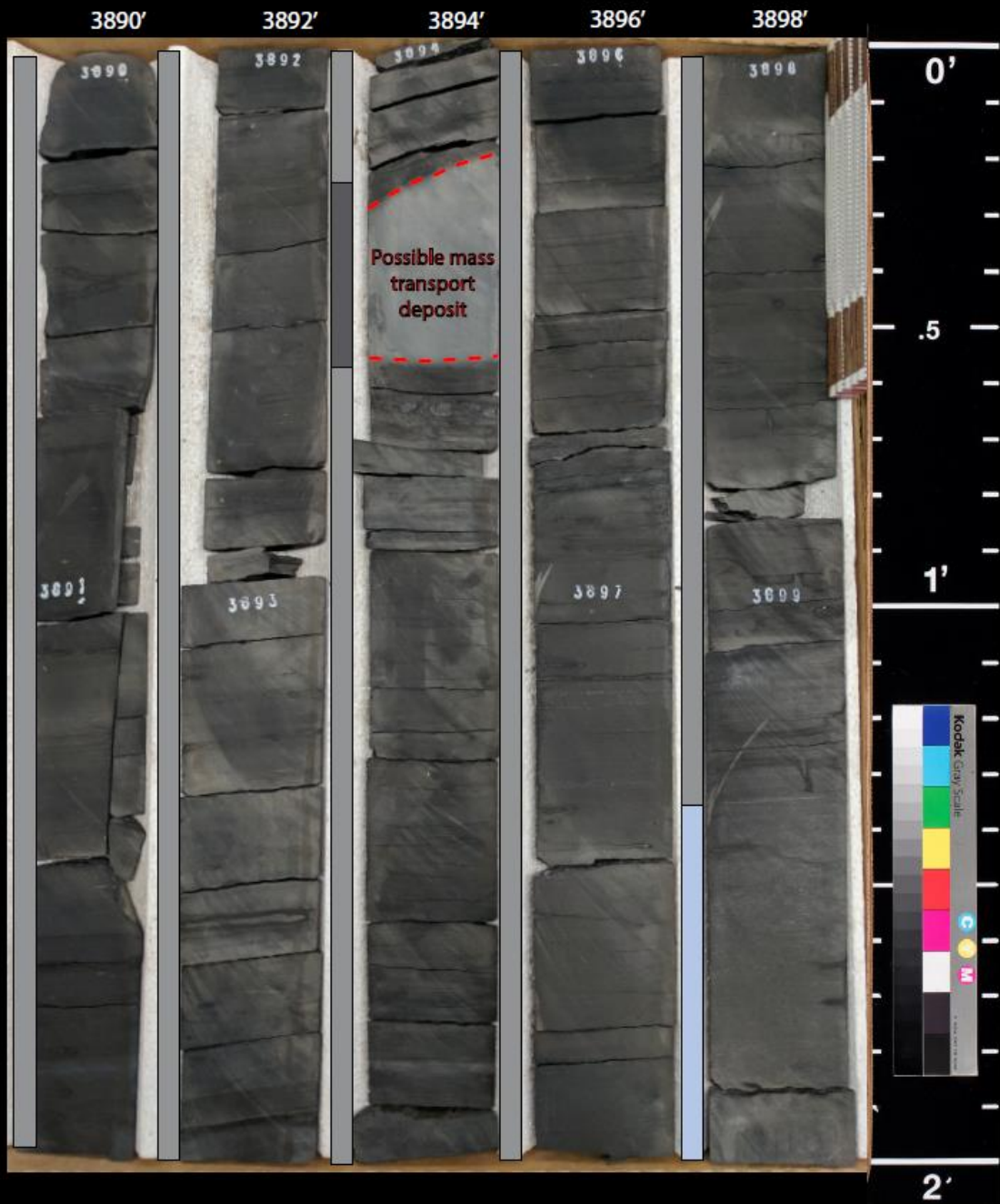
.5

1'

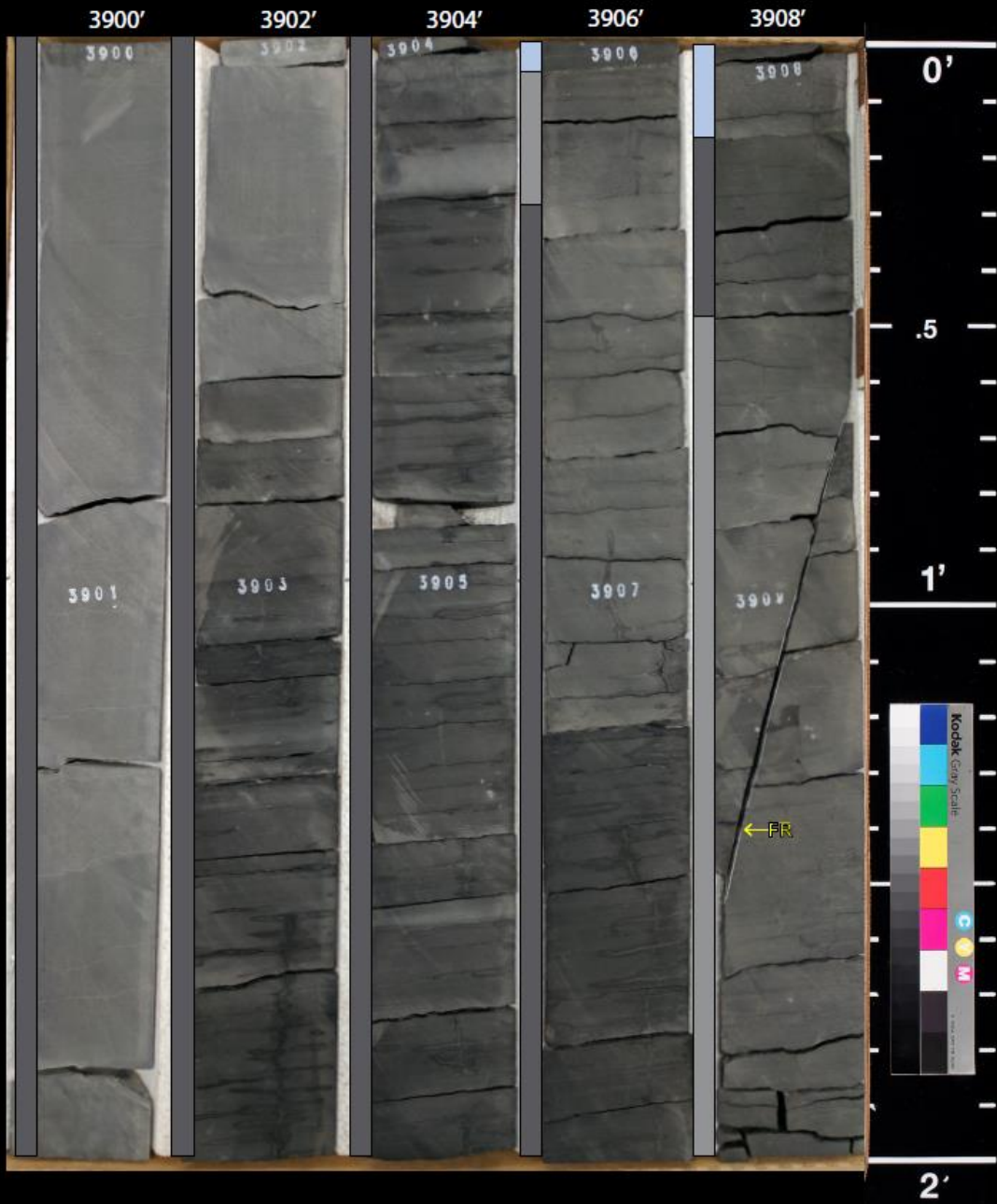
2'



Wise 1-20
Okfuskee County, OK



Wise 1-20
Okfuskee County, OK



Wise 1-20
Okfuskee County, OK

3910'

3912'

3914'

3916'

3918'

3910

3912

3914

3916

3918

0'

.5

1'

← 限

3911

3913

3915

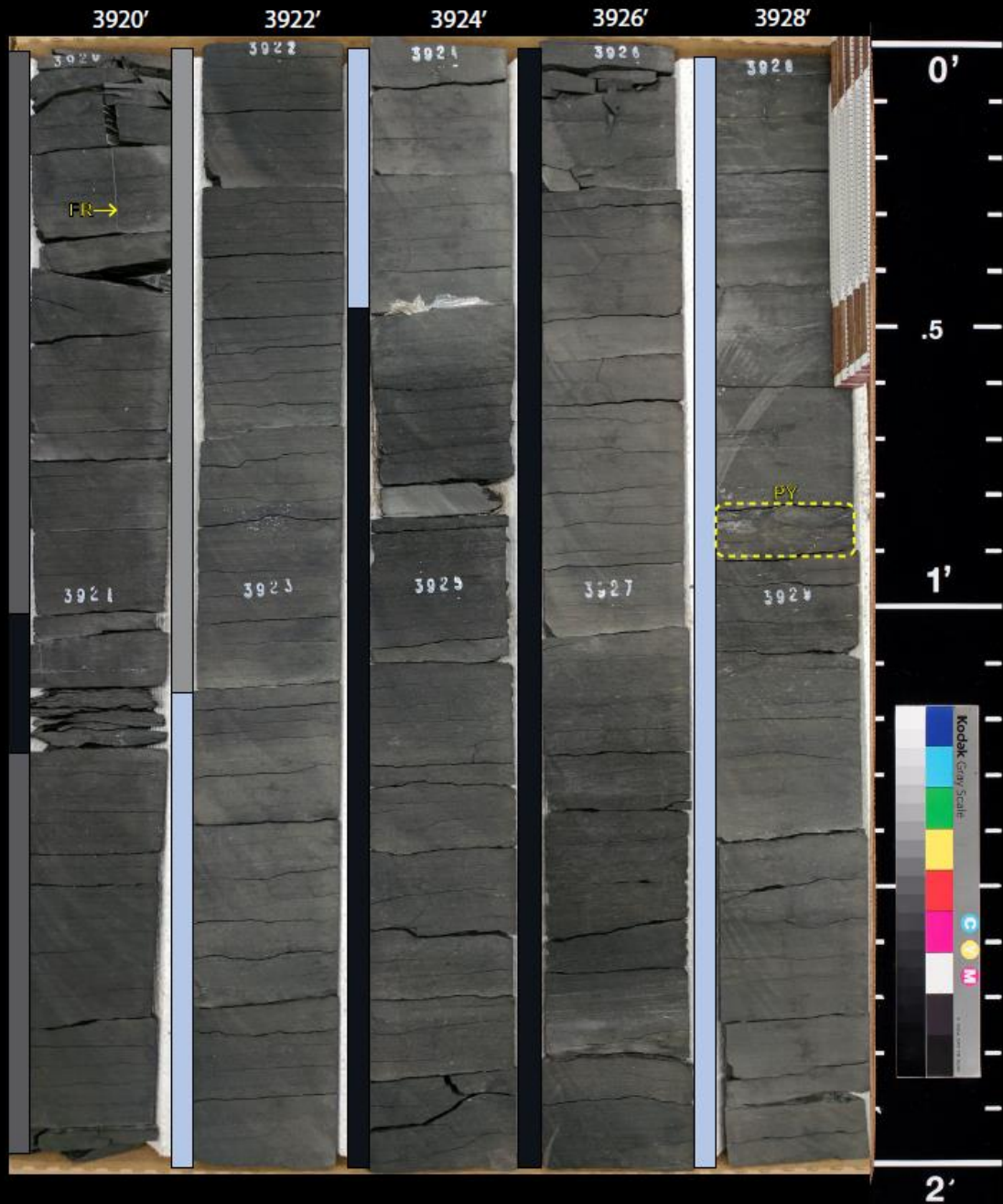
3917

3919



2'

Wise 1-20
Okfuskee County, OK



Wise 1-20
Okfuskee County, OK

3930'

3932'

3934'

3936'

3938'



0'

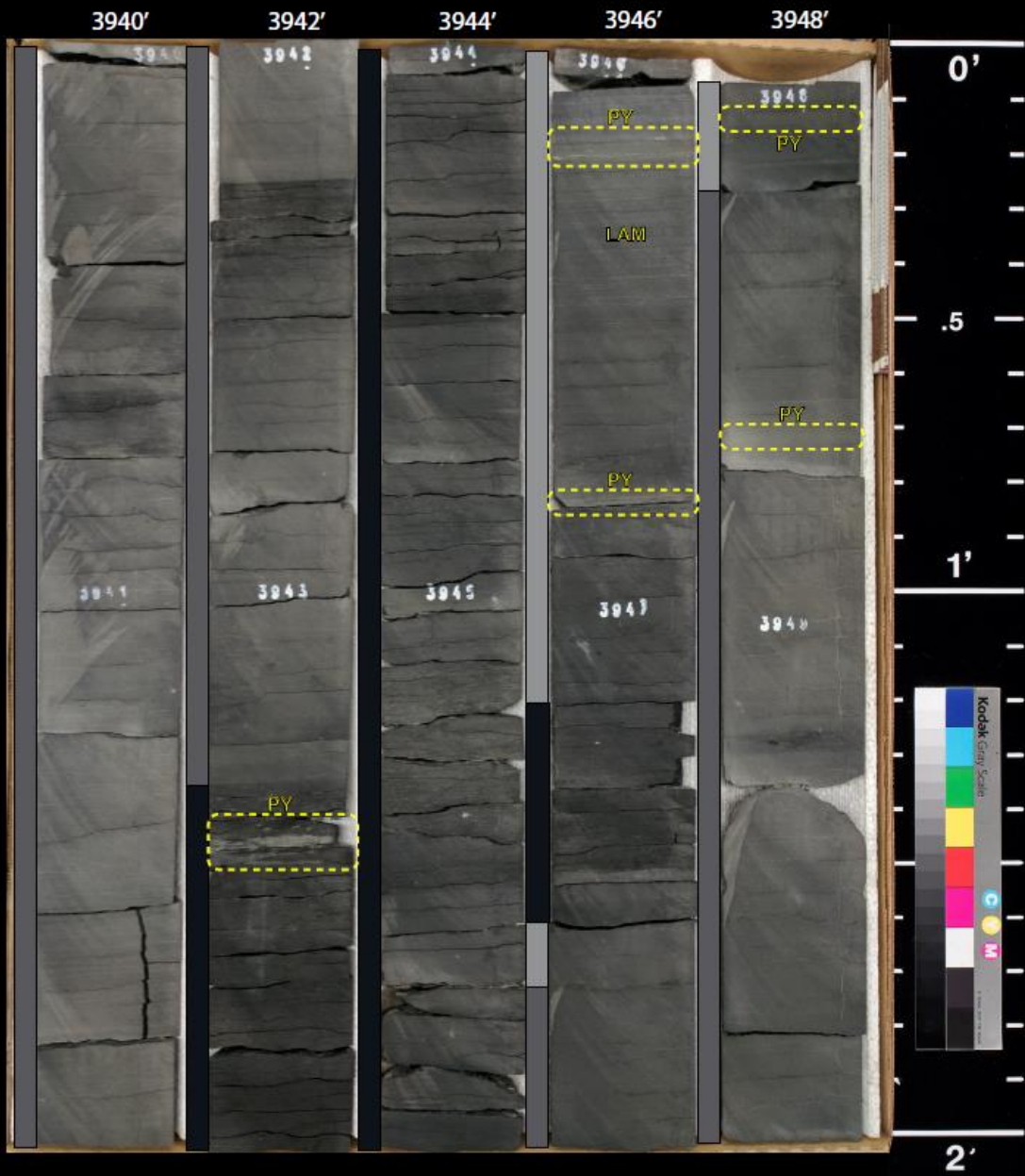
.5

1'

2'



Wise 1-20
Okfuskee County, OK



Wise 1-20
Okfuskee County, OK

3950'

3952'

3954'

3956'

3958'



0'

.5

1'

2'



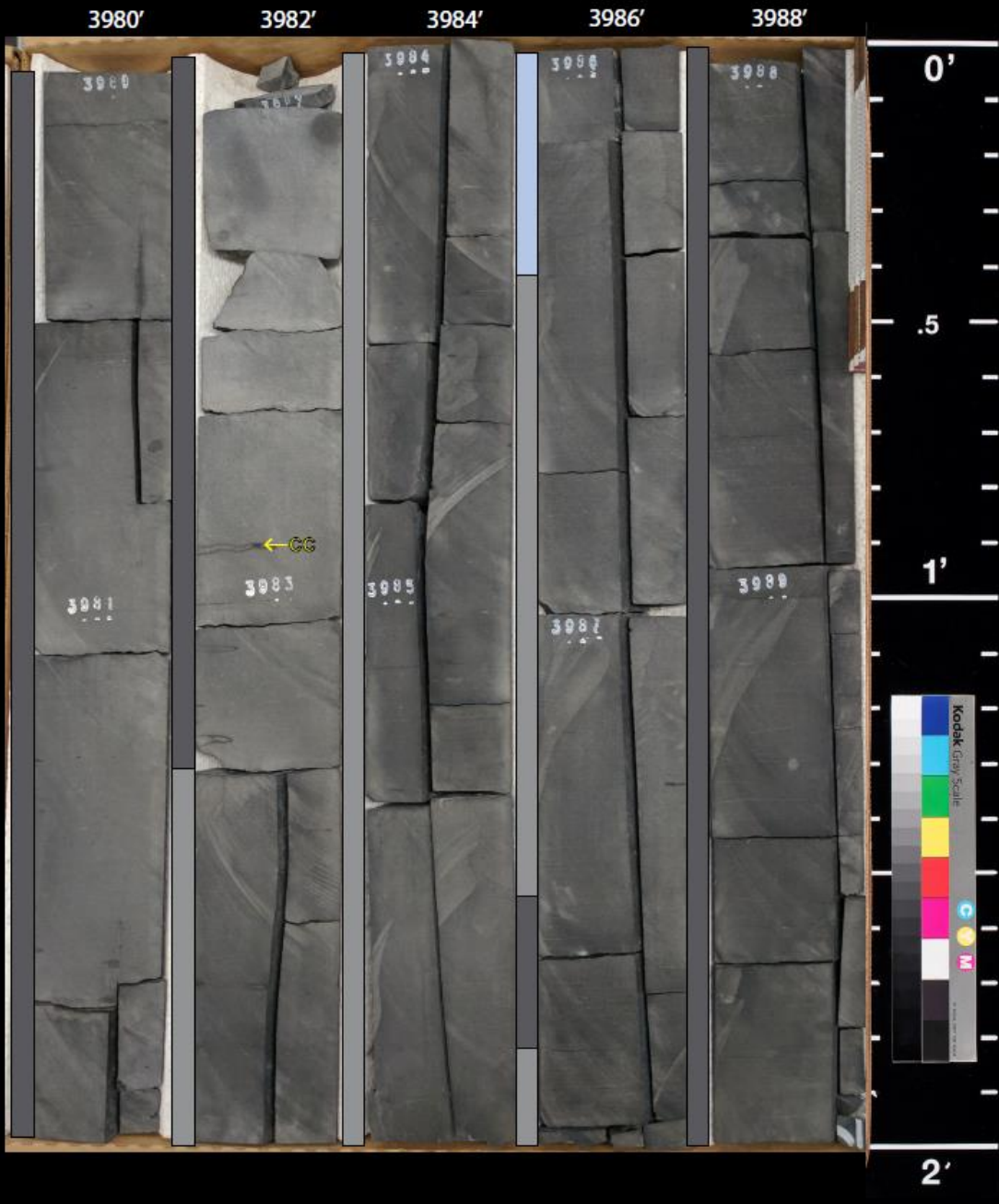
Wise 1-20
Okfuskee County, OK



Wise 1-20
Okfuskee County, OK



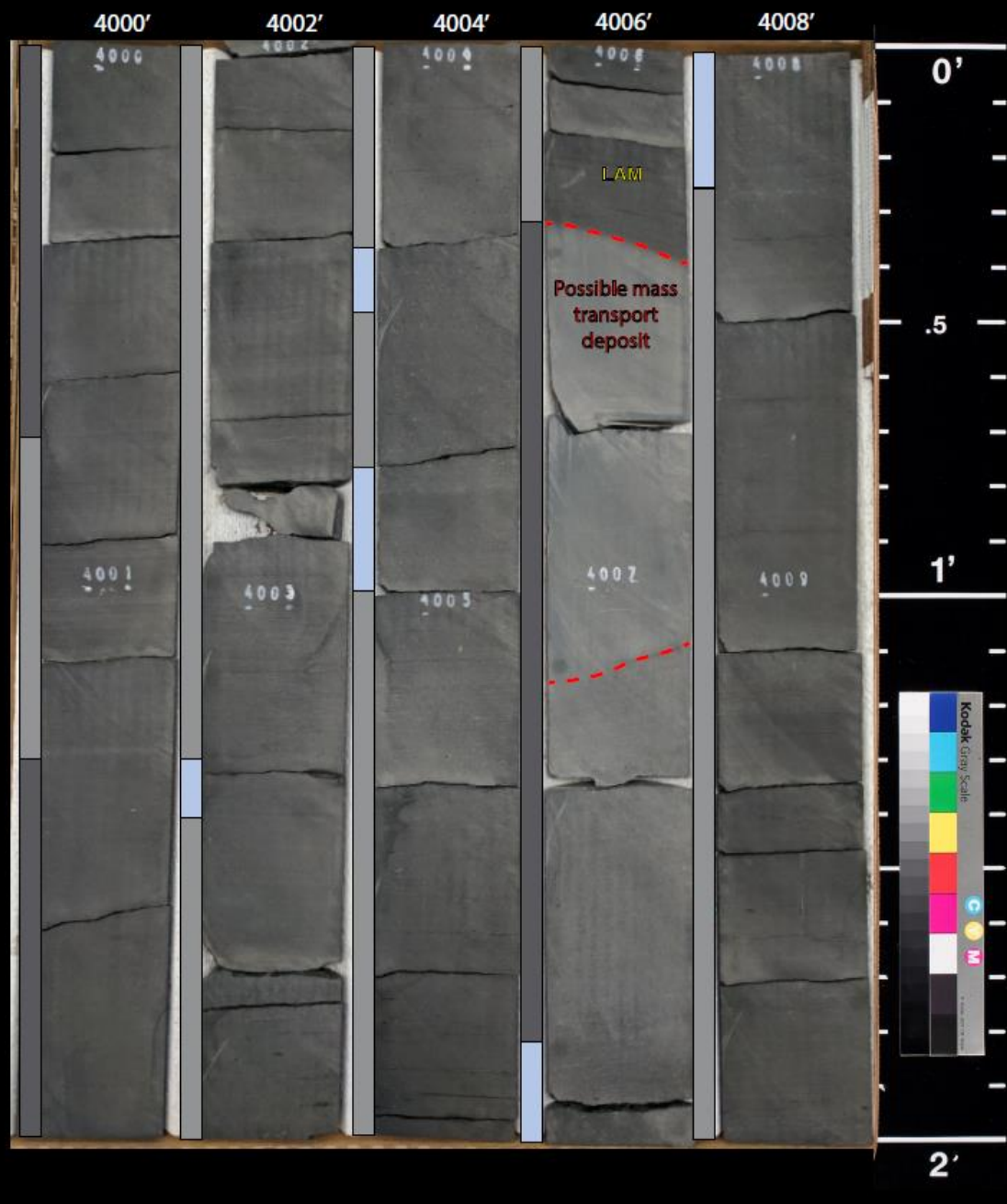
Wise 1-20
Okfuskee County, OK



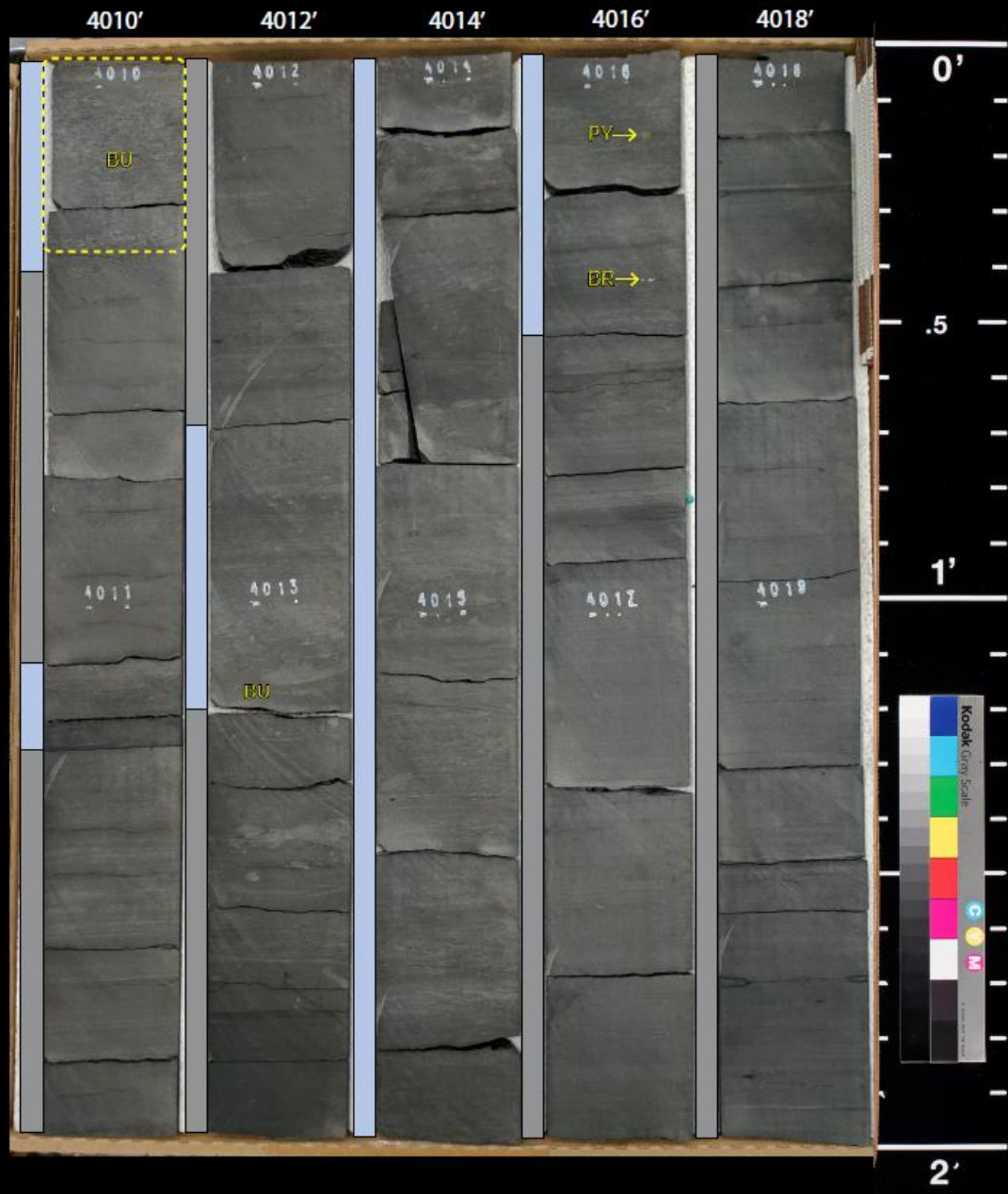
Wise 1-20
Okfuskee County, OK



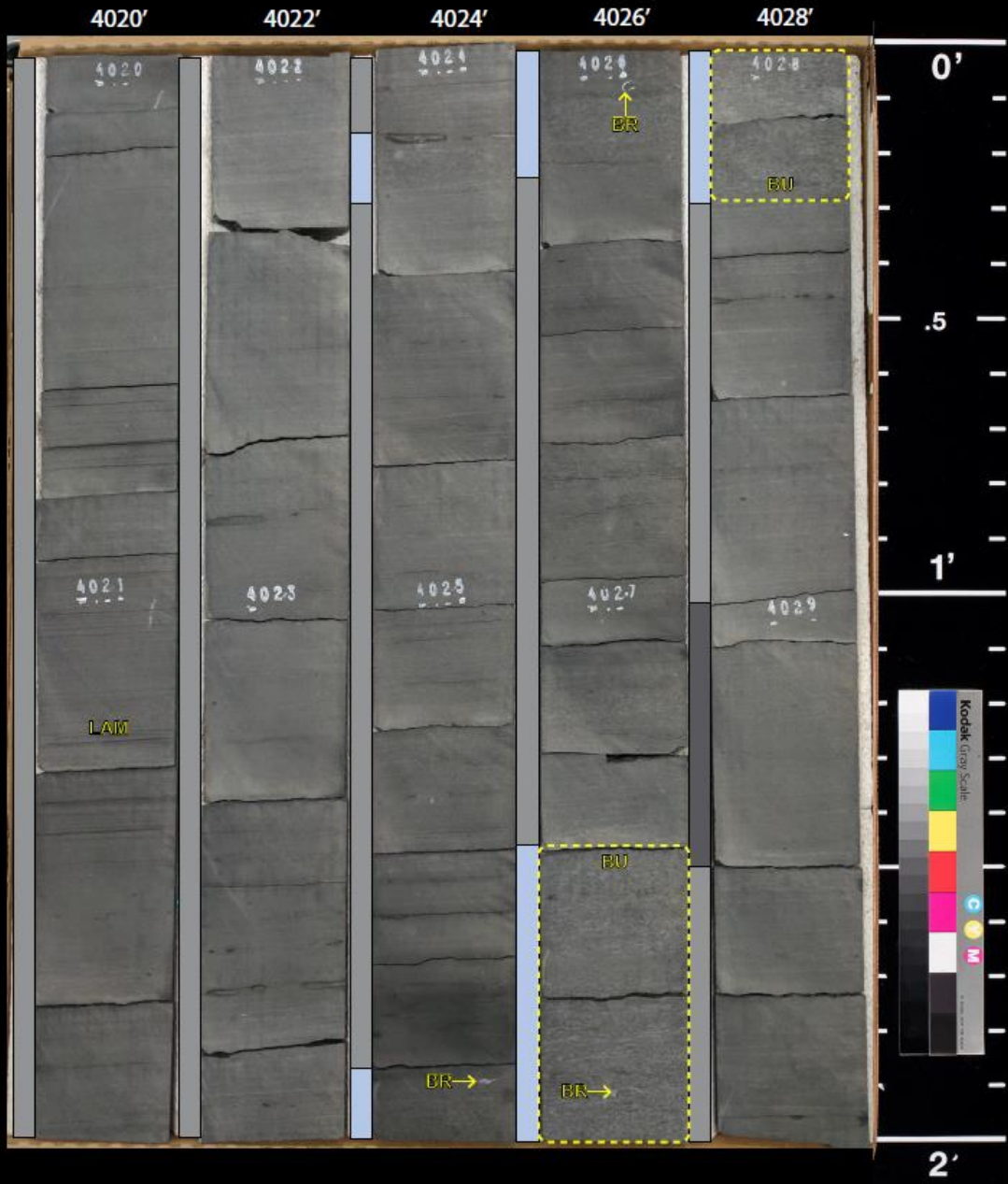
Wise 1-20
Okfuskee County, OK



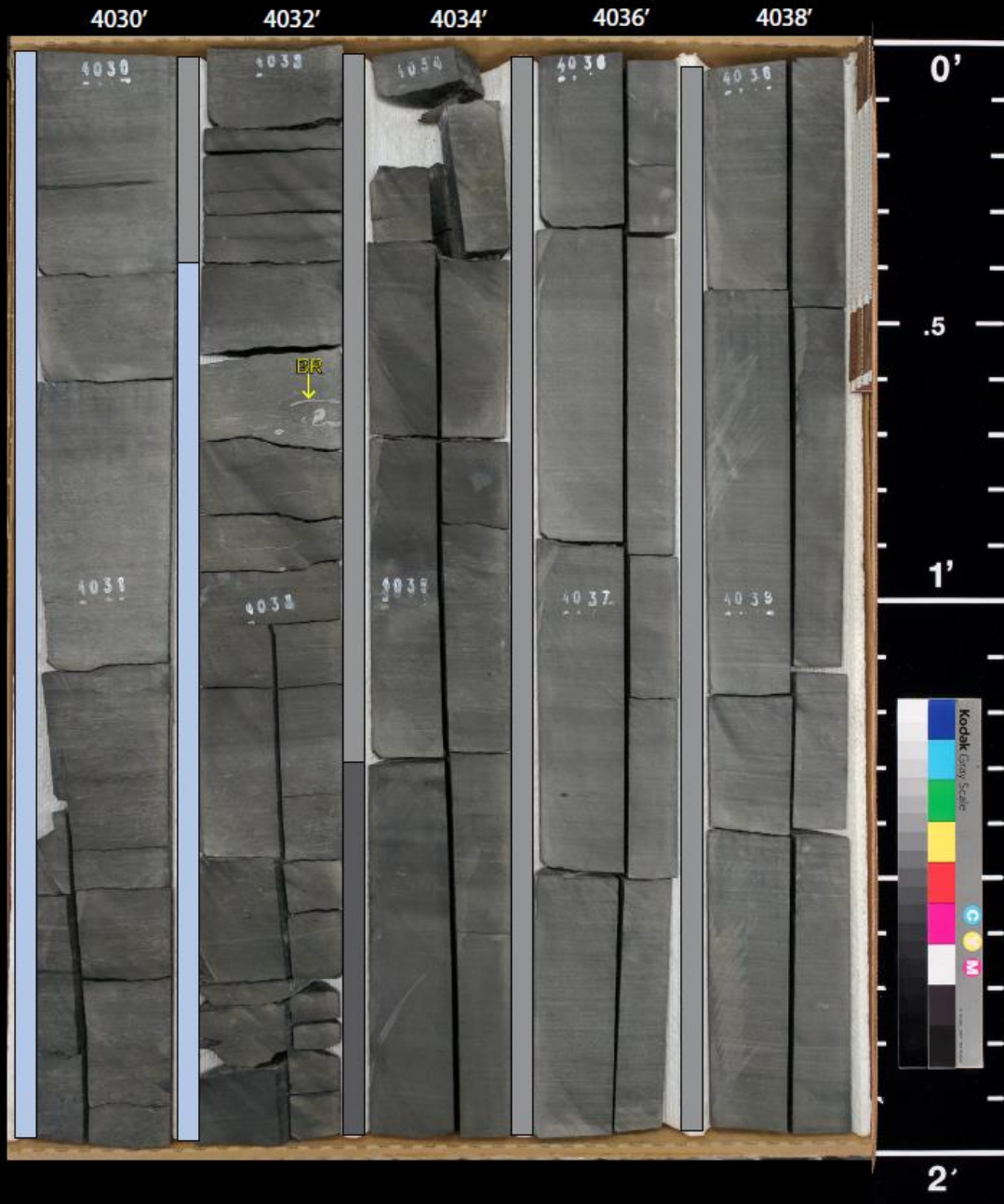
Wise 1-20
Okfuskee County, OK



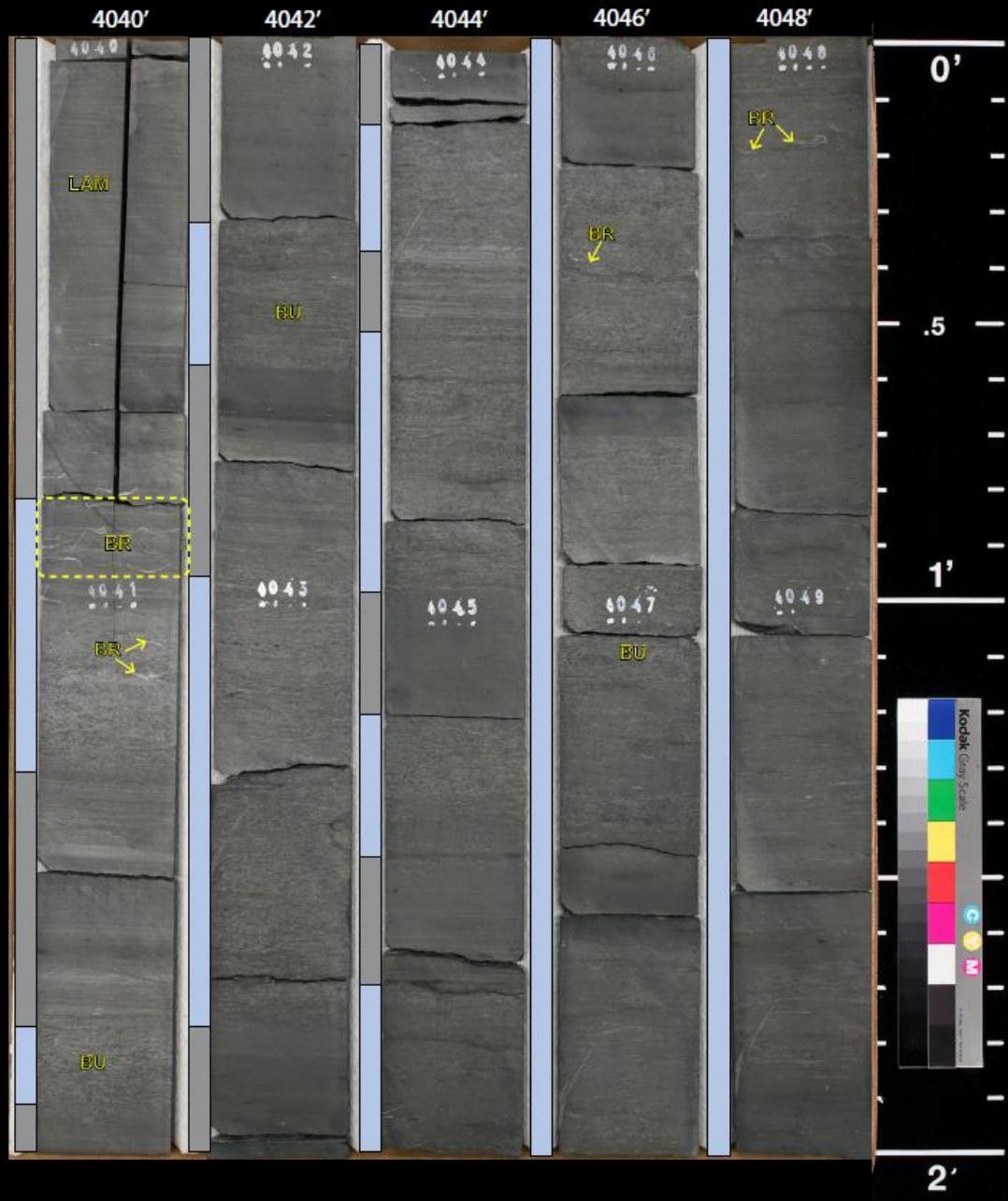
Wise 1-20
Okfuskee County, OK



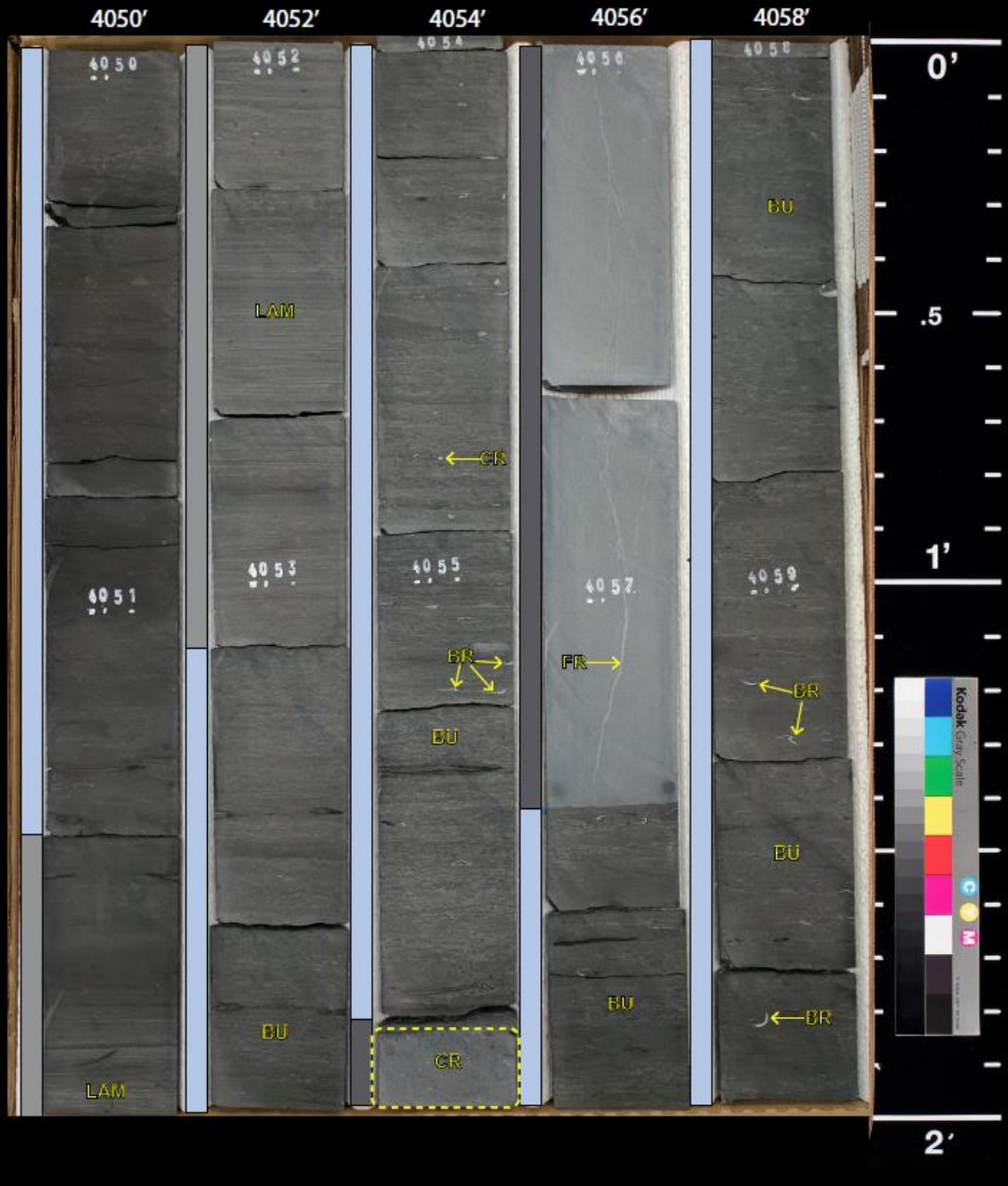
Wise 1-20
Okfuskee County, OK



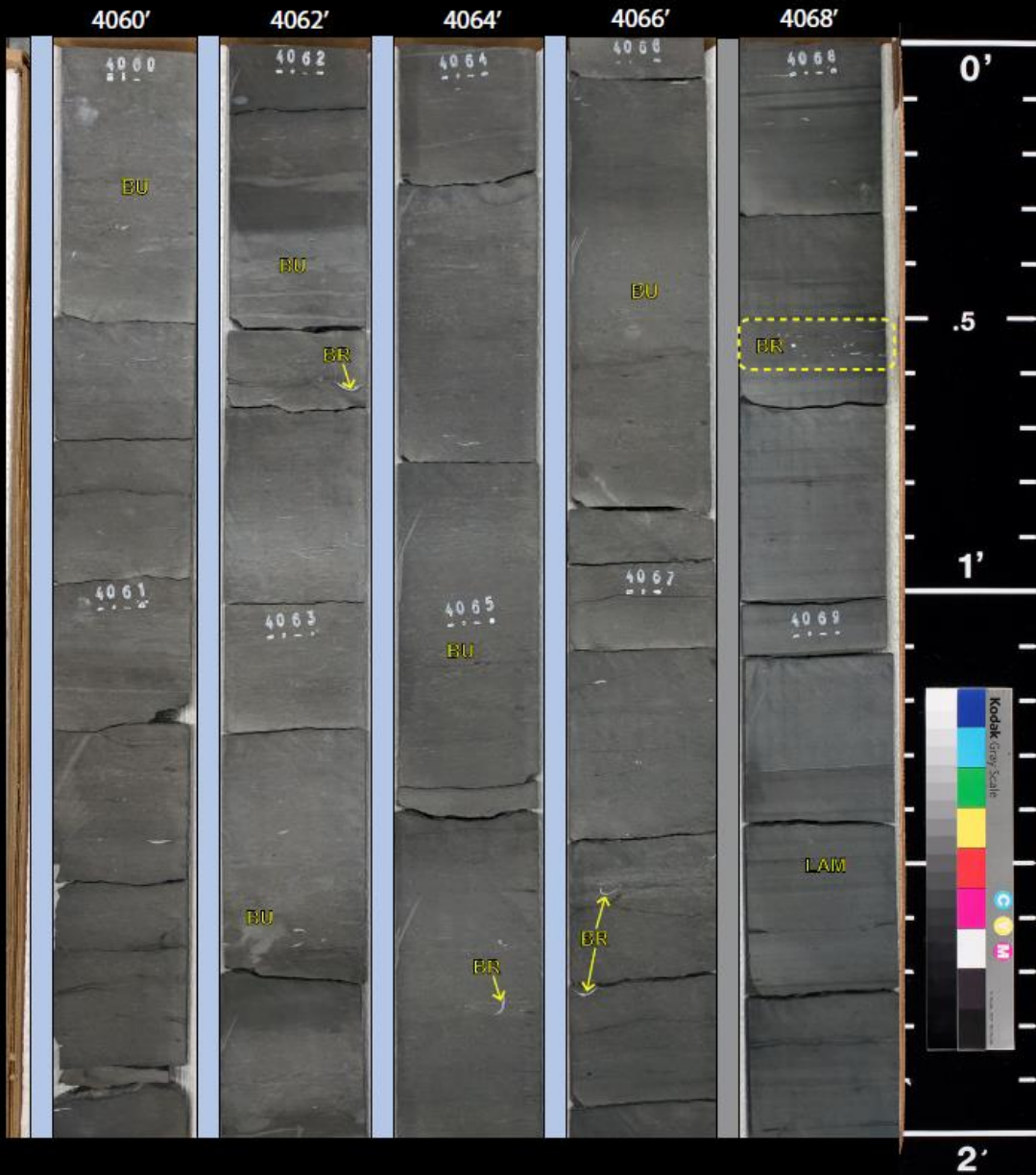
Wise 1-20
Okfuskee County, OK



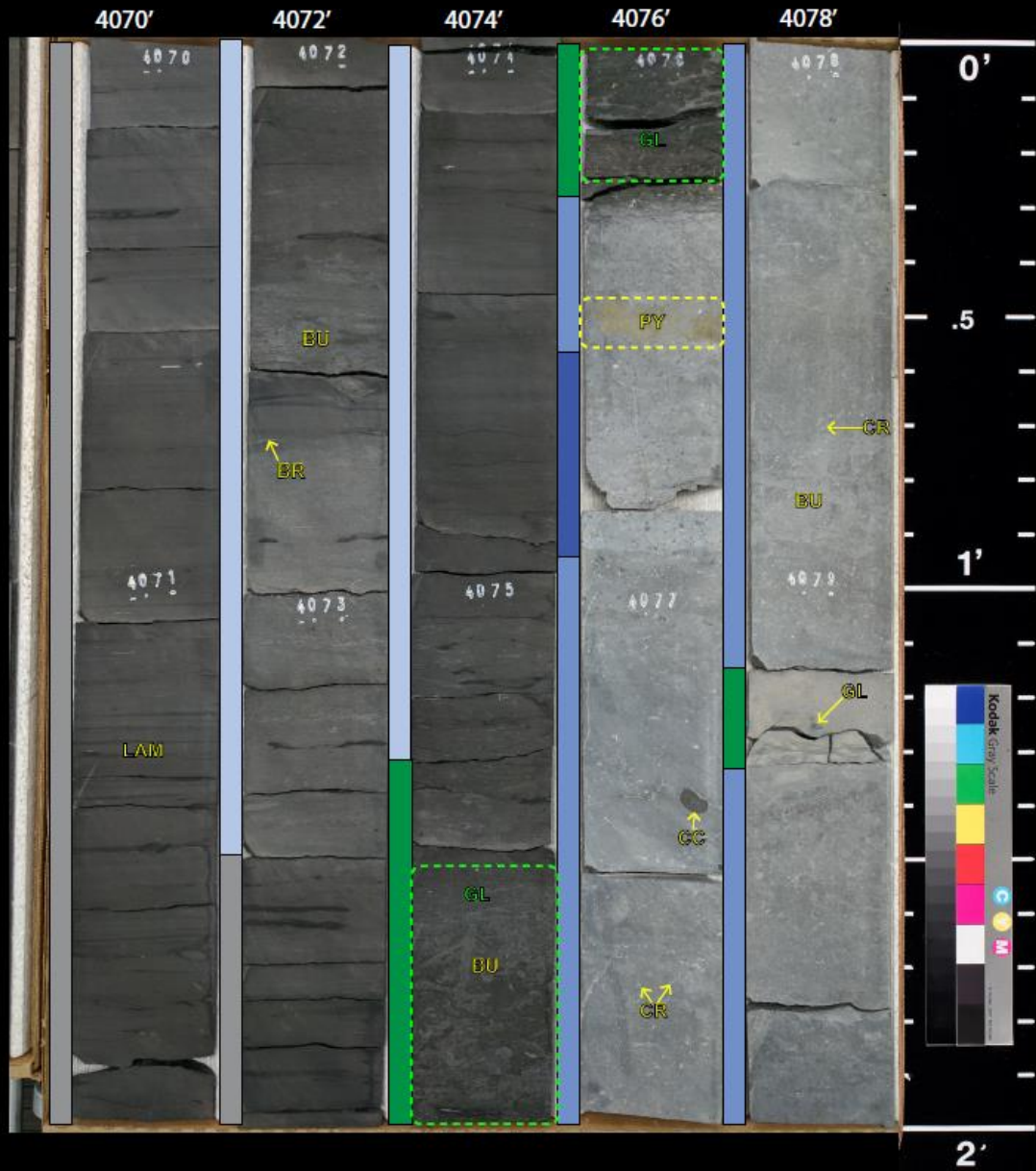
Wise 1-20
Okfuskee County, OK



Wise 1-20
Okfuskee County, OK



Wise 1-20
Okfuskee County, OK



Wise 1-20
Okfuskee County, OK



II. Wise 1-20 Core Description

The Wise 1-20 core was described using the Dunham (1962) classification scheme where applicable (i.e. – carbonate dominant intervals). Siliciclastic dominant intervals were classified based on grain type and composition. The descriptions of bioturbation uses a bioturbation index implemented from Bann et al., 2008 (Table 6).

Wise 1-20 Core Description Key




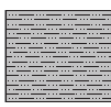


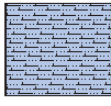


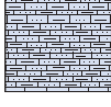

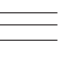
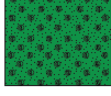


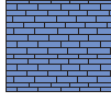




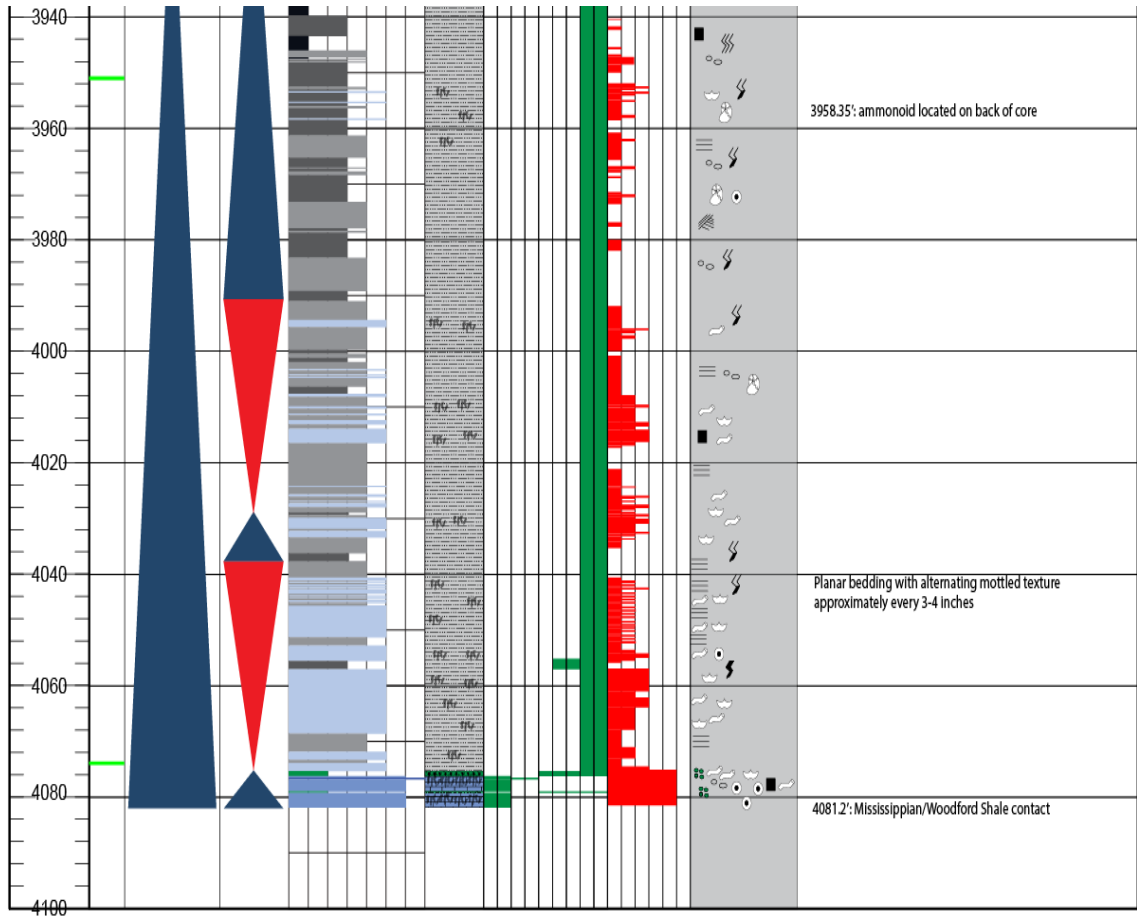
Lithology	Sedimentary Structures		
	No core recovered	Ammonoids 	Fracture (partially filled) 
	Siltstone	Bioturbated 	Fracture swarm 
	Calcareous Siltstone	Brachiopods 	Glaucanite 
	Interbedded Limestone & Siltstone	Burrows 	Horizontal laminae 
	Glaucanitic Sandstone	Crinoids 	Intraclast 
	Limestone	Cross-bedded 	Nodule 
		Fracture (filled) 	Pyrite 

Figure 33: Key for core description of Wise 1-20



III. Wise 1-20 X-Ray Diffraction Analysis

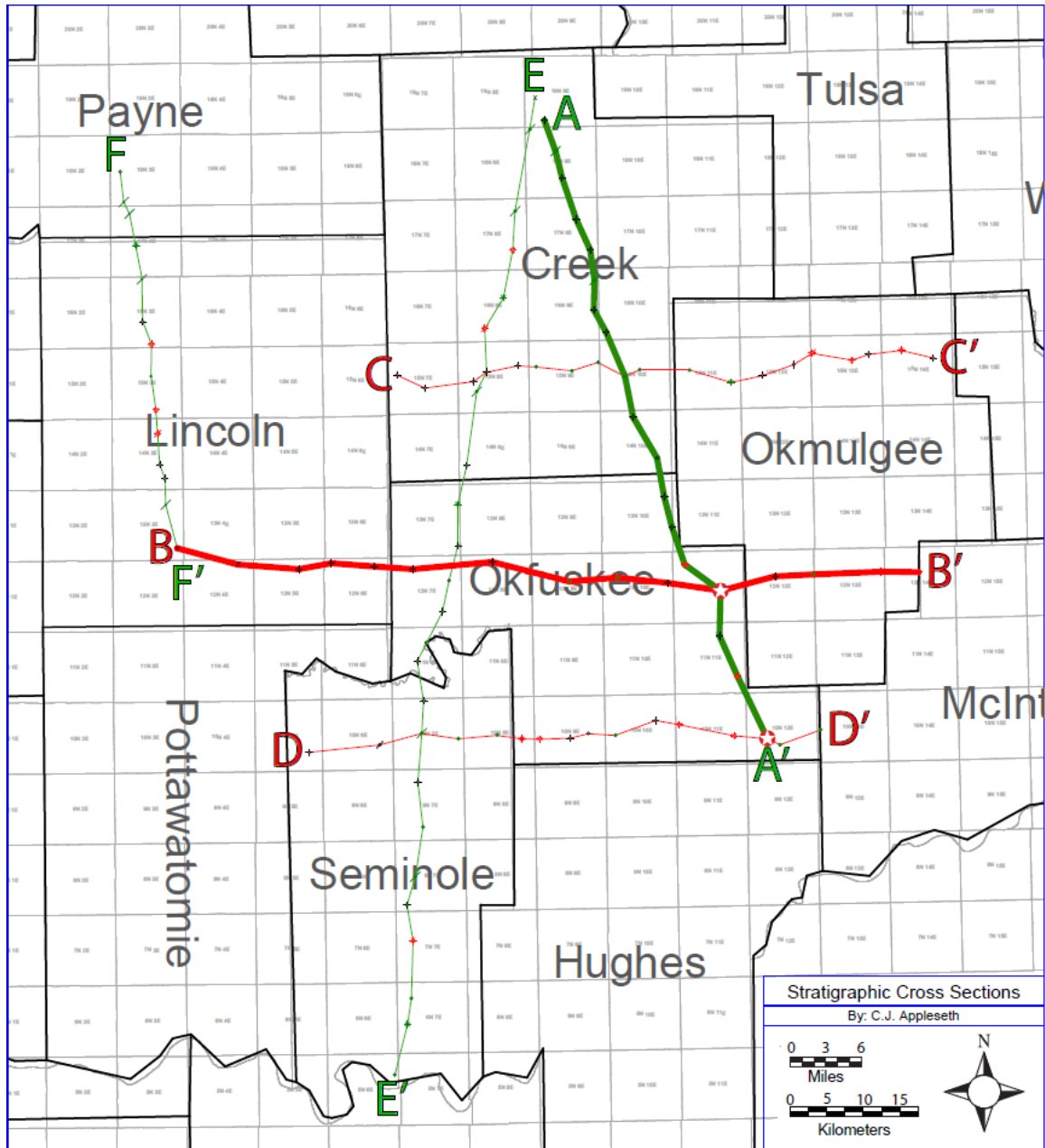
X-ray diffraction (XRD) is a diagnostic tool for identifying crystalline materials and provides quantitative estimates of bulk and clay mineralogy. Devon Energy sampled the butt section of the core. These samples were evaluated utilizing whole-rock bulk mineralogy to identify and quantify the abundances of common framework grains and cements.

Facies	Sample Depth (ft)	CLAYS				Carbonates		OTHER MINERALS				TOTALS			
		Chlorite	Kaolinite	Illite/Mica	I/S	Calcite	Dolomite (Fe/Ca+)	K-spar	Plag.	Pyrite	Apatite	Quartz	Clays	Carb.	Other
3	3745.1	1	Tr	21	3	1	Tr	1	2	1	2	68	25	1	6
3	3777.3	2	0	30	4	2	Tr	1	3	2	6	50	36	2	12
4	3803.3	5	1	39	5	Tr	Tr	2	4	2	1	41	50	0	9
4	3855.3	4	1	39	5	5	2	1	3	3	1	36	49	7	8
3	3957.1	3	Tr	27	2	Tr	1	1	7	2	1	56	32	1	11
5	4074.8	1	Tr	24	3	Tr	5	2	6	2	2	55	28	5	12

Table 8: XRD analysis for the Wise 1-20

C. Mississippian Architecture

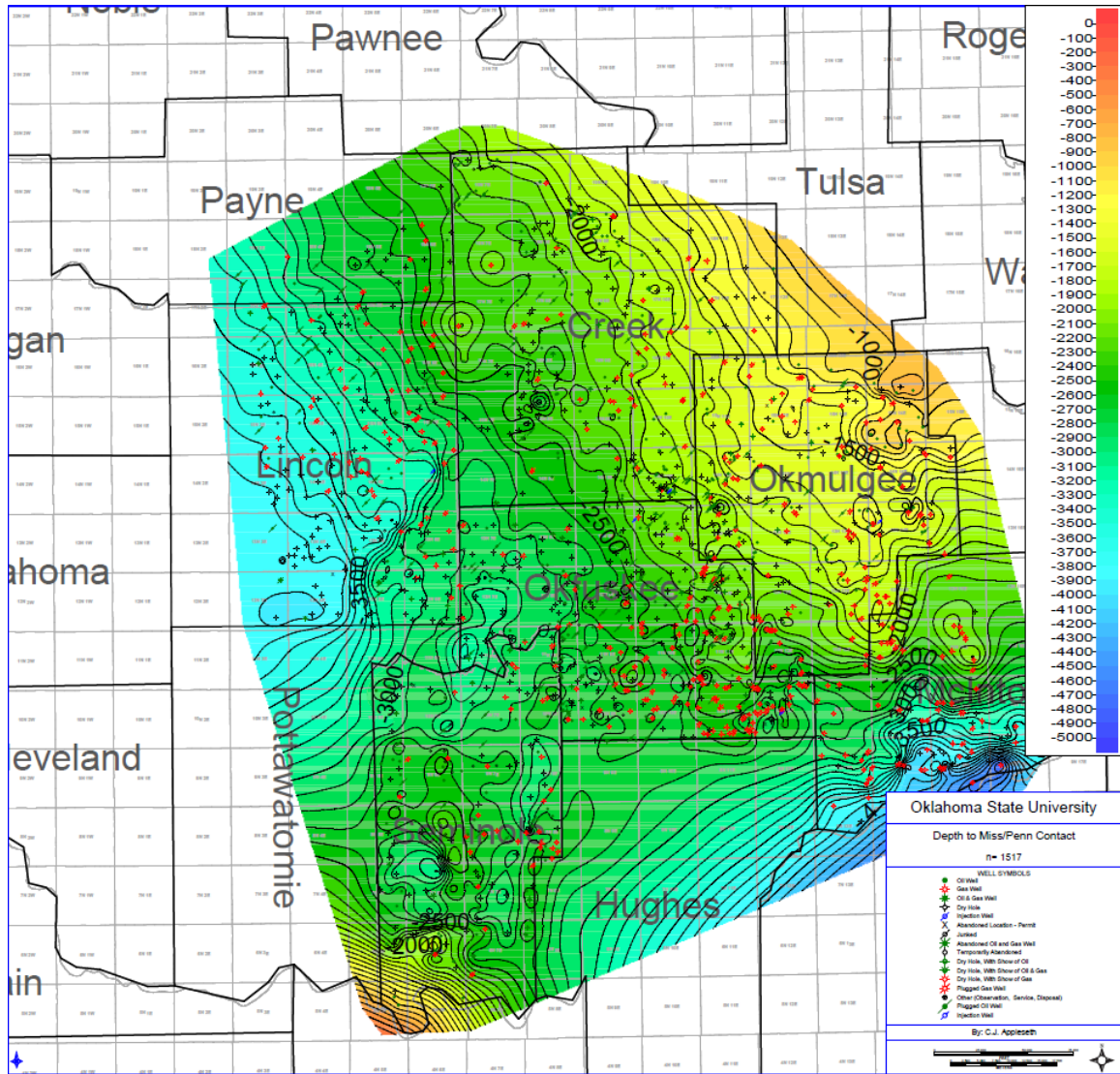
I. Subsurface Cross Section Reference Map



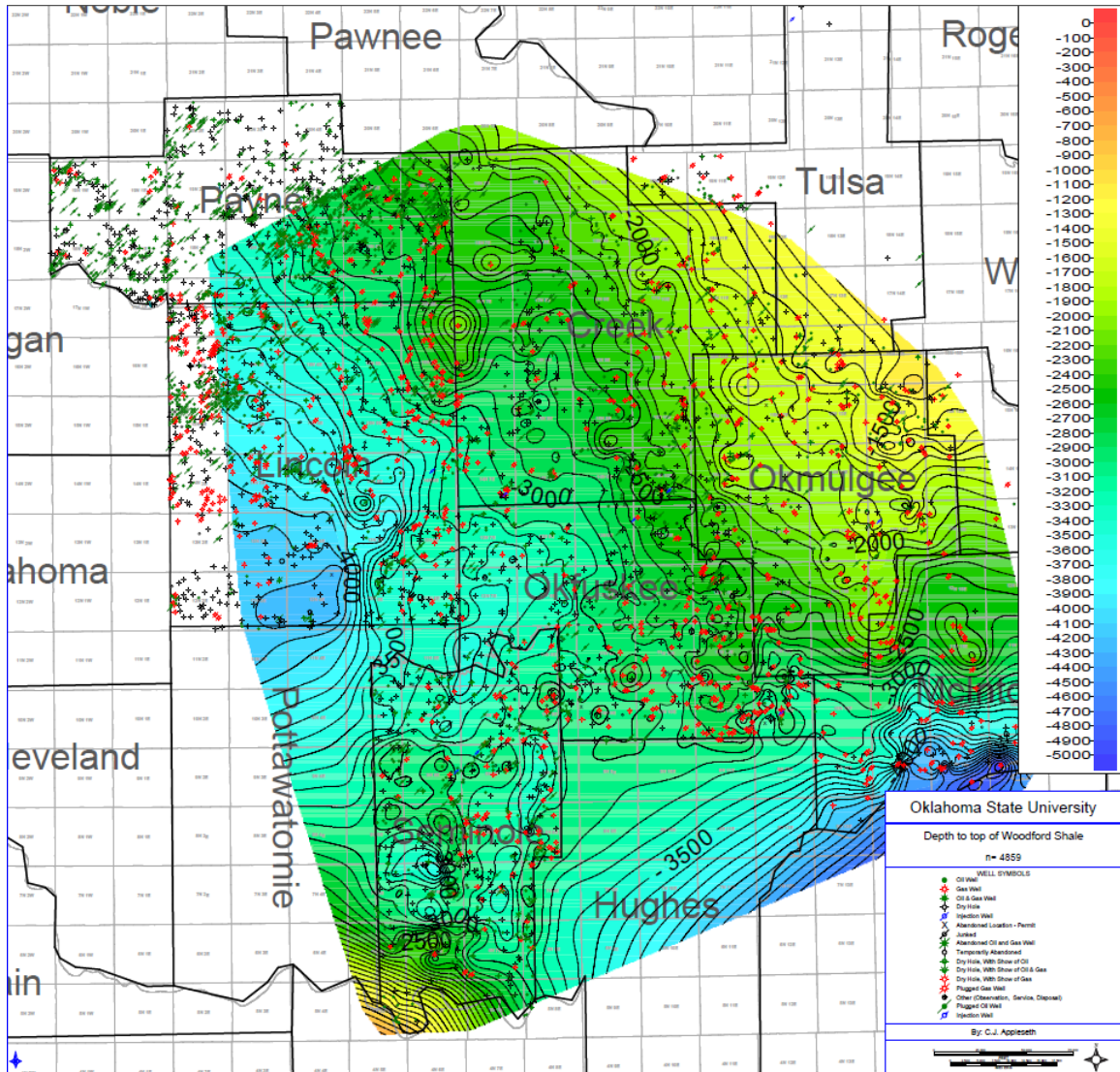
II. Subsurface Cross Sections

See attached Plates.

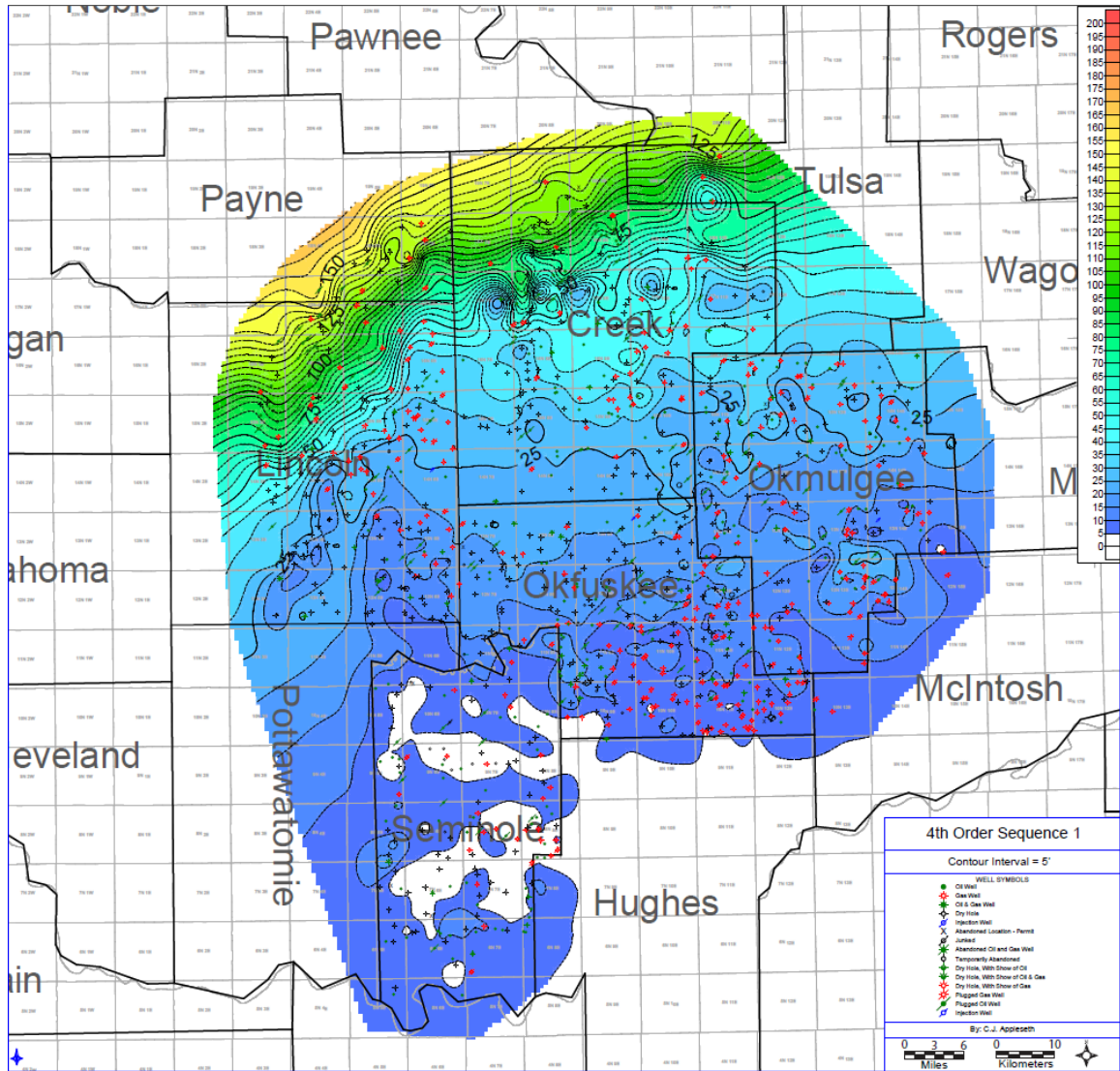
III. Depth to Mississippian-Pennsylvanian Contact Structure Map

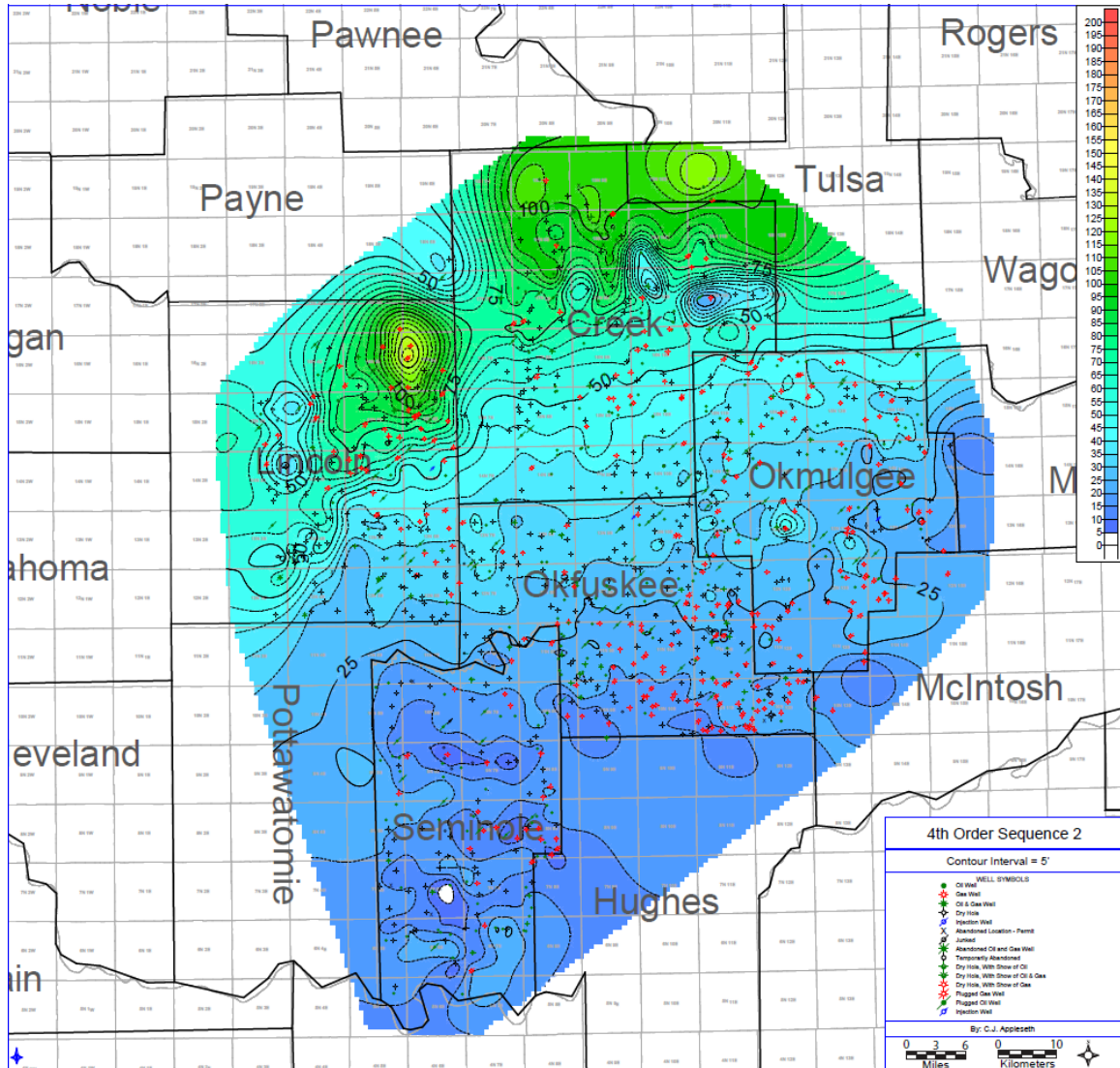


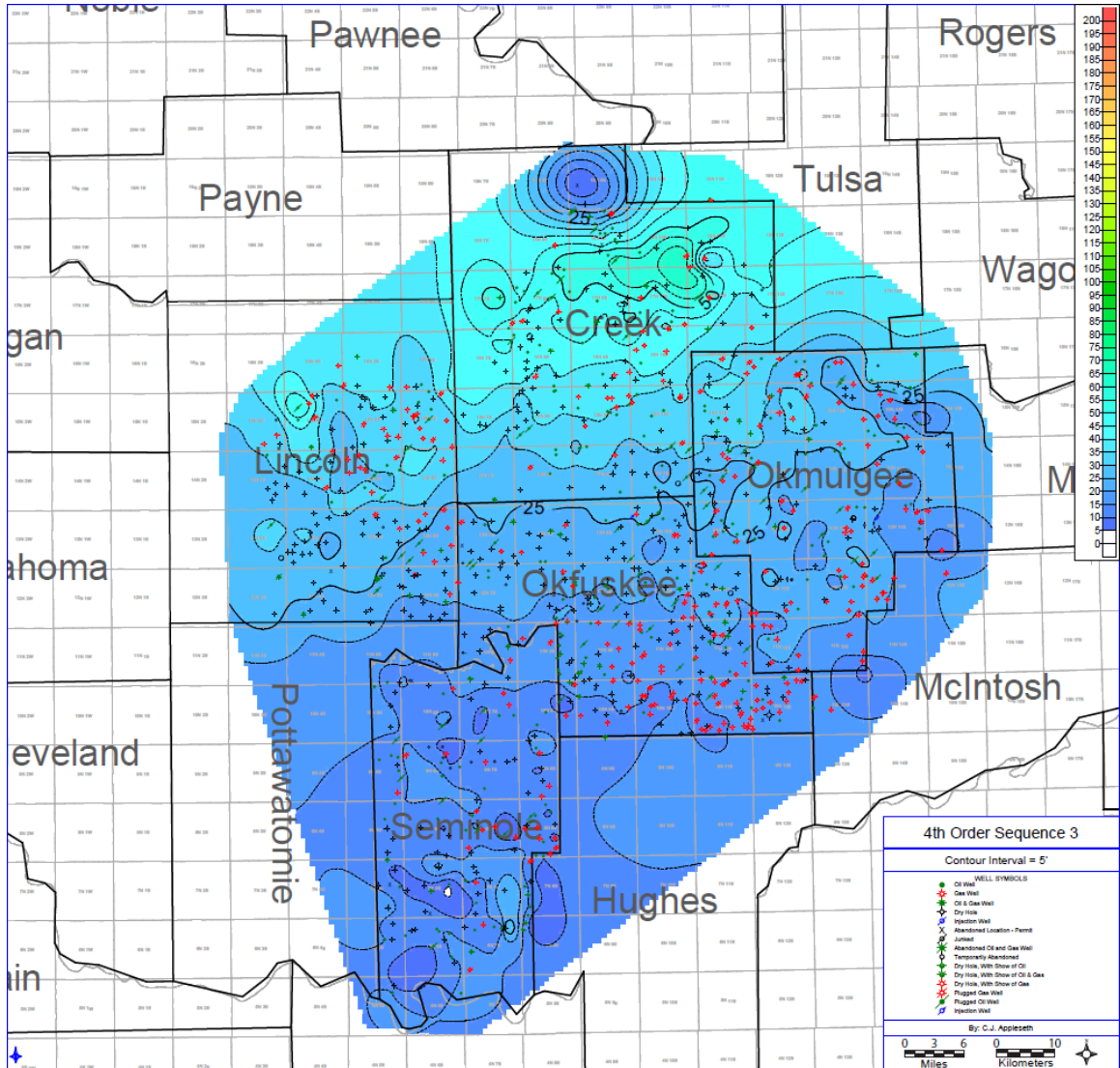
IV. Depth to Basal Mississippian Contact (Top of Woodford Shale) Structure Map

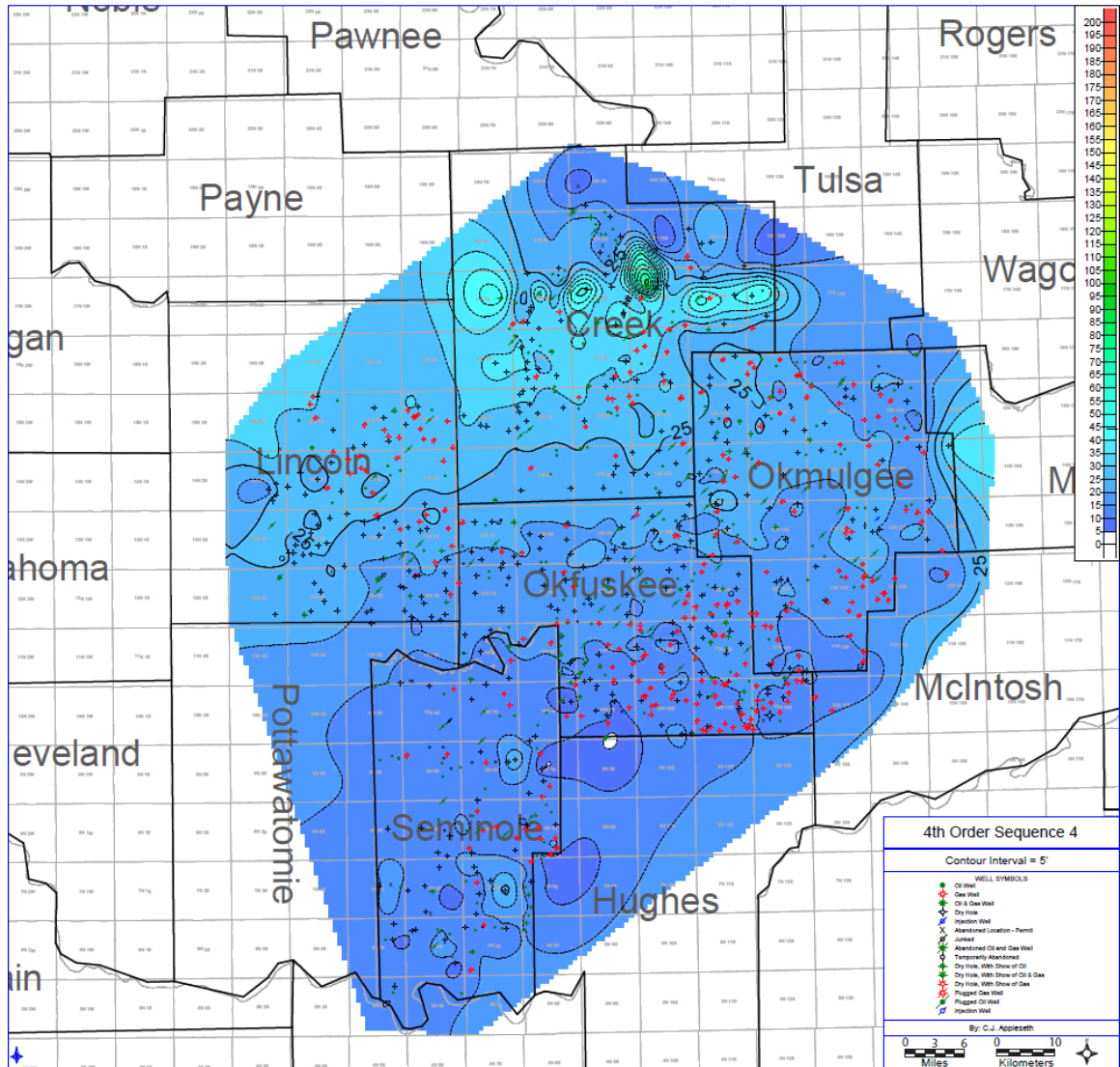


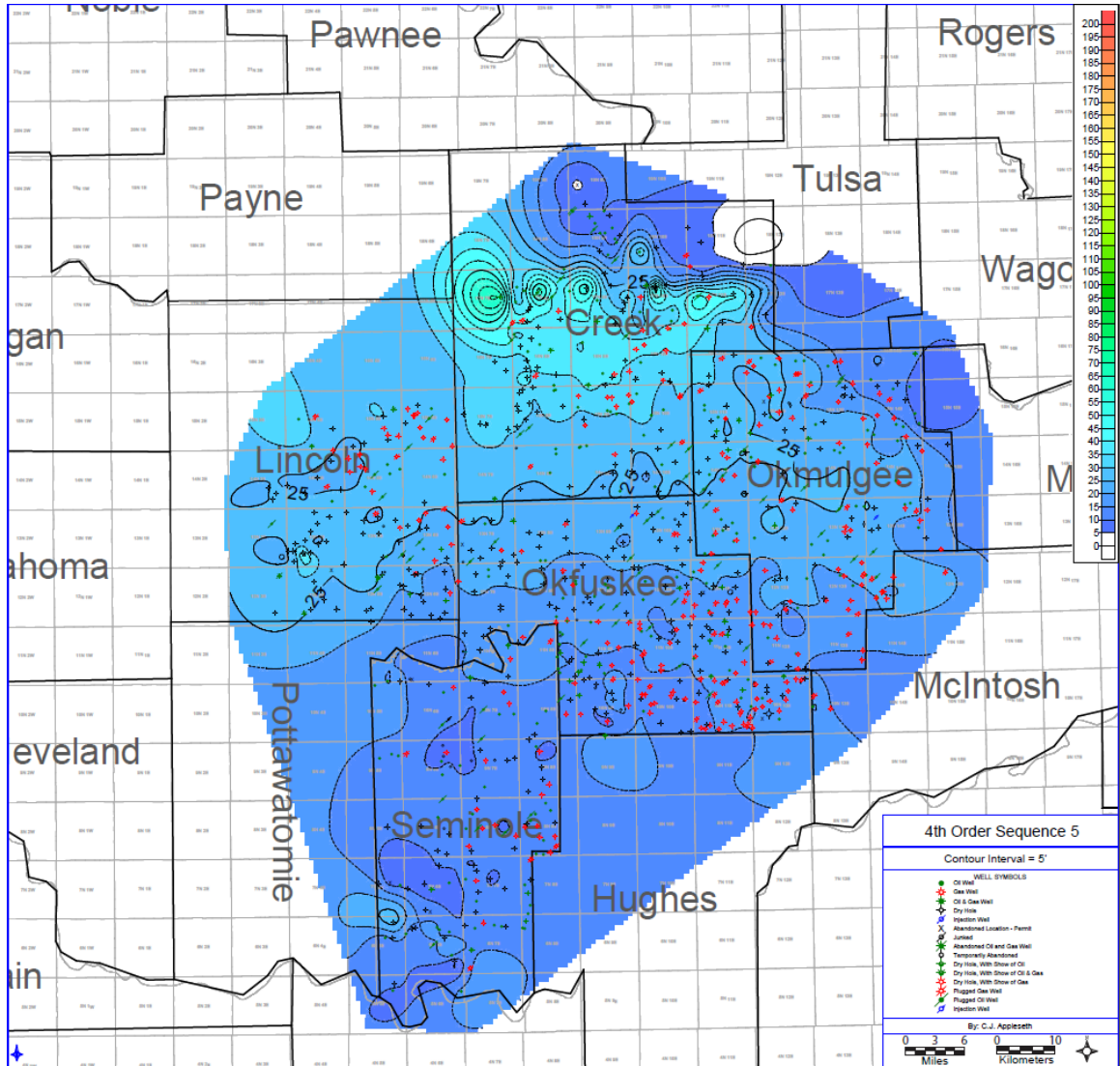
V. "4th Order" Sequence Thickness Maps

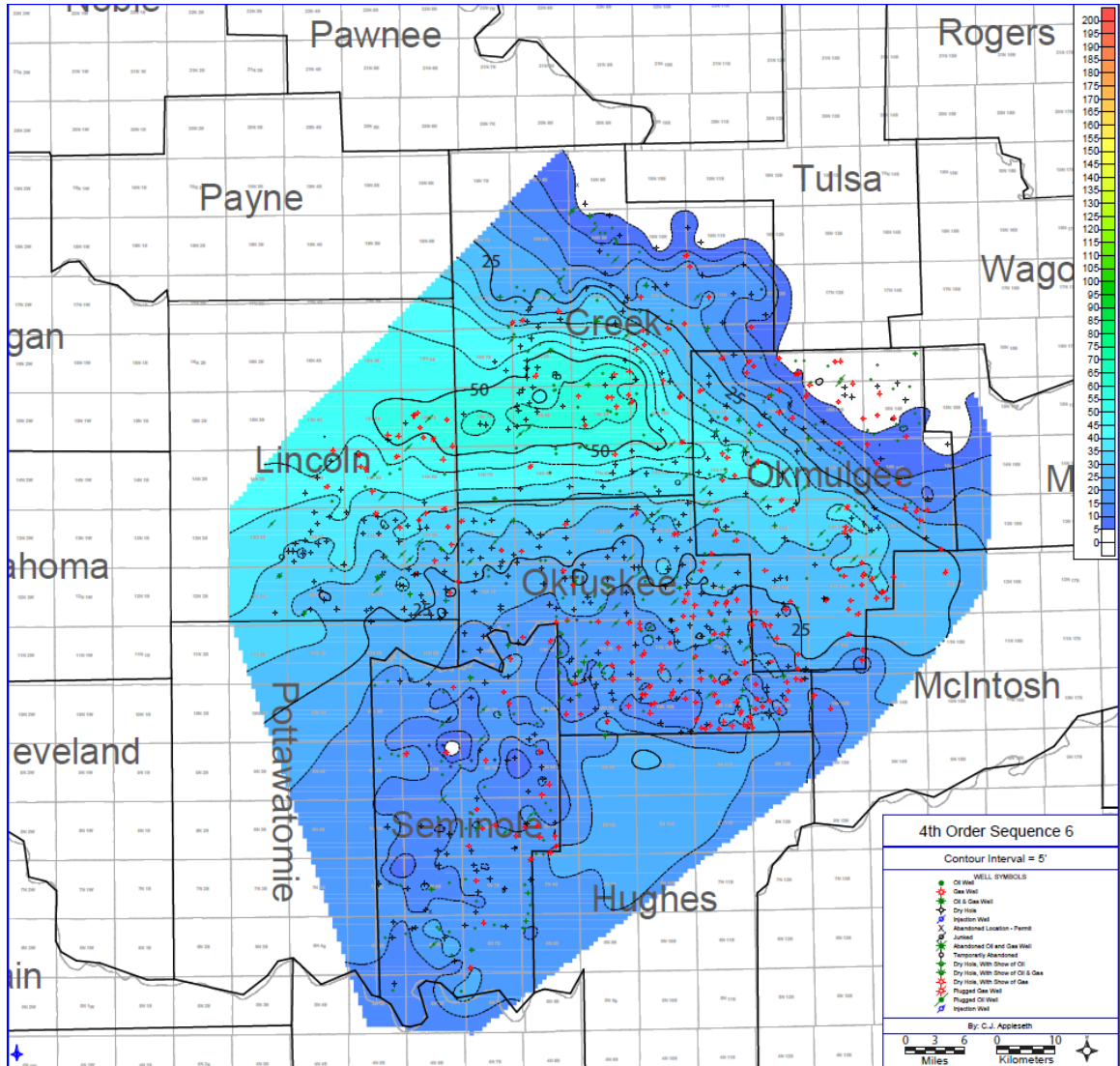


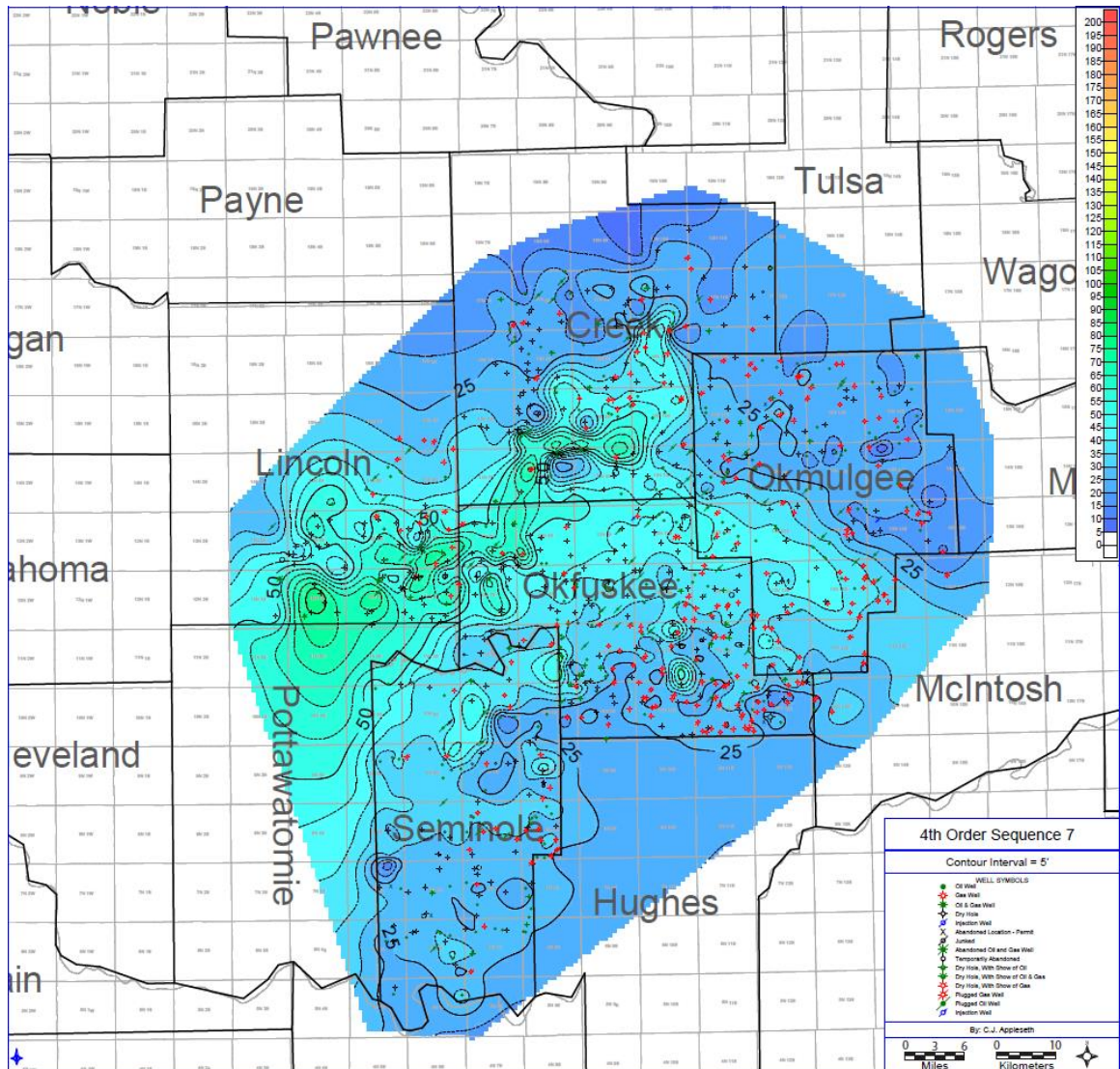


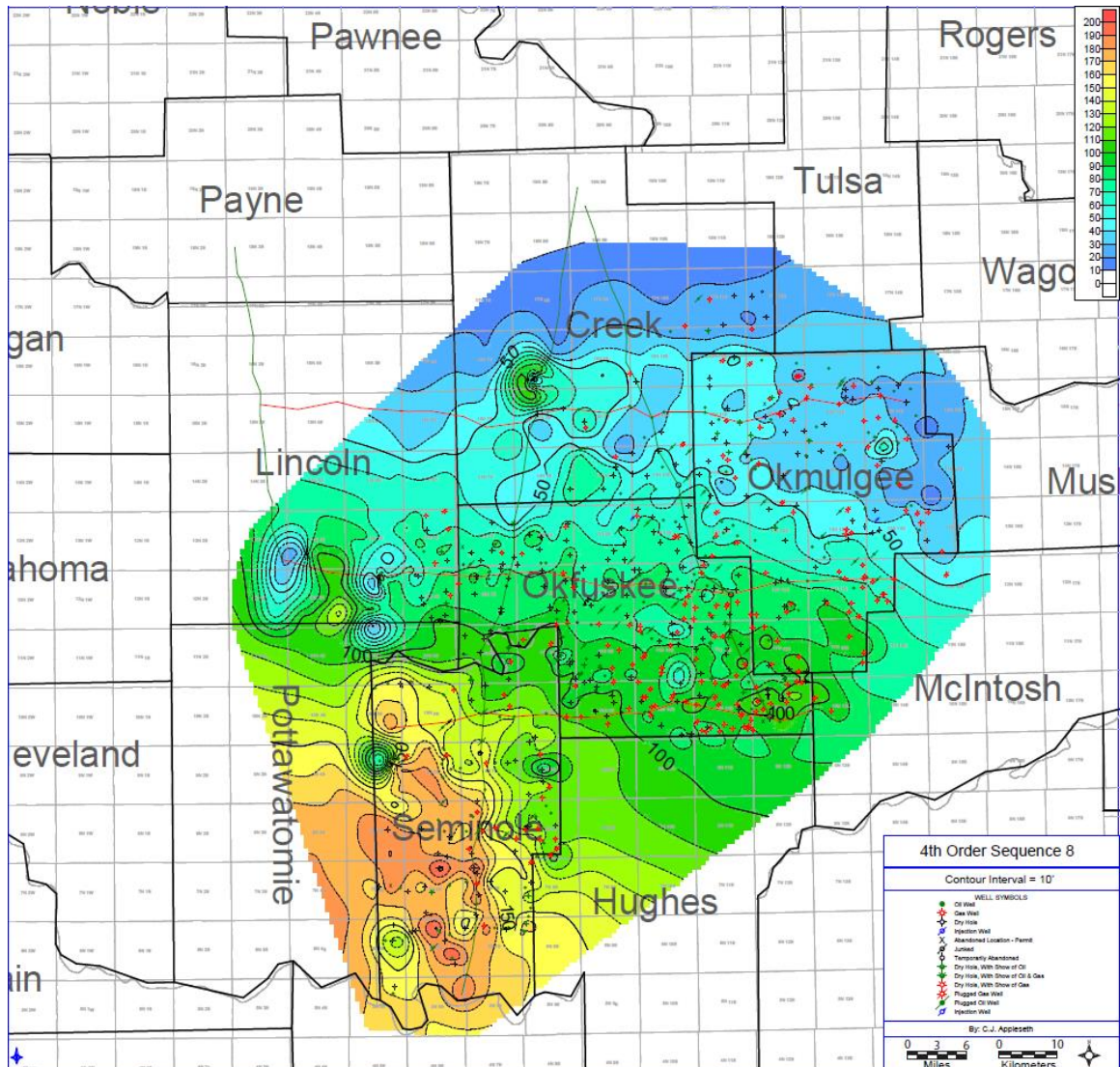


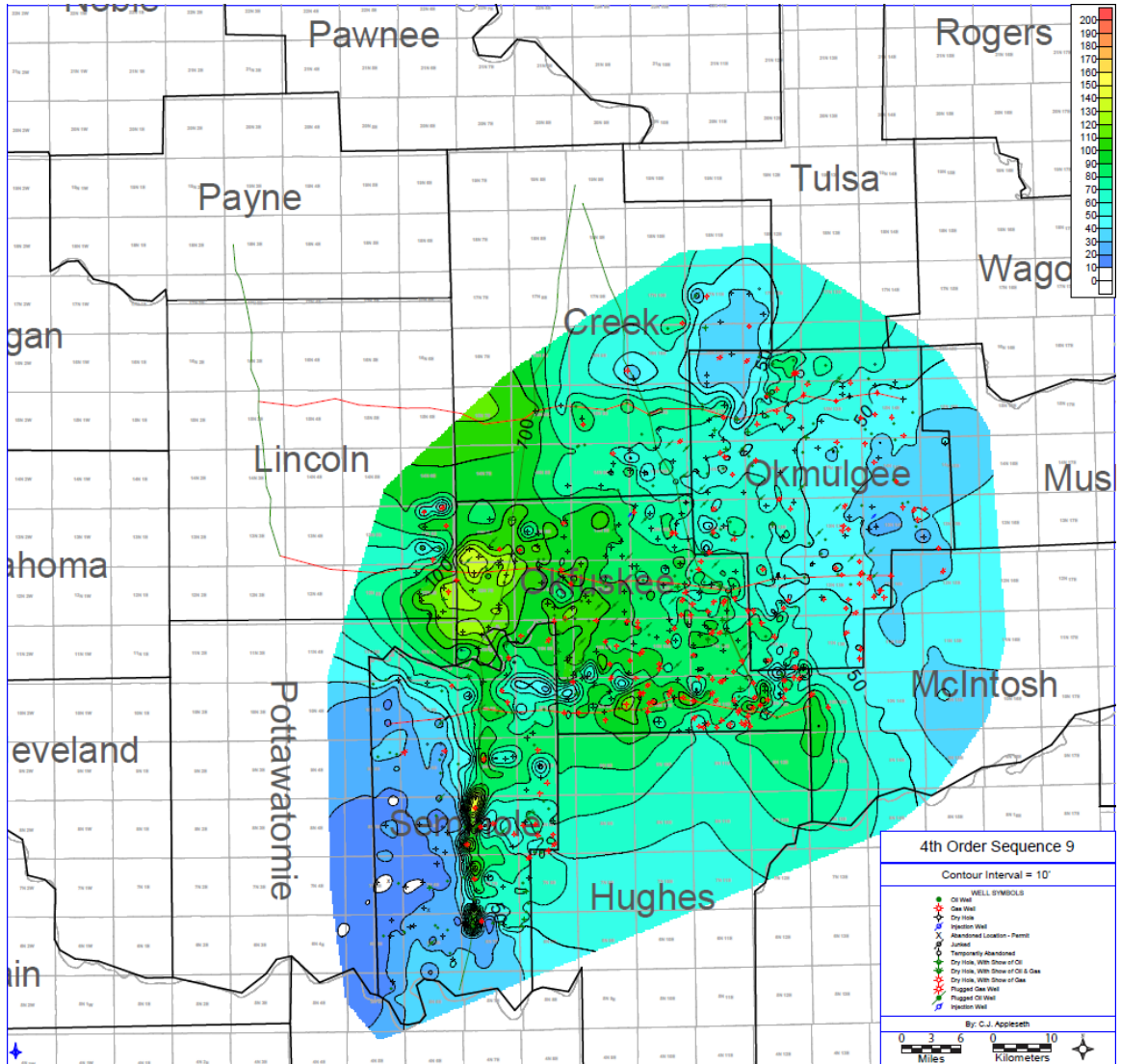












VITA

C.J. Appleseth

Candidate for the Degree of

Master of Science

Thesis: HIGH RESOLUTION SEQUENCE STRATIGRAPHY AND RESERVOIR
CHARACTERIZATION OF MISSISSIPPIAN STRATA IN CENTRAL AND EASTERN
OKLAHOMA

Major Field: Geology

Biographical:

Education:

Completed the requirements for the Master of Science in Geology at Oklahoma State University, Stillwater, Oklahoma in May, 2019.

Completed the requirements for the Bachelor of Arts in Business Administration at University of Central Oklahoma, Edmond, Oklahoma in 2008.

Experience:

Geology intern at FourPoint Energy, in Denver, CO in 2016.

Geoscience intern at Devon Energy, in Oklahoma City in 2015.

Professional Memberships:

American Association of Petroleum Geologists

Society for Sedimentary Geology

Oklahoma City Geological Society